THE UNIVERSITY OF BIRMINGHAM

Multiphase Catalytic Reactions in a Trickle Bed Reactor

By

Mansour Ali Al Herz

A thesis submitted to
The University of Birmingham
for the degree of
DOCTOR OF PHILOSOPHY

Abstract

Successful transfer of multiphase catalytic reactions from laboratory to commercial scale depends on proper understanding of all the parameters involved. This thesis aims to further understand these aspects with regards to trickle beds. A detailed discussion of reaction kinetics, hydrodynamics and mass transfer is presented for three industrially important reactions.

The catalytic hydrogenation of dimethyl itaconate was studied in lab-scale shake flask and transferred to continuous flow with recirculation in a trickle bed reactor (TBR). The TBR was operated in the trickle flow regime using the catalyst complex [Rh((R,R)-Me-DuPhos)(COD)]BF_4 supported on ion-exchange resins and trilobe alumina. Under optimized conditions in the TBR, 99% conversion and enantioselectivity of up to 99.9% were achieved. After elimination of all diffusional resistances, the experimental data could be fitted well by means of a kinetic model based on the Osborn-Wilkinson reaction mechanism.

The selective hydrogenation of 1-heptyne over a 2 wt. % Pd/Al_2O_3 catalyst was studied in a TBR operating in both batch recycle and continuous modes. Solvent selection and liquid flow rate were found to have a noticeable effect on reaction rate and selectivity. The concentration profiles were fitted according to a Langmuir-Hinshelwood kinetic expression. Under optimized conditions in the TBR, 100% selectivity to 1-heptene was maintained up to 84% conversion of 1-heptyne.

The selective hydrogenation of soyabean oil over a 2 wt. % Pd/Al_2O_3 catalyst was assessed in a TBR operating in a batch recycle mode. Reaction temperature, hydrodynamics and oil volume were found to have a noticeable influence on reaction rate and selectivity. It was demonstrated that under proper reaction conditions, the composition of soyabean oil can be upgraded to produce base oils for lubricants.

This thesis is dedicated to my father and mother, who have been a source of encouragement and inspiration to me throughout my life.

Also, this thesis is dedicated to my wife's father and mother for the sacrifices they made in life so that their daughter could have the best.

Acknowledgements

Contents

4

15

LIST OF TABLES

NOMENCLATURE

$[A]$ Catalyst concentration, mol m^{-3}. *(Equation 4.2)*

C_i H$_2$ concentration in EtOH at the EtOH-H$_2$ interface , mol m^{-3}. *(Equation 3.2)*

C_{H_2} H$_2$ concentration in isopropanol, kmol m^{-3}. *(Equations 6.3 & 6.4)*

$C_{1-heptyne}$ Concentration of 1-heptyne, kmol m^{-3}. *(Equations 6.3 & 6.4)*

$C_{1-heptene}$ Concentration of 1-heptene, kmol m^{-3}. *(Equations 6.3 & 6.4)*

$C_{heptane}$ Concentration of heptane, kmol m^{-3}. *(Equation 6.6)*

D_{AB} The diffusivity of solute A in solvent B , m^2 s^{-1}. *(Equations 5.5 & 7.3)*

De Effective diffusivity, m^2 s^{-1}. *(Equation 5.2)*

d_p Diameter of catalyst particle, m. *(Equations 6.1 & 6.2)*

d_R Inner diameter of reactor, m. *(Equations 6.1 & 6.2)*

d_v Equivalent volume diameter, $d_v = (6V_p/\pi)^{1/3}$, m. *(Equation 5.3)*

Fr_L Liquid Froude number, $Fr_L = V_{SL}^2/gd_v$. *(Equation 5.3)*

G_l Superficial mass velocity of liquid, kg m^{-2} s^{-1}. *(Equation 5.4)*

g Gravitational constant, m s^{-2}. *(Equation 5.3)*

K_1, K_2 Equilibrium constants, m^3 mol^{-1}. *(Equation 4.2)*

$K_{1-heptyne}$ Adsorption coefficient of 1-heptyne, m^3 kmol^{-1}. *(Equations 6.3 & 6.4)*

$K_{1-heptene}$ Adsorption coefficient of 1-heptene, m^3 kmol^{-1}. *(Equations 6.3 & 6.4)*

K_c Mass transfer coefficient, m s^{-1}. *(Equation 5.4)*

k_1, k_2 Rate constants, kmol kg s. *(Equations 6.3 & 6.4)*

k', k'' Rate constants, m^3 mol^{-1} s^{-1}. *(Equation 4.2)*

M_B The molecular weight of the solvent. *(Equations 5.5 & 7.3)*

Mo_L Liquid Morton number, $Mo_L = g\,\mu_L^4/\rho_L\sigma_L^3$. *(Equation 5.3)*

m Catalyst loading, kg of catalyst / m^3 of solution. *(Equations 6.3 & 6.4)*

P Concentration of hydrogen in the solution, mol m^3. *(Equation 4.2)*

R	Pellet radius, m. *(Equation 5.2)*
R_A	Rate per volume of solution, mol / (m^3 of solution $\cdot$ s). *(Equation 3.2)*
Re	Reynolds Number, $Re = G_l d_p / \mu_l$. *(Equation 5.4)*
r_b	Resistance to gas absorption, s. *(Equation 3.2)*
r_{cr}	Specific combined resistance to internal diffusion, reaction, and external Diffusion, kg cat $\cdot$ s / m^3. *(Equation 3.2)*
$[S]$	Substrate concentration, mol l^{-1}. *(Equation 4.2)*
S_a	Surface area per unit mass of catalyst, m^2 g^{-1}. *(Equation 5.2)*
Sc	Schmidt number, $Sc = v D_{AB}^{-1}$. *(Equation 5.4)*
Sh	Sherwood number, $Sh = K_c d_p \alpha / D_{AB}$. *(Equation 5.4)*
S_T	Surface tension of liquid, dyne cm^{-1}. *(Equation A.2)*
S_{TW}	Surface tension of water, dyne cm^{-1}. *(Equation A.2)*
T	The temperature, K. *(Equation 7.3)*
u_g	Gas superficial velocity, cm s^{-1}. *(Figures 5.5, 6.4 and 7.11)*
u_L	Liquid superficial velocity, cm s^{-1}. *(Figures 5.5, 6.4 and 7.11)*
V_A	The molecular volume of the solute, m^3 mol^{-1}. *(Equations 5.5 & 7.3)*
V_{SL}	Superficial liquid velocity, m s^{-1}. *(Equation 5.3)*

Greek symbols

α	Fraction of external surface that is wetted. *(Equation 5.4)*
ε	Bed porosity, dimensionless.
ε_B	Porosity of the alumina particle bed. *(Equation 5.3)*
ϵ_L	Liquid holdup, dimensionless. *(Equations 6.1 & 6.2)*
η	Internal effectiveness factor. *(Equation 5.1)*
λ	Baker co-ordinate, dimensionless. *(Figures 5.5, 6.4 and 7.11)*
μ	The viscosity of the solution, Pa · s. *(Figures 5.5, 6.4 and 7.11)*
μ_L, μ_l	Liquid viscosity, Pa · s. *(Figures 5.5, 6.4 and 7.11)*
ρ_p	Density of catalyst particle, kg m^{-3}. *(Equation 3.1)*
ρ_L	Liquid density, kg m^{-3}. *(Figures 5.5, 6.4 and 7.11)*
σ_L	Liquid surface tension, kg s^{-2}. *(Equation 5.3)*
ϕ	Thiele modulus. *(Equation 5.1)*
$\emptyset_B$	The association factor for the solvent. *(Equations 5.5 & 7.3)*
ψ	Baker co-ordinate, dimensionless. *(Figures 5.5, 6.4 and 7.11)*

LIST OF APPREVIATIONS

BINAP   2,2'-bis(diphenylphosphino)-1,1'-binaphthyl

CDC   Concurrent downflow contactor

CHD   Coronary heart disease

COD   *Cis,cis*-1,5-cyclooctadiene

C16   Palmitic acid

C18:0   Stearic acid

C18:1   Oleic acid

C18:2   Linoleic acid

C18:3   Linolenic acid

DIOP   1,4-Bis(diphenylphosphine(1,4-dideoxy-2,3-O-isopropylidene-threitol

DMI   Dimethyl itaconate

Ee   Enantioselectivity

EtOH   Ethanol

FDA   Food and drug administration

GC   Gas chromatography

IPA   Isopropanol

IV   Iodine value

Me-DUPHOS   1,2-Bis(2,5-dimethylphospholano)benzene

MeOH   Methanol

MCM-41   Mobile composition of matter No. 41

NBD   Norbornadiene

Si   Isomerization index

S_L Linoleic selectivity

S_{Ln} Linolenic selectivity

TAG	Triglycerides
TBR	Trickle bed reactor
TFA	*Trans* fatty acids
TOF	Turnover frequency
TON	Turnover number
STR	Stirred tank reactor
50WX2-100	Ion exchange resin

CHAPTER 1

INTRODUCTION

1.1 Background and motivation

1.1.1 Enantioselective compounds

Optically active compounds are the constituents of many medicines, vitamins, flavours, fragrances, herbicides and pesticides. They are also the building blocks of proteins, carbohydrates and DNA which are the principal components of life itself. Baiker (1997) demonstrated that research in this field has been driven by the fact that the 'wrong' enantiomer of a chiral product may have negative side effects which outweigh the beneficial value of the 'right' enantiomer, a well known example being birth defects caused by the drug thalidomide. Such cases drive today's emphasis towards production of enantiomerically pure active ingredients.

Enantioselective catalysis is an attractive method of producing a single enantiomer, which has been applied to reactions involving the hydrogenation of carbon-carbon, carbon-nitrogen, and carbon-oxygen bonds (Crosman and Hoelderich, 2005) with high efficiency and low environmental impact. Moreover, information on industrial applications of enantioselective catalytic reactions has increased both in quantity and in quality with the enantioselective hydrogenation of olefins being a prime example with industrial relevance (Blaser *et al*. 2005). Homogeneous transition-metal-catalyzed asymmetric hydrogenation has attracted increased attention for the production of enantiopure pharmaceuticals and agrochemicals (Simons *et al*. 2004). However, large-scale applications of this mature methodology are hindered by the difficulty of catalyst separation and reuse. To overcome these issues, attention has recently focused on heterogenisation or immobilisation of metal complexes upon supports. Hems *et al*. (2005) claimed that poorer enantioselectivities are usually achieved with the immobilised

complex when compared to homogeneous catalysts although for some rare cases improved enantioselectivity can occur.

Despite the various well described procedures which allow for the immobilisation of a metal complex onto a solid support, it is still a challenge to synthesize efficient catalysts from these precursors. Once immobilised, the complex must maintain its activity and selectivity, be easily recovered and not leach under the reaction conditions (Quignard and Choplin, 2003). Among these conflicting requirements, covalently bound catalysts display possibly the broadest scope due to the link stability towards most solvents or additives such as salts or acids and bases (Blaser *et al*. 2000).

The enantioselective hydrogenation of β-ketoesters to chiral β-hydroxyesters using nickel catalysts and the hydrogenation of α-ketoesters or acids to chiral α-hydroxyesters or acids using platinum catalysts are two of the most feasible methods to result from over 40 years of research (Augustine *et al*. 2004). However, the potential of homogeneous catalysts as candidates for immobilisation could be realised through novel methods of attachment to the support. Augustine *et al*. (2003) developed a new technique of immobilisation that involves attaching catalytically active complexes to solid supports via heteropoly acids (HPAs). The active complex is attached to the support through the metal atom, delivering "anchored homogeneous catalysts". The attachment can be either covalent between the metal atom of the complex and the HPA or an ion pair with a metal cation and the oxygen anion of the HPA (Augustine *et al*. 2003). This type of attachment avoids the use of the ligand which may be prone to leaching. By applying this technique, turnover frequencies (TOFs) of up to 7000 h^{-1} and enantioselectivities of 97% have been achieved for the hydrogenation of dimethyl itaconate (DMI) together with good recyclability (Augustine *et al*. 2004).

1.1.2 Industrial methods

Production of small volumes of enantiopure compounds and fine chemicals in general are delivered on the industrial scale using batch processing (Maranhão and Abreu, 2005). In contrast, production of large volumes of bulk chemicals employs continuous processing, which affords lower plant inventories, lower production and labour costs and greater process control compared with batch plant at the expense of reduced process flexibility (www.manufacturingchemist.com). However, due to the expected increase in production volumes of fine chemicals, the replacement of batch plant with continuous (Toukoniitty *et al*. 2002) is a natural step forward for large scale production of some optically pure compounds (Turek *et al*. 1983; Gallezot *et al*. 1998; Bogdan *et al*. 2007). Examples of large production volumes of fine chemicals include ibuprofen, a painkiller at 10,000 tonnes/annum (t/a) (Stahly and Starrett, 1997), S,S-aspartame, a sweetener at 14,000 t/a (Sheldon, 1993) and (R)-mecropol, a herbicide at 14,000 t/a (Wang and Kienzle, 1998).

Hermán *et al*. (2007) stated that heterogeneous catalysts are more suitable for use in continuous processes and that chirally modified metal catalysts are the most promising alternatives for large scale production of optically pure compounds. Heterogeneous catalysts are more suitable for use in continuous reactors, since they do not require separation and recycling. Therefore efficient immobilisation, or heterogenisation, of homogeneous complexes onto supports is a key issue for the transfer of enantioselective synthesis from batch to continuous operation.

Various parameters have been reported in the literature for controlling the catalytic performance such as reactor design and operating conditions. Among these parameters, selection of solvent or mixture of solvents as a medium in which to conduct the reaction has particularly demonstrated a crucial impact upon the reaction behaviour (Hu *et al*. 2007; Bennett *et al*. 2009). Moreover, Toukoniitty *et al*. (2002) mentioned that in the production of

fine chemicals over heterogeneous catalysts, the choice of the solvent influences selectivity and/or activity of the catalytic system significantly. They pointed out that a bad selection of solvent destroys the possible utilization of a potentially efficient process in practice. Consequently, the proper choice of a solvent and the understanding of solvent effects are very crucial and require a careful investigation.

Multiphase catalytic processes have been expanding into diverse areas of applications and continue to make a significant impact on the development of new synthetic routes and high-value added products (Chaudhari and Mills, 2004). A wide variety of reactions have been carried out via this process using predominantly heterogeneous catalysts. Considering the diversity of its product values and volumes, and despite its application for over a century, it is somewhat surprising that these reactions are carried out for the most part in just one reactor type: the stirred tank reactor, (Fishwick *et al*. 2007). According to Stitt *et al*. (2003) this type of reactor has found extensive industrial applications for over a century. Fishwick *et al*. (2007) stated that there are a number of other well-established alternatives used in the large-scale chemical industries including the trickle bed reactor.

A trickle-bed reactor is a type of three-phase reactors in which a gas and a liquid phase concurrently flow downward over a packed bed of catalyst particles. Lopes and Quinta-Ferreira (2009) reported that trickle-bed reactors (TBRs) incorporate similar behaviour to plug flow which can ensure a high degree of conversion of the liquid reactants. They pointed out that this is one of the advantages of trickle-bed reactors over three-phase reactors, where the catalyst is introduced as either a suspension or a fluidized bed. Furthermore, TBRs are also distinguished by their flexibility and simplicity in operation for low as well as high throughputs (Gunjal *et al*. 2005). The application of these reactors is increasing every year (Dudukovic *et al*. 2002) with specific use in refineries and in the chemical and petrochemical industries (Lopes and Quinta-Ferreira, 2009).

Trickle-bed reactors may be operated in several flow regimes. At present, steady state operation in the trickle flow regime is the most frequently used in practice (Lopes and Quinta-Ferreira, 2009). However, frequent problems such as liquid maldistribution, back mixing, incomplete wetting of the catalyst bed and decreased selectivity are serious problems encountered during trickle flow operation. Moreover, trickle-flow characteristics are extremely complex and associated with the strong interactions of the fluids in the bed (Lopes and Quinta-Ferreira, 2009). Therefore, accurate understanding of hydrodynamics of trickle-bed reactors and how it influences basic phenomena such as wetting efficiency of catalyst bed, mass transfer and selectivity is essential.

A significant challenge in assessment of the effectiveness of heterogeneous or immobilised homogeneous catalysts for continuous processing at the laboratory scale is the low conversion achieved per pass within the fixed bed. This can be overcome by closed loop operation by recirculation of the reactant/product mixture. Indeed, the application of a closed-recycling configuration has been found to be useful in various research studies (Winterbottom *et al*. 2000; Heiszwolf *et al*. 2001; Gao *et al*. 2006) offering advantages such as achieving high conversions of substrates through prolonged exposure to the catalyst within the fixed bed. This type of operation has also been found applicable to small volume fine-chemical heterogeneous catalytic liquid-phase reactions, as it ensures efficient saturation of hydrogen in the recycling mixture (Gao *et al*. 2006).

The work presented in this thesis addresses and discusses the influence of hydrodynamics and solvent selection upon reaction performance in a recirculating trickle-bed reactor. The effect of these parameters is investigated using model reactions with fast kinetics which allow the influences of mass transfer limitations to be examined (enantioselective hydrogenation of dimethylitaconate to succinnic acids) and using a model selective series reaction (hydrogenation of 1-heptyne) and also using a model selective series-parallel reaction where

the residence time of the phases is known to alter the ratio of the products (hydrogenation of soyabean oil). The overall aim of this thesis is to develop better fundamental understanding of the relevant phenomena which enables the development of design rules for an optimised trickle-bed reactor. The evident lack of knowledge in the literature that covers these very important phenomena was the major incentive for this study, which if bridged will serve as a firm basis for further optimisations towards greener conditions of these industrially important reactions.

1.2 Scope of the work

From the brief background described above, a project with the following aims was conceived. The main aims of the work presented in this thesis are:

1) To apply high throughput methodologies to the optimisation of enantioselectivity for hydrogenation of dimethylitaconate.

2) To optimize catalyst formulation for hydrogenation of dimethylitaconate (catalyst precursor complex, ligand, support, catalyst loading) and investigate catalyst leaching under optimized reaction conditions.

3) Understanding mass transfer processes for simple single product reaction such as dimethylitaconate hydrogenation, series reaction such as 1-heptyne hydrogenation, and series-parallel reaction such as soyabean oil hydrogenation.

4) To determine whether studied reactions are limited by kinetics or mass transfer and test measured reaction kinetics against existing models.

5) To obtain understanding of the hydrodynamics of a trickle-bed reactor, and understand the influence of gas and liquid superficial velocities upon reaction rate, selectivity to the desired product, wetting efficiency of catalyst particles, liquid holdup in the reactor and mass transfer.

6) Study the role of transport parameters and solvent effects in trickle-bed and their influence on reaction rate and selectivity.

1.3 Thesis layout

The work presented in this thesis is introduced in this Chapter (Chapter 1). A literature review is presented in Chapter 2 which covers basic concepts of enantioselective hydrogenation reactions and the various methods used for immobilizing homogenous catalysts. Chapter 2 also covers literature survey on reactions considered, kinetics in trickle bed reactors and multiphase catalytic reactors. Selected examples of continuous hydrogenation of the studied reactions are also viewed in Chapter 2. Chapter 3 is the compilation of detailed description of experimental systems, operating procedures, equipment calibrations employed in this study and properties of materials used. The results from hydrogenation of dimethylitaconate over catalyst complexes immobilized on organic and inorganic supports are given in Chapters 4 and 5, respectively. Chapter 6 is concerned with the selective hydrogenation of 1-heptyne with the intermediate being the desired product, which is typical in the fine chemical industries. Chapter 7 is concerned with soyabean oil hydrogenation to improve its fatty acid composition for different industrial applications. In Chapter 8, the conclusion and recommendation for future work in this context are given. The Appendices include sample of calibration curves, sample calculations and some supporting graphs.

1.4 Publications

Publications resulting from work in this thesis are listed below, and copies are provided in Appendix 9.4.

1.4.1. Journals

1. M.A. Al Herz, M.J.H. Simmons, J. Wood. "Selective Hydrogenation of 1-Heptyne in a Mini Trickle Bed Reactor." (2011). Industrial & Engineering Chemistry Research. (Accepted for publication, Industrial & Engineering Chemistry Research, October 2011)

2. M.A. Al Herz, A.N. Tsoligkas, M.J.H. Simmons, J. Wood. "Enantioselective hydrogenation of dimethyl itaconate with immobilised rhodium-duphos complex in a recirculating fixed-bed reactor." (2011). Applied Catalysis A: General (Accepted for publication, Applied Catalysis A: General, February 2011).

1.4.2. Conference presentations

1. M.A. Al Herz, A.N. Tsoligkas, M.J.H. Simmons, J. Wood. "Selective Hydrogenation of 1-Heptyne over Pd/Al$_2$O$_3$ Catalyst in a Mini Fixed-Bed Reactor: Effect of Operating Parameters and Choice of Solvent. Catalysis in Multiphase Reactors CAMURE-8 International Symposium on Multifunctional Reactors ISMR-7, Finland, May 2011. Oral presentation

2. M.A. Al Herz, A.N. Tsoligkas, J. Wood, M.J.H. Simmons. "CONTINUOUS ENANTIOSELECTIVE HYDROGENATION IN FIXED-BED REACTOR". 8th World Congress of Chemical Engineering, Montreal, Canada, September 2009. Oral presentation.

3. M.A. Al Herz, A.N. Tsoligkas, J. Wood, M.J.H. Simmons. "CONTINUOUS ENANTIOSELECTIVE HYDROGENATION IN FIXED-BED REACTOR". Liverpool Summer School in Catalysis, Liverpool, UK, July 2009. Poster presentation.

4. M.A. Al Herz, A.N. Tsoligkas, J. Wood, M.J.H. Simmons. "CONTINUOUS ENANTIOSELECTIVE HYDROGENATION IN FIXED-BED REACTOR". Catalytic Flow Chemistry, Birmingham, UK, April 2009. Poster presentation.

5. M.A. Al Herz, A.N. Tsoligkas, J. Wood, M.J.H. Simmons. "CONTINUOUS ENANTIOSELECTIVE HYDROGENATION IN FIXED-BED REACTOR". IChemE Catalysis Subject Group Student Conference, Bath University, November 2008. Poster presentation.

CHAPTER 2

LITERATURE REVIEW

2.1 Introduction

This chapter reviews the literature with reference to the enantioselective hydrogenation reactions, selective hydrogenation of alkynes, hydrogenation of vegetable oils and multiphase reactors. § 2.2-2.4 introduce the concept of chirality and stereoselective synthesis. § 2.5 discusses the importance of using homogeneous catalysis as a tool to obtain chiral products and explains the mechanism of rhodium-catalyzed enantioselective hydrogenation. The different procedures of immobilization of metal complexes on organic and inorganic supports are described in § 2.6, followed by discussion of the importance of continuous enantioselective hydrogenation § 2.7. § 2.9 covers various aspects of selective hydrogenation of alkynes with particular emphasis on long-chain hydrocarbons such as 1-heptyne. § 2.10 approaches partial hydrogenation of vegetable oil and reports useful tips for minimization of *trans* fatty acid formation. § 2.10 concludes with the benefits and potential applications of continuous hydrogenation of vegetable oil. § 2.11 reviews the multiphase reactors in general and trickle bed reactor in particular. Parameters such as flow regime in the reactors, mass transfer, liquid holdup and wetting efficiency are discussed.

2.2 Chirality of molecules and chiral carbon atoms

A molecule is said to be chiral when it cannot be superimposed upon its mirror-image. In this case, the molecule and its mirror-image are considered to be different compounds and the pair are called enantiomers. Apart from chirality, a pair of enantiomers has the same structure and thus same physical and chemical properties. For example, each pure enantiomer of a pair has the same melting point and the same boiling point. Only two sets of properties are

39

different for a single pair of enantiomers: interactions with other chiral substances and interactions with polarized light.

A chiral carbon atom has four different groups attached to it and the order of arrangement of the groups is called absolute configuration. The actual arrangement of groups around a chiral carbon is defined by the (R) and (S) system. Any chiral carbon atom has either an (R) configuration or an (S) configuration and therefore, one enantiomer is (R) and the other is (S). Furthermore, a mixture of equal amounts of any pair of enantiomers is called a racemic mixture. A solution of either a racemic mixture or of an achiral compound is considered to be optically inactive (Fessenden *et al*. 1998).

2.3 Synthesis of chiral compounds

To synthesize one enantiomer of a chiral compound, two common synthetic approaches have been reported in the literature. The first is to synthesize the compound as a racemic mixture and then separate the enantiomers. The separation of enantiomers, called resolution, is recognized as a viable tool for obtaining certain optically active compounds. Moreover, D'Oria *et al*. (2010) pointed out that crystallization of a racemic solution or melt can sometimes lead to a conglomerate, which is known as spontaneous resolution. However, De Vries and Elsevier (2007) pointed out that the theoretical yield of this type of reaction is only 50%, because the unwanted enantiomer is discarded. This generates a huge waste stream, and is an undesirable situation from both environmental and economic points of view. Sekhon (2010) also reported that separation of racemates via crystallization from a proper solvent has a lot of disadvantages: i) complete enantiomer separation cannot be achieved in one step, ii) a small amount of the wanted form is retained in the mother liquor, iii) a large amount of active resolution agent is needed, iv) the widely used organic solvents cause impurities in the product.

The second approach is to synthesize the compound with a chiral auxiliary (a chiral catalyst, reagent, solvent, or intermediate). This technique is called asymmetric synthesis. Ojima (2010) stated that among the types of asymmetric reactions, the most desirable and the most challenging is catalytic asymmetric synthesis because one chiral catalyst molecule can create millions of chiral product molecules, just as enzymes do in biological systems. Ojima (2010) also reported that catalytic asymmetric synthesis offers significant economic advantages, and hence it is preferred over other types of asymmetric reactions for the industrial-scale production of enantiomerically pure compounds. Due to the above advantages of chiral catalysis, it is chosen as the subject of study in this work.

2.4 Important criteria for enantioselective catalysts

Since chiral catalysis is the subject of study in this thesis, some basic relevant terminology will be defined.

Enantioselectivity: since many asymmetric syntheses are not 100 % efficient, the term enantiomeric excess (*% ee*), i.e., % desired – undesired enantiomer is often used to describe the products.

$$\% \: ee = (R - S) \: / \: (R + S) \times 100 \tag{2.1}$$

Where (*S*) and (*R*) are concentrations of a pair of enantiomers in mol/litre.

Blaser *et al*. (2005) pointed out that for pharmaceuticals, the *ee* of a catalyst should be $\square$ 99% in the case where no purification is possible whereas for agrochemicals *ees* $\square$ 80% will be sufficient.

Catalyst productivity: expressed as turnover number (TON), determines catalyst costs. TON is defined as the number of moles of substrate converted per moles of catalyst used. De Vos

et al. (2000) stated that TONs for homogeneous enantioselective hydrogenation reactions ought to be > 1000 for small-scale, high-value products and >50 000 for large-scale or less expensive products. They pointed out that for C-C coupling reactions and other reactions with high added value or for very inexpensive catalysts, lower TONs might be acceptable. Moreover, much lower limits might apply if catalyst reuse is possible without much loss in selectivity and activity.

Catalyst activity: expressed as turnover frequency (TOF) determines the production capacity. TOF is defined as the number of moles of substrate converted per moles of catalyst used per unit time (or TON per unit time). De Vos *et al*. (2000) stated that TOFs ought to be >500 h^{-1} for small-scale products and >10 000 h^{-1} for large-scale products.

2.5 Asymmetric homogeneous hydrogenation

Asymmetric homogeneous hydrogenation constitutes an important synthetic procedure and is one of the most extensively studied reactions of homogeneous catalysis. The homogeneous hydrogenation of organic unsaturated substrates is usually performed with molecular hydrogen. The significant advancement of coordination and organometallic chemistry has led to the preparation of a wide variety of soluble metal complexes active as homogeneous hydrogenation catalysts under very mild conditions. These complexes are usually derived from transition metals with phosphine ligands. These transition metal complexes demonstrated the ability to stabilize a large variety of ligands with a variability of the coordination number and oxidation state. Among these ligands are unsaturated substrates such as alkenes.

Industrial hydrogenation reactions are common-place syntheses, but because the reaction of hydrogen with alkenes is exothermic; the high activation energy required inhibits the occurrence of the reaction in the absence of catalyst. Therefore, the addition of hydrogen to

alkenes doesn't occur without catalyst according to orbital symmetry rules. In contrast, transition metals have the appropriate orbitals to interact readily with molecular hydrogen, forming metal hydride species, allowing the transfer of the hydride to the coordinated alkene. De Vries and Elsevier (2007) reported that rhodium is a good example of such transition metals that has played a major role in the understanding of homogenous hydrogenation.

2.5.1 Chiral modification of metal catalysts

Chiral modification of metal catalysts is achieved by a very small quantity of an adsorbed chiral auxiliary (modifier), which is deposited on the catalyst surface in a special pre-treatment step before reaction. The modifier adsorbs on the active metal surface and controls the enantioselectivity of the catalytic process by interacting with the reactant(s). Therefore, knowledge concerning the adsorption of the modifier on the metal surface and its interaction with the reactant(s) is very important for synthesizing this class of catalysts. The design of suitable modifiers requires some understanding of the reaction mechanism as well as the crucial interactions occurring in the catalytic system which are summarized in Figure 2.1. De Vos *et al*. (2000) pointed out that the ultimate goal from considering these interactions is to gain some understanding of the transition state which determines the enantioselectivity of the reaction. They reported that the transition state structure is generally not available.
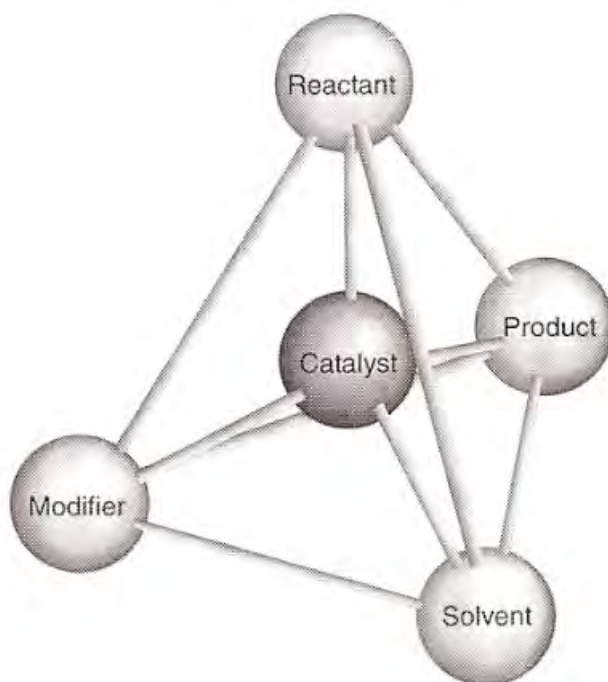
Figure 2.1. Interactions to be considered in optimisation of an enantiodifferentiating catalytic system based on chirally modified metals, De Vos *et al*. (2000).

Today, thousands of efficient chiral phosphorus ligands with diverse structures have been developed, and their applications in asymmetric hydrogenation have been extensively utilized in both academic research and industry (Tang and Zhang, 2003). Tang and Zhang (2003) stated that numerous unsaturated compounds can be hydrogenated with excellent *ee's* using a metal catalyst associated with an appropriate chiral ligand.

Denticity refers to the number of atoms in a single ligand that bind to a central atom in a coordination complex. In many cases, only one atom in the ligand binds to the metal, so the denticity equals one, and the ligand is said to be monodentate. Similarly, ligands that bind with two atoms, providing more tight binding with the metal atom, are called bidentate ligands. Bernsmann *et al*. (2005) reported that transition-metal-catalyzed enantioselective hydrogenation has been dominated by chiral bidentate ligands for more than three decades. They stated that bidentate ligands were considered essential to achieve high enantioselectivity in catalytic asymmetric hydrogenation reactions. A huge library of chiral bidentate ligands

has been developed for enantioselective hydrogenation, but only a limited number including DIOP, DuPhos and its analogues, and BINAP (Figure 2.2) are commercially available (Bernsmann *et al.* 2005).
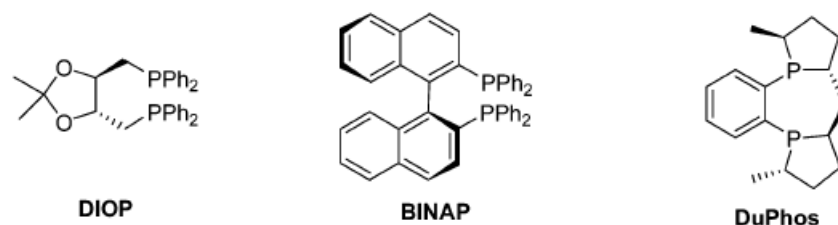
Figure 2.2. Examples of effective bidentate ligands in transition-metal-catalyzed enantioselective hydrogenation.

2.5.2 Enantioselective hydrogenation of alkenes with rhodium catalysts

Following Wilkinson's discovery of [RhCl(PPh₃)₃] as an homogeneous hydrogenation catalyst for unhindered alkenes (Young *et al.* 1965), various chiral phosphine ligands have been developed. Several authors have then shown that, with the use of optically active phosphines as ligands in complexes of rhodium, the enantioselective asymmetric hydrogenation of prochiral C=C double bonds is possible (De Vries and Elsevier, 2007).

Knowles and Sabacky (1968) reported the hydrogenation of α-phenylacrylic acid and itaconic acid with 15% and 3% ee, respectively, by using [RhCl₃(P*)₃][P* = (R)-(-)-methyl-n-propylphenylphosphine] as homogeneous catalyst. Although the ee's achieved were relatively low, they established the validity of the hydrogenation method and paved the way for further optimisation of the results.

An important breakthrough was the finding, by Dang and Kagan (1971), who efficiently catalyzed the reduction of unsaturated α-acetamidocinnamic acid and α-phenylacetamidoacrylic acid with 72 and 68% ee, respectively, using rhodium complex containing the chiral diphosphine (-)-DIOP ((-)-2,3-O-isopropylidene-2,3-dihydroxy-1,4-

bis(diphenylphosphine)butane. Dang and Kagan (1971) presented two assumptions for achieving a high degree of stereoselectivity in enantioselective catalysis:

- The ligand conformations must have maximum rigidity;
- Ligands must stay firmly bonded to the metal.

Dang and Kagan (1971) concluded that diphosphines fulfil both of these conditions. Furthermore, it has been reported that the possibility of geometric isomerization can be avoided by choosing diphosphine having two equivalent phosphorous atoms. De Vries and Elsevier (2007) stated that these conditions strongly conditioned the subsequent development of the field, with the greater research effort being subsequently laid on metallic compounds with chiral diphosphines with C_2 symmetry as ligands.

The following years witnessed the development of new diphosphine ligands with chiral carbon backbones, and at a very impressive pace. Among these, two examples were of particular interest.

The first example was the 2,2'-bis(diphenylphosphino)-1,1'-binaphthyl (BINAP) ligand synthesized by Noyori and Takaya in 1980 (Miyashita *et al*. 1980). BINAP is C_2 diphosphine that forms a seven-membered chelate ring through coordination to metals (Figure 2.2). BINAP complexes exhibit high enantioselectivity in various catalytic reactions, and readily catalyze the hydrogenation of prochiral α-acylaminoacrylic acids with up to 100% ee (De Vries and Elsevier, 2007).

The second example was the bis(phospholanyl)benzenes (DuPHOS) ligands developed by Burk some years later (Burk, 1991). De Vries and Elsevier (2007) pointed out that these ligands are electron-rich diphosphines and that chirality lies in the carbon atoms adjacent to the phosphorous atoms and therefore, in the derived catalysts, it lies in the immediacy of the rhodium atoms. By choosing the appropriate alkyl substituent, a large variety of substrates, including unsaturated carboxylic acids and itaconic acids, are efficiently hydrogenated by

cationic rhodium complexes of the type [Rh(COD)(bisphospholane)]X (X= weakly coordination anion) with exceedingly high enantioselectivities (Burk, 2000).

Encouraged by the excellent results of the chiral ligands BINAP and DuPhos developed in 1980s and in the early 1990s, many research groups have devoted their efforts toward the design and discovery of new efficient chiral phosphorus ligands (Tang and Zhang, 2003).

2.5.3 Mechanism of rhodium-catalyzed enantioselective hydrogenation

Rhodium-catalyzed enantioselective hydrogenation is one of the most thoroughly studied mechanisms of all metal-catalyzed processes (De Vries and Elsevier, 2007). They pointed out that these studies have focused on cationic rhodium chiral diphosphine complexes as catalyst precursors, and on prochiral enamides as hydrogenation substrates. Notably, the case of achiral hydrogenation of alkenes by Wilkinson's catalyst served as a basis for early mechanistic studies. In the catalytic cycle proposed for Wilkinson's catalyst, dihydride rhodium complexes were obtained by reversible oxidative addition of dihydrogen to the active species $[RhCl(PP_3)_2]$ (Halpern, 1981). Thus, the formation of similar intermediates was expected to occur upon hydrogenation of the catalyst precursors employed in asymmetric hydrogenation. Moreover, further investigations showed that the formation of $[Rh(PP^*)S_2]^+$ (PP* = chiral diphosphine; S = solvent molecule) complexes by hydrogenation of the catalyst precursors is a general behaviour of chelating diphosphine rhodium complexes (De Vries and Elsevier, 2007). It has been concluded that, under catalytic conditions, a molecule of the prochiral alkene coordinates to the rhodium metal, affording a bischelate catalyst-substrate complex (Scheme 2.1). Depending on the alkene enantioface that coordinates with the metal, two diastereomeric catalyst-substrate complexes can be formed.

From the above observations it was concluded that for diphosphine chelate complexes, the hydrogenation stage takes place after alkene coordination with the metal, and thus the

unsaturated pathway depicted in Scheme 2.1 was proposed. As shown in Scheme 2.1, addition of dihydrogen to the catalyst-substrate complex followed by transfer of a single hydride results in the formation of monohydride-alkyl complex. Reductive elimination of the product regenerates the active catalysts and restarts the cycle.

De Vries and Elsevier (2007) reported that the spectroscopic detection and characterization of dihydride intermediates opened a new insight into the mechanism of enantioselective hydrogenation reactions including hydrogenation of dimethylitaconate with an enantiomerically pure bis(phosphinite)rhodium(I) catalyst.
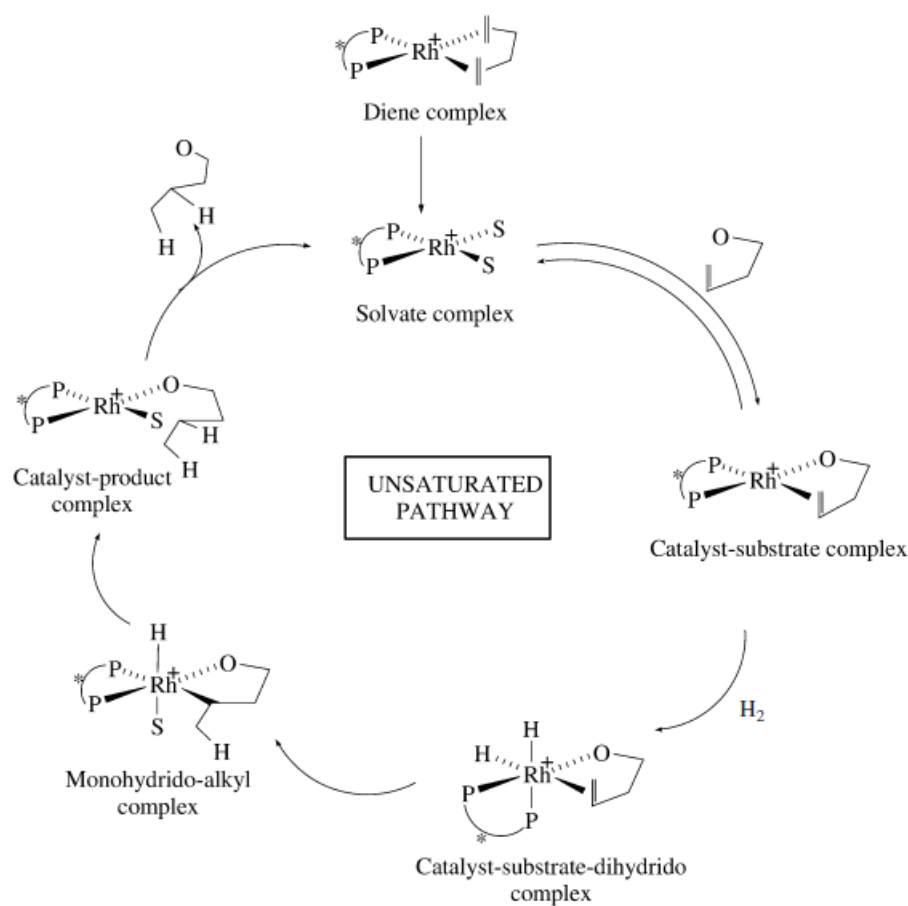
Scheme 2.1. Unsaturated pathway in rhodium-catalyzed enantioselective hydrogenation. From De Vries and Elsevier, 2007.

Based on a study by Gridnev *et al*. (2000), the hydrogenation of the diene complex could also lead to the formation of reversible catalysts-solvate dihydride complex. The authors concluded that in this case the dihydride mechanism depicted in Scheme 2.2 was operating.

The catalyst-substrate complexes dissociate, yielding the solvate complex that is hydrogenated to the solvate-dihydride complex. Reaction of the solvate-dihydride complex with the substrate gives the monohydride-alkyl complex, and the hydrogenation product is obtained after the reductive elimination step.
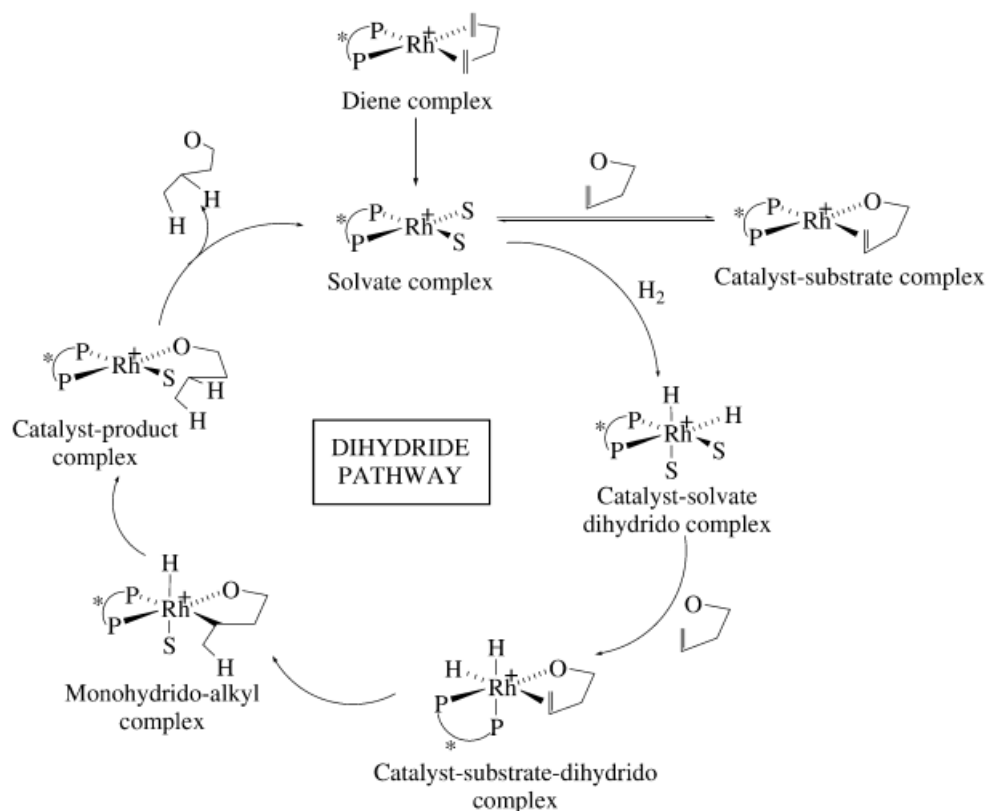
Scheme 2.2. Dihydride pathway in rhodium-catalyzed enantioselective hydrogenation (De Vries and Elsevier, 2007).

It is noteworthy that under catalytic conditions reaction steps prior to the formation of catalyst-substrate dihydrido complexes are shown to be in rapid equilibrium. Thus, stereoselection is believed to occur at a later step in the catalytic cycle. It has been suggested that it is the migratory insertion step that is responsible for enantio-determining and turnover-limiting of enantioselective hydrogenation. De Vries and Elsevier (2007) pointed out that following Gridnev *et al.* (2000) contribution; the boundaries between unsaturated pathway and dihydride pathway are considered blurred. They suggested that in some cases, both mechanisms could be operating, joining in a single pathway before stereoselection occurs.

Due to their excellent and versatile catalytic performance, [Rh (NBD)$_2$]BF$_4$ and [Rh (COD)$_2$]BF$_4$ precatalysts were selected in this work. According to a study by Börner and Heller (2001), precatalysts rhodium complexes bearing NBD counter ligand to the chiral diphosphine demonstrated much higher reaction rates compared to the usually sold and applied COD complexes. Consequently, in this work, initial optimisations were carried out using [Rh (NBD)$_2$]BF$_4$ precatalyst modified with the commercial and privileged bidentate ligands BINAP, (S,S)-DIOP.

2.6 Immobilization of metal complexes on solid supports

Immobilization of transition-metal-complexes on supports generates heterogeneous catalysts that are generally more complicated than the homogenous catalysts. Thus, it is not surprising that, in practice, the mechanism of immobilized catalysts is still very often unpredictable. Generally, most immobilized homogeneous catalysts experience reduced activity or lose part of it upon recycling. However, in some cases, the activities of the heterogenized systems are superior to their homogenous counterparts.

Thomas *et al*. (1999) stated that an improved performance of a heterogeneous catalyst as compared with the homogeneous one, can sometimes be explained by the '*confinement concept*' (Figure 2.3), in which the substrate interacts favourably with both the pore wall and the chiral directing group. When compared to the situation in solution, this confinement of the substrate in small pores leads to a larger influence of the chiral directing group on the orientation of the substrate relative to the reactive catalytic centre (De Vos *et al*. 2000). However, De Vos *et al*. (2000) pointed out that the confinement is a two-edged sword: in other cases, a tight caging of the immobilized catalyst molecules can cause lower enantioselectivities and activities. The lower activities can be due to reduced or even blocked mass transport in the small pores, imposing limits to the effective range of substrates that can

be utilized. On the other hand, the reduced enantioselectivity can result from too strong physisorption of the complex on the wall of the support, or a restricted environment that prevents the chiral transition-metal-complexes to take the spacial configuration that is required to induce chiral recognition (De Vos *et al*. 2000).
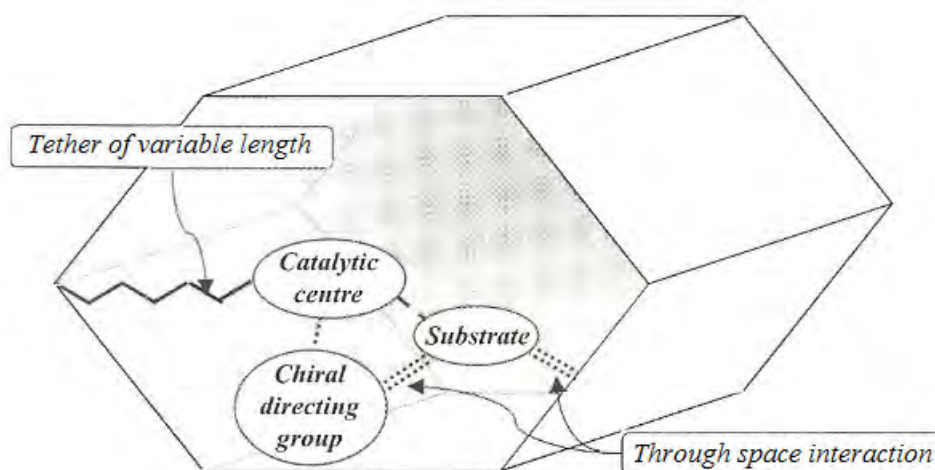
Figure 2.3. Schematic representation of the confinement concept (De Vos *et al*. 2000).

Quignard and Choplin (2003) reported that there are three main methods for the synthesis of supported metal complex catalysts:

1) The complex catalyst or a precursor is directly reacted with the solid support.

2) The complex is copolymerized with monomeric precursors of the solid.

3) The complex is immobilized in a liquid phase (i.e., in solution) on a solid: the interaction between the solvent and the solid is the driving force of heterogenization.

In the first two methods, the complex (i.e. the homogenous catalyst) and the solid are either reacted together directly or are modified to be able to react with each other. In the third method, modification of the complex is essential in order to acquire a high solubility in the liquid solvent, which acts as the immobilizing agent. The choice of a suitable method and a solid support depends mainly on the catalyst used as well as the target reaction. Figure 2.4

summarizes the main approaches to immobilize or heterogenize soluble catalysts which have been described in the literature.
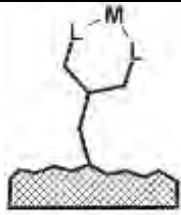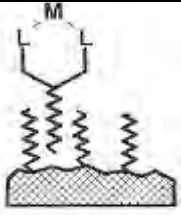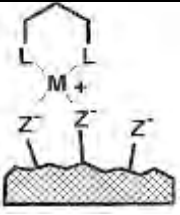
Immobilization method	Covalent binding	Adsorption	Ion pair formation	Entrapment or 'ship in a bottle'
Applicability	Broad	Restricted	Restricted	Restricted
Problems	Preparation	Competition with solvents and substrates	Competition with ionic substrates and salts	Size of substrate and diffusion

Figure 2.4. Schematic view and important properties of immobilized complexes, L: Ligand ; M: Metal complex, De Vos *et al*. (2000).

2.6.1 Heterogenization via covalently bound ligands

Covalent binding is the most frequently used strategy which is accomplished by grafting functionalized ligands or metal complexes with reactive groups of a preformed support. Many parameters such as type of support, solvent, spacer length and flexibility, degree of surface coverage have to be optimized to obtain acceptable catalytic performance.

De Vos *et al*. (2000) stated that the highest activities (expressed as turnover frequencies (TOF's)), productivities (given as turnover numbers (TON's)) and very good *ee's* have so far been obtained in hydrogenations with chiral Rh-diphosphines which are immobilized on solid inorganic supports or on soluble polymers.

2.6.2 Heterogenization via adsorption and ion-pair formation

Various adsorptive interactions between a carrier and a metal complex are involved in this approach. Binding cationic Rh-diphosphine complexes to anionic resins resulted in hydrogenation catalysts which could be recycled 20 times with almost constant activity and

selectivity and with little leaching. Augustine *et al*. (2003) developed an innovative method by using heteropoly acids as anchoring agents to attach various metal complexes to different supports. Immobilized Rh-catalysts exhibited approximately equal and even better activities and enantioselectivities when compared to their homogeneous counterparts. By applying this technique, turnover frequencies (TOFs) of up to 7000 h^{-1} and enantioselectivities of 97% have been achieved for the hydrogenation of dimethyl itaconate (DMI) together with good recyclability.

2.6.3 Heterogenization via entrapment

In this approach, a very important factor is the size of the metal complex rather than a specific adsorptive interaction. There are two different preparation strategies. The first strategy which is often called 'ship in a bottle' is based on building up catalysts in well-defined cages of porous supports. The other approach is to build up an inorganic sol gel or organic polymeric network around a preformed catalyst. The size and the solubility of the metal complex and the swelling of the polymer influence leaching of the metal complex.

In both cases, the heterogenized complexes have shown a greater stability than the same complexes in solution (Quignard and Choplin, 2003). The degree of confinement of the metal complex inside the pores of the zeolite controls metal leaching.

In conclusion, the problems encountered with trapped complexes are driving researchers to find new porous solids capable of accommodating the metal complexes of interest and consequently leading to good diffusion of the reactants and the products. Due to limitations in mass transport through the pores of entrapped catalysts, more often other methods of heterogenization are preferred, such as covalent bonding of catalyst to the support. Moreover, De Vos *et al*. (2000) reported that covalently bound catalysts display possibly the broadest

scope due to the link stability towards most solvents or additives such as salts or acids and bases.

2.6.4 Supported catalysts design and characterisation

Many authors indicate that preformed, solid, insoluble supports for single-site heterogenization of homogeneous catalysts should fulfil certain requirements (Barbaro, 2006) which may be listed as:

- Readily available in a number of varieties.

- Be inexpensive.

- Need the minimum amount of chemical manipulation before use.

- Compatible with the solvent employed.

- Thermally and mechanically stable.

- Chemically resistant.

- Easily filterable or decantable.

- Be of reliable quality.

- Easily custom tailored.

- Have a defined amount of single anchoring sites.

On the other hand, heterogenized catalysts for enantioselective hydrogenation reactions should (Barbaro, 2006):

- Not required synthetic modifications before attachment to the support.

- Be easily prepared and handled.

- Operate under smooth reaction conditions.

- Show turnover frequencies (TOF) and enantiomeric excesses (*ee*) comparable to those of the parent homogeneous catalyst.

- Be quantitatively and easily recoverable.

- Be recyclable (as many times as possible).

- Feature negligible catalyst leaching.

Based on these criteria, various organic and inorganic supports demonstrated high potential for the heterogenization of rhodium metal complexes used for enantioselective hydrogenation reactions. Steiner *et al*. (2004) stated that both types of supports have their strengths and their weaknesses. Advantages of organic polymers are their large variety and high loading capacities of functional groups. Disadvantages are the often high price and their restricted solvent compatibility, since they usually have to be used in a solvent in which they swell. In contrast, inorganic supports are relatively cheap, can be used in most organic solvents, but on the other hand loading capacities are lower than for organic polymers.

Accordingly, the following sections discuss the literature of these two classes of supports as candidates for immobilizing homogeneous Rh-diphosphine complexes. The review approaches their applications for the enantioselective hydrogenation of alkenes with particular emphasis on DMI as a substrate. DMI reacts with hydrogen to form two isomers as products namely, dimethyl (*S*)-(-)-methylsuccinate and dimethyl (*R*)-(+)-methylsuccinate (Scheme 2.3). The incentive for studying DMI hydrogenation is the importance of succinnic acid derivatives as valuable intermediates for several pharmaceutical preparations including potent renin inhibitors (Inoguchi *et al*. 1989).
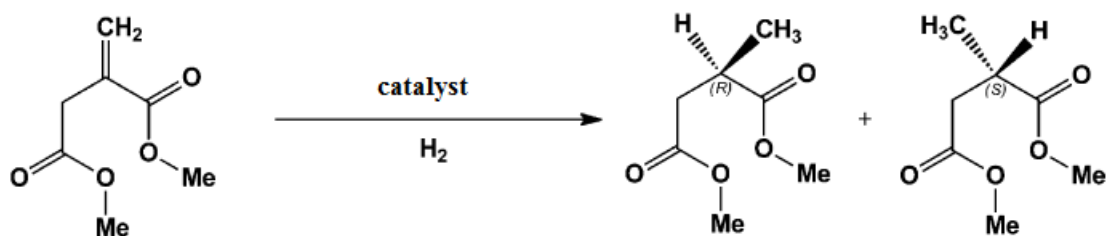
Scheme 2.3. Enantioselective hydrogenation of DMI.

2.6.5 Catalyst immobilization on inorganic supports

Inorganic supports are generally inert porous structures with highly specific surface area. These solids are chosen for their high thermal and mechanical stability, their chemical surface properties (acid-base, redox, hydrophilicity). Amorphous oxides, in particular silica and, to a lesser extent, alumina, zirconia or ZnO, are the most used supports. A wide range of these materials with different pore size, pore size distribution and particle size are commonly available. Clay minerals such as pillared clays, which contain stable metal oxide clusters that separate the layers that build the clay, are another type of commonly applied supports.

Other popular supports include zeolites, these crystalline materials, mostly aluminosilicates; have well-defined pores and channels in the micropore range (Figure 2.5). According to IUPAC definition, porous materials are divided into three classes; microporous (pore size < 2nm), mesoporous (2-50nm), and macroporous (> 50nm) materials. Taguchi and Schüth (2005) stated that among the family of microporous materials, the best known members are zeolites which have a narrow and uniform micropore size distribution due to their crystallographically defined pore system. However, when large reactant molecules are involved, zeolites present severe limitations due to the fact that mass transfer limitations are very severe for microporous solids. The first mesoporous material was synthesized in 1969. However, the remarkable features of this product were not recognized at that time due to a lack of analysis. Taguchi and Schüth (2005) reported that in 1992, a similar material was obtained by scientist in Mobil Oil Corporation who opened up a whole field of research by discovering the remarkable features of this novel type of silica. MCM-41, which stands for Mobil Composition of Matter No. 41, has a very narrow pore size distribution and is of highly ordered hexagonal array of unidimensional pores of diameters varying between 1.5 nm and 100 nm.
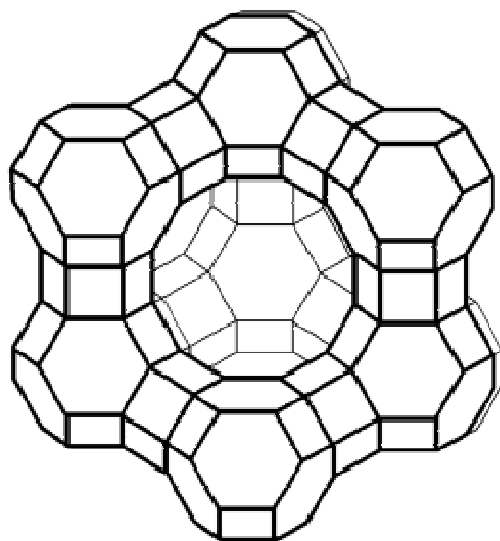
Figure 2.5. Schematic representation of a zeolite Y cage.

Wagner *et al*. (2001) prepared heterogeneous chiral catalysts for the enantioselective hydrogenation of dimethyl itaconate (DMI) from chiral rhodium diphosphine (S,S-Me-Duphos) complexes and Al-MCM-41. They claimed that impregnation of the mesoporous carrier Al-MCM-41with the organometallic complexes in dichloromethane leads to active hydrogenation catalysts which are not prone to leaching (Figure 2.6). In order to get a first impression of whether the chosen carrier system would be a suitable host for the homogeneous catalysts, a computer simulation of the structures of several Rh diphosphine complexes was carried out whereby the Rh complexes were placed in a simulated tube of Al-MCM-41. The graphical illustration of CODRhDuphos fixed in Al-MCM-41 showed that the complex fits easily in a tube of 2.2 nm.

When used in the reaction, the immobilized catalysts showed high activity and excellent enantioselectivity. Up to 92% ee and 100% conversion were obtained. In their study, several diphosphine ligands (Figure 2.7) have been tested and the results are shown in Table 2.1. As can be seen in Table 2.1, the *S*,*S*-Me-Duphos ligand achieved the best results with 92% *ee* at 100% conversion to dimethyl (*R*)-methylsuccinate. In this single batch reaction the

substrate/rhodium ratio was 4000, resulting in a turnover number of 4000 for the immobilized Me-Duphos rhodium complex. Moreover, this catalyst could be recycled at least four times without any loss in activity giving a total TON of >16,000.
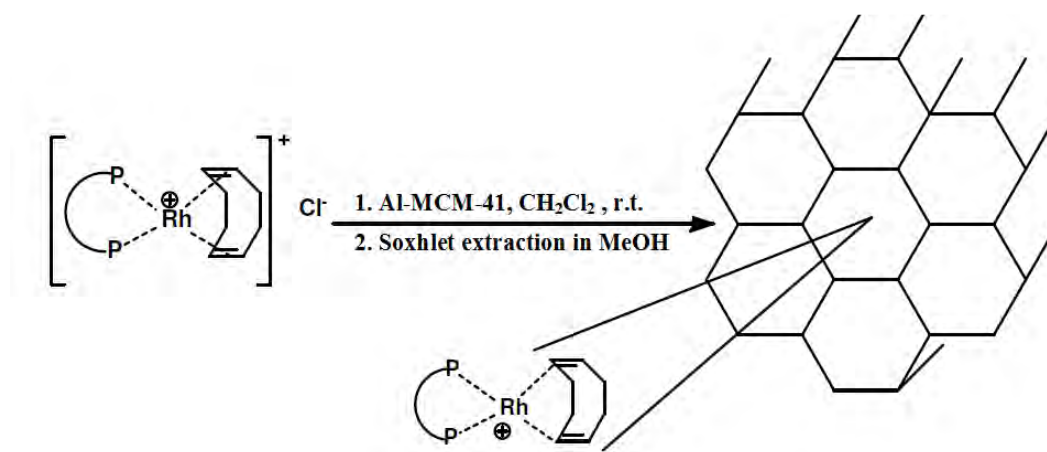
Figure 2.6. Impregnation of Al-MCM-41 with rhodium diphosphine complex, Wagner *et al*. (2001).
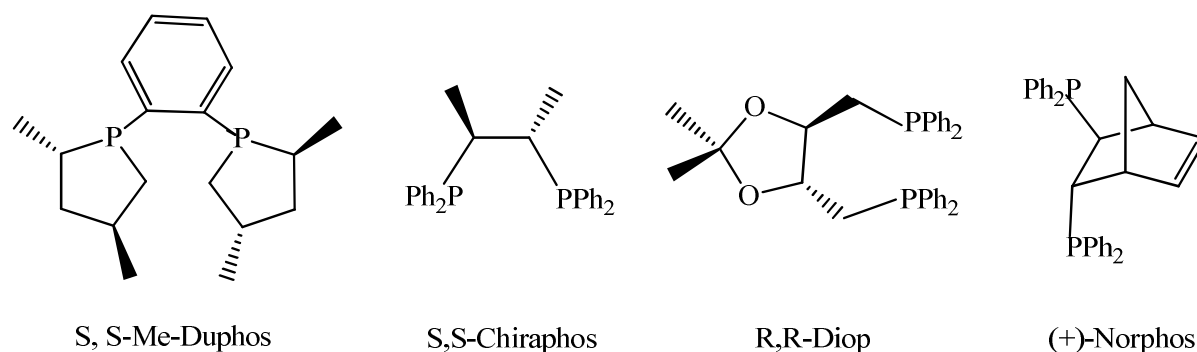
Figure 2.7. Diphosphine ligands in the rhodium complexes, Wagner *et al*. (2001).

Ligand	Conversion (%)	TON	*ee (%)*
S,S-Me-Duphos	100	>4000	92 (R)
R,R-DIOP	57	2280	35 (S)
S,S-Chiraphos	8	320	47 (R)
(+)-Norphos	16	640	48 (S)

Table 2.1. The catalytic activity and *ee* of immobilized rhodium diphosphine complexes, Wagner *et al*. (2001).

Hems *et al*. (2005) immobilized Rh diphosphine complexes using R,R-MeDuPhos **1** and JosiPhos **2** as chiral ligands (Figure 2.8) by ion exchange into the mesoporous material MCM-41.

1 DuPHos   2 JosiPhos
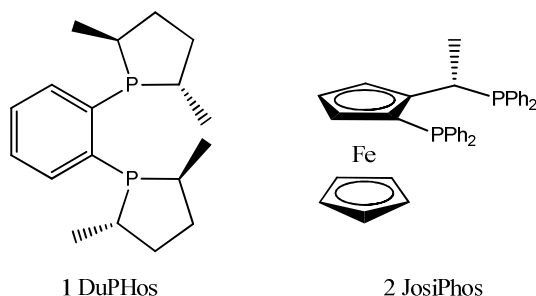
Figure 2.8. Diphosphine ligands in the rhodium complexes, Hems *et al*. (2005).

They introduced a second immobilization strategy in which $[Rh(COD)_2]^+BF_4^-$ is initially immobilized by ion exchange and subsequently modified by the chiral diphosphine. It was claimed that this method gives comparable catalyst performance and that such strategy is suitable for ligand-screening for parallel synthesis and libraries. The catalyst was anchored using electrostatic forces which did not require ligand modification. They argued that this is a common method to immobilize catalysts using covalent linking of the ligand to the inorganic support. They reported that their method of anchoring the catalyst is more specific than using physical adsorption which gives extensive leaching of the active components, leading to poor stability. The immobilised catalysts gave comparable enantioselection (95 – 99 %) and conversion (95 -99 %) even after 8 reuses, using a substrate to catalyst ratio of 250 : 1. Use of higher substrate : Rh molar ratio of 5000 : 1 was also possible, but some activity was lost on reuse, which was claimed to be due to loss of the chiral ligand, but the *ee* was retained and was comparable to the homogeneous catalyst.

The catalyst [Rh(R,S-JosiPhos)(COD)]-Al-MCM-41 was used for the hydrogenation of DMI using a substrate: Rh molar ratio of 500 : 1 at 20 ℃ with a reaction time of 15 min. The catalyst could be reused several times without marked loss of catalyst performance. The

59

catalyst achieved conversions (98 – 99%) and *ee's* (90 – 96) with a comparable performance to the homogenous catalyst.

Crosman and Hoelderich (2005) prepared heterogeneous chiral catalysts from rhodium diphosphine complexes and aluminated SBA-15. They claimed that impregnation of mesoporous Al-SBA-15 with organometallic complexes led to strongly bounded hydrogenation catalysts (Figure 2.9). The recently discovered pure silica phase, designated SBA-15 has long-range order, large monodispersed mesoporous (up to 50 nm), and thicker walls (typically between 3 and 9 nm), which make it more thermally and hydrothermally stable than the M41S-type zeolite materials such as MCM-41. When [(S,S-MeDuPhos)Rh(COD)]-SBA-15 was used in the hydrogenation of DMI , 89% ee at > 99% conversion and TOF of 44 h^{-1} were obtained.
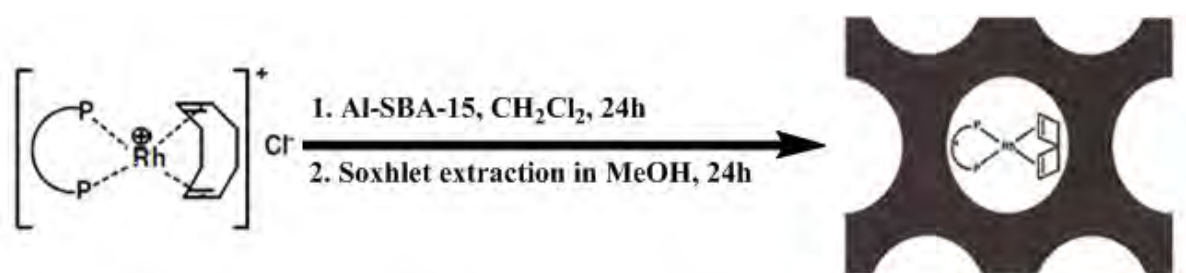
Figure 2.9. Immobilization of rhodium diphosphine complexes on Al-SBA-15, Crosman and Hoelderich (2005).

Augustine *et al*. (2003) developed a new technique of immobilization that involves attaching catalytically active complexes to solid supports via heteropoly acids (HPAs). The active complex is attached to the support through the metal atom and provides what has been termed "anchored homogeneous catalysts". The attachment can be either covalent between the metal atom of the complex and the HPA or an ion pair with a metal cation and the oxygen anion of the HPA as pictured in Figure 2.10. This type of attachment avoids the use of the ligand which may be prone to leaching. By applying this technique, turnover frequencies (TOFs) of

up to 19000 h^{-1} and enantioselectivities of 97% were achieved for the hydrogenation of DMI, together with good recyclability (Augustine *et al*. 2004).
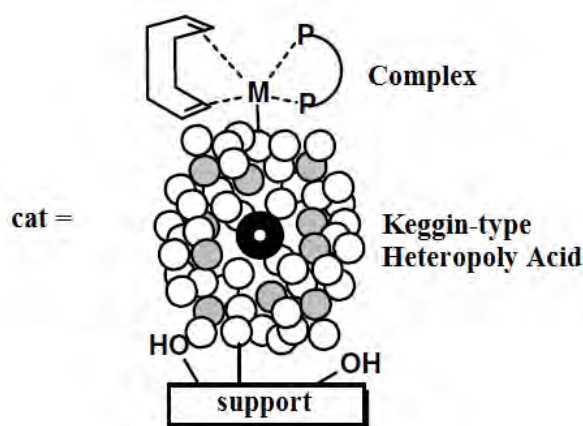
Figure 2.10. Schematic drawing showing the presumed structure of an anchored homogenous catalyst, from Kunna (2008).

Brandts and Berben (2003) immobilized two different precursors, [Rh(COD)$_2$]BF$_4$ and [Rh(COD)Cl]$_2$, on phosphotungstic acid-modified alumina to form γ-Al$_2$O$_3$/PTA/Rh(COD)$_2$BF$_4$ (1b) and γ-Al$_2$O$_3$/PTA/[Rh(COD)Cl]$_2$ (2b), respectively (In their paper, different complexes were assigned different notations for easy reference during the discussion of their results). These immobilized complexes have been modified with (R,R)-MeDuPHOS to form the immobilized chiral catalysts γ-Al$_2$O$_3$/PTA/Rh((R,R)-MeDuPHOS)(COD)BF$_4$ (1c) and γ-Al$_2$O$_3$/PTA/Rh((R,R)-MeDuPHOS)(COD)Cl (2c). They claimed that immobilization and subsequent modification by ligand exchange reactions is useful in case of having to screen various ligands. They also reported that this method tends to give better reproducibility results in terms of activity and leaching stability.

Enantioselective hydrogenation of DMI showed that the activity and selectivity differences between the homogenous catalysts [((R,R)-MeDUPHS)Rh(COD)}BF$_4$ (1a) and the in situ prepared [((R,R)-MeDUPHS)Rh(COD)}Cl (2a) are larger than the differences between the immobilized analogues (1c,2c), as shown in Table 2.2. Table 2.2 also shows that complex 2a was approximately 20 times less active compared to 1a and the enantioselectivity was also

lower (92% vs 96%). Moreover, slow deactivation of 2a was observed during the reaction. It was pointed out that these differences can be ascribed to the influence of the anion and that the (R,R)-MeDuPHOS based rhodium catalysts work best with noncoordinating anions such as OTf^-, BF_4^{-} or PF_6^-.

catalyst	solvent	H_2 pressure (bar)	T (^oC)	TOF $(h^{-1})^c$	ee (%)^d
1a	MeOH	3.3	20	30000	96
2a	MeOH	3.3	20	1200	92
1c	2-propanol	6.6	50	17000	96
2c	2-propanol	6.6	50	13000	97

Table 2.2. hydrogenation of DMI using different catalysts. Standard reaction conditions: 2-4 µmol Rh catalyst, 3.54 mmol dimethyl itaconate, 20 mL of solvent, 1000 rpm. ^{c} Approximate turnover frequencies calculated at 20% conversion. ^{d} *ee's* determined at 98% conversion. Brandts And Berben (2003).

2.6.6 Use of organic supports for catalyst recovery

One of the aims of heterogenizing a homogeneous catalyst is to facilitate the recycling and reuse of the expensive catalyst complex, rather than losing it in the product, as occurs with homogeneous reactions. De Vos *et al*. (2000) reported the following materials as common organic supports used to immobilize or heterogenize soluble catalysts:

- Linear, non-cross-linked polymers and, more recently, also better defined dendrimers (Köllner *et al*. 1998) are soluble in suitable solvents and give catalyst with high mobility and good mass transport properties. However, separation is not trivial (precipitation or ultrafiltration has to be used). Dendrimers are repeatedly branched, roughly spherical large molecules. Köllner *et al*. (1998), claim that the preparation and characterization of dendrimers containing transition-metal-complex fragments has received considerable attention in recent years. However, the application of chiral

organometallic dendrimers in asymmetric catalysis is a field still very much in its infancy (Seebach *et al*. 1996).

- <u>Swellable, slightly cross-linked polymers</u> such as polystyrene cross-linked with 0.5-3% 1,4-divinylbenzene, can easily be separated by filtration or sedimentation. These polymers must be used in solvents in which they swell to allow good mass transport.

- <u>Highly cross-linked polymers</u> hardly swell and use of different solvents does not change texture or mass transport properties.

Barbaro (2006) stated that swelling of the resin in the adopted solvent is crucial for both catalyst anchoring and efficiency. Slightly cross-linked, gel-type resins are preferred over macroporous ones, owing to enhanced mass transport inside the polymer beads, hence giving a good active-site accessibility, as a consequence of swelling of the resin into methanol, which is commonly used as solvent. Swelling volumes have been carefully investigated using 0.5–4% cross-linked polymers and was found to increase up to 800% upon decreasing the cross-linking percentage (Selke *et al*. 1989). Because of the high solvation of lithium, swelling is also highest for Li^+-derivatised resins. Mechanical instability and difficulty of preparation prevented the use of very low cross-linked resins (Barbaro, 2006). Barbaro (2006) also pointed out that the lower the cross-linking percentage, the higher the moisture content, the equilibrium rate, the capacity (usually expressed as millimole of catalyst equivalent to gram of support), the fragility and the ability to accommodate larger ions.

De Vos *et al*. (2000) reported that several issues must be addressed when organic polymers are used as a catalyst recovery vehicle. It should be decided whether the polymer should be insoluble throughout the reaction or should be soluble at some point in the reaction scheme. The decision depends upon the desired separation method of catalyst and ligands from reaction products. In case of solid/liquid separation, which is the most commonly deployed

method, both soluble and insoluble polymer-bound catalysts have been used. For the less commonly used liquid/liquid separation case, a soluble polymeric catalyst must be used.

De Vos *et al*. (2000) reported that use of organic polymers as vehicles for enantioselective catalyst recovery originated from the success of the commercial development of ion-exchange resins. They stated that necessary feature of both the older work and the more recent work with enantioselective polymer-bound hydrogenation catalysts is the need to prepare ligands that have attachment points for coupling to a polymer.

Rhodium complexes immobilized onto strong cation-exchange resins have been tested as catalysts for the asymmetric hydrogenation of various prochiral olefins. Examples were provided by a recent review article by Barbaro (2006) and summarized in Table 2.3. As shown in Table 2.3, appropriate selection of the support allow better resin swelling in methanol, which results in enhanced rates as a consequence of the kinetic reaction control through substrate diffusion to the active sites inside the polymer beads, thus leading to high conversion and *ee* under very mild reaction condition.

complex	substrate	resin	t [min]	Yield [%]	*ee* [%]
$[Rh(Ph\text{-}\beta\text{-glup})(cod)]^+$	MAC	G-4-H$^+$	500[b]		94.1
		G-2-H$^+$	135[b]		94.9
		G-1-H$^+$	60[b]		95.5
		G-0.5-H$^+$	38[b]		95.3
	MAA	Wofatit KP2	15[b]		94.3
$[Rh(propraphos)(cod)]^+$	MAC	G-0.5-Li$^+$	10[b]		84.6
$[Rh(norphos)(cod)]^{+\,[c,d]}$	ACA	DOWEX HCR-S	2460	100	67
		DOWEX MSC-1	1200	100	87
$[Rh\{bdpp(p\text{NMe}_2)_4\}(nbd)]^+$	PAC	Nafion-NR-50	15	100	50
$[Rh(diop)(nbd)]^+$	MAA	DOWEX 50WX2	150	99.9	54.6
$[Rh(tmbtp)(nbd)]^+$	MAA	DOWEX 50WX2	120	99.9	99.9

Table 2.3. Examples of asymmetric hydrogenation reactions with catalysts immobilized onto ion-exchange resins. In methanol, room temperature, H_2 pressure 1-5 bar. Substrate/catalyst ratio was 100:1 in all cases, except for ACA for which it was 90:1. [b] Half-life time t/2. [c] 50 °C. [d] H_2 pressure 20 bar. Barbaro 2006.

In his review article, Barbaro (2006) pointed out that, in principle, ion-exchange resins meet all requirements defined for the catalysts supports. Nowadays, they are widely available from numerous commercial suppliers and reasonably priced. They consist mainly of styrene–divinylbenzene cross-linked copolymers bearing a charged ion-exchanging group. Barbaro (2006) reported that such immobilization leads to an optically active complex that is anchored to the support though ion-pair formation.

Barbaro (2006) reported the following as remarkable advantages of such immobilization strategy:

- The catalysts are easily prepared.

- The immobilized catalysts combine the high activity and selectivity of the homogeneous catalysts with a facile product separation, minimization of waste production and use of environmentally friendly experimental conditions.

- The catalysts' active sites are easily characterized.

- Catalyst loadings can be chosen and optimized.

- Problems arising from metal-loading processes are minimized.

- A systematic design of new catalysts is enabled.

Barbaro (2006) also reported that anchoring of Rh complexes onto ion-exchange resins is an equilibrium process that is usually attained after only few hours in methanol by using batch operations (i.e., stirring a solution of the complex in the presence of the support at room temperature, followed by filtration, washing and drying).

Barnard *et al*. (2005) presented a new method of anchoring homogeneous catalysts onto different types of carbon (Figure 2.11). They claim that their method of anchoring is superior to the commonly used approach in which the catalyst is grafted to the support via a tether. They argue that such methods present a synthetic challenge when tethering the ligand and that enantioselectivity can be reduced/lost at reaction conditions. It was also claimed that

heterogenization methods based on non-covalently bonded catalysts are not robust, and the catalyst can be removed by an exchange reaction occurring under the catalytic reaction conditions. Their method is distinguished by the ease of preparation, as no modification of support is required, and its suitability for scaling up. By comparison with literature, they speculated that the Rh(diphosphine) complexes in their case are attached to the support via a covalent Rh-O bond. The immobilized Rh-diphosphine complexes exhibited higher enantioselectivities that their homogeneous counterparts. It was reported that the change in stereoselectivity emphasizes the role played by supports in these systems during the chiral selection process. Activity was in each case remarkable, being little different from the homogeneous reaction. The catalysts retained activity going from 500 TON to 1000 TON. The reuse test of [Rh(nbd)(Skewphos)]/carbon showed the catalyst conserves its enantioselectivity and activity. It was suggested that this result is an indication of the stability toward reuse of the catalyst under these conditions. It was also reported that this contrasted with most Rh-(diphosphine)-like catalysts, which upon exposure to air demonstrate reduced activity due to fairly inactive species.
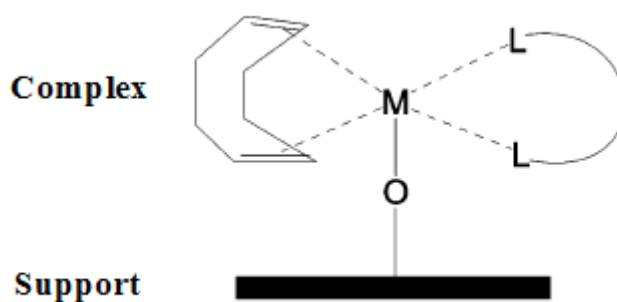
Figure 2.11. Proposed structure of the homogeneous catalyst anchored onto carbon support, Barnard *et al*. (2005).

2.7 Continuous enantioselective hydrogenation

Very few examples of use of continuous processes for production of products using enantioselective catalysts appear in the literature. Künzle *et al.* (2003) demonstrated the feasibility of continuous enantioselective hydrogenation over cinchona-modified Pt/alumina for some reactants, including ethyl pyruvate, ketopantolactone and 1-phenyl-1,2-propanedione. However, these reactions required a continuous feed of minute amounts of cinchona modifier to maintain enantioselectivity which is a significant drawback. In addition, continuous operation was found to require higher cinchona alkaloid/reactant ratios to achieve good enantioselectivity compared with the batch reactor (Künzle *et al.* 2002). Besides, the catalyst used was in the form of very small particles leading to high pressure drop which is not ideal for fixed bed operation.

In an attempt to tackle high pressure drop across the catalyst bed, Toukoniitty *et al.* (2001) studied the enantioselective hydrogenation of 1-phenyl-1,2-propanedione in a fixed bed reactor using knitted silica fiber support material impregnated with platinum. In their work, the modifier was continuously fed to the reactor; the initial enantioselectivity of 23% was extremely low but it increased to a steady state value of 57%.

2.8 Hydrogenation of non-saturated hydrocarbons

Hydrogenation reactions are becoming increasingly important in academic and industrial research (Molnár *et al*. 2001; Liprandi *et al*. 2006). Moreover, Molnár *et al*. 2001 stated that the topic of selective hydrogenations has been extensively studied and covered since the 1960s. In particular, selective hydrogenation of non-saturated hydrocarbons gives various products that are used as the starting point for producing high added value substances related to commercial chemistry, for example, the fine chemicals and pharmaceutical industries (Ulan *et al*. 1987; Chen *et al*. 2005). Mekasuwandumrong *et al*. (2009) reported that catalytic hydrogenation is one of the most useful, versatile, and environmentally acceptable reaction routes for organic synthesis. This is because many functional groups can be hydrogenated with high selectivity and high conversion.

2.9 Selective hydrogenation of alkynes

The selective hydrogenation of double bonds has been extensively studied in the literature. However, more challenging, from an academic and industrial point of view, is the selective hydrogenation of alkynes (Mekasuwandumrong *et al*. 2009). The selective hydrogenation of alkynes is an industrially significant reaction; Bennett *et al*. (2009) pointed out that this reaction has a particular relevance in the petrochemical industry, where alkene streams of high purity are required for the synthesis of polymers. Furthermore, Acetylenic hydrocarbons, which are very unstable compounds in petroleum cuts, could be converted to more stable olefinic compounds by selective hydrogenation at mild conditions. Alkenes produced via semi-hydrogenation reactions of alkynes are also used as raw materials in industries such as pharmaceutical and agrochemicals (Lederhos *et al*. 2010). They are also used for the synthesis and manufacture of industrial chemicals, such as food additives, flavours and

fragrances (Liprandi *et al*. 2009) as well as the synthesis of natural products, such as biologically active compounds (Lederhos *et al*. 2005).

Several authors pointed out that the majority of research in the area has focused on low molecular weight substrates in the gas phase, with molecules above C4 (i.e. butyne, butadiene) receiving little attention (Jackson and Shaw, 1996; Lennon *et al*. 2000; Hamilton *et al*. 2002; Bennett *et al*. 2009). In particular, the mechanisms and kinetics of ethyne semihydrogenation have been the most extensively studied (Bond *et al*. 1958; Bond and wells 1965; Bond and wells 1966; Hamilton *et al*. 2002; Quiroga *et al*. 2005; Lederhos *et al*. 2006; Quiroga *et al*. 2007). More recently, it has been of interest to find out whether the same effects occur in the hydrogenation of higher hydrocarbons (Jackson *et al*. 2001). However, it has been difficult to predict behaviour patterns based on the existing knowledge.

Doyle *et al*. (2003) stated that hydrogenation of unsaturated hydrocarbons occurs efficiently on noble-metal catalysts, such as platinum, rhodium and palladium. The reaction mechanism first proposed by Horiuti and Polanyi (1934) proceeds by a) hydrogen dissociation on the metal surface, b) alkene adsorption, c) subsequent hydrogen addition to alkene and, finally d) desorption of the product (alkane). The semi hydrogenation of an alkyne to the corresponding alkene is possible since the alkyne is more strongly adsorbed at the catalyst surface than the alkene and thus competes more efficiently for the catalytic sites. As a result of this, the re-adsorption of the alkene, once formed, is limited or displaced by the alkyne; hence its further over hydrogenation is decreased (Lederhos *et al*. 2005; Lederhos *et al*. 2006). The strong chemisorption of the alkyne species on the active centre was believed to be due to the restricted rotation of the C-C triple bond and to the high electron density in the alkyne species as reported by Liprandi *et al*. (2009). Moreover, to compromise between avoiding overhydrogenation and keeping a high reaction rate, milder conditions of hydrogen pressure

and temperature are normally used (Lederhos *et al*. 2005; Lederhos *et al*. 2006; Quiroga *et al*. 2007; Lederhos *et al*. 2010).

Molnár *et al*. (2001) reported that the variation of the product selectivity or hydrogenation of ethene in the presence of ethyne has frequently been explained in such a way that aging generates different sites on the surface. Kinetic studies by Borodzinski using Pd/Al_2O_3 (Borodzinski and Cybulski, 2000) and commercial catalysts (Borodzinski, 1999) suggest that the deposits formed during ethyne hydrogenation generate two types of active sites. They argue that short-spaced active sites on the palladium surface (A sites) are inaccessible to ethene. It was proposed that hydrogenation of ethene to ethane takes place on large-spaced sites on the palladium surface where competitive adsorption of ethene and ethyne occurs (E sites). A simplified representation of the suggested model is shown in Figure (2.12). It was assumed that ethyne species adsorbed on A sites is a key intermediate in the hydrogenation of ethyne, whereas π-bonded ethene adsorbed on E sites is a key intermediate in the hydrogenation of ethene. Molnár *et al*. (2001) stated that a large steric hindrance of the adsorbed ethene compared to that of adsorbed ethyne is caused by the difference in position of the molecules in the adsorbed state: π-adsorbed ethyne is flat lying, while adsorbed ethene is either perpendicular or tilted with respect to the surface.

Various ways have been reported in the literature for controlling the activity and selectivity of a catalytic reaction, such as varying the active species, the support, adding a promoter or a poison, adding a modifier and a suitable selection of solvent (Molnár *et al*. 2001).
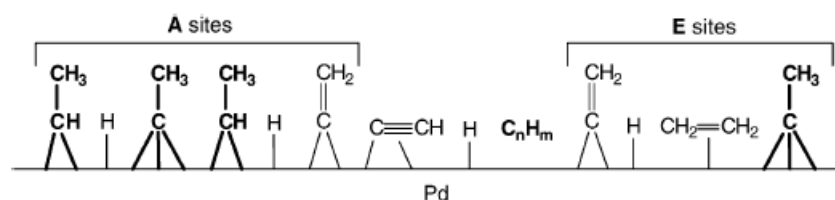
Figure 2.12. The simplified representation of the palladium surface during the hydrogenation of the ethyne-ethene mixture (Molnár *et al*. 2001). Irreversibly adsorbed species creating the carbonaceous overlayer are printed boldface.

2.9.1 Catalysts for selective hydrogenation of alkynes

The typical commercial catalyst used, since 1952, for selective hydrogenation of alkynes is the Lindlar catalyst (Pd/CaCO$_3$ modified with Pb(OAc)$_2$). Nijhuis *et al*. (2003) have found that during the preparation of Lindlar catalyst, palladium becomes more electron deficient thus leading to efficient Pd-alkyne interaction. However, Lederhos *et al*. (2010) reported that the Lindlar catalyst has the disadvantage that it cannot be pelletized and must be operated under slurry conditions; hence, the reactant solution must be purified after reaction by an expensive procedure to recover the catalyst. Moreover, Klasovsky *et al*. (2009) pointed out that irrespective of the advantages of Lindlar catalyst, the content of toxic lead, the need for the addition of an amine promoter could conflict with the tightened environment and safety regulations as well as the ongoing move towards green chemistry.

As reported by several authors, high activity and selectivity may be obtained over other catalyst systems in which modifiers are not necessary such as homogeneous Pd complexes (Kerr and Suckling, 1988), homogeneous Ru complexes (Atencio *et al*. 1995), supported Pd complexes (Sladkova *et al*. 1985; L'Argentière *et al*. 2002; L'Argentière *et al*. 2003), bimetallic Pd-Cu/SiO$_2$ (Nijhuis *et al*. 2003) Pd-Ni/γ-Al$_2$O$_3$(Lederhos *et al. 2010*), Pd/C (Lennon *et al*. 2000), Pd/C and Pd/γ-Al$_2$O$_3$ (Lederhos *et al*. 2005).

Significant work in recent years considered the role of hydrogen located within bulk Pd, as hydride or sub-surface hydrogen, in the over hydrogenation of alkynes (Teschner *et al*. 2006). They studied the hydrogenation of 1-pentyne over various palladium catalysts and showed that significant amounts of subsurface carbon and a Pd-C surface phase built up during the early stages of the reaction. These species limited the diffusion of bulk-dissolved hydrogen to the surface and thus caused changes in the selectivity of the reaction. Thus at lower pressures and lower H$_2$/C$_5$ ratios, hydrogenation was slow but highly selective towards 1-pentene, rather than pentane, which was formed at high pressure and hydrogen excess. Studt

et al. (2008) observed similar effects in the hydrogenation of acetylene, where the modification of the surface with carbon led to weaker adsorption of acetylene and ethylene, thus giving higher selectivity to ethylene. Jackson *et al*. (2001) studied the hydrogenation of C5 alkynes over a palladium catalyst. It was found that the internal triple bond hydrogenated faster than the terminal and a particle size effect was observed on the rate of hydrogenation and isomerisation. Hamilton *et al*. (2002) studied the competitive hydrogenation reactions between alkynes over a palladium/carbon catalyst, including 1-phenyl-1-propyne, 1-phenylacetylene, 1-pentyne and 2-pentyne as substrates. It was found that terminal alkynes reduced the rate of hydrogenation of a competing alkyne more effectively than internal alkynes.

2.9.2 Selective hydrogenation of 1-heptyne

Over the last ten years, various catalysts based on Pd, Rh, Ru and Ni metals have been investigated for the selective hydrogenation of heptyne with a terminal triple bond (Scheme 2.4). These catalysts have been immobilized on several supports including alumina (Lederhos *et al*. 2005, Lederhos *et al*. 2006), carbon (Lederhos *et al*. 2005, Lederhos *et al*. 2006) and silica (Somboonthanakij *et al*. 2007; Mekasuwandumrong *et al*. 2009; Mekasuwandumrong *et al*. 2010). It has been found that the choice of an efficient support can have a considerable effect on activity, selectivity, recycling, and reproducibility of the above metal-catalysts. Moreover, the operational parameters such as temperature and pressure, catalyst pre-treatment with hydrogen, and proper selection of a ligand could significantly improve the performance of the catalytic system.
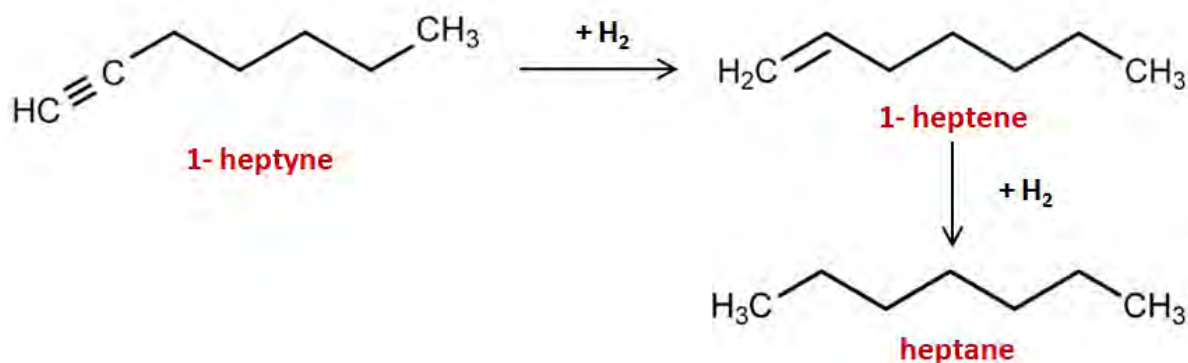
Scheme 2.4. Reaction scheme for 1-heptyne hydrogenation.

Quiroga *et al.* (2007) reported that evaluation of the best catalytic systems for the hydrogenation of 1-heptyne is based on two factors: (a) maximum conversion values to 1-heptene versus 1-heptyne total conversion and (b) maximum selectivity values to 1-heptene, and the range of 1-heptyne total conversion in which they are self-maintained. Bennett *et al.* (2009) stated that palladium is known to be one of the most selective catalysts for the hydrogenation of highly unsaturated hydrocarbons in terms of selectivity towards alkyne versus alkene hydrogenation. In particular, Pd-based/Al_2O_3 and Pd-based/C catalysts are known to be proven catalysts for the selective hydrogenation of 1-heptyne. Lederhos *et al.* (2005) investigated 1-heptyne hydrogenation using Pd supported on γ-Al_2O_3 and on carbon GF-45 and found that γ-Al_2O_3 was more active in terms of 1-heptyne total conversion, whereas the selectivity towards 1-heptene was slightly higher at high conversion values for Pd/C. They concluded that these differences can be attributed to the differences in the support porosities. Hydrogenation of 1-heptyne has also been carried out over catalysts prepared by flame-spray pyrolysis (Somboonthanakij *et al.* 2007; Mekasuwandumrong *et al.* 2010). High selectivities towards 1-heptene (> 90%) at complete conversion of 1-heptyne were observed (Mekasuwandumrong *et al.* 2010). Pd-based/Al_2O_3 catalysts are also known to exhibit high selectivities during hydrogenation of other terminal alkynes such as 1-butyne (Alves *et al.* 2011) and 1-pentyne (Jackson and Monaghan, 2007).

73

2.9.3 Influence of solvent selection on selective hydrogenation reactions

Toukoniitty *et al*. (2003) reported that the effects observed from the use of different solvents appear as variations in activity, selectivity and stereoselectivity. These variations can result from various factors, such as solubilities of liquid and gaseous reactants and their adsorption on the catalyst surface, competitive adsorption of solvent molecules, interaction of solvent with the reactant(s) either in the liquid phase or on the catalyst surface as well as catalyst deactivation caused by the solvent (Khodadadi-Moghaddam *et al*. 2009). Also, a possible role of solvents donating a proton, i.e. being involved in the reaction may influence the catalytic behaviour (Rajadhyaksha and Karwa, 1986).

Kobayashi *et al*. (2000) pointed out that organic transformations in aqueous media, particularly in water, have gained increasing attention, as water is easily available, economical, and friendly to the environment. They found that water can accelerate the rate of palladium-catalyzed allylic alkylation in a colloidal dispersion system created by a neutral surfactant, Triton X-100, in water. In this type of system, reactions proceeded rapidly without using high temperature, and the desired products were obtained in high yields. However, it was claimed that the usefulness of such system is limited by the solubility of the organic substrate in water. Tike and Mahajani (2007) studied the kinetics of hydrogenation of palm stearin fatty acid over Ru/Al_2O_3 catalyst in the presence of a small quantity of water. In their study, the rate of reaction could be improved by adding 2 % (w/w) water to the n-dodecane solvent. The reaction kinetics were investigated and fitted using a Langmuir-Hinshelwood expression. Yang *et al*. (2008) studied the aerobic oxidation of benzyl alcohol over Au/TiO_2 catalyst. The conversion of benzyl alcohol at a molar ratio of water to solvent (p-xylene) of 7 was 7 times higher than in the absence of water. It was found that water has dual promotional functions in the reaction system: to help form unique microdroplets in a multiphase reaction system and to assist the oxygen adsorption and activation. It was envisaged that hydrogen

species could be released from the dissociation of water to react with oxygen adsorbed on the catalyst, yielding very reactive OOH species that further decompose to form activated O* and OH groups. The O* species participate in the formation of benzaldehyde, and thus help to improve the catalytic activity of Au/TiO_2.

Hu *et al*. (2007) studied the selective hydrogenation of 2-butyne-1,4-diol in a stirred reactor as a function of solvent composition (isopropanol/water), while observing bubble sizes in the reactor using a microscope-video-imaging system. The maximum reaction rate was obtained with the smallest bubbles at an isopropanol concentration of 5 % (v/v). This was explained by the larger interfacial area available for gas-liquid mass transfer for the smallest bubble size. When the concentration of isopropanol was increased from 5 % up to 100 %, a complicated relationship between reaction rate and bubble size was observed, the rate first decreasing and then increasing as the pure isopropanol was approached. This was attributed to a combination of larger bubbles of lower interfacial areas and higher solubility of hydrogen in the pure alcohol.

The influence of the addition of an acid or a base in a reaction appears to be more complex, as this could modify the reaction pathway and greatly alter the physical effects involved in the system such as the adsorption characteristics of reactant(s) and/or products. Arterburn *et al*. (2000) demonstrated that catalytic transfer hydrogenation using palladium (II) chloride ($PdCl_2$), in aqueous sodium hydroxide containing formic acid was effective for the reduction of unsaturated carboxylic acids, azalactones, and α-ketocarboxylic acids. The procedure facilitated the transfer of hydrogen in the reaction without the use of compressed hydrogen gas. It was concluded that the implemented reaction conditions should be suitable for the reduction of a wide variety of organic substrates, and offers an economical, safe, and environmentally benign alternatives to available procedures. Huck *et al*. (2003) reported that the use of acidic or basic solvents influenced the enantioselectivity during the hydrogenation

of 2-pyrones. These solvents were found to diminish the enantioselectivity by disturbing the O-H-O interaction between the OH group of the alkaloid and the carbonyl O atom of the reactant.

Bennett *et al*. (2009) investigated the influence of solvent selection for the hydrogenation of 2-pentyne over 1 wt. % Pd/Al$_2$O$_3$ in a 2.65 L baffled stirred vessel. Solvent selection was found to have a very strong effect upon reaction rate and selectivity and in heptane the reaction rate was faster than isopropanol. In a 50/50 mixture of heptane and isopropanol the rate of alkyne hydrogenation was intermediate to that observed in the solvents individually while selectivities were up to 5 times greater.

2.9.4 Kinetics of alkyne hydrogenation reactions

A revision on the catalytic hydrogenation of alkynes was published by Molnár *et al*. (2001). They noted that kinetic studies are scarce and that they were performed under narrow ranges of experimental conditions.

Alkyne hydrogenation reactions typically follow Langmuir-Hinshelwood-type kinetic expressions of the type (Rode *et al*. 2006; Wood *et al*. 2009):

$$R_1 = -\frac{dC_{alkyne}}{dt} = \frac{mk_1 C_{H_2} C_{alkyne}}{(1 + K_{alkyne} C_{alkyne} + K_{alkene} C_{alkene})^2} \tag{2.2}$$

For the alkene hydrogenation, the rate is give by

$$R_2 = \frac{mk_2 C_{H_2} C_{alkene}}{(1 + K_{alkyne} C_{alkyne} + K_{alkene} C_{alkene})^2} \tag{2.3}$$

Thus, the rate of consumption of alkene is determined by the difference of the aforementioned rates:

$$\frac{dC_{alkene}}{dt} = R_1 - R_2 \qquad\qquad (2.4)$$

The rate of production of alkane is found from the rate of consumption of alkene:

$$\frac{dC_{alkane}}{dt} = R_2 \qquad\qquad (2.5)$$

Using these kinetic expressions, Wood *et al*. (2009) obtained a good fit of their experimental values for the hydrogenation of 2-butyne-1,4-diol using novel bio-palladium catalysts in a 500-mL high-pressure stainless steel reactor. In their work, the predicted adsorption coefficient of the alkyne (2-butyne-1,4-diol) was higher than that of the alkene (2-butene-1,4-diol) for the two implemented solvents, namely, 100% 2-propanol and 5% 2-propanol in water. The alkene adsorption coefficient was predicted to be higher in the mixed solvent and zero in pure 2-propanol. They stated that although one must be cautious of overinterpreting a mathematically fitted value, the predicted adsorption coefficient of 2-butene-1,4-diol suggests that adsorption of the alkene does not occur in the pure alcohol.

Winterbottom *et al*. (2003) studied the liquid phase hydrogenation of 2-butyne-1,4-diol to cis-2-butene-1,4,-diol in a monolith cocurrent downflow contactor reactor. A model based on Langmuir–Hinshelwood kinetic allowed quite reasonable prediction of reactant and product concentration profiles.

Natividad *et al*. (2004) studied Pd-catalysed hydrogenation of 2-butyne-1,4-diol in a monolith cocurrent downflow contactor reactor and in a single channel capillary reactor. A model based upon a Langmuir-Hinshelwood mechanism was applied and found to predict reasonably well reaction rates and product distribution.

Alves *et al*. (2011) also proposed a kinetic expression of the Langmuir–Hinshelwood–Hougen–Watson type to describe the hydrogenation of 1-butyne, 1-butene hydrogenation rate. The kinetic model predicted their experimental data with an average deviation of 17.1%.

2.9.5 Continuous hydrogenation of alkynes

According to Rode *et al*. (2006), continuous hydrogenation of alkynes in a fixed-bed reactor could control the selectivities to alkenes and alkanes by varying the hydrodynamics, which is an attractive option to obtain the desired products distribution depending on the fluctuation in the market demand. They studied continuous and batch catalytic hydrogenation of 2-butyne-1,4-diol (B_3D) over 1% $Pt/CaCO_3$ catalyst to give 2-butene-1,4-diol (B_2D) and butane-1,4-diol (B_1D). In case of continuous hydrogenation, higher selectivity (66%) to B_2D could be obtained and the selectivity pattern was completely different from that found in case of batch slurry operation in which B_1D selectivity was very much higher (83%) than the B_2D selectivity (17%). In the continuous operation, the ratio of butene-and butane diols could be manipulated by tailoring the operation conditions for the same catalyst. The liquid flow rate showed a significant effect on the conversion of B_3D and overall rate of hydrogenation. The conversion of B_3D decreased almost proportionately (from 70% to 12%) with increase in liquid flow rate from 10 to 60 mL/h. It was reported that as the liquid flow rate was increased, the residence time of B_3D in the reactor was reduced and less time was available for the intimate contact of H_2 with liquid B_3D and with catalyst pellets; thus, proper diffusion was not possible. They also reported that, at lower liquid velocity, catalyst particles were partially wetted; under these conditions the rate would increase due to direct transfer of the gas-phase reactant to the catalyst surface.

2.10. Hydrogenation of vegetable oil

2.10.1 Introduction

Partial hydrogenation of vegetable oil is a very important process in the chemical industry. Lee *et al.* (2007) reported that the first target from such a process was to produce different base oils for lubricants that are generally produced from petroleum oil. However, lubricants extracted from crude oil are not easily biodegradable thus causing environmental problems. Besides, the reserves of crude oil are decreasing leading to sharp rises in oil prices. Therefore, there is a need to replace fossil fuels with other energy sources in order to make the production of lubricants economically feasible. Thus, vegetable oils, which are easily biodegradable, attaining high demand and production worldwide, besides easy reutilization of recovered frying oil have become an attractive starting material for lubricants (Lee *et al.* 2007). Partial hydrogenation of vegetable oil is also an important reaction in the food industry, used widely in the manufacture of margarines, shortenings, salad oils and other food products (Bailar 1971). Bailar (1971) pointed out that world production of soyabean oil is much greater than that of any other edible vegetable oil. In the U.S. alone, the annual production of margarines and shortenings reached 8 billion pounds in 2007. Although the annual production of soyabean oil in China achieved 6.21 million tons in 2005, 1.70 million tons of oil is still imported to cover the domestic demand (Lee *et al.* 2007).

2.10.2 Vegetable oil

Vegetable oils are mixtures of triglycerides which are composed of one molecule of glycerol attached to three molecules of fatty acids as shown in Figure 2.13. The three fatty acids, which are also termed as mixed triglycerides, often have different structures. To facilitate G.C. analysis, the triglycerides are usually converted to methyl esters so as to have each alcohol group attached to a single acid chain instead of three. The composition of the oil

depends upon the plant it is produced from and the soil and climatic conditions in which the plant grew (Bailar 1971). A typical composition of vegetable oil contains 10% palmitic acid (C16:0; nomenclature: 16 carbon atoms with zero double bonds), 4% stearic acid (C18:0, m.p. 70°C), 27% oleic acid (C18:1), 50% linoleic acid (C18:2), 7.5% linolenic acid (C18:3, m.p. -11°C).
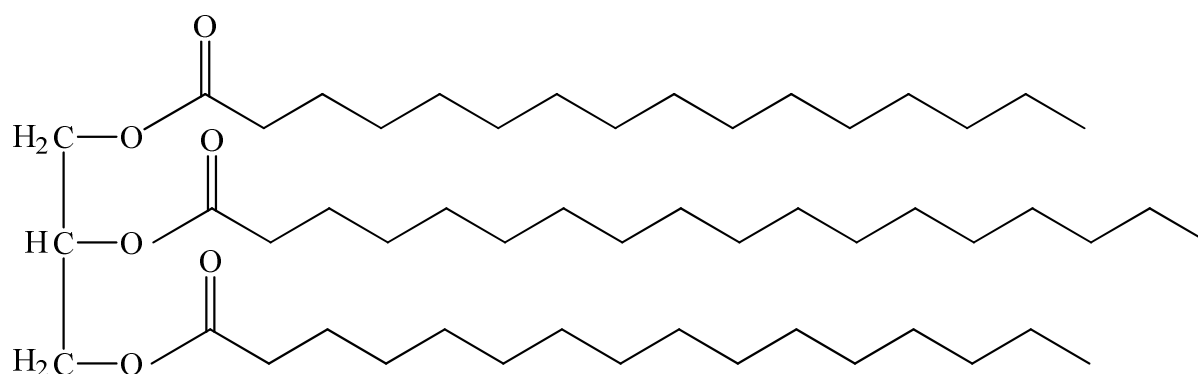
Figure 2.13. Structure of a mixed triglyceride with one stearic and two palmitic acids attached to the glycerol molecule (Dipalmito stearin).

For the vegetable oil to be used as lubricant, its low viscosity needs to be increased. This is accomplished by hydrogenation of the diene linoleic acid and triene linolenic acid, targeting maximum formation of oleic fatty acid and a minimum increase of stearic acid, while maintaining a low cis-trans isomerisation (Lee *et al*. 2007). In general, the bulk physical and chemical properties of vegetable oil such as melting characteristics and oxidative stability are determined by the composition of the major fatty acids. The resistance of different fatty acids to oxidative rancidity is in the following order: C18:1 > C18:2 > C18:3. Table 2.4 demonstrates the relative oxidation rates and melting points of some common fatty acids, which shows that the behavior of oil is significantly influenced by the fatty acid composition. For example, a triglyceride with three oleic acids is ten times more stable to oxidation than a triglyceride with three linoleic acids.

Fatty Acid	Relative oxidation rate	Melting point, ^{o}C
Stearic	1	70
Oleic	10	14
Linoleic	100	-5
Linolenic	150	-11

Table 2.4. Listing of relative oxidation rates and melting points of fatty acids, (Formo 1968; Grau *et al*. 1988).

All of the double bonds in naturally occurring oils are essentially in the *cis* configuration, which is desirable from a practical point of view. In soyabean oil which is to be used in food industry, linolenic acids are considerably objectionable due to their bitter taste, and palmitic and stearic acids are somewhat undesirable since they are difficult to digest if available in excess amounts (Bailar 1971). To upgrade soyabean oil, research has been focused on selective hydrogenation as a tool to convert linolenic and linoleic acids to oleic acid while keeping composition of stearic acid to a minimum. On the other side, hydrogenation of vegetable oil can produce *trans* fatty acids (TFA) which have been associated with adverse health effects (Willett *et al*. 1993).

The molecular structures of some common *cis* and *trans* fatty acids are displayed in Figure 2.14. A *cis* configuration designates that the two adjacent hydrogen atoms on the double bond are on the same side. In the case of *cis* isomer, the double bond bends the chain and constrains the flexibility of the fatty acid. Hence, the more double bonds the chain has with the *cis* configuration, the less conformational freedom it has. For instance, oleic acid, with one double bond, has a "kink" in its structure, while linoleic acid, with two double bonds, has a more evident curve. Linolenic acid, with three double bonds, has a hooked chain. A *trans* configuration, on the other hand, has the next two hydrogen atoms bound to opposite sides of the double bond. Therefore, they do not enhance the chain to bend, maintaining a straight

shape of the fatty acid similar to that of saturated fats. Hence, *trans* fatty acids pack better in the crystal lattice which increases their melting points, that falls between the melting point of *cis* unsaturated and saturated fatty acids (Singh, 2009).
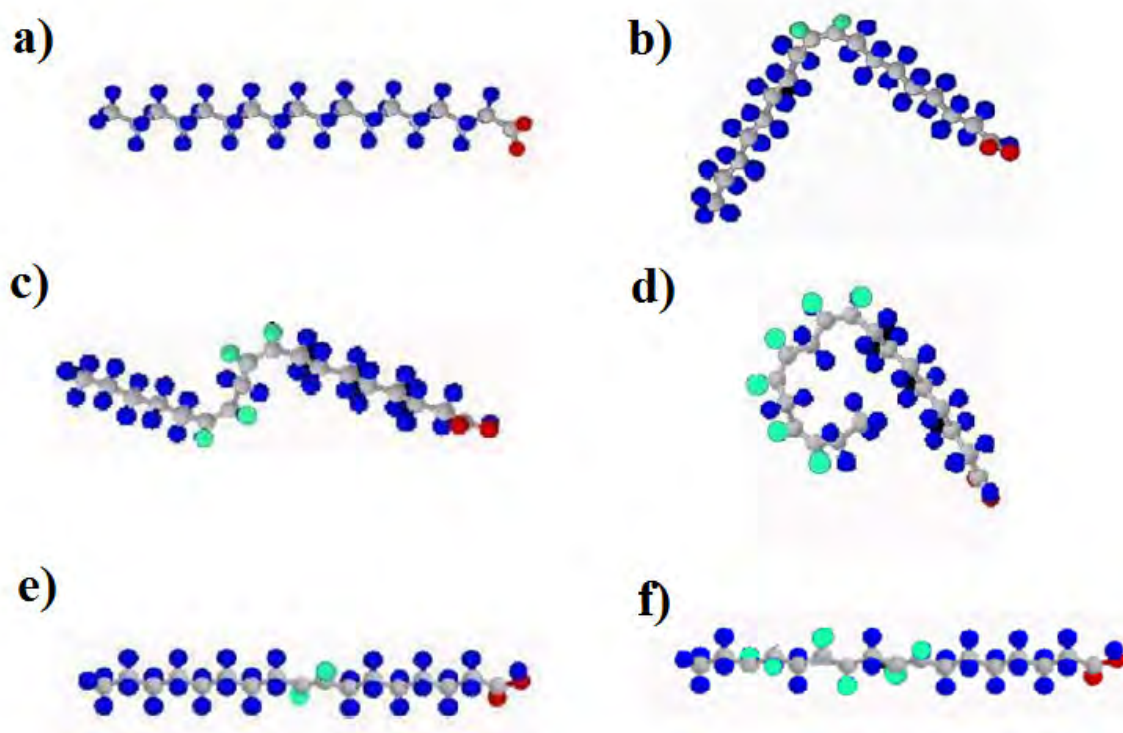
Figure 2.14. Structures of fatty acids commonly present in processed vegetable oil: a) Stearic acid (C18:0), b) Oleic acid (C18:1 9c), c) Linoleic acid (C18:2 9c 11c), d) Linolenic acid (C18:3 9c 11c 13c) e) Elaidic acid (C18:1 9t) f) . All cis unsaturated fatty acids have a kink in their structure while all the trans unsaturated acids have straight structures similar to saturated fats (Singh, 2009).

2.10.3 Health effects of trans fatty acids

The resemblance of *trans* fatty acids (TFA) structure to that of saturated fatty acids has raised health concern that high intake of TFA could develop the risk of coronary heart disease (CHD) (Willett *et al*. 1993). As a result, in 2006, the US Food and Drug Administration (FDA) mandated the declaration of the total *trans* fat content on the Nutrition Fact label of food products. Besides, dietary supplements were requested for products containing 0.5 or more grams of *trans* fatty acid per serving; the minimum corresponding *trans* fat content is estimated to be approximately 2% of total fat (Mossoba *et al*. 2009).

2.10.4 Partial hydrogenation of vegetable oil

The hydrogenation of edible oils, which is a very important operation in the chemical industry, has been carried out since the beginning of the 20th century (Nohair *et al*. 2005; Tike and Mahajani 2006; Fernández *et al*. 2009). Hydrogenation of vegetable oil incorporates the modification of fatty acids compositions to increase the melting point, improve the oxidation properties and obtain a solid fat content most suited for a particular application (Coenen 1976). Therefore, partial hydrogenation of the oil should aim to minimize C18:3 due to its poor oxidative stability, maintain C18:2 due to its importance in human diet or minimize it if the oil to be used as lubricant, maximize C18:1, and finally minimize the formation of saturated C18:0. In the case of food industry, partial hydrogenation has to avoid the formation of TFA due to the recent health concerns. Nohair *et al*. (2005) stated that the selective hydrogenation of vegetable oil must lead to a minimum of 80% toward *cis* oleic acid to correspond to the industrial needs. Consequently, selectivity is very important in the hydrogenation of vegetable oil.

Fernández *et al*. (2009) reported that hydrogenation of vegetable oil involves three simultaneous reactions: saturation of double bonds, and geometric (*cis – trans*) and positional isomerisation. It has been reported that these reactions can presumably be described as first order consecutive reaction, and if *cis - trans* compositions are combined together a simple accepted general model can be represented as shown below (Eq. 2.6) (Veldsink *et al*. 1997; Tike *et al*. 2006; Bernas *et al*. 2009; Fernández *et al*. 2009), where k_1, k_2, k_3 are pseudo-first-order rate constants.

$$\text{Liolenic acid (C18:3)} \xrightarrow{k_1} \text{Linoleic acid (C18:2)} \xrightarrow{k_2} \text{Oleic acid (C18:1)} \xrightarrow{k_3} \text{Stearic acid (C18:0)} \qquad (2.6)$$
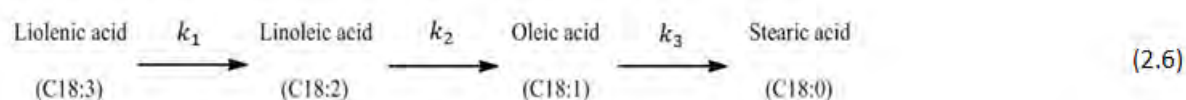
With these simplifications and assumptions, the apparent reaction rates depicted in Eq. 2.6 can be expressed as (Tike and Mahajani, 2006):

$$-\frac{d(C_{linolenic\ acid})}{dt} = k_1(C_{linolenic\ acid}) \tag{2.7}$$

$$-\frac{d(C_{linoleic\ acid})}{dt} = k_1(C_{linolenic\ acid}) - k_2(C_{linoleic\ acid}) \tag{2.8}$$

$$-\frac{d(C_{oleic\ acid})}{dt} = k_2(C_{linoleic\ acid}) - k_3(C_{oleic\ acid}) \tag{2.9}$$

$$-\frac{d(C_{stearic\ acid})}{dt} = k_3(C_{oleic\ acid}) \tag{2.10}$$

Where $(C_{linolenic\ acid}) = (C_{linolenic\ acid})_0$, $(C_{linoleic\ acid}) = (C_{linoleic\ acid})_0$, $(C_{oleic\ acid}) = (C_{oleic\ acid})_0$, and $(C_{stearic\ acid}) = (C_{stearic\ acid})_0$ at t=0.

Based on the above scheme, the selectivities can be defined as:

$$S_{Ln} = \frac{k_1}{k_2} \tag{2.11}$$

$$S_L = \frac{k_2}{k_3} \tag{2.12}$$

Linolenic selectivity (S_{Ln}) is the preferential reduction of trienes over dienes; while (S_L) represents the preferential saturation of dienes over monoenes. High values of these selectivities are desirable since at equivalent conversion this designates lower amounts of linolenic and stearic acid. A specific isomerization index is also used to designate the *cis-trans* isomerization and is defined as:

$$S_i = \frac{trans\ \text{double bond formed}}{\text{double bonds hydrogenated}} \tag{2.13}$$

The hydrogenation process of vegetable oil can be described by the Horiuti-Polanyi mechanism (Horiuti and Polanyi 1934; Dijkstra 2006). The demonstration of this mechanism for the hydrogenation of linoleic acid (C18:2) to oleic acid (C18:1) is outlined in Figure 2.15. After diffusion of hydrogen through the liquid oil, it is adsorbed on the catalyst surface where it dissociates into two hydrogen atoms. The adsorbed hydrogen atom then reacts with the adsorbed fatty acid molecule resulting in an unstable half-hydrogenated intermediate complex. The unstable complex either gains a hydrogen atom and saturates or loses a hydrogen atom and isomerizes. The saturation or isomerization of the unstable complex depends upon the concentration of hydrogen at the catalyst surface. Veldsink *et al.* (1997) pointed out that the low solubility of hydrogen in oils is behind the gas-liquid mass transfer limitations experienced when operating industrial hydrogenation slurry reactors. The hydrogen-starved catalyst-surface in these reactors often encouraged the production of TFAs. Singh (2009) also reported that these reactors are often run under high temperatures which increase the hydrogen consumption rate which in turn aggravates the starvation of the catalyst enhancing the formation of TFAs.
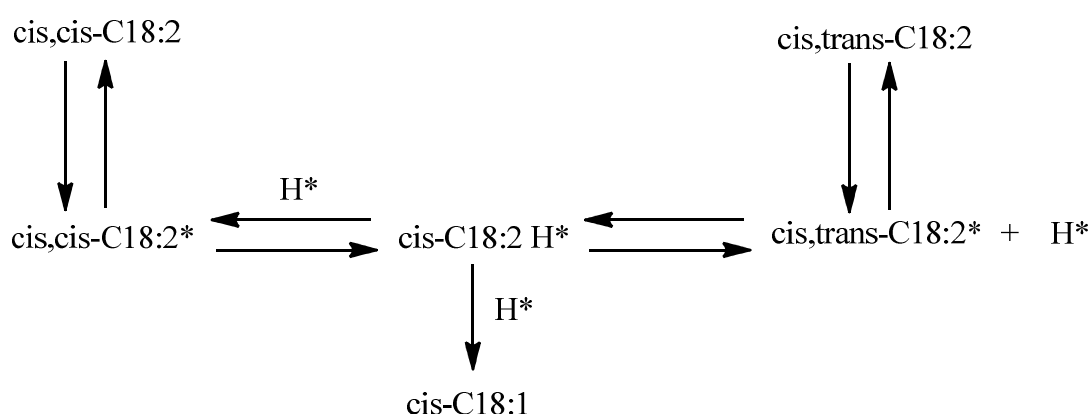
Figure 2.15. Horiuti-Polanyi mechanism for the hydrogenation of linoleic acid (C18:2) to oleic acid (C18:1) (*indicates species adsorbed on the catalyst surface), from Singh (2009).

2.10.5 Minimization of trans fatty acid formation

Based on Horiuti-Polanyi mechanism described above, the formation or dissociation steps of the half-hydrogenated intermediates are the key factors for the formation of TFAs. Low hydrogen concentration favours dissociation and isomerization of these unstable intermediates, while high hydrogen concentrations promote hydrogenation and hence avoid the formation of TFAs. The effect of process conditions on hydrogen concentration and hydrogenation selectivity, for a standard nickel catalyst in a stirred batch reactor, is summarized by Dijkstra (2006) and is demonstrated in Table 2.5. Among these conditions, reducing the temperature could be the only viable option since achieving high pressure and agitation require high cost, and reducing the amount of catalyst will make the process unstable (Dijkstra 2006).

	Effect upon		
Increase of	$[H_2]_{bulk}$	S_L	S_i
Pressure	+	-	-
Agitation	+	-	-
Temperature	-	+	+
Amount of catalyst	-	+	+
Activity of catalyst	-	+	+
Reactivity of oil	-	+	+

Table 2.5. Influence of process conditions on hydrogen concentration and selectivity, (+) and (-) designate the impact on $[H_2]_{bulk}$, S_L and S_i upon increasing reaction parameter, from Dijkstra (2006).

Babaee *et al*. (2007) claim that nickel catalyst is the most common catalyst used for the hydrogenation of fats and oils. Nevertheless, other precious metal catalysts are gaining increasing interest since they are active at much lower temperatures and hence produce less TFA when compared to conventional Ni catalysts (Singh 2009). Singh (2009) reported that

the order of catalytic activity of precious metal catalysts is Pd > Rh > Pt > Ru, while the cis-trans isomerization follows the order Pd > Rh > Ru > Pt.

Pintauro *et al*. (2005) pointed out that the catalytic hydrogenation of edible oils is carried out industrially in a stirred batch reactor operating at 150 - 225 ^{o}C and 10 – 60 psig with supported nickel catalyst. However, operating at such high temperatures favours the formation of the undesired *trans*-fatty acids. Lower levels of *trans* isomers have been achieved with precious metal powder catalysts such as Pd and Pt, but these catalysts are difficult to separate from the hydrogenated oil (Rylander 1970).

Singh (2009) reported some attempts from literature aiming to decrease the amount of TFA formation. These include using a solvent to increase hydrogen solubility in oil under supercritical conditions (King *et al*. 2001; Piqueras *et al*. 2008), using novel reactors such as electrochemical hydrogen cell (Yusem *et al*. 1996; Pintauro *et al*. 2005; Mondal and Lavani (2008) besides other novel reactor configurations.

2.10.6 Continuous hydrogenations in fixed-bed reactors

Heldal *et al*. (1989) pointed out that continuous reactor systems have been reported to offer several advantages over a batch system for the hydrogenation of vegetable oils. Some of these advantages include improved heat economy, equipment and labour utilization, and product uniformity (Albright, 1973; Satterfield, 1975; Coenen, 1976). Hydrogenation of soyabean oil in continuous catalyst/oil slurry systems has shown marginal improvement as compared to that over batch systems in terms of selectivity or specific isomerization (Snyder *et al*. 1982; Koritala et al. 1984). Hastert, however, claimed that hydrogenation of vegetable oils over fixed-bed reactors reduces the formation of *trans* isomers in partially hydrogenated oils. Lush (1930) reported that the reason behind the lower formation of *trans* isomers is the efficiency in supplying hydrogen during continuous hydrogenation process.

Moulton and Kwolek (1982) stated that continuous hydrogenation over a stationary catalyst bed is not new to fats and oil processing. Bolton (1922), Lush (1923), Bolton (1927) and Lush (1930) performed oil hydrogenation by passing the oil over nickel turnings in a tube reactor aimed at producing stearine, where control of selectivity was not a factor. Mukherjee *et al*. (1975) evaluated various stationary catalysts for soyabean oil hydrogenation under non optimized conditions; and Coenen (1976) obtained low selectivity values from fixed-bed hydrogenation.

Moulton and Kwolek (1982) studied continuous hydrogenation of soyabean oil in a trickle-bed reactor with a stationary copper catalyst bed. Hydrogenation was performed at 110-180 ^{o}C, 30-75 psig hydrogen and liquid hourly spaced velocities (LHSV) of 0.25-0.6 cc/hr/cc catalyst. It was claimed that continuous hydrogenation was accomplished at a lower temperature compared to batch operations with no need to postfilter the product. At 100% conversion of triene, both systems showed similar fatty acid composition, *trans* content of 29% and linolenate selectivity of 5. It was concluded that under reduced temperatures, continuous trickle-bed hydrogenation with a copper catalyst is capable of reducing the unsaturates in soyabean oil to the same degree as a batch hydrogenation. It was suggested that amendments in the continuous operation such as a pump with lower rate, a longer catalyst bed, or more selective catalyst would improve the extent of triene hydrogenation.

Heldal *et al*. (1989) studied continuous hydrogenation of soyabean oil in a trickle-bed reactor with Pd and Ni catalysts. Under optimized conditions, both the Pd and Ni catalysts gave significantly lower *trans* isomers when compared to reported values for batch hydrogenation with similar type catalysts. The linolenate and linoleate selectivities were also considerably lower for the continuous operation. At same conditions, heterogenized homogeneous Pd-on-polystyrene catalyst gave lower *trans* isomers and higher selectivity than Pd supported on carbon. It was claimed the low *trans* isomers and low selectivity during hydrogenation in the

trickle-bed reactor resulted from the large interfacial area existed between the oil and hydrogen. It was concluded that, under the proper operating conditions, Pd-on-polystyrene, Pd-on-carbon and extruded Ni catalysts can be used in fixed-bed continuous hydrogenation of soyabean oil without excessive formation of isomeric products.

Winterbottom *et al*. (2000) studied the hydrogenation of soyabean oil in a concurrent downflow contactor (CDC) reactor using slurry and fixed-bed Pd-catalysts. The linolenic selectivity (S_{Ln}) was better for the fixed bed CDC reactor which was attributed to the greater degree of plug flow behaviour in the fixed bed operation. Furthermore, the fixed bed CDC gave lower production of stearic acid than the slurry CDC reactor which could be explained by the RTD measurements. For both types of reactor, the *trans*-fatty acid (TFA) production was in the range 20-28% for an iodine value (IV) change in the range 137 to 103. They stated that for a palladium catalyst such TFA values are relatively low and are indicative of the fact that the reaction was operated under surface reaction rate control. It was concluded that, careful choice of catalyst type with a reactor that can reduce transport resistances to a minimum could increase reaction selectivity significantly. It was also suggested that carefully designed structured packings could further improve selectivity by reducing dispersion, i.e. giving increased plug flow behaviour.

2.11 Multiphase reactors

A multiphase reactor is a system in which gas and liquid phases are contacted with a solid-phase catalyst. In most applications, the reaction occurs between a dissolved gas and a liquid-phase reactant in presence of a solid catalyst (Ramachandran and Chaudhari, 1983). These reactors have a broad range of applications areas and are becoming increasingly important in the chemical industry. Examples of applications include upgrading and conversion of petroleum feed stocks and intermediates, synthesis gas into fuels, hydrocarbons and oxygenates, bulk commodity chemicals and polymers, pharmaceuticals, herbicides and

pesticides, in refining ores, waste water treatment and pollution abatement (Dudukovic *et al*. 1999). Mills and Chaudhari (1997) listed some examples and references of gas-liquid-solid catalytic reactions for the pharmaceutical and fine chemical industry. These include hydrogenation, oxidation, carbonylation and hydroformylation reactions.

Three-phase catalytic reactors used in industry can be classified into two main categories: (a) fixed-bed reactors in which the solid catalyst is stationary, and (b) slurry reactors in which the solid catalyst is suspended and in motion (Ramachandran and Chaudhari, 1983).

In fixed bed reactors, gas and liquid phases move over a stationary bed of catalyst particles. There exist three basic modes of operation in fixed bed reactors: (a) concurrent downflow of both gas and liquid, (b) downflow of liquid and countercurrent upflow of gas, and (c) concurrent upflow of both gas and liquid. The reactor with concurrent downflow of gas and liquid is conventionally referred to as a trickle-bed reactor (TBR), while a reactor with concurrent upflow of gas and liquid is referred to as a packed bubble-bed reactor.

Depending upon the nature of suspension of catalyst particles, it is possible to classify slurry reactors into three basic types: (a) mechanically agitated slurry reactors, in which catalyst particles are kept in suspension by means of mechanical agitation, (b) bubble column slurry reactors, in which the particles are suspended by means of gas-induced agitation, (c) Three-phase fluidized-bed reactors, in which the particles are suspended by means of a combined action of bubble movement and concurrent liquid flow (Ramachandran and Chaudhari, 1983).

2.11.1 Stirred tank reactors (STRs)

Mechanically-agitated slurry reactors have found extensive applications in many chemical processes, and are generally considered to be the most common choice for carrying out multiphase reactions (Fishwick *et al*. 2007). These reactors, which are convenient for use in

batch processes, are simple and consist of a tank containing a stirrer and, usually, fixed baffles to improve mixing. Ramachandran and Chaudhari (1983) reported that these reactors have some specific advantages over other three-phase reactors because a high efficiency for mass and heat transfer is achieved. Moreover, as small particle sizes can be used, the intraparticle diffusional resistance is also minimal, thus leading to maximum utilization of the catalyst. Since these reactors offer higher mass and heat transfer rates, they are also most suitable for kinetic studies in the laboratory. However, these reactors have disadvantages, such as non-uniform suspension of catalyst, difficulties in handling of the slurry from the perspective of feeding, separation, catalyst recovery and recycle (Kulkarni *et al.* 2005). Furthermore, scale up of these reactors is far from straightforward leading to possible problems such transport limitations, which in turn affects productivity, rate and selectivity. Another major drawback of these reactors is the occurrence of possible side reactions due to backmixing of liquid with the reactant. Nevertheless, these reactors are commonly used in small and medium scale batch operations due to their flexibility and moderate cost.

The choice of a reactor for a particular process depends upon the requirements and characteristics of the process as well as some engineering aspects. For hydrogenation of organic compounds, which is a common class of catalytic reactions, gas to liquid mass transfer efficiency and control of temperature play a major role in the selection of reactor type.

2.11.2 Comparison of multiphase catalytic reactors

Pangarkar *et al.* (2008) stated that, among the multiphase reaction systems, the stirred tank slurry reactor, slurry bubble column and the trickle bed reactor are being used most extensively. In their review article, the pros and cons of the various reactor types are summarized and are shown in Table 2.6. As can be seen in Table 2.6, an optimum has still

not been reached with respect to reliable reactor performance. Every type has its pros and cons. While smaller particles can be used in bubble columns and stirred tank reactors, trickle bed reactors are privileged with easy catalyst separation. The major drawback of the stirred tank and slurry bubble column reactors is the need to separate product and catalyst from reaction mixture. Furthermore, when operated in the continuous mode, backmixing lowers the conversion and usually the selectivity. Pangarkar *et al*. (2008) pointed out that a packed bed reactor, such as the trickle bed reactor, is much more convenient if pressure drop is limited by use of large particles (> 1 mm). Trickle bed reactors are considered ideal for slow reactions due to their advantage of high catalyst loading, longer residence time and its narrower distribution. In order to avoid the development of stagnant liquid zones, trickle bed reactors are operated with limited liquid flow rates due to the low porosity of the packed bed. Consequently, due to the limitations imposed on the flow rates, trickle bed reactors should be operated at optimized conditions to avoid incomplete catalyst wetting and poor mass transfer rates.

Kulkarni *et al*. (2005) pointed out that, in the last decade, intensive work has been done to extend the application of monoliths to liquid-gas systems. Monoliths are structures consisting of straight and uniform channels that can serve as a catalyst support in fixed bed reactors (Winterbottom *et al*. 2003). Winterbottom *et al*. (2003) stated that although these catalysts have been shown to possess distinct advantages due to low pressure drop, easy scale-up and improved mass transfer resistance, their use is not widespread.

Kulkarni *et al*. (2005) reported that despite the various advantages of monoliths, the successful engineering of a monolith reactor is still a challenge, in terms of cost, achieving uniform gas-liquid distribution at the inlet and understating reaction behaviour. They carried out a comparative study of the performance of a TBR and a monolith concurrent downflow contactor (CDC) reactor in terms of selectivity and residence time distribution (RTD) for the

selective hydrogenation of 2-butyne-1,4-diol to 2-butene-1,4diol. Pd/Al_2O_3 catalyst was used in both reactors. For the experiments in the monolith CDC, an α-Al_2O_3 wash-coated cordierite monolith was impregnated with Pd at 1% loading. In the TBR, the catalyst was in form of 6 mm spherical alumina support, impregnated with Pd. Under the studied range of gas and liquid velocities, the liquid RTD was almost identical in both reactors. However, selectivity to butene-diol was higher in the monolith compared with the TBR. It was suggested that the difference in selectivities could be due to the thicker film surrounding the catalyst particles in the TBR, thus leading to lower H_2 population on the catalyst surface.

Use of the above catalytic systems at the industrial scale is affected by complexities of scale-up and the shift towards continuous processing. Therefore, a challenge exists to develop supported catalysts which may be used in continuous reactors, such as stirred tanks and trickle beds. The choice of reactor for a particular process is a complex one depending not only on kinetics of reaction but also on practical considerations such as desired throughput, need for temperature and frequency of catalyst regeneration or replacement. Nigam and Larachi (2005) illustrated that fixed bed reactors, such as trickle beds, are of great value for continuous operation and large scale reactions; this is due to the ease of recovering the catalyst and separating the product, thus enabling a clean and selective production route to various organic compounds.

aspects considered		stirred tank slurry reactor	slurry bubble column	trickle bed reactor
reactor catalyst	type	mixed	plug flow/mixed	dispersed plug flow
	separation	difficult	difficult	simple
	replacement	simple	simple	difficult
	manufacture	established	established	established
	loading	low-moderate	low-moderate	high-low pure/egg shell catalysts
mass transfer	utilization	high	high	low-moderate
	internal	good	good	bad-good
	liquid-solid	good particles in suspension small particles	good particles in suspension small particles	fair particles stationary larger particles
	gas-liquid	moderate larger bubble size	moderate larger bubble size	fair sufficient gas-liquid interaction
residence time distribution (RTD)	gas and liquid	backmixing for both gas and liquid	backmixing for liquid and small bubbles	axially dispersed plug flow for both gas and liquid

94

heat transport	to outside	very good	very good	low-moderate
	hydrodynamics	difficult	difficult	medium
scale-up	high pressure	costly	fair	fair

Table 2.6. Qualitative comparison of existing multiphase catalytic reactors, Pangarkar *et al.* (2008)

2.11.3 Trickle bed reactors

Trickle bed reactors (TBRs) are multifunctional reactors and their industrial applications lie in petroleum, petrochemical, wastewater treatment, pharmaceuticals, pesticides, herbicides, biochemical and specialty chemical industries. They are three phase catalytic reactors in which gas and liquid flow in concurrent downward mode over a fixed bed of catalyst. The advantage of co-current flow over the counter current is the flexibility in terms of higher gas and liquid throughput, lower pressure drop and overcomes flooding limitation.

Kulkarni (2006) mentioned that in refining industry, the majority of TBRs run at a pressure of 20-30 MPa and temperature of 350-425 $^{\circ}$C while the typical height of industrial trickle beds is 3-6 m and the diameter is 3 m. A typical industrial set up of TBR is shown in Figure 2.16. Recent trends and research have focused in understanding hydrodynamics and its application of TBR on process intensification (Nigam and Larachi, 2005).
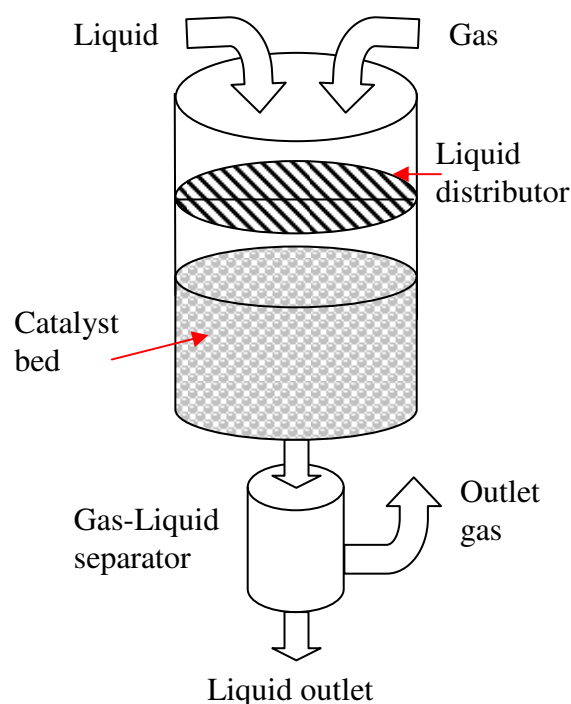
Figure 2.16. A typical industrial set up of TBR, Kulkarni (2006).

A thorough understanding of the various parameters involved can lead to a successful design of any TBR as demonstrated in Figure 2.17. Many of these factors are interlinked, for instance flow rate controls the operating regime, wetting efficiency, holdup, dispersion and mass transport. Catalyst particle size determines the bed structure and packing method influences the bed porosity. Heat transfer is connected to fluid flows, kinetics, and bed characteristics. A proper understanding of all these parameters is crucial for better utilization of catalyst, prolonging catalyst lifetime, increasing throughput in the reactor and improving selectivity. Some of the key parameters are discussed further in detail in the following sections.

GAS   LIQUID

Operating conditions:
- Flow rate
- Concentration
- Temperature
- Pressure

Kinetics:
- Catalyst composition and carrier materials
- Adsorption
- Surface reaction
- Desorption

Holdup:
- Dynamic
- Static
- Internal and external

Wetting efficiency:
- Internal
- External

Dispersion:
- Axial and Radial
- Mass and Heat

Bed Structure:
- Catalyst particle shape
- Catalyst particle size
- Filling method
- Addition of fines

Mass Transfer:
- Gas-Liquid
- Gas-Solid
- Liquid – Solid
- Intraparticle diffusion

Heat Transfer
- Gas
- Liquid
- Catalyst
- Wall of the reactor

CONVERSION, RATE, SPACE-TIME, YIELD, SELECTIVTY

Figure 2.17. Overview of various parameters on performance of trickle bed reactors, (Nigam and Larachi, 2005).

2.11.3.1 Flow patterns

It has been reported that four basic flow regimes may exist in concurrent gas-liquid flows through trickle beds in normal gravity conditions. The type of flow regime inside the reactor, which is determined by the properties of the fluids, the flow rates, the structure and the characteristics of the catalyst bed, can affect heat and mass transfer rates and hydrodynamics at large. Figure 2.18 shows the different flow regimes for different gas and liquid flow rates. Trickle flow is observed at very low gas and liquid flow rates and is characterized by liquid phase flowing in the form of films or rivulets (Munteanu and Larachi, 2009). This regime is also known as a low interaction regime. At low liquid and high gas flow rates the liquid film is broken down by high shear rate at gas-liquid interface resulting in spray flow or mist flow regime. At high liquid and low gas flow rates, the gas is entrained in form of bubbles and the regime is called bubble flow regime. Pulse flow occurs at moderate to high gas and liquid flow rates and characterized by alternating gas-rich and liquid-rich regions. In this region, the interaction between the gas and liquid phases is very high and is known as a high interaction regime. Ramachandran and Chaudhari (1983) stated that knowledge of this is essential in understanding the hydrodynamics and mass transfer characteristics.
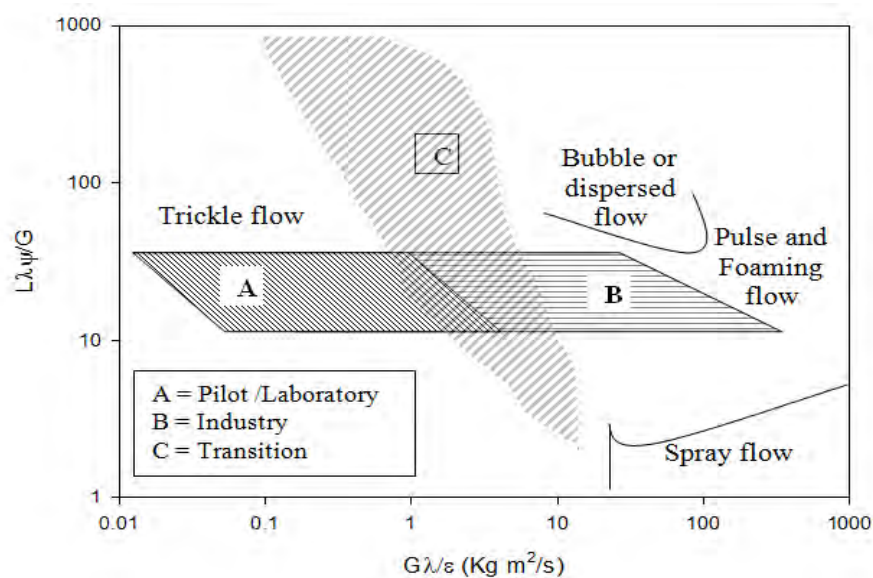
Figure 2.18. Flow regime maps in concurrent gas – liquid flows through trickle beds (Baker, 1954).

2.11.3.2 Mass transfer

The basic reaction and transport steps in TBRs are similar to those in slurry reactors with the main difference being the correlations used to determine the mass transfer coefficients. Mass transfer takes place in several steps as follows, (1) Transport from the bulk gas phase to the gas-liquid interface, (2) Equilibrium at the gas-liquid interface, (3) Transport from the interface to bulk liquid, (4) Transport from the bulk liquid to external catalyst surface, and (5) diffusion and reaction in the pellet. Determination of the rate-limiting step is vital for the design of TBRs. If the gas-liquid or liquid-solid mass transfer rates are lower than the intrinsic reaction rate, the hydrodynamics will have a noticeable influence upon the conversion achieved in the TBR (Fogler, 1999). If different catalyst pellet sizes give different reaction rates then reaction is deemed internal diffusion limited. External diffusion can be said to take place if there are changes in reaction rates with variations in liquid velocity. If the reaction is neither internal diffusion limited nor external mass transfer limited then reaction is in the kinetic regime and observed kinetics can be considered to be true kinetics.

The various parameters required for the evaluation of mass transfer coefficients depend on a number of factors, such as packing type, flow rates, extent of particle wetting and column size. A collection of typical correlations is provided by Winterbottom and King (1999) and is shown in Table 2.7.

Transport step	Correlation	Typical values	Reference
Gas-to-gas interface	$k_g a_i = 2 + 0.91\, E_g^{2/3}$ E_g is in ft $1b_f$ / ft^3 s $E_g = (\dfrac{\Delta P}{\Delta L})_g U_g$ $k_g a_i = 2 + 0.12\, E_g^{2/3}$ $E_g = \text{kW/m}^3$	$k_g a_i = 7.4\ \text{s}^{-1}$ for $U_g = 10$ ft/s $\dfrac{\Delta P}{\Delta L} 10^{-2}$ psi/ft	*IEC Proc. Des. Dev.*, 6, 486 (1967)
Liquid interface to bulk liquid			
Aqueous	$\dfrac{k_l a_i}{D_l} = 8.08\, (\dfrac{G_l}{\mu})^{0.41} Sc^{1/2}$	$k_l a_i \sim 0.01\ \text{s}^{-1}$ for $U_l = 0.2$ cm/s	*Chem. Eng. Sci.*, 34, 1425 (1979)
Organic	$\dfrac{k_l a_i}{D_l} = 16.8 \left(\dfrac{Re_l^{\frac{1}{4}}}{Ga^{0.22}} \right) Sc^{\frac{1}{2}}$ cm^2 $k_l a_i$ in s^{-1}, D_l in cm^2/s, $Re_l = \dfrac{G_l d_p}{\mu_l}$		*Chem. Eng. Sci.*, 36, 569 (1981)
Bulk liquid-to-solid interface			*AlChE J.*, 24, 709 (1978)
For $Re < 60$	$Sh' = 0.815 Re_l^{0.822} Sc^{1/3}$	$k_c a_c \sim 0.2\ \text{s}^{-1}$ for $Re_l = 50$ and $d_p = 0.5$ cm	
For $Re < 20$	$Sh' = 0.266 Re_l^{1.15} Sc^{1/3}$		

$$Ga = \text{Galileo number} = \frac{d_p^3 \rho_l^2 g}{\mu_l^2}, \quad g = 9.8 \text{ m/s}^2,$$

G_l = superficial mass velocity of liquid (g/cm^2 s), U_l = superficial velocity of liquid (cm/ s)

$$Sh' = \frac{k_c d_p \alpha}{D_l}, \quad \alpha = \text{fraction of external surface that is wetted}$$

$$a_s = \frac{6}{d_p} = \frac{\text{interfacial area}}{\text{volume of pellet}} \, , \quad a_c = \frac{6}{p_p d_p} = \frac{\text{interfacial area}}{\text{mass of pellet}}, \quad a_i = \frac{6(1 - \epsilon_b)}{d_p} = \frac{\text{interfacial area}}{\text{volume of reactor}}$$

Table 2.7. Sample mass-transfer correlations for trickle beds, Winterbottom and King (1999).

2.11.3.3 Liquid holdup

Total liquid hold up is defined as the total volume of the liquid phase in the catalyst bed volume at a specific time. Liquid holdup volume influences the mean residence time and hence the conversion achieved. It also relates to pressure drop, catalyst wetting efficiency, heat and mass transfer of gas via liquid to solid (Kulkarni, 2006). Total liquid holdup is composed of static and dynamic fractions. The dynamic liquid holdup is the freely flowing liquid volume relative to the reactor volume, while the static liquid holdup is the fraction of the liquid that is trapped in catalyst pores and stagnant liquid between catalyst particles. Static liquid holdup leads to formation of stagnant zones, which leads to increase in dispersion (Rajashekharam *et al*. 1998).

2.11.3.4 Wetting efficiency

Wetting efficiency in TBR is defined as the fraction of outer surface area wetted by liquid phase. Wetting of the porous catalysts can be classified into two types: (a) Internal wetting, which is the amount of internal active area wetted by the liquid, and (b) External effective wetting, which is the amount of external area wetted by the flowing liquid. If the reaction is external mass transfer limited, the partial wetting of external surface can have a detrimental influence on reaction rate (Ramachandran and Chaudhari, 1983). Mogalicherla *et al*. (2009) stated that it is essential to estimate the partial wetting of catalytic beds in order to predict the performance of trickle-bed reactors.

Partial wetting in trickle bed reactors has been experimentally investigated by five main techniques: the dynamic tracer technique, chemical reaction method, and, more recently the hydrodynamic technique, magnetic resonance imaging (MRI), and dye adsorption technique. However, all of these techniques, except the last two, are overall and indirect and require a model of the reactor involving hydrodynamic, transfer, and/or kinetic parameters. Moreover,

MRI method requires both complex equipment and a delicate treatment, and dye adsorption technique has not been able to predict wetting efficiency with convenient accuracy in a wide range of operating conditions (Julcour-Lebigue *et al.* 2009).

Various correlations have been introduced to calculate the global wetting efficiency in TBR. However, these correlations have been found to give very dispersed results over the same range of operating conditions. More recently, a new correlation for wetting efficiency was proposed by Julcour-Lebigue *et al.* (2009). The correlation, which uses a bounded function and only three dimensionless groups, is able to predict wetting efficiency with a very good precision on a large database.

Based on the literature review provided, it is clear that further research is required to investigate the viability of heterogeneous/heterogenized-homogeneous catalysts in flow reactors such as trickle beds. It is also evident that little work has been made to compare batch and continuous operations under similar conditions. For an immobilized catalyst, a realistic comparison with the corresponding homogenous systems is quite often lacking and, in addition, little information on catalyst activity or productivity is provided. For the described catalyst immobilization techniques, much remains to be done to progress the field of heterogeneous enantioselective catalysis. It comprises the preparation of such widely different materials as polymers, inorganic supports, complex organic molecules and organometallic complexes. This presents a real challenge as many of the heterogeneous systems are very difficult to characterize and are not well understood. For the catalyst user, this means to adapt catalysts and processes to industrial conditions, as many of the new systems, as described in the literature, are often unsuited for industrial application (exotic solvents, reactions conditions, too low productivity and activity, etc.).

CHAPTER 3

EXPERIMENTAL METHODS

This chapter discusses the experimental methods, apparatus and parameters used for the reactions described in this thesis. For enantioselective hydrogenation of DMI, § 3.1 describes the procedure implemented to prepare the supports, modify the complexes and produce the immobilized catalysts. Then their characterization along with the 2 % Pd/Al_2O_3 used to catalyze the selective hydrogenation of 1-heptyne and soyabean oil are described in § 3.2. § 3.3.1 provides an illustration of the experimental set up of the three reactors used to carry out the catalytic reactions, namely, shake-flask, trickle-bed and autoclave reactors. This includes a schematic diagram of the reactors and a general step-by-step description of how the experiments were conducted in these reactors. § 3.3.2 contains a specific description of the reactions conducted along with experimental conditions. The sampling method for the GC is then described in § 3.3.3, followed by an overview of the GC used for product analysis § 3.4.

3.1 Catalyst preparation

3.1.1 Materials

All chemicals and solvents used in the studies are shown in Table 3.1. All solvents (Analytical reagent grade, Fisher Scientific, UK) were degassed by bubbling nitrogen through for several hours before use to ensure absence of oxidation during the experiments.

Material	Supplier	Specification/treatment
DOWEX 50WX2-100 support	Sigma Aldrich, UK	Washed with deionised water to remove impurities
[Rh (NBD)$_2$]BF$_4$	Sigma Aldrich, UK	Purity 98+%, stored under N$_2$
[Rh (COD)$_2$]BF$_4$	Sigma Aldrich, UK	Purity 98+%, stored under N$_2$
BINAP, (S,S)-DIOP, and (R,R)-MeDUPHOS ligands	Sigma Aldrich, UK	Purity 98+%, stored under N$_2$
1-heptyne, 1-heptene and heptane	Sigma Aldrich, Germany	Purity 99+%, stored under N$_2$
Soyabean oil	Sigma Aldrich, UK	Purity 99+%, stored under N$_2$
methyl linolenate, methyl linoleate, methyl oleate, methyl elaidate, methyl stearate and methyl palmitate	Sigma Aldrich, UK	Purity 99+%, stored under N$_2$
Phosphotungstic acid (PTA)	Sigma Aldrich, UK	Purity 99+%, stored under N$_2$
Powder alumina support (neutral γ-alumina), 97%	Strem Chemicals, Inc, UK	Washed with ethanol to remove fine particles.
Trilobe alumina support	Johnson Matthey, UK	Washed with ethanol to remove fine particles.
Dimetyl itaconate (DMI), dimethyl (S)-(-)-methylsuccinate and dimethyl (R)-(+)-methylsuccinate	ACROS ORGANICS, USA	Purity 99+%, stored under N$_2$
[Rh((R,R)-Me-DuPhos)(COD)]BF$_4$	Strem Chemicals, Inc, USA	Purity 98+%, stored under N$_2$

Table 3.1. Chemicals used in the studies.

3.1.2 Manipulation of air-and moisture-sensitive materials

Operations such as material transfer, sampling, weighing and reactions were conducted inside a Zipper-lock AtmosBag under inert atmosphere of N_2. The AtmosBag, supplied by Sigma-Aldrich UK, is a flexible, inflatable polyethylene chamber with built-in gloves that enables a totally isolated and controlled environment. 99.99+ % pure nitrogen has been reported as an acceptable inert atmosphere for many applications and hence was used in this work (www.sigmaaldrich.com). A portable lattice system was set inside the AtmosBag to stabilize the bag during operations as well as support the bag when inflation is not required.

After placing air-and moisture-sensitive materials and equipment inside the bag, the following procedure was used to purge the AtmosBag with inert gas:

a) The end of AtmosBag was sealed opened and the Zipper-lock track was closed.

b) The bag was inflated by pumping N_2 through via a gas flow meter.

c) The end of bag was opened slightly to allow gas to escape. The AtmosBag was deflated by pushing down on bag with hands to force gas out. The end of the bag was then closed. After inflation/deflation cycle was repeated 3 to 5 times, the bag was finally inflated with inert gas to a very soft pillow level that allowed easy insertion of hands. The gas supply was then turned off.

d) The end of bag was folded over two times and clipped.

e) The AtmosBag was observed for several minutes to ensure that the inflation pressure was maintained.

3.1.3 Resin preparation

As previously stated by (Barbaro, 2006) (see § 2.6.6), catalysts loadings are highest for lower cross-linking percentages and for lithiated resins. Therefore, in this project, strong cation-exchange resins, DOWEX 50WX2-100, with 2% cross-linking were selected as an organic support for rhodium complexes. Due to their low cross-linking, their capacity (expressed as millimole of catalyst equivalent to gram of support) is also high (4.8 mequiv g^{-1}).

The preparation procedure of Barbaro *et al*. (2002) was followed to prepare the resin. 5 g of DOWEX 50WX2-100 strong cation-exchange resin in H^+ form was washed with deionised water (100 ml) every hour in air for 6 hours in order to remove any impurities. The resin was then washed with methanol (3 × 100 ml), dichloromethane (2 × 100 ml), methanol (2 × 100 ml), diethyl ether (3 × 100 ml) respectively and was dried in a stream of nitrogen. It was then rinsed with a 1 M solution of lithium hydroxide (120 ml deionised water) and was left on the agitator over night to swell the resin before performing ion-exchange. This process is illustrated in scheme 3.1.
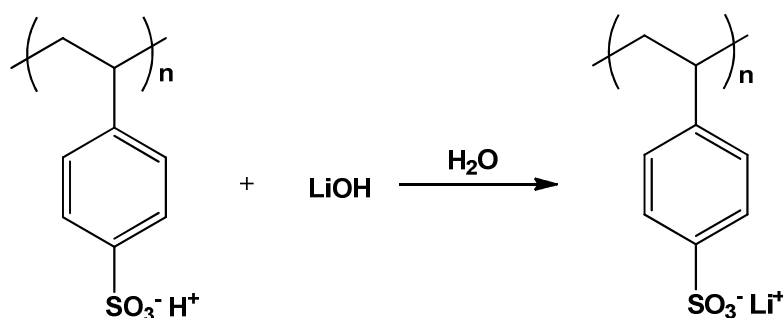
Scheme 3.1. Lithiation of the resin to improve its swelling.

Due to their sensitivity to air, all catalysts preparations in § 3.1.4 and § 3.1.5 were made under an inert atmosphere of nitrogen in the AtmosBag, and this inert atmosphere was maintained until the start of the reaction when the inert gas was replaced by H_2.

3.1.4 Preparation of the catalyst/ligand and immobilisation on the lithiated resin

For efficient utilization of the resin capacity, 4.8 meq g $^{-1}$ catalyst was prepared and mixed with 4.8 meq g $^{-1}$ ligand and both were dissolved in 5 ml tetrahydrofuran (THF). The mixture was stirred via stirring bar for 3 hours and was dried in a stream of nitrogen.

To perform the immobilisation, 7.5 ml of methanol was added together with 1 g of resin overnight. The beads were then washed with methanol (3 × 50 ml), diethyl ether (3 × 50 ml) respectively and were dried in a stream of nitrogen. This process is illustrated in scheme 3.2. The influence of ligand/metal molar ratio was studied by varying the amount of ligand while keeping the amount of [Rh (NBD)$_2$]BF$_4$ precatalyst the same. Subsequent experiments were conducted with the proven [Rh ((R,R)-Me-DuPhos)(COD)]BF$_4$ catalyst immobilized on 1 g of resins. The optimum catalyst/support ratio was investigated by varying the amount of catalyst over same amount of support.
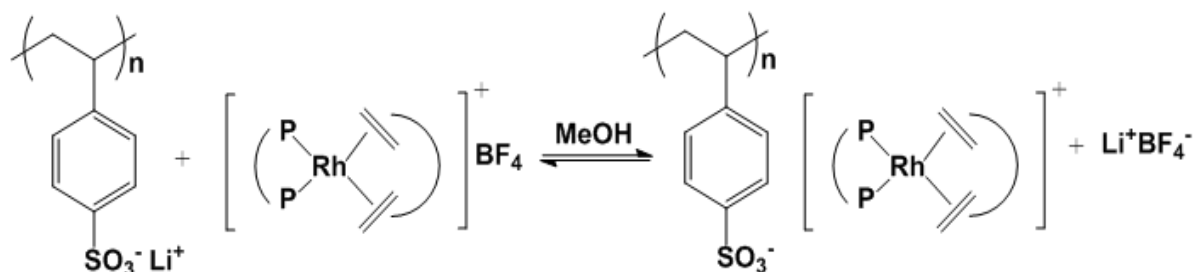
Scheme 3.2. Immobilization of the modified Rh-metal catalyst on the lithiated resin.

3.1.5 Preparation of Rh [(R,R)-Me-DuPhos]/phosphotungstic acid/Al$_2$O$_3$

The preparation procedure of Augustine *et al.* (2003) was followed to prepare the catalyst complex. 9 g of alumina was placed in a glass flask and washed 4 times with 50 ml portions of EtOH. 75 ml of EtOH (95%) was added to the flask. 1.95 g of phosphotungstic acid (PTA) was dissolved in 25 ml of 95% EtOH and the solution was added drop-wise to the well agitated alumina solution. The mixture was then shaken for a further 4 h. After the reaction

liquor was removed, the Al_2O_3/PTA was washed 3 times with 50 ml portions of EtOH and re-suspended in another 75 ml of EtOH. A solution of 0.012 M of [Rh ((R,R)-Me-DuPhos)(COD)]BF_4 in 50 ml of EtOH was prepared and added drop-wise to the Al_2O_3/PTA and then shaken overnight. The liquor was then removed and the resulting Rh((R,R)-Me-DuPhos)/PTA/Al_2O_3 was washed with 50 ml portions of EtOH until the wash liquid became colourless.

3.2 Catalyst characterization

Data on BET surface area, pore size and pore volume of the powder and trilobe supports as well as the 2 wt. % Pd/Al_2O_3 catalyst are given in Table 3.2. BET surface areas and pore volumes were determined from nitrogen adsorption and desorption isotherm data obtained at 77.3 K on a constant-volume adsorption apparatus (Micromeritics, ASAP-2010). The pore volumes were determined at a relative pressure (P/P_0) of 0.99. Notably, the BET surface area of the powder is almost double that of the trilobe support, with the average pore size within the trilobes being slightly over twice that of the powder support.

Support/catalyst	BET area ($m^2 g^{-1}$)	Average pore size (nm)	Pore volume ($cm^3 g^{-1}$)
Powder alumina	258	9.4	0.6
Trilobe alumina	149	19.3	0.72
2 wt. % Pd/Al_2O_3	149	21.8	0.81

Table 3.2. Characteristics of powder and trilobe alumina supports, 2 wt. % Pd/Al_2O_3 catalyst.

The characteristics of the ion-exchange resin support (DOWEX 50WX2-100) are shown in Table 3.3. The typical appearance of immobilized catalyst is shown in Figure 3.1, in which the colour of the resin is due to the presence of the attached rhodium complex.

% cross-linking	2
Matrix	Gel (microporous)
Mesh/Bead size (μm)	100
Ionic form	H
% Moisture	78
Maximum operating temp. ^{o}C	150
Total exchange capacity (meq/g)	4.8

Table 3.3. properties of the ion-exchange resin support (DOWEX 50WX2-100) supplied by Sigma Aldrich.

Figure 3.1. Conventional optical microscope images of DOWEX 50WX2-100 resin beads (200 magnifications). From left: commercial resin, lithiated resin and resin with supported [Rh(diop)(nbd)]$^{+}$ complex. From Barbaro (2006).

3.3 Catalytic test

3.3.1 Experimental equipment

3.3.1.1 Shake-flask reactor

The experiments were carried out in a 100 ml Erlenmeyer flask. After transferring the catalyst, solvent and substrate into the reactor, it was sealed with rubber septa. The reactor

was then fixed onto the shaking plate of the agitator using adhesive tape. The hydrogen (H_2) flow was set at the desired rate using a flow meter and was then fed into the mixture through a needle attached to a rubber tube. A continuous flow of H_2 was applied to the reactor by venting the gas through another needle inserted into the rubber septa. The experimental setup of the reactions conducted in the shake flask is demonstrated in Figure 3.2.
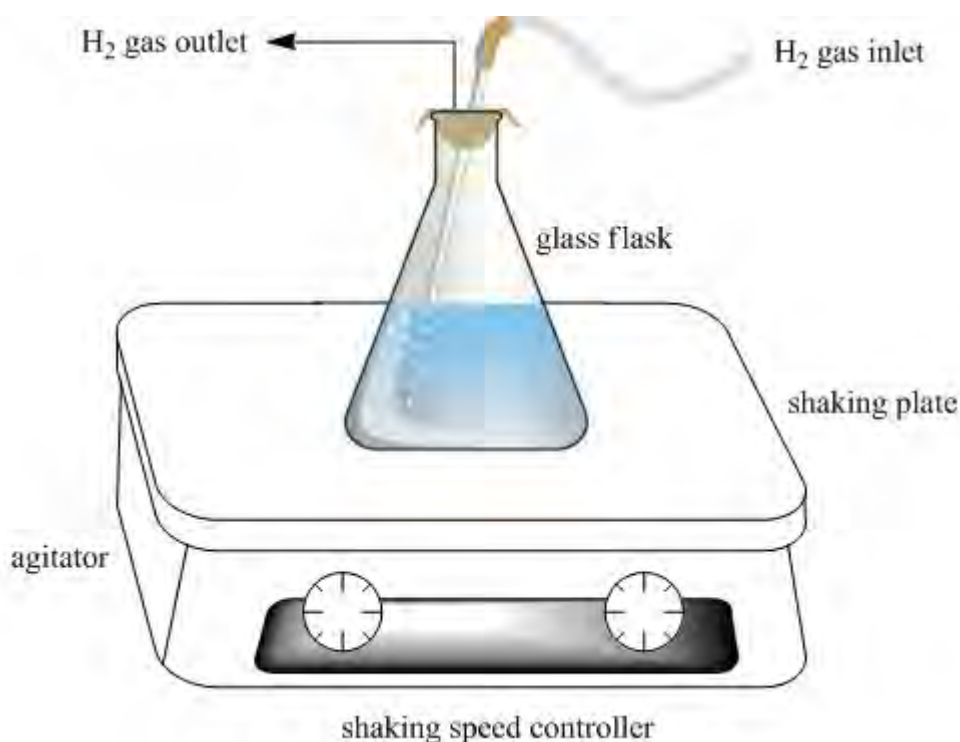
Figure 3.2. Experimental setup of the shake-flask reactor.

3.3.1.2 Trickle bed reactor (TBR)

The experimental setup of reactions is demonstrated in Figure 3.3 and the schematic diagram of the TBR is shown in Figure 3.4. The bed was of 6 mm diameter with a total height of 100 mm. The catalyst was loaded into the reactor to a depth of 95 mm and topped with a 5 mm layer of glass beads to ensure good contact between gas and liquid before entering the bed. H_2 and liquid flows were set at the desired rates using a flow meter and a pump, respectively.

Both gas and liquid were admitted simultaneously into the Y-shape mixer before entering the catalyst bed. At the bottom of the reactor, gas was vented and liquid was recycled back to the top of the reactor via the pump, thus forming a recirculating flow through the bed.

Determination of bed porosity

The porosity of a packed bed was determined from measurements of the single particle density ρ_p and of the bulk density ρ_{bed} (Gupta *et al*. 2002):

$$\varepsilon = 1 - \frac{\rho_{bed}}{\rho_p} \tag{3.1}$$

The porosity of a packed bed was also measured using the water substitution method (Sharma *et al*. 2001). The porosity of packed beds of trilobes reported by (Sharma *et al*. 2001) ranged from 0.49 for a 0.19 m inside diameter column, rising to 0.54 for a 0.05 m column, owing to wall effects. In this work the very small bed diameter of 6 mm leads to larger wall effects in the packing and thus the higher porosity.
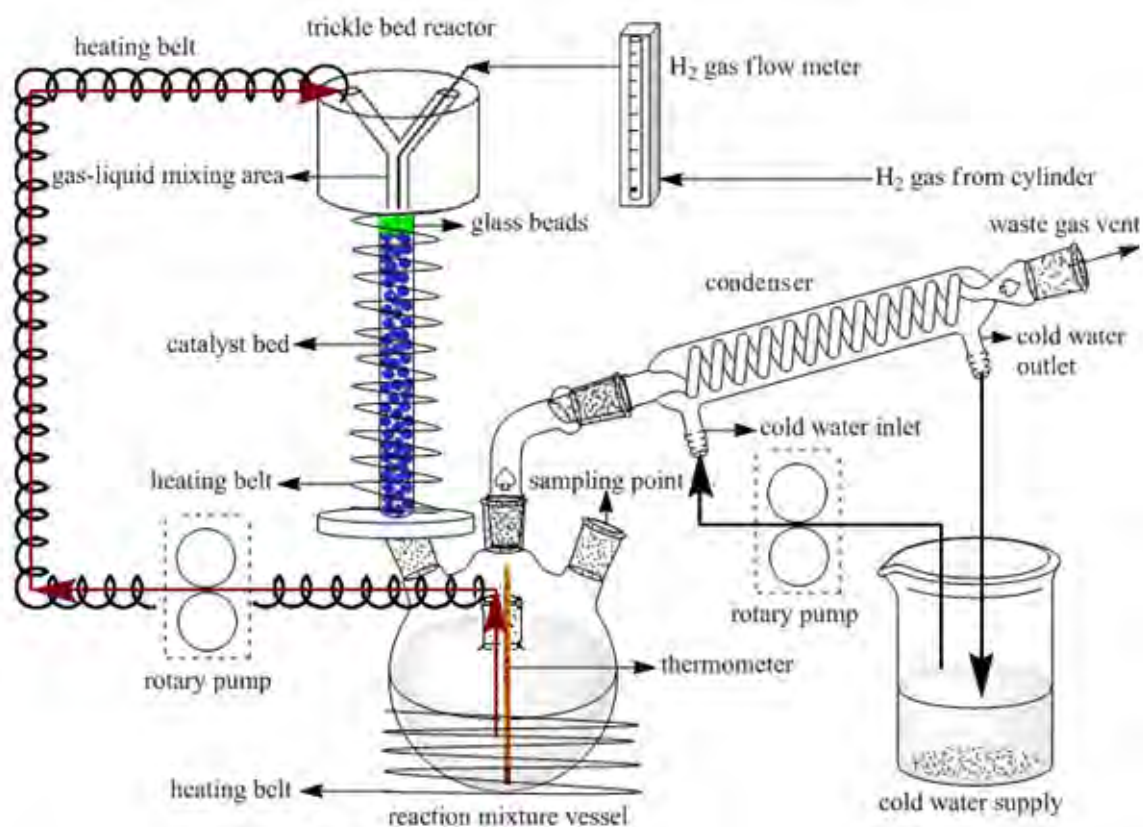
Figure 3.3. Experimental setup of the TBR.
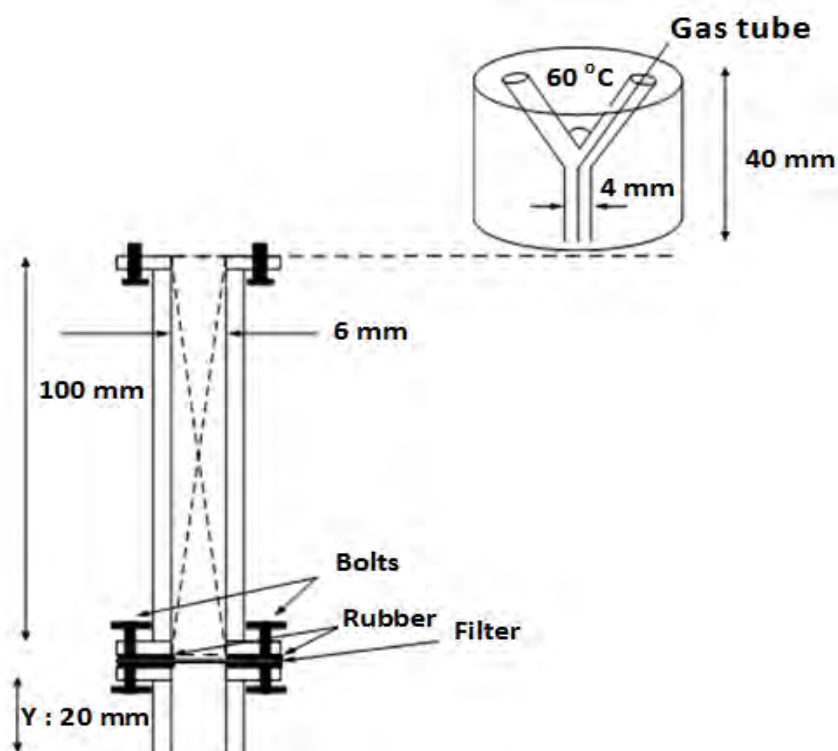
Figure 3.4. A schematic diagram of the TBR.

3.3.1.3 Autoclave reactor

The schematic diagram of the autoclave is shown in Figure 3.5. The 500- mL-stainless-steel autoclave is a three-phase reactor manufactured by Baskerville, Manchester, U.K. The reactor is composed of a heating jacket, a cooling coil, a thermocouple and a sample line. Mixing in the reactor is accomplished via an agitator. The agitator is a gas-inducing pipe impeller consisting of four inclined round-shaped blades. The hollow shaft of the agitator contains two holes at the bottom. The holes enable the sparging of nitrogen gas bubbles into the liquid phase for removing any dissolved oxygen in the reaction mixture. The holes also introduce hydrogen gas into the liquid phase efficient enough to reach the saturation state. During the experiments, gas uptake, heat flow, temperatures and pressures in the reactor are controlled and recorded by a computer through an interface system by Eurotherm Instruments, Inc. The reactor could be operated in a semi-batch mode, at a temperature range of 10 to 350 ^{o}C, at a maximum pressure of 60 bar and with a stirring rate ranging from 50 to 1500 rpm.
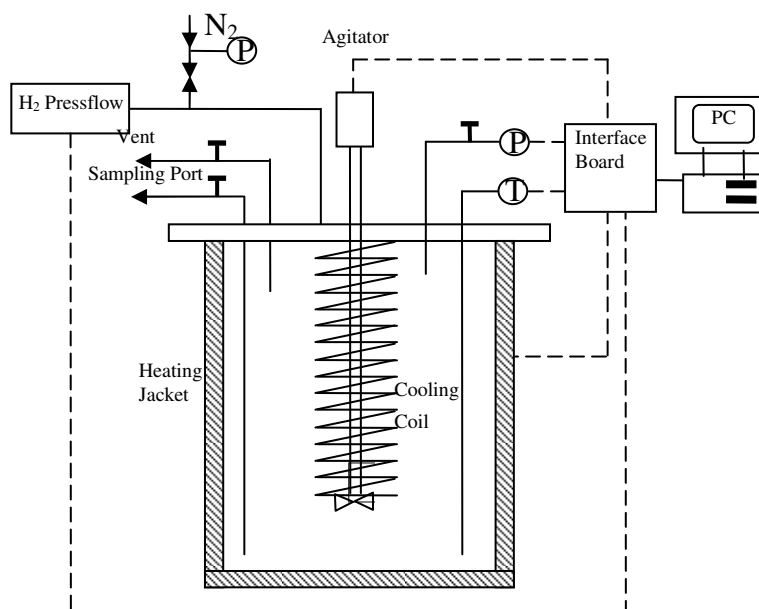
Figure 3.5. A schematic diagram of the autoclave reactor.

3.3.2 Hydrogenation tests

To compare slurry batch operation with fixed-bed recirculation mode, enantioselective hydrogenation of DMI was carried out in shake-flask (§ 3.3.2.1) and trickle-bed reactor (§ 3.3.2.2). For consistent comparison, same amount of catalyst and reaction mixture (solvent and DMI) was used in both reactors. For selective hydrogenation of 1-heptyne, reactions were conducted in the TBR only, as it was not possible to carry out the reactions in the shake-flask or autoclave reactors due to the high volatility of 1-heptyne and reaction products (1-heptene and heptane). For selective hydrogenation of soyabean oil, reactions were conducted in the TBR and performance was compared to slurry batch reactions in the autoclave reactor (§ 3.3.2.3).

3.3.2.1 Catalytic hydrogenations in the shake-flask reactor

For all experiments in the shake-flask reactor, prior to the reaction, the catalyst was reduced in situ under flowing hydrogen for 2 h.

Enantioselective hydrogenation of DMI with rhodium complex immobilized onto organic supports

After preparing the catalyst as in § 3.1.4 above, the required concentration of DMI was prepared in 15 ml solvent and was poured into the flask. The flask was then purged with a continuous flow of hydrogen in order to remove nitrogen and then hydrogen was set at the desired flow rate. The flask was put on a shaking device and the speed was set at the desired rate.

The procedure of conducting the reaction heterogeneously is similar to the homogeneous one except that the catalyst was used after immobilisation on the support.

Table 3.4 provides detailed conditions under which the experiments were conducted. The parameters investigated were: influence of solvent on homogeneous reactions (run 1-3),

influence of agitation speed (run 4-7), influence of substrate to catalyst ratio (run 8-10) and influence of catalyst phase (homogeneous vs heterogeneous) (run 11).

Enantioselective hydrogenation of DMI with rhodium complex immobilized onto alumina

The amount of catalyst support used was adjusted to provide 20 µmol of catalyst precursor complex upon the desired support, which was then placed in the flask. The required weight of DMI corresponding to the desired turnover number (TON) was dissolved in 15 ml of solvent and the solution was added to the flask. After sealing the top of the flask with septa it was taken off the inert atmosphere and put on the agitator. H_2 was bubbled into the reactor for five minutes to ensure a full displacement of N_2. The orbital agitator was then started by setting the controller at the desired speed. Samples of 40 µL volume were taken at regular intervals using a syringe and analyzed by GC.

To ensure that the rates of reaction obtained were representative of the reaction kinetics and not influenced by mass transfer, two checks were made. Firstly, the dependence of initial reaction rate on the speed of agitation was investigated and the optimal TOF was detected by optimizing the concentration of DMI. Secondly, to identify the presence of rate limiting resistances, the mass of immobilised catalyst precursor complex [Rh((R,R)-Me-DuPhos)(COD)]BF$_4$, m, was varied and the corresponding rate of reaction was measured. Using the following rate expression by Fogler 1999:

$$\frac{C_i}{R_A} = r_b + \frac{1}{m} r_{cr} \qquad (3.2)$$

a plot of C_i/R_A versus $1/m$ enables the resistance to gas adsorption, r_b and the combined resistance to internal and external diffusion for the catalyst, r_{cr}, to be determined.

Table 3.4 provides detailed conditions under which the experiments were conducted. The parameters investigated were: influence of agitation speed (run 12-15), influence of DMI concentration (run 16-20), influence of mass of catalyst (run 21-24) and influence of support (run 25).

Run	Precatalyst/catalyst	Support*	Catalyst loading** (g catalyst/ g support)	Solvent (15 ml)	DMI Conc. (M)	Gas flow rate (ml min⁻¹)	Speed of agitation (rpm)	S/C molar ratio (TON)
1	[Rh ((R,R)-Me-DuPhos)(COD)]BF$_4$	—	—	MeOH	0.08	100	200	30
2	[Rh ((R,R)-Me-DuPhos)(COD)]BF$_4$	—	—	EtOH	0.08	100	200	30
3	[Rh ((R,R)-Me-DuPhos)(COD)]BF$_4$	—	—	50%v/v MeOH in water	0.08	100	200	30
4	[Rh ((R,R)-Me-DuPhos)(COD)]BF$_4$	50WX2-100	0.024	50%v/v MeOH in water	0.08	100	175	30
5	[Rh ((R,R)-Me-DuPhos)(COD)]BF$_4$	50WX2-100	0.024	50%v/v MeOH in water	0.08	100	200	30
6	[Rh ((R,R)-Me-DuPhos)(COD)]BF$_4$	50WX2-100	0.024	50%v/v MeOH in water	0.08	100	250	30
7	[Rh ((R,R)-Me-DuPhos)(COD)]BF$_4$	50WX2-100	0.024	50%v/v MeOH in water	0.08	100	300	30
8	[Rh ((R,R)-Me-DuPhos)(COD)]BF$_4$	50WX2-100	0.024	50%v/v MeOH in water	0.04	100	250	15
9	[Rh ((R,R)-Me-DuPhos)(COD)]BF$_4$	50WX2-100	0.024	50%v/v MeOH in water	0.16	100	250	60
10	[Rh ((R,R)-Me-DuPhos)(COD)]BF$_4$	50WX2-100	0.024	50%v/v MeOH in water	0.30	100	250	113
11	[Rh ((R,R)-Me-DuPhos)(COD)]BF$_4$	—	0.024	50%v/v MeOH in water	0.16	100	250	60
12	[Rh ((R,R)-Me-DuPhos)(COD)]BF$_4$	Powder alumina	0.040	EtOH	0.01	100	100	9
13	[Rh ((R,R)-Me-DuPhos)(COD)]BF$_4$	Powder alumina	0.040	EtOH	0.01	100	150	9
14	[Rh ((R,R)-Me-DuPhos)(COD)]BF$_4$	Powder alumina	0.040	EtOH	0.01	100	200	9
15	[Rh ((R,R)-Me-DuPhos)(COD)]BF$_4$	Powder alumina	0.040	EtOH	0.01	100	300	9
16	[Rh ((R,R)-Me-DuPhos)(COD)]BF$_4$	Powder alumina	0.040	EtOH	0.03	100	200	26
17	[Rh ((R,R)-Me-DuPhos)(COD)]BF$_4$	Powder alumina	0.040	EtOH	0.08	100	200	61
18	[Rh ((R,R)-Me-DuPhos)(COD)]BF$_4$	Powder alumina	0.040	EtOH	0.16	100	200	122
19	[Rh ((R,R)-Me-DuPhos)(COD)]BF$_4$	Powder alumina	0.040	EtOH	0.26	100	200	196
20	[Rh ((R,R)-Me-DuPhos)(COD)]BF$_4$	Powder alumina	0.040	EtOH	0.41	100	200	311
21	[Rh ((R,R)-Me-DuPhos)(COD)]BF$_4$	Powder alumina	0.040	EtOH	0.08	100	200	60
22	[Rh ((R,R)-Me-DuPhos)(COD)]BF$_4$	Powder alumina	0.040	EtOH	0.08	100	200	48
23	[Rh ((R,R)-Me-DuPhos)(COD)]BF$_4$	Powder alumina	0.040	EtOH	0.08	100	200	90
24	[Rh ((R,R)-Me-DuPhos)(COD)]BF$_4$	Powder alumina	0.040	EtOH	0.08	100	200	121
25	[Rh ((R,R)-Me-DuPhos)(COD)]BF$_4$	Trilobe alumina	0.012	EtOH	0.08	100	200	60

Table 3.4. Experimental conditions used for DMI hydrogenation in the shake-flask reactor. Ligand [(R,R)-Me-DuPhos] /catalyst molar ratio was (1/1). All experiments were performed under ambient conditions (20 °C and atmospheric pressure). * 50WX2-100 is sulfonated ion-exchange resin. ** Runs (1-3) were carried out using 0.024 g of catalyst.

3.3.2.2 Catalytic hydrogenations in the TBR

Due to catalysts sensitivity to air, enantioselective hydrogenation reactions were carried out in the AtmosBag. For all experiments in the TBR, prior to the reaction, the catalyst was reduced in situ under flowing hydrogen for 2 h.

Enantioselective hydrogenation of DMI with rhodium complex immobilized onto trilobe alumina and ion-exchange resin

To achieve acceptable pressure drop in the TBR, trilobe-shaped alumina pellets were used as the powder was found to be unsuitable. The reactor was packed with 20 µmol of catalyst precursor complex immobilised into 2.7 g of trilobe alumina or 1 g of ion-exchange resin. The hydrogenation was begun by setting the H_2 and liquid flows at the desired rates. The effect of catalyst loading was investigated by varying the amount of immobilised complex over 2.7 g of trilobe alumina or 1 g of ion exchange resins. TON was optimized by testing different concentrations of DMI in 15 ml of solvent.

Table 3.5 provides detailed conditions under which the experiments were conducted. The parameters investigated were: different combinations of ligand and support systems (run 1-6), the parameters investigated for $[Rh(NBD)_2]BF_4$ precatalyst modified with (S,S)-DIOP ligand and supported on 50WX2-100 were: influence of solvent (run 7-12), influence of ligand/metal molar ratio (run 13-15). The parameters investigated for [Rh ((R,R)-Me-DuPhos)(COD)]BF_4 catalyst supported on 50WX2-100 were the influence of catalyst loading (run 16, 17) and influence of DMI concentration (run 18-23).

The parameters investigated for [Rh ((R,R)-Me-DuPhos)(COD)]BF_4 catalyst supported on trilobe alumina were: influence of catalyst loading (run 24, 25), influence of DMI concentration (run 26-29), influence of gas superficial velocity (run 30, 31) and influence of liquid superficial velocity (run 32, 33).

Run	Precatalyst/catalyst	Ligand	Catalyst loading*	Support**	Solvent (15 ml)	DMI Conc. (M)	V_G (cm s^{-1})	V_L (cm s^{-1})	S/C molar ratio (TON)
1	[Rh(NBD)₂]BF₄	BINAP	0.042	50WX2-100	MeOH	0.03	2.4	2.4	9
2	[Rh(NBD)₂]BF₄	(S,S)-DIOP	0.042	50WX2-100	MeOH	0.03	2.4	2.4	9
3	[Rh(NBD)₂]BF₄	BINAP	0.042	AC	MeOH	0.03	2.4	2.4	9
4	[Rh(NBD)₂]BF₄	(S,S)-DIOP	0.042	AC	MeOH	0.03	2.4	2.4	9
5	[Rh(NBD)₂]BF₄	BINAP	0.042	MSC	MeOH	0.03	2.4	2.4	9
6	[Rh(NBD)₂]BF₄	(S,S)-DIOP	0.042	MSC	MeOH	0.03	2.4	2.4	9
7	[Rh(NBD)₂]BF₄	(S,S)-DIOP	0.042	50WX2-100	100 % water	0.03	2.4	2.4	9
8	[Rh(NBD)₂]BF₄	(S,S)-DIOP	0.042	50WX2-100	10%v/v MeOH in water	0.03	2.4	2.4	9
9	[Rh(NBD)₂]BF₄	(S,S)-DIOP	0.042	50WX2-100	33.3%v/v MeOH in water	0.03	2.4	2.4	9
10	[Rh(NBD)₂]BF₄	(S,S)-DIOP	0.042	50WX2-100	50%v/v MeOH in water	0.03	2.4	2.4	9
11	[Rh(NBD)₂]BF₄	(S,S)-DIOP	0.042	50WX2-100	70%v/v MeOH in water	0.03	2.4	2.4	9
12	[Rh(NBD)₂]BF₄	(S,S)-DIOP	0.042	50WX2-100	90%v/v MeOH in water	0.03	2.4	2.4	9
13	[Rh(NBD)₂]BF₄	(S,S)-DIOP	0.018	50WX2-100	50%v/v MeOH in water	0.03	2.4	2.4	9
14	[Rh(NBD)₂]BF₄	(S,S)-DIOP	0.03	50WX2-100	50%v/v MeOH in water	0.03	2.4	2.4	9
15	[Rh(NBD)₂]BF₄	(S,S)-DIOP	0.21	50WX2-100	50%v/v MeOH in water	0.03	2.4	2.4	9
16	Rh ((R,R)-Me-DuPhos)(COD)]BF₄	[(R,R)-Me-DuPhos]	0.024	50WX2-100	50%v/v MeOH in water	0.08	2.4	2.4	30
17	Rh ((R,R)-Me-DuPhos)(COD)]BF₄	[(R,R)-Me-DuPhos]	0.012	50WX2-100	50%v/v MeOH in water	0.08	2.4	2.4	60
18	Rh ((R,R)-Me-DuPhos)(COD)]BF₄	[(R,R)-Me-DuPhos]	0.012	50WX2-100	50%v/v MeOH in water	0.035	2.4	2.4	26
19	Rh ((R,R)-Me-DuPhos)(COD)]BF₄	[(R,R)-Me-DuPhos]	0.012	50WX2-100	50%v/v MeOH in water	0.08	2.4	2.4	60
20	Rh ((R,R)-Me-DuPhos)(COD)]BF₄	[(R,R)-Me-DuPhos]	0.012	50WX2-100	50%v/v MeOH in water	0.16	2.4	2.4	121
21	Rh ((R,R)-Me-DuPhos)(COD)]BF₄	[(R,R)-Me-DuPhos]	0.012	50WX2-100	50%v/v MeOH in water	0.3	2.4	2.4	227
22	Rh ((R,R)-Me-DuPhos)(COD)]BF₄	[(R,R)-Me-DuPhos]	0.012	50WX2-100	50%v/v MeOH in water	0.662	2.4	2.4	500
23	Rh ((R,R)-Me-DuPhos)(COD)]BF₄	[(R,R)-Me-DuPhos]	0.012	50WX2-100	50%v/v MeOH in water	1.324	2.4	2.4	1000
24	Rh ((R,R)-Me-DuPhos)(COD)]BF₄	[(R,R)-Me-DuPhos]	0.012	Trilobe alumina	EtOH	0.08	5.9	1.2	25
25	Rh ((R,R)-Me-DuPhos)(COD)]BF₄	[(R,R)-Me-DuPhos]	0.004	Trilobe alumina	EtOH	0.08	5.9	1.2	65
26	Rh ((R,R)-Me-DuPhos)(COD)]BF₄	[(R,R)-Me-DuPhos]	0.004	Trilobe alumina	EtOH	0.105	5.9	1.2	85
27	Rh ((R,R)-Me-DuPhos)(COD)]BF₄	[(R,R)-Me-DuPhos]	0.004	Trilobe alumina	EtOH	0.170	5.9	1.2	128
28	Rh ((R,R)-Me-DuPhos)(COD)]BF₄	[(R,R)-Me-DuPhos]	0.004	Trilobe alumina	EtOH	0.237	5.9	1.2	179

29	[Rh ((R,R)-Me-DuPhos)(COD)]BF$_4$	0.004	[(R,R)-Me-DuPhos]	Trilobe alumina	EtOH	0.3	5.9	1.2	223
30	[Rh ((R,R)-Me-DuPhos)(COD)]BF$_4$	0.004	[(R,R)-Me-DuPhos]	Trilobe alumina	EtOH	0.3	2.95	1.2	223
31	[Rh ((R,R)-Me-DuPhos)(COD)]BF$_4$	0.004	[(R,R)-Me-DuPhos]	Trilobe alumina	EtOH	0.3	11.8	1.2	223
32	[Rh ((R,R)-Me-DuPhos)(COD)]BF$_4$	0.004	[(R,R)-Me-DuPhos]	Trilobe alumina	EtOH	0.3	5.9	0.6	223
33	[Rh ((R,R)-Me-DuPhos)(COD)]BF$_4$	0.004	[(R,R)-Me-DuPhos]	Trilobe alumina	EtOH	0.3	5.9	0.9	223

Table 3.5. Experimental conditions used for DMI hydrogenation in the TBR. All experiments were performed under ambient conditions (20 °C and atmospheric pressure). Ligand/metal molar ratio: 1 except for Run 13,14 and 15 where it was 0, 0.5 and 5, respectively.*(g catalyst/ g support).**AC is activated carbon and MSC is sulfonated ion-exchange resin.

Selective hydrogenation of 1-heptyne

The catalytic performance of 2 wt. % Pd/Al$_2$O$_3$ catalyst in the liquid-phase semi-hydrogenation was evaluated using a 100 ml mixture containing 5 % v/v 1-heptyne in the corresponding solvent at the temperature 20 ^{o}C and atmospheric pressure of H$_2$. Due to the high volatility of 1-heptyne, its evaporation during continuous recirculation of reaction mixture was likely to occur, and therefore, it was necessary to investigate this matter further. The evaporation of 1-heptyne was investigated by recirculating a 100 ml mixture containing 5 % v/v 1-heptyne in isopropanol. The reaction mixture was flowed at 5 ml min^{-1} into the catalyst bed containing 2.8 g of catalyst. 1-heptyne concentration was monitored by taking samples every 30 minutes for 3 hours. As can be seen from Figure 3.6, concentration of 1-hepytne dropped to half its value after 2 h indicating considerable evaporation that could be attributed to the system not being sealed and the turbulence induced by the catalyst bed. The experimental data shown in Figure 3.6 are average values for the same experiment carried out in triplicate and the obtained relative experimental error for each is approximately ± 5 %.
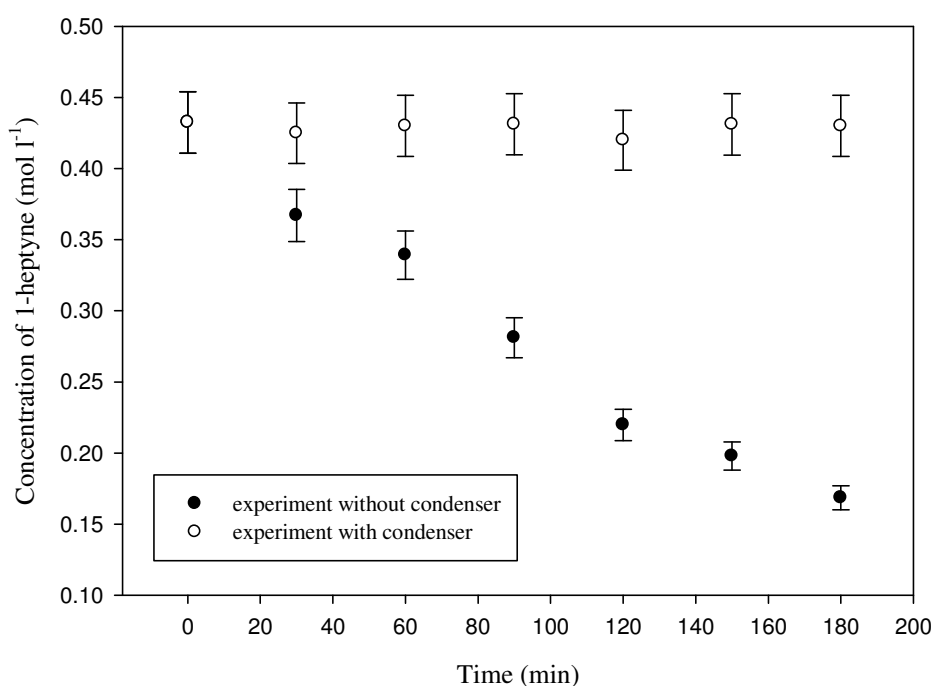
Figure 3.6. Investigation of 1-heptyne evaporation.

To overcome the evaporation problem, a condenser was fitted into the experimental setup and is shown in Figure 3.3. The condenser has a gas or vapour pathway that is enclosed by a jacket through which a cooling water was passed. The cooling water cools the outer surface of the vapour tube and this cooling effect reaches the inner wall of the vapour tube to cool the vapour and cause it to condense. After conducting the experiment with the fitted condenser, a constant concentration of 1-heptyne was obtained for 3 h, and therefore, the modified experimental setup was implemented in the experiments.

Table 3.6 provides detailed conditions under which the experiments were conducted. The parameters investigated were: influence of solvent (run 1-6), influence of liquid superficial velocity (run 7-9), influence of initial concentration of 1-heptyne during recirculation operation (run 10-13) and influence of liquid superficial velocity during continuous operation with a single pass through the catalyst bed (run 14-18).

Run	Solvent	Initial conc. of 1-heptyne ($mol\ l^{-1}$)	Substrate/catalyst molar ration (TON)	V_G ($cm\ s^{-1}$)	V_L ($cm\ s^{-1}$)
1	100 % IPA	0.4	72	5.9	0.59
2	50 % IPA / 50 % hexane	0.4	72	5.9	0.59
3	100 % hexane	0.4	72	5.9	0.59
4	99.6 % IPA / 0.4 % water	0.4	72	5.9	0.59
5	99 % IPA / 1 % water	0.4	72	5.9	0.59
6	99 % IPA / 1 % NaOH	0.4	72	5.9	0.59
7	100 % IPA	0.4	72	5.9	0.29
8	100 % IPA	0.4	72	5.9	0.88
9	100 % IPA	0.4	72	5.9	1.2
10	100 % IPA	0.1	18	5.9	1.2
11	100 % IPA	0.2	36	5.9	1.2
12	100 % IPA	0.3	54	5.9	1.2
13	100 % IPA	0.5	90	5.9	1.2
14	100 % IPA	0.0273	5	5.9	0.17
15	100 % IPA	0.0273	5	5.9	0.21
16	100 % IPA	0.0273	5	5.9	0.24
17	100 % IPA	0.0273	5	5.9	0.32
18	100 % IPA	0.0273	5	5.9	0.62

Table 3.6. Experimental conditions used for 1-heptyne hydrogenation in the TBR (catalyst 2 % Pd on trilobe Al_2O_3 support). All experiments were performed under ambient conditions (20 °C and atmospheric pressure).

Continuous operations with a single pass of reaction mixture through the catalyst bed were performed by supplying the mixture from a separate feedstock instead of recycling the reaction mixture. The overall volume of liquid processed continuously was 100 ml. Other conditions remained the same as those used in the batch recycle experiments.

Selective hydrogenation of soyabean oil

The catalytic performance of 2 wt. % Pd/Al_2O_3 catalyst in the selective hydrogenation of soyabean oil was evaluated using 12.5 and 25 ml of oil. The fatty acid composition of soyabean oil used in this work is demonstrated in Table 3.7. The soyabean oil was passed through alumina prior to hydrogenation to remove impurities that might act as catalyst poisons and interfere with catalyst evaluation.

The continuous hydrogenation system consisted of oil charging vessel, two rotary pumps, hydrogen supply, a condenser and a heater. The TBR reactor was packed loosely with 2.7 g of catalyst before being surrounded by an electric heating belt. A layer of glass beads on top of the catalyst bed provided a zone for preheating the incoming oil and gas to reaction temperature. To ensure a uniform heating across the hydrogenation system, the charging vessel and the recirculating mixture were also surrounded by the electric heating belt. Temperature of the reaction mixture was measured with a thermometer inserted into the charging vessel as shown in Figure 3.3. The desired gas (H_2 or N_2) was admitted to the top of the reactor just upstream to the catalyst bed. A preconditioning procedure was followed to activate the catalyst. The catalyst was activated by first purging with N_2, raising the bed temperature to operating conditions and then introducing H_2. Soyabean oil was then started through the bed at the desired rate. To study the effect of operating temperature and to calculate the activation energy of the reaction, temperatures of 50, 60, 70, 85, 105 ^{o}C were selected. The influence of changing the hydrodynamics was investigated by testing gas flow

rates of 250, 500, 750 and 1000 ml min^{-1} and liquid flow rates of 3.5, 5, 6.5 and 8 ml min^{-1}. The rate of soyabean oil flow was selected as to ensure even distribution over the catalyst bed surface and efficient wetting of catalyst particles.

		Fatty Acid Composition (mass %)
Palmitic acid	C16:0	11.2
Stearic acid	C18:0	3.8
Oleic acid	cis-C18:1	21.5
Linoleic acid	C18:2	55.8
Linolenic acid	C18:3	7.7

Table 3.7. Composition of untreated soyabean oil (determined in situ by injecting a sample into GC).

Table 3.8 provides detailed conditions under which the experiments were conducted. The parameters investigated were: influence of temperature (run 1-5), influence of gas superficial velocity (run 6-8), influence of liquid superficial velocity (run 9-11), influence of hydrodynamics at reaction temperature of 50 ºC (run 12) and influence of oil volume (run 13).

Run	Volume of oil (ml)	Temperature (ºC)	Gas velocity (cm s^{-1})	Liquid velocity (cm s^{-1})
1	12.5	50	14.7	0.21
2	12.5	60	14.7	0.21
3	12.5	70	14.7	0.21
4	12.5	85	14.7	0.21
5	12.5	105	14.7	0.21
6	12.5	105	29.4	0.21
7	12.5	105	44.2	0.21
8	12.5	105	58.9	0.21
9	12.5	105	58.9	0.29
10	12.5	105	58.9	0.38
11	12.5	105	58.9	0.47
12	12.5	50	58.9	0.47
13	25	50	58.9	0.47

Table 3.8. Experimental conditions used for soyabean oil hydrogenation in the TBR (catalyst 2 % Pd on trilobe Al$_2$O$_3$ support). All experiments were performed under atmospheric pressure.

3.3.2.3 Catalytic hydrogenations in the autoclave reactor

(The reactions were carried out by Ju Zhu- a PhD student in Catalysis and Reaction Engineering Group)

To the autoclave reactor, a volume of 200 mL solvent and 0.170 g of ground powdered catalyst were added, followed by 50 mL soybean oil. The reactor was purged with nitrogen in order to remove the remaining oxygen, and the mixture was programmed to heat to the reaction temperature. The reaction was then started at a steady temperature of 50 ^{o}C and at 1 bar hydrogen pressure, by switching from a nitrogen gas flow to a hydrogen gas flow. Total reaction time was 2-5 h depending on the operating conditions, the catalyst activity and the catalyst amount. Prior to reaction and before introducing the soybean oil, the catalysts were pre-reduced in situ under 2 bar of hydrogen by bubbling an outflow of hydrogen (0.6 L/min) through the system for 25 min with gentle stirring (500 rpm). The Pd catalyst weight was adjusted in order to keep the weight of exposed Pd constant along the various experiments. The course of the reaction was followed by withdrawing samples smaller than 0.5 ml out of a total of 250 mL from the system periodically through the sample pipe, hence the liquid-to-catalyst ratio could be considered to remain constant.

3.3.3 Sampling method

3.3.3.1 Enantioselective hydrogenation of DMI

Samples of 40 µL (40 x 10^{-9} m^{3}) were taken at regular intervals throughout the course of the reaction for GC analysis (Varian GC Model, 30m × 0.25mm × 0.25µm film thickness, Gamma DEX^{TM} 225 Capillary Column, injection port: 175 ^{º}C; detector: 180 ^{º}C; column oven: initial temperature 80 ^{º}C, ramp at 3 ^{º}C/min to 140 ^{º}C/min, head pressure 15 psig, split ratio −90/1).

The enantioselectivity (ee) of the reaction was determined as the enantiomeric excess defined as $(S - R)/(S + R)$, where R and S are the concentrations of the enantiomers in mol l^{-1}.

To check the reproducibility of results, experiments were carried out in triplicate and the obtained relative experimental error was about $\pm$ 2.5 %.

3.3.3.2 Selective hydrogenation of 1-heptyne

Samples of 80 µL (80×10^{-9} m^3) were taken at regular intervals throughout the course of the reaction for GC analysis (Varian GC Model, 30m $\times$ 0.25mm $\times$ 0.25µm film thickness, Gamma DEX^{TM} 225 Capillary Column, injection port: 60 $^{\circ}$C; detector: 60 $^{\circ}$C; column oven: initial temperature 24 $^{\circ}$C, ramp at 3 $^{\circ}$C/min to 40 $^{\circ}$C/min, head pressure 5 psig, split ratio $-40/1$).

The selectivity of the reaction was calculated as: $C_{1\text{-heptene}} / (C_{1\text{-heptene}} + C_{heptane})$.

To check the reproducibility of results, experiments were carried out in triplicate and the obtained relative experimental error was about $\pm$ 2.5 %.

3.3.3.3 Selective hydrogenation of soyabean oil

Liquid samples collected from reactions, were placed into test tubes and subjected to derivatization (Christy *et al*. 2009). The aim of the derivatization is to convert fatty acids to fatty acid methyl esters which offer excellent stability, and provide quick and quantitative samples for GC analysis. The derivatization was conducted using an alkylation derivatization reagent and was performed following a typical procedure. The test tubes containing reaction samples were added 2 mL of 0.5 M sodium hydroxide in methanol which were then placed in a water bath at 60 $^{\circ}$C for 15 min. After cooling, to each test tube was added 2 mL of BF$_3$/methanol and returned in the water bath for another 10 min. After each test tube was

added 2 mL of a saturated solution of NaCl and 1 mL hexane, it was shaken to aid separation and dissolution of the fatty acid methyl esters (FAMEs) in the hexane layer. The glass tubes were then allowed to stand for a few minutes to help settling the formed layers. The hexane layer floating at top of the tube was extracted and placed in a small clean vial and stored in dark until GC analysis.

The GC analysis was carried out using (Varian GC Model, 75m × 0.18mm × 0.14µm film thickness, SP^{TM}-2560 Capillary Column, injection port: 250 $^{\circ}$C; detector: 265 $^{\circ}$C; column oven: initial temperature 200 $^{\circ}$C, ramp at 4 $^{\circ}$C/min to 240 $^{\circ}$C/min, head pressure 50 psig, split ratio −150/1).

Selectivity toward *cis*-C$_{18:1}$ was calculated as the number of moles of *cis*-C18:1 divided by the total number of moles of all products detected.

To check the reproducibility of results, experiments were carried out in triplicate and the obtained relative experimental error was about ± 2.5 %.

3.4 Analytical methods

3.4.1 Gas chromatograph (GC)

The Gas Chromatograph (Varian GC Model) is composed of an injector, a capillary column, an oven, a temperature controller, a monitor and a detector. The GC was fitted with a flame ionisation detector (FID). A hydrogen – oxygen flame was produced in the FID to combust the compounds of the sample as they elute from the column. A temperature ramp profile was applied for the sample analysis based upon the boiling points of the compounds expected to be found. The carrier gas was helium, a part of which was used as make up gas. Helium, hydrogen and air were measured with soap bubble flow meter and electronic flow meter. Liquid samples were injected using a 1 µm microsyringe fitted with 7 cm length needle. The GC output was processed using the chromatographic software CSW 32 (Data Apex Ltd.,

Czech Republic). CSW 32 provides highly configurable 32-bit data handling capability. Prior to collecting and processing the chromatographic signal by the computer the analogue signal of a detector must be converted to digital form by an analog/digital (A/D) converter. An integrating converter is installed capable of integrating the input signal for a short time, and transforms the resulting integral to the digital form.

3.4.2 Calibration

The GC was calibrated with standard samples of components to be analysed. The GC was calibrated for (i) DMI, (ii) dimethyl (*S*)-(-)-methylsuccinate and dimethyl (*R*)-(+)-methylsuccinate (iii) 1-heptyne (IV) 1-heptene and heptane (V) soyabean oil (VI) palmitic acid (C16:0), stearic acid (C18:0), oleic acid (C18:1), linoleic acid (C18:2) and linolenic acid (C18:3). A calibration set was constructed from reference spectra of samples containing known concentrations of components. The concentration covered the entire range from maximum to minimum expected during actual experiments. The calibration curves are shown in Appendix C, p 308-312.

CHAPTER 4

ENANTIOSELECTIVE HYDROGENATION OF DIMETHYL ITACONATE OVER RHODIUM COMPLEXES IMMOBILIZED ON ORGANIC SUPPORTS

4.1 Introduction

In this chapter, the rhodium-catalyzed enantioselective hydrogenation of dimethyl itaconate (DMI) has been studied using three asymmetric hydrogenation catalysts: [Rh (NBD){(S,S)-DIOP}]BF$_4$ (hereinafter referred to as " catalyst (1)", [Rh (NBD) (BINAP)]BF$_4$ (hereinafter referred to as " catalyst (2)" and [Rh (COD){(R,R)-Me-DuPHOS}]BF$_4$ (hereinafter referred to as " catalyst (3)". The catalysts were supported on ion-exchange resins which proved to be effective for heterogenisation. Initial optimisation studies were carried out using the most common and least expensive ligands, (S,S)-DIOP and BINAP, in order to achieve the optimum conversion and enantioselectivity in the trickle bed reactor (TBR). In §4.2, different combinations of ligand and support were tested in the TBR in order to find the best combination for optimisation. §4.3 & §4.4 show the significant influence of solvent upon the activity of catalyst (1) supported on 50WX2-100 ion-exchange resin. Efforts were then made to optimize the enantioselectivity by studying the influence of the ligand/metal molar ratio (§4.5) and type of ligand (§4.6). §4.6 also contains a brief background which justifies the selection of the expensive R,R-MeDUPHOS ligand for optimizing the enantioselectivity of the reactions.

Using catalyst (3) supported on 50WX2-100 ion-exchange resin, the catalytic hydrogenation of DMI was studied in lab-scale shake flask (§4.7) and transferred to continuous flow with recirculation in the TBR (§4.8). Tests were conducted in the shake flask to ensure that the reaction was not influenced by mass transfer limitations by varying the shaking speed (§4.7.1). In the shake-flask, the substrate to catalyst molar ratio was optimized (§4.7.2), and a

130

reaction was carried out homogenously for the purpose of comparing the effectiveness of both catalyst phases at the optimized agitation speed (§4.7.3). In the TBR, the effect of catalyst loading (g complex/ g support) and substrate to catalyst molar ratio were discussed in §4.8.1 and §4.8.2. The fitting of DMI concentration profiles to Osborn-Wilkinson kinetic expression is then demonstrated in §4.8.3, followed by conclusions (§4.9).

4.2 Selection of suitable ligand and support systems

Different combinations of ligand and support were tested in the TBR in order to find the best combination for optimisation. The results obtained are summarized in Table 4.1. It is clear from the data obtained that experiment 2 gave the best results in terms of conversion and enantioselectivity and for this reason (S,S)-DIOP ligand and 50WX2 resin were selected for further optimisation studies. The rest of the experiments did not achieve good results possibly due to leaching of the catalyst and/or the ligand into the solution.

Run	Catalyst	Ligand	Support*	Time (h)	Conversion (%)	*ee* (%)
1	$[Rh(NBD)_2]BF_4$	BINAP	50WX2	2	0	0
2	$[Rh(NBD)_2]BF_4$	(S,S)-DIOP	50WX2	2	66	29
3	$[Rh(NBD)_2]BF_4$	BINAP	AC	2	0	0
4	$[Rh(NBD)_2]BF_4$	(S,S)-DIOP	AC	2	6	35
5	$[Rh(NBD)_2]BF_4$	BINAP	MSC	2	3	7
6	$[Rh(NBD)_2]BF_4$	(S,S)-DIOP	MSC	2	0	0

Table 4.1. Testing different combinations of ligand and support for optimisation. Conditions: room temperature; solvent: 15 ml MeOH, liquid and gas flow rates: 40 ml min^{-1}, concentration of DMI: 0.03 M, substrate/catalyst ratio: 9 and ligand/catalyst ratio: 1.
*DOWEX 50WX2 and DOWEX MSC are sulfonated ion-exchange resins; AC is activated carbon.

4.3 Influence of dimethyl itaconate (DMI) concentration and water addition

The effect of DMI concentration upon the conversion and *ee* was then studied under the conditions given in Table 4.1. Conducting a reaction with a higher DMI concentration of 0.1 M decreased the conversion to 38%, while the *ee* remained unaffected at about 24%. When a reaction was conducted with a lower DMI concentration of 0.02 M, a conversion of 19% and ee of 28% were obtained after 2h. Consequently, a DMI concentration of 0.03 M, and the ligand/support of experiment 2 in Table 4.1, was chosen as a basis for further optimisation studies. When conducting experiment 2, evaporation of methanol with time was experienced due to its high volatility. Therefore, in later studies methanol was mixed with deionised water (30%$_{v/v}$) in order to reduce evaporation of the solvent. When the experiment was conducted using a mixture of methanol and water, 100% conversion and 27% *ee* were obtained in twenty minutes. Consequently, this mixed solvent was selected for further optimisation studies.

The concentration versus time results for experiment (room temperature, solvent: 50%$_{v/v}$ MeOH in water, liquid and gas flow rates of 40 ml min^{-1}, 0.03 M concentration of DMI, substrate/catalyst ratio: 9 and ligand/catalyst ratio: 1) were fitted to the integrated rate equation for first order reaction:

$$\ln C = -kt + \ln C_0 \tag{4.1}$$

where C is reactant concentration at time t, k is first order rate constant, C_0 is initial reactant concentration. From Figure 4.1 it is observed that the data are a good fit to a straight line, thus confirming that the reaction follows first order behaviour. The rate constant, k, was found from slope of line to be 0.234 s^{-1}.
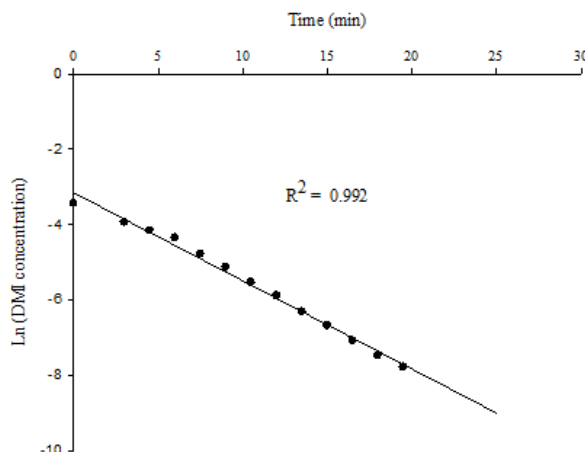
Figure 4.1. Plot of $\ln C$ vs time (t) to determine order of reaction. Conditions: room temperature; solvent: $50\%_{v/v}$ MeOH in water, liquid and gas flow rates: 40 ml min^{-1}, concentration of DMI: 0.03 M, substrate/catalyst ratio: 9 and ligand/catalyst ratio: 1.

4.4 Solvent effects

Since a mixed solvent was chosen, the influence of different ratios of methanol to water (within the range 0 - 90 % methanol) upon the initial reaction rate and enantioselectivity was examined in the TBR. Figure 4.2 and Table 4.2 summarize these results. For consistency, all experiments were conducted at same conditions: room temperature, 1 atm, hydrogen pressure: 2 bar, liquid and gas flow rates: 40 ml min^{-1}, 1% [Rh (NBD)$_2$]BF$_4$ and (S,S)-DIOP loadings, ligand/catalyst ratio:1.

The trend of reaction rate with methanol concentration reaches an optimum at $50\%_{v/v}$ methanol in water, which corresponds to a TOF of 27 h^{-1}. By increasing the ratio of methanol to water up to 50%, the reaction rate increased by a factor of 1.3 and full conversion of DMI was obtained. Increasing the concentration further from 50% to 90% decreased the reaction rate significantly by a factor of 2.3 and led to dramatic drop of conversion. Different solvents can influence the catalytic behaviour differently due to different solubility of reactants (DMI and hydrogen), and can change interactions between the modifier [(S,S)-DIOP], reactant and metal surface. Toukoniitty *et al*. (2002) pointed out that the use of different solvents affects

activity and enantioselectivity of the catalytic system due to different strengths of adsorption

of reactant(s) on the catalyst surface, competitive adsorption of solvent molecules, and

interaction of solvent with the reactant, either in the liquid phase or on the catalyst surface.

Khodadadi-Moghaddam *et al*. (2009) reported that deactivation of the catalyst can also be

caused by the solvent. Moreover, a possible role of solvents donating a proton, i.e. being

involved in the reaction may influence the catalytic behaviour (Rajadhyaksha and Karwa,

1986).
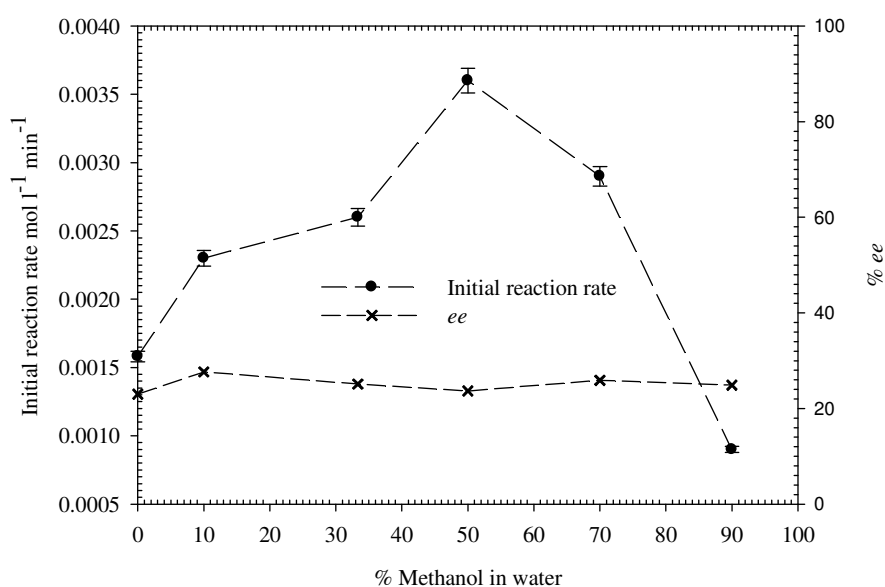
Figure 4.2. Effect of solvent on reaction rate and enantioselectivity. Conditions: room temperature, 1 atm, hydrogen pressure: 2 bar, liquid and gas flow rates: 40 ml min^{-1}, 1% [Rh (NBD)$_2$]BF$_4$ and (S,S)-DIOP loadings, ligand/catalyst ratio:1.

Run	%$_{v/v}$ MeOH in water	Conversion (%)	Time (min)	Initial Reaction rate (mol l^{-1} min^{-1})*	ee (%)
7	0	100	34	0.00158	23
8	10	100	20	0.00229	28
9	33.333	100	20	0.00258	23
10	50	100	18	0.00360	23
11	70	91	30	0.00290	24
12	90	15	18	0.00093	25

Table 4.2. Influence of solvent on conversion, reaction rate and *ee*. * calculated after 7 min from the start of the reaction. Conditions are given in Figure 4.2.

In order to explain the obtained trend of the reaction rate, adsorption of DMI onto the catalyst surface was investigated in a shake-flask containing 0.03 M of DMI in 15 ml of solvent. After running the experiments for twenty minutes, 0.00012 moles of DMI adsorbed onto the catalyst surface using pure water and 33%$_{v/v}$ methanol in water compared to 0.00018 moles of DMI adsorbed onto the catalyst surface when 50%$_{v/v}$, 70%$_{v/v}$ and 90%$_{v/v}$ ratios of methanol to water were used. The higher adsorption of DMI into catalyst surface at high ratios of methanol to water can explain the drop in conversion and reaction rate by the increased coverage of the rhodium surface by DMI and the resulting loss of free active sites on the catalyst. For optimal reaction rate, approximately equal surface coverage of DMI and hydrogen is required to maximise the probability of adjacent adsorbed molecules reacting. Excessive adsorption of DMI would lead to reduction of the number of available sites for hydrogen to adsorb. Despite the fact that hydrogen is more soluble in methanol than in water, the optimum reaction rate obtained at 50 %$_{v/v}$ methanol in water could be due to this mixture falling in between low and high solubility of hydrogen as well as low and high adsorption of DMI into the catalyst surface.

Furthermore, different swellings of the resin in the adopted solvents was likely to occur which could further explain the obtained trend of reaction rate. Barbaro (2006) reported that swelling of the resin is crucial for both catalyst anchoring and efficiency owing to enhanced mass transport inside the polymer beads, hence giving efficient active-site accessibility. Therefore, swelling of resin in methanol, $50\%_{v/v}$ methanol in water and pure water was studied under the microscope. The findings of the study together with the microscope images of the swollen resin are displayed in Table 4.3 and Figure 4.3, respectively. As can be seen in Table 4.3, the resin diameter increased by almost 50% when immersed in water and $50\%_{v/v}$ methanol in water compared to 12.5% in methanol solvent. The significantly lower swelling of resin in methanol could explain the dramatic drop of reaction rate and conversion for ratios of methanol in water higher than 50%, due to limited mass transport inside the beads. On the other hand, the relatively high swelling of resin obtained with water and $50\%_{v/v}$ methanol in water could lead to efficient mass transfer inside the resin, and therefore could explain the full conversion of DMI achieved with the solvents within this range as demonstrated in Table 4.2. Moreover, it has been reported that mixtures of short-chain alcohols and water cause a greater degree of swelling in resin than either the short-chain alcohol or water alone (Gebel *et al*. 1993).

Solvent	% increase in resin diameter
Methanol	~12.5
50%v/v methanol in water	~50
Water	~50

Table 4.3. Swelling properties of resin examined under the microscope.
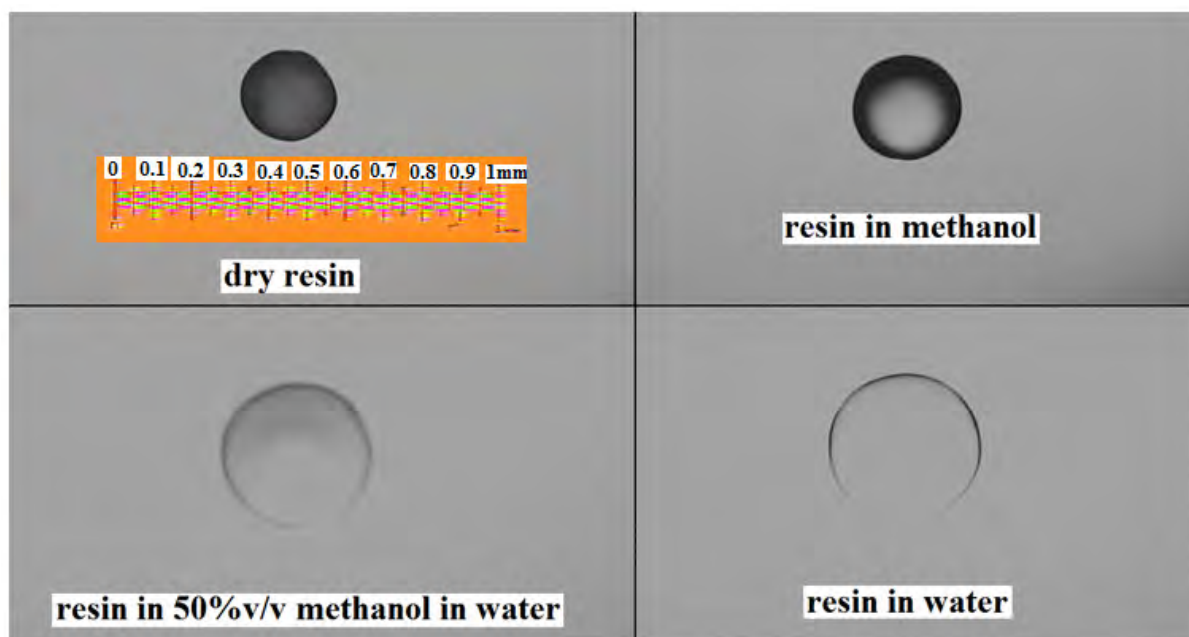
Figure 4.3. Microscope images of the swollen resin in methanol, $50\%_{v/v}$ methanol in water and pure water (100 maginifications, Olympus, UPlanFI, 100x/1.30 Oil, Japan).

Although solvent selection was found to have a noticeable effect upon the reaction rate, the achieved *ee* of ~23% and TOF of 27 h^{-1} are considerably lower than the 54.6% *ee* and 40 h^{-1} TOF reported for the same catalyst for the asymmetric hydrogenation of the prochiral olefin methyl 2-acetamidoacrylate (Barbaro, 2006). Hence, it is desirable to increase the *ee*, TON and TOF with regard to possible commercial application for the resin and to improve catalyst performance to the levels reported in the literature (Barbaro, 2006). Therefore, the effect of ligand/metal ratio, ligand, substrate concentration, catalyst loading upon *ee* and DMI conversion were studied and are discussed in the following sections.

4.5 Influence of ligand/metal molar ratio

The mechanism of rhodium-catalyzed hydrogenation of functionalized olefins using bidentate organophosphine ligands such as DIOP has not been well addressed in the literature. Reetz *et al*. (2005) reported that the prevailing viewpoint for monodentate phosphine ligands was that two ligand molecules would bond to rhodium in the active catalytic species. However, Fu *et al*. (2004) and Tang *et al*. (2006) found that in the asymmetric hydrogenation of (Z)-2-

(acetamido)cinnamate catalyzed by Rh-monodentate phosphine, a faster reaction was obtained with 1:1 Ligand/Rh than that with 2:1 Ligand/Rh ratio, and that ligand/Rh ratio had little influence upon the conversion and enantioselectivity. Van den Berg *et al.* (2003) proved that a number of different complexes are formed during hydrogenation. They found that the rate of the asymmetric hydrogenation of dehydroamino acids with Rh/monodentate MonoPhos was positively affected by reducing the L/Rh ratio from two to one without compromising the enantioselectivity. It was thought that their finding was due to very strong binding of phosphoramidites ligands to rhodium metal. It was claimed that despite their reduced sigma donating properties, phosphoramidites have greater enhanced π acceptor properties when compared to phosphines. It is noteworthy that these studies have been conducted on homogeneous reactions using monodentate ligands while different interactions might occur in heterogeneous systems that are significantly influenced by the physical and chemical properties of the support such as those of the ion exchange resins.

This leads to a point of practical interest, namely, the optimum choice of the ligand to metal ratio. The effect of ligands on the catalytic properties is dependent on their relative amounts in the catalyst with regard to the quantity of metal. For example the molar ratio of ligand to rhodium in a complex. Therefore, in this study, the amount of Rh complex was fixed and the number of moles of DIOP ligand was varied that gave DIOP/Rh molar ratios from 0:1 to 5:1. The influence of DIOP/Rh molar ratio upon conversion is shown in Figure 4.4. A full conversion of DMI was obtained with DIOP/Rh molar ratios of 0:1, 0.5:1 and 1:1, while the catalytic activity was substantially decreased upon increasing the ratio to 5:1. Increasing DIOP/Rh molar ratio from 0:1 to 0.5:1 prolonged reaction time from 8 min to 35 min, whereas further increase in the molar ratio to 1:1 led to full conversion of DMI obtained after 18 min. Modification of [Rh (NBD)$_2$]BF$_4$ incorporates the loss of one equivalent of NBD where the role of NBD in the catalyst causes short induction periods and high hydrogenation

rates. Hence, the fastest reaction rate obtained in absence of a chiral modifier indicates that the metallic sites neighboured by two NBD configurations are more active than the modified catalytic sites. Decreasing DIOP/Rh molar ratio to 0.5:1 could affect the stability of the metal atoms by creating additional complications due to the formation of hydroxo complexes, which could explain the better catalytic activity obtained upon increasing the molar ratio to 1:1. On the other hand, the dramatic drop in DMI conversion upon increasing DIOP/Rh molar ratio to 5:1 could be ascribed to metal leaching caused by excessive coordination (Hanfan and Guoping 1993). Gampp (1987) pointed out that if ligand to metal ratio is too large, precipitation of the ligand or of a complex may occur, hence affecting the catalytic activity of the system. Conducting the reaction in absence of ligand (on the catalyst) does not show enantiomeric enhancement (Figure 4.5), confirming that a chiral molecule is necessary for the generation of modified catalytic sites responsible of the production of a given enantiomer. For the other DIOP/Rh molar ratios, the enantioselectivities displayed by the catalysts did not significantly change with the conversion level, although it was affected by the DIOP/Rh molar ratio as shown in Figure 4.5. Urbina *et al*. (2010) claimed that increasing ligand to metal molar ratio could decrease the metal particle size. As a result, the ligand remaining linked to the metal surface also increases but not in the right position. Consequently, the metal surface should lie parallel to the aromatic ring, leading to a decrease in the *ee*.
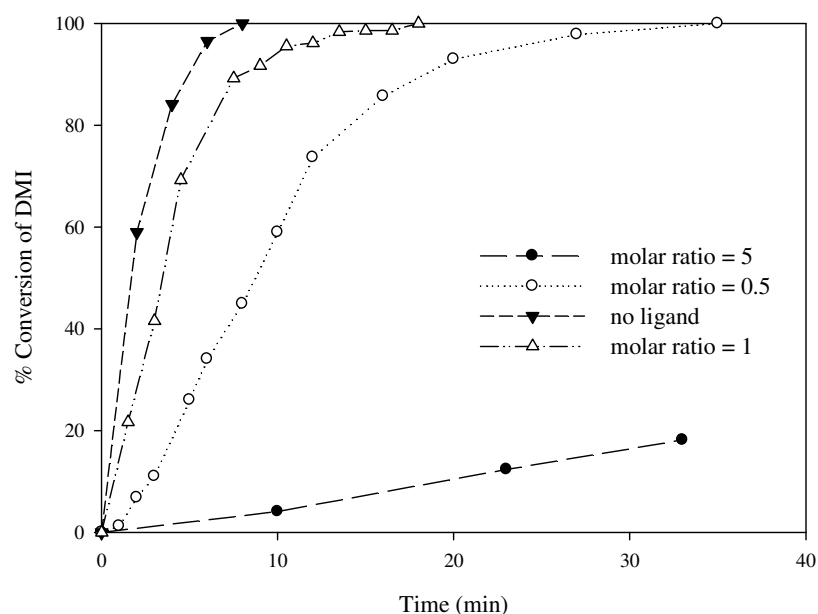
Figure 4.4. Effect of ligand/catalyst molar ratio upon DMI conversion. Conditions: room temperature, 1 atm, hydrogen pressure: 2 bar, liquid and gas flow rates: 40 ml min $^{-1}$, solvent: 50%$_{v/v}$ MeOH in water, S/C molar ratio: 9.
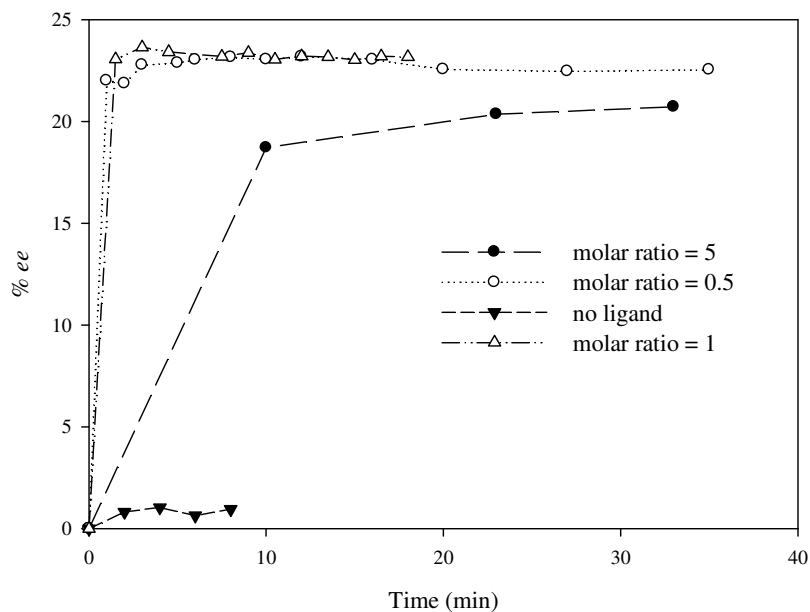
Figure 4.5. Effect of ligand/catalyst molar ratio upon *ee*. Conditions: : room temperature, 1 atm, hydrogen pressure: 2 bar, liquid and gas flow rates: 40 ml min $^{-1}$, solvent: 50%$_{v/v}$ MeOH in water, S/C molar ratio: 9.

Even though the obtained *ee* values are moderate, which confirms the difficulty of this reaction to induce chirality, they are not too far from the best reported values (0.4 – 29.6%)

for (S,S)-DIOP ligand in the hydrogenation of itaconates (Sento *et al*. 1999). Tang and Zhang

(2003) reported that DIOP itself only provides moderate to good enantioselectivities in

asymmetric hydrogenation of dehydroamino acid derivatives and that its applications in

highly enantioselective asymmetric hydrogenation have rarely been disclosed. They pointed

out that a possible reason is that the seven-membered chelate ring of DIOP metal complex is

conformationally flexible which could be responsible for its low efficiency. To rigidify the

conformational flexibility of DIOP ligand, several rigidified DIOP-type ligands have been

developed. Li and Zhang (2000) and Yan and RajanBabu (2000) have independently reported

the development of DIOP by introducing two alkyl substituents at α positions of the

diphenylphosphine groups (Figure 4.6). It was found that the (S,R,R,S)-DIOP provides

excellent enantioselectivity in Rh-catalyzed hydrogenation of arylenamides, whereas its

isomeric ligand (S,S,S,S)-DIOP provides much lower enantioselectivity. It is believed that

the two methyl groups of (S,R,R,S)-DIOP are oriented at pseudoequatorial positions in the

"effective" conformer of the DIOP metal complex, which help in stabilizing it, therefore

promoting high enantioselectivity. However, its isomeric ligand (S,S,S,S)-DIOP has two

methyl groups at pseudoaxial positions which destabilize the " effective" conformer and

hence lead to diminished *ee's* (Tang and Zhang, 2003) as shown in Figure 4.6.
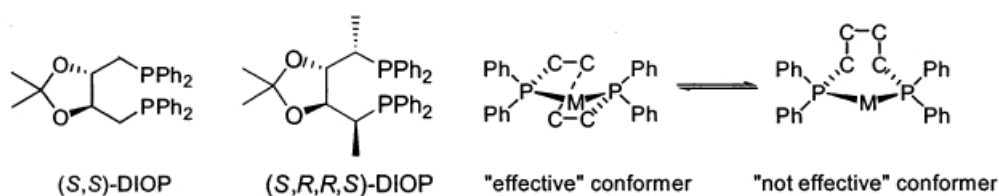
Figure 4.6. Modification of DIOP ligand to rigidify its conformational flexibility (Tang and Zhang, 2003).

The fact that all the above optimisation efforts for (S,S)-DIOP ligand display almost no

change in the *ee* values for the reactions, with all maxima close to 23%, was a major

incentive for studying the influence of ligand type, as reported in the following sections.

4.6 Influence of ligand

Certain classes of ligands are enantioselective over a wide range of different reactions. These ligands are called "privileged chiral ligands". Most of these ligands are C_2-symmetrical, possess a rigid structure and are bidentate ligands. The presence of a C_2-symmetrical axis in a catalyst can reduce the number of possible competing diastereomeric transition states (Whitesell, 1989). This can have a beneficial effect on the enantioselectivity due to the possible elimination of less-selective pathways. However, the reason why a C_2-symmetrical ligand should be superior to a C_1-symmetrical ligand is far from straightforward. In some cases, a C1-symmetrical ligand can give better enantioselectivities than the corresponding C2-symmetrical ligand (Pfaltz and Drury, 2004).

Fabrello *et al*. (2010) stated that bidentate diphosphine ligands coordinated to the metal centre play a major role in homogeneous catalysis since they allow the adjustment of both the steric and electronic features of the catalysts. For example, this approach has found intensive application in homogeneous hydrogenation reaction of alkenes, enamides and ketones (De Vries, 2007). However, the weak point of the design of these chelating phosphorous-containing ligands is that it is difficult to anticipate the control of the activity and the selectivity of all the species involved in the catalytic process (Fabrello *et al*. 2010).

Various techniques have been evolved to probe the stereo-electronic properties of a metal complex, and the most widely used method is to record the IR frequency of the corresponding CO analog (Tolman, 1977). Tolman (1977) used this method to quantify the electronic and steric effects of phosphine ligands via measuring and comparing the CO-stretching frequency on a common metal fragment such as $Ni(CO)_3$. Based on same reference, Tolman (1977) extracted a transferable electronic parameter called *Tolman electronic parameter (TEP).*

Similarly, IR data for *cis*-[Mo(CO)$_4$(diphosphine)] were introduced for describing bidentate phosphine electronic effects, and found to correlate very well with the *TEP*.

Fabrello *et al*. (2010) reported that the monitoring of carbonyl stretching frequency has been proven to be an efficient tool for ranking stereo-electronic effects of diphosphine ligands. However, it has been only recently shown that this approach failed to clearly discriminate between the donor properties of some chiral diphosphine ligands (DIOP, BINAP and MeDUPHOS) largely employed in catalysis. Diphosphine ligands donor properties are defined as their affinity to the Rh centre via ligand exchange reaction. Fabrello *et al*. (2010) reported a systematic ^{103}Rh NMR study on representative rhodium cationic [Rh(diene)(diphosphine)]$^+$ complexes bearing bidentate DIOP, BINAP and MeDUPHOS ligands. Unlike the IR methodology, their technique represented a very powerful tool to access the global electronic and steric contribution of the ligands, and particularly diphosphines, on the metal centre. After validation of this technique for DIOP, BINAP and MeDUPHOS, the following order of donor properties was extracted: MeDUPHOS > DIOP > BINAP.

The above study clearly highlights the enhanced donor ability of the MeDUPHOS with respect to DIOP, compared to the one of DIOP with respect to BINAP. Fabrello *et al*. (2010) also proposed the following trend on the basis of the metal-diphosphine binding strength: MeDUPHOS > DIOP > BINAP. These findings are expected to influence the charge distribution on the metal and the atoms directly linked to it, and thus could explain the remarkable performance of the MeDUPHOS ligand in the hydrogenation of alkenes. Consequently, in this work, the catalyst precursor complex, [Rh((R,R)-Me-DuPhos)(COD)]BF$_4$, which is a proven catalyst for this reaction, was immobilised on the ion exchange resin DOWEX 50WX2, and used in the reactions under the previously optimized

reaction conditions: room temperature, 1 atm, hydrogen pressure: 2 bar, liquid and gas flow rates: 40 ml min $^{-1}$, solvent: 50%$_{v/v}$ MeOH in water, S/C molar ratio: 9.

To assess the efficiency of the immobilization, a comparison was drawn with the homogenous reaction in the shake-flask reactor under same conditions. From these results, a base case was then established which served as a basis for further optimisations. In the shake-flask reactor, the optimum agitation speed was determined and the substrate to catalyst ratio was optimized. Comparisons were then drawn between DMI conversion and *ee* obtained from both the shake-flask and the trickle-bed reactors. To achieve optimum conditions in the recirculating mode in the TBR, the catalyst loading and substrate to catalyst ratio were optimized.

4.7 Reactions in the shake-flask reactor

4.7.1 Base case

Reactions conducted in lab-scale shake-flask reactor were taken as base cases for comparison with the TBR; an initial substrate to catalyst ratio of 30 was selected as a basis for optimisation. The influence of solvent upon DMI conversion and *ee* was investigated homogeneously using the catalyst precursor complex [Rh ((R,R)-Me-DuPhos)(COD)]BF$_4$. From the results shown in Table 4.4, it can be seen clearly that the best DMI conversion and *ee* were obtained with 50%$_{v/v}$ MeOH in water solvent. The superior performance of this solvent could be explained by DMI adsorption and H$_2$ solubility effects described earlier.

Run	Solvent	Time (h)	% Conversion	% ee
1	MeOH	1	30	100
2	EtOH	1	38	84
3	50%v/v MeOH in water	1	100	96

Table 4.4. Influence of solvent upon DMI conversion and *ee* for reactions conducted homogeneously in the shake flask reactor. Conditions: In 15 ml solvent, 20 ^{o}C temperature, atmospheric pressure, 24 mg of catalyst precursor complex, substrate to catalyst molar ratio: 30, H_2 flow of 100 ml min^{-1} and shaking speed of 200 rpm.

The reaction was then conducted heterogeneously by immobilizing 24 mg of catalyst precursor complex onto 1 g of the ion exchange resin DOWEX 50WX2. As can be seen in Figure 4.7, the reaction achieved 97% conversion of DMI and 88% *ee* in about 3h. The expected decrease in the catalytic activity of the immobilized complex compared to the homogenous one is believed to be due to some diffusional limitations to and within the catalyst inside the pores of the resins. De Vos *et al*. (2000) reported that this type of weakness is inherent to heterogeneous catalysts and represents a special challenge for both academia and industry.
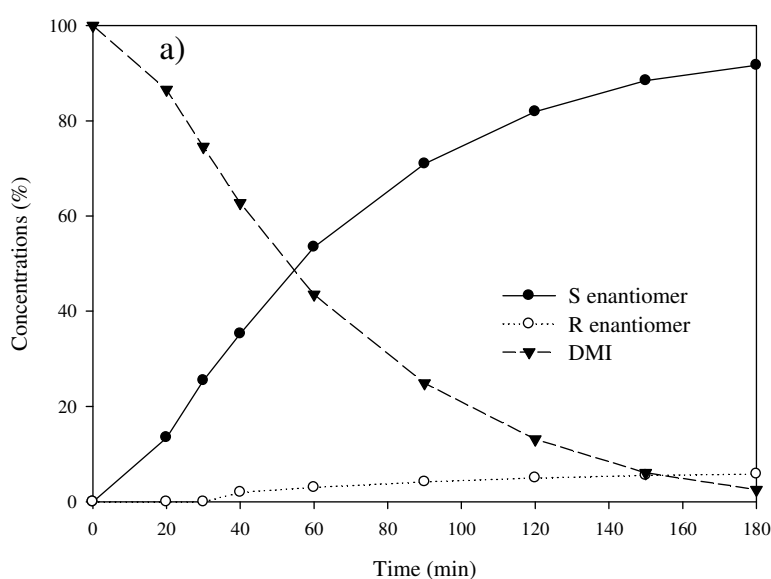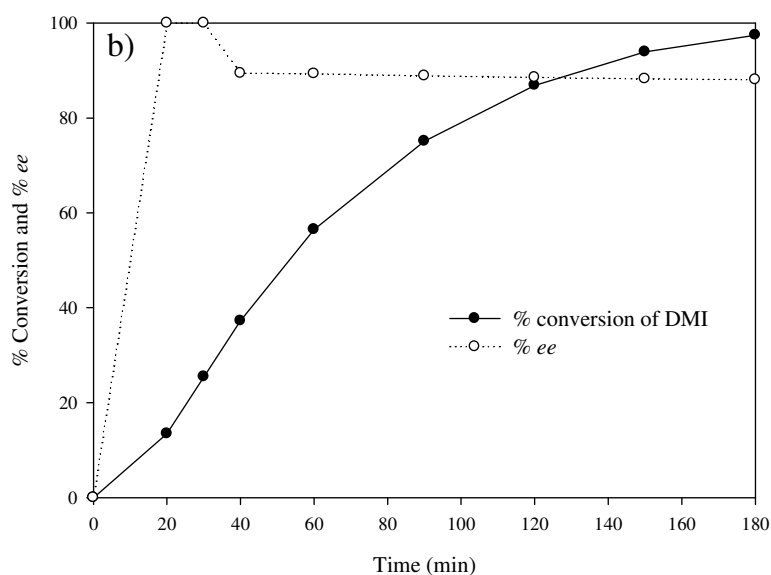
Figure 4.7. Results from the reaction catalyzed by [Rh ((R,R)-Me-DuPhos)(COD)]BF$_4$ immobilised into ion exchange resin in the shake flask reactor. Conditions: In 15 ml solvent, 20 °C temperature, atmospheric pressure, 24 mg of catalyst precursor complex, substrate to catalyst molar ratio: 30, H$_2$ flow of 100 ml min^{-1} and shaking speed of 175 rpm. a) Profiles of reaction components. b) Conversion of DMI and *ee* profiles.

The rotational speed (rpm) of the agitator affects mixing and thus mass transport between gas-liquid and liquid-solid. This was quantified in terms of the dependence of initial reaction rate on the speed of agitation. The results obtained from testing different agitation speeds are shown in Table 4.5 and the influence upon initial reaction rate is plotted in Figure 4.8. As shown in Table 4.5 and Figure 4.8, the initial reaction rate increased with an increasing speed of agitation up to 250 rpm, after which it was independent of agitation speed. Therefore, all experiments were conducted at 250 rpm to eliminate external particle mass transfer resistance as a limiting factor for the immobilized catalyst. Referring back to Table 4.5, the TOF increased with increasing speed of agitation from 17 h^{-1} at 175 rpm up to 30 h^{-1} at 250 and 300 rpm. Table 4.7 demonstrates also that the agitation speed influences not only reaction rate and TOF, but also had a profound effect upon the enantioselectivity. Over the range of agitation speeds studied, the enantioselectivity increased from 88 to 99.9%. Investigations of the interplay between gas-liquid mass transfer and other rate processes, as well as methods

146

for determining the rate-controlling step, have been discussed extensively using a wide range of catalytic applications as an example (Paul, 1988). However, the influence of these concepts on enantioselectivity in complex organic reactions has been brought to light only recently (Sun, 1996). The improved enantioselectivities associated with the increased agitation speeds indicate that hydrogen availability to the catalyst could play a role in determining the enantioselectivity of the reaction. Marked shifts in enantioselectivity in the asymmetric hydrogenation of several prochiral substrates were observed as a function of the availability of hydrogen to the catalyst in both heterogeneous and homogeneous catalytic reactions (Sun *et al*. 1996; Berger *et al*. 2001; Pestre *et al*. 2006).

Run	Speed of agitation (rpm)	Initial reaction rate *	% Conversion	TOF (h^{-1})	% *ee*
4	175	0.0007	97	17	88
5	200	0.0012	100	27	99.9
6	250	0.0017	100	30	99.9
7	300	0.0017	100	30	99.9

Table 4.5. Influence of speed of agitation in the shake-flask reactor with the immobilized catalyst. Conditions: In 15 ml solvent ($50\%_{v/v}$ MeOH in water), 20 ^{o}C temperature, atmospheric pressure, 24 mg of catalyst precursor complex, substrate to catalyst molar ratio: 30, H_2 flow of 100 ml min^{-1}. * mol DMI l^{-1} min^{-1} ;calculated after 25 min from the start of the reaction.
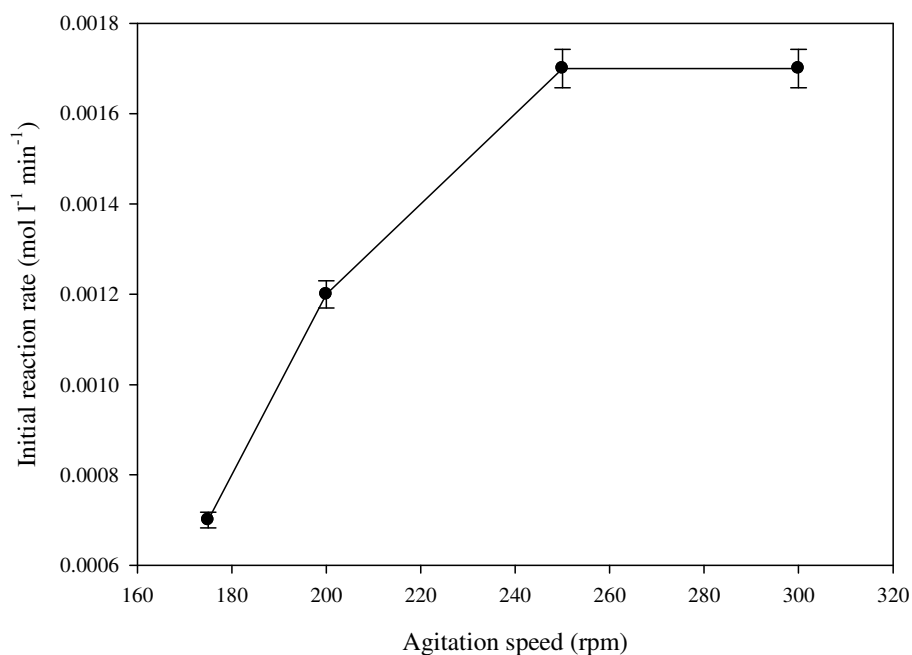
Figure 4.8. Effect of speed of agitation on initial reaction rate in the shake-flask reactor with the immobilized catalyst. Conditions: In 15 ml solvent (50%$_{v/v}$ MeOH in water), 20 ^{o}C temperature, atmospheric pressure, 24 mg of catalyst precursor complex, substrate to catalyst molar ratio: 30, H$_2$ flow of 100 ml min^{-1}.

4.7.2 Influence of the substrate concentration

The optimum TOF of 30 h^{-1}, achieved with the immobilized catalyst [Rh ((R,R)-Me-DuPhos)(COD)]BF$_4$, was relatively low and therefore optimisation of the TOF in the current study was carried out by changing the DMI concentration, with substrate to catalyst ratios of 60 and 113 as shown in Table 4.6. To further elucidate the impact of the substrate to catalyst ratio upon the TOF and *ee*, a lower substrate to catalyst ratio of 15 was also incorporated in the study. As can be seen in Table 4.6, the initial reaction rate increased by more than 10 folds upon increasing the substrate to catalyst ratio from 15 to 30. However, the initial reaction rate remained unaffected (at about 0.001 mol l^{-1} min^{-1}) when the substrate to catalyst molar ratio was increased to 60. Further increase in the substrate to catalyst ratio to 113 decreased the initial reaction rate significantly to 0.0003 mol l^{-1} min^{-1}. Moreover, the increase in the initial reaction rate was accompanied by a slight improvement in the TOF, from 5 h^{-1} at

substrate to catalyst ratio of 15 to about 38 h^{-1} at substrate to catalyst ratio of 60. However, doubling the substrate to catalyst ratio to 113 led to a substantial drop in the TOF to 8 h^{-1}. It is noteworthy that over the range of the studied substrate to catalyst ratios, the enantioselectivity maintained a high value of about 99.9%.

Run	DMI concentration	Substrate/catalyst molar ratio (TON)	Initial reaction rate*	Time (min)	% Conversion	TOF (h^{-1})	% ee
8	0.04	15	0.00009	120	71	5	99.9
6	0.08	30	0.001	60	100	30	99.9
9	0.16	60	0.001	90	89	38	99.9
10	0.30	113	0.0003	120	11	8	99.9

Table 4.6. Results from testing different concentrations of DMI in the shake-flask reactor. Conditions: In 15 ml solvent (50%$_{v/v}$ MeOH in water), 20 ^{o}C temperature, atmospheric pressure, 24 mg of catalyst precursor complex, agitation speed of 250 rpm.
* mol DMI l^{-1} min^{-1} ; calculated at 10% conversion of DMI.

4.7.3 Effect of homogenous and heterogeneous reactions

Due to the relatively low TOFs observed with the immobilized catalyst [Rh ((R,R)-Me-DuPhos)(COD)]BF$_4$, a reaction was carried out homogenously in the shake-flask reactor for the purpose of comparing the effectiveness of both catalyst phases at the optimized agitation speed. For consistent comparison, the homogeneous reaction was carried out under the same conditions as those quoted in Table 4.6 and using a substrate to catalyst ratio of 60. The results of the comparison are shown in Table 4.7 and Figure 4.9. As expected, the reaction rate and hence TOF of the homogenous reaction were higher than the reaction conducted with the immobilized catalyst. Despite the noticeable swelling of the ion-exchange resin into the mixed solvent (50%$_{v/v}$ MeOH in water), it is believed that the superior performance of the homogeneous catalyst was due to the larger surface area provided as well as the restricted mass transport inside the polymer beads, hence offering limited active-site accessibility.

Run	Reaction phase	Initial reaction rate*	Time (min)	% Conversion	TOF (h^{-1})	% ee
11	Homogeneous	0.005	60	100	60	97
9	Heterogeneous	0.001	90	89	38	99.9

Table 4.7. Comparison of homogeneous and heterogeneous reactions in the shake-flask reactor. Conditions: In 15 ml solvent ($50\%_{v/v}$ MeOH in water), 20 ^{o}C temperature, atmospheric pressure, 24 mg of catalyst precursor complex, substrate to catalyst ratio of 60 and agitation speed of 250 rpm. * mol DMI l^{-1} min^{-1} ; calculated after 20 min from the start of the reaction.
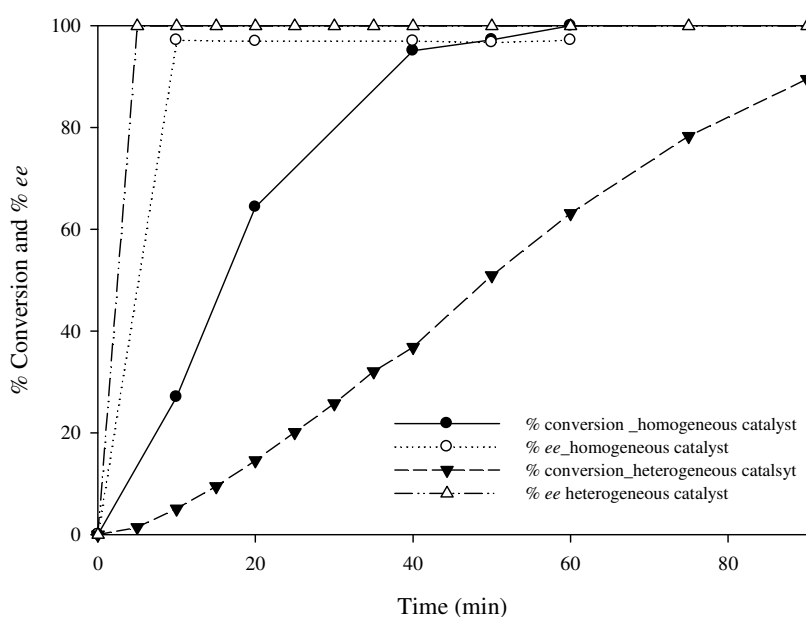
Figure 4.9. Comparison of DMI conversion and *ee* profiles for the homogeneous and heterogeneous reactions in the shake-flask reactor. In 15 ml solvent ($50\%_{v/v}$ MeOH in water), 20 ^{o}C temperature, atmospheric pressure, 24 mg of catalyst precursor complex, agitation speed of 250 rpm.

4.8 Reactions in the trickle bed reactor (TBR)

In this section results for the TBR using [Rh ((R,R)-Me-DuPhos)(COD)]BF$_4$ catalyst immobilized on 50WX2-100 ion exchange resin are presented and compared with those obtained in the shake flask reactor. Thereafter optimisation of catalyst loading and kinetic modelling of reactions in the TBR are presented.

In the TBR, liquid and gas flow rates were both set at the previously optimized flow rates of 40 ml min^{-1}, based on Baker flow map in order for the reaction to fall in the trickle flow

regime (Ramachandran and Chaudhari, 1983). Table 4.8 shows a comparison between the trickle-bed reaction at these conditions and the results from the shake-flask. A comparison of DMI conversion and *ee* profiles from both reactors is also presented in Figure 4.10. As can be seen in Table 4.8, the initial reaction rate and eventually the TOF were higher in the shake-flask reactor compared to the TBR. A significant drop in the *ee* was also observed in the trickle-bed reactor, 78% compared to 99.9% in the shake-flask reactor. The difference in reaction rates could be due to the suspension of the catalyst particles in the shake-flask resulting in higher interparticle diffusion and hence a more efficient utilization of the catalyst. Frequent problems in packed bed reactors such as non-uniform flow distribution with flow channelling could have caused concentration gradients affecting the performance of the TBR (Nedovic and Willaert, 2004).

Run	Reactor	Initial reaction rate*	Time (min)	% Conversion	TOF (h^{-1})	*% ee*
6	Shake-flask	0.0016	60	100	30	99.9
16	Trickle-bed	0.0012	120	75	17	78

Table 4.8. Comparison of DMI conversion and *ee* in the shake-flask and trickle-bed reactors. In 15 ml solvent (50%$_{v/v}$ MeOH in water), 20 ^{o}C temperature, atmospheric pressure, 24 mg of catalyst precursor complex, substrate to catalyst ratio: 30, in the shake-flask: agitation speed of 250 rpm, in the TBR: liquid and gas flow rates: 40 ml min $^{-1}$. * mol DMI l^{-1} min^{-1}; calculated after 20 min from the start of the reaction.
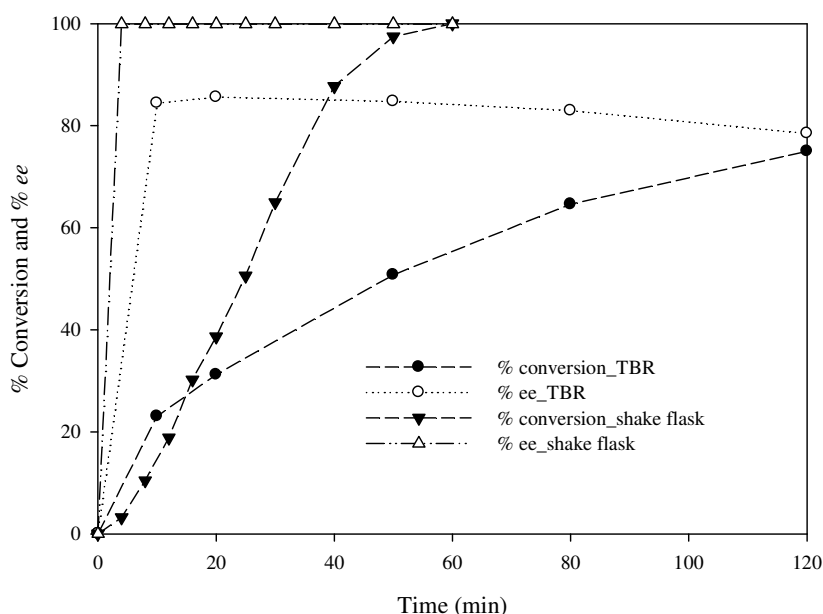
Figure 4.10. Comparison of DMI conversion and *ee* profiles in the shake-flask and trickle-bed reactors. In 15 ml solvent ($50\%_{v/v}$ MeOH in water), 20 ^{o}C temperature, atmospheric pressure, 24 mg of catalyst precursor complex, substrate to catalyst ratio: 30, in the shake-flask: agitation speed of 250 rpm, in the TBR: liquid and gas flow rates: 40 ml min $^{-1}$.

4.8.1 Effect of catalyst loading

In order to achieve the optimum complex to support ratio in the catalyst bed, two different catalyst loadings upon the support were tested in the TBR and the results are summarized in Table 4.9. A comparison between the DMI conversion and *ee* is presented in Figure 4.11. As can be seen in Table 4.9, a conversion of 75% with 78% *ee* was achieved when a catalyst loading of 0.024 g complex/g of support was used. However, when the loading was decreased to 0.012 g complex/g of support, 98% conversion with 95% *ee* was obtained with more than a double increase in reaction rate.

The effect of catalyst loading can be explained by the *site isolation theory* presented by Pugin (1996). Isolated sites are those attached to the support in sufficiently low density that they do not interact with each other, and thus are able to maintain their activity and selectivity. In contrast, if the complexes are packed onto the support too densely, they have a strong tendency to react irreversibly with each other, forming dimers that are no longer active.

152

Pugin (1996) developed a mathematical rate model on these bases which matched very well

with their experimental data.

Run	Catalyst loading (g complex/g support)	Initial Reaction rate[*]	% Conversion	% ee	Time (min)
16	0.024	0.0012	75	78	120
17	0.012	0.0027	98	95	60

Table 4.9. Optimizing catalyst bed by testing different catalyst loadings. In 15 ml solvent (50%$_{v/v}$ MeOH in water), 20 ^{o}C temperature, atmospheric pressure, 1 g of support, concentration of DMI: 0.08M, liquid and gas flow rates: 40 ml min $^{-1}$. *mol DMI l^{-1} min^{-1}; calculated after 20 min from the start of the reaction.
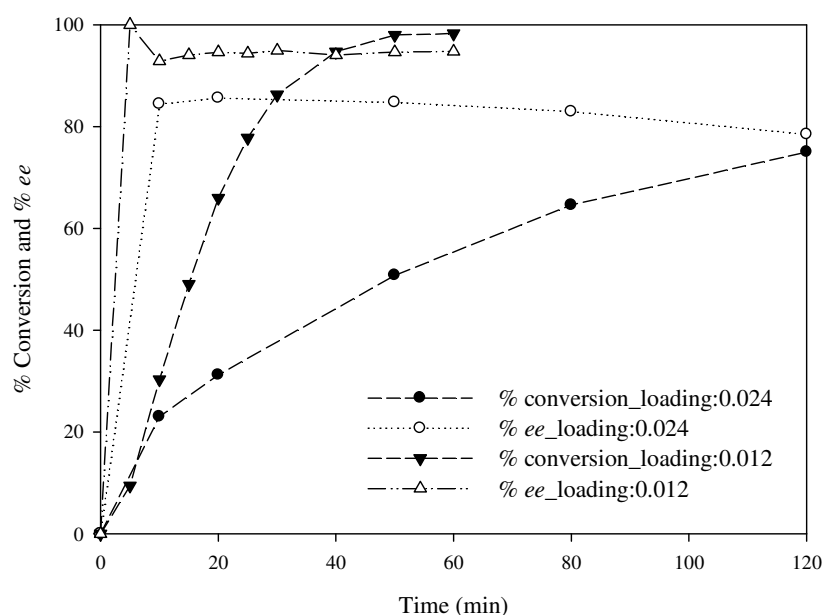
Figure 4.11. Optimizing catalyst bed by testing different catalyst loadings. In 15 ml solvent (50%$_{v/v}$ MeOH in water), 20 ^{o}C temperature, atmospheric pressure, 1 g of support, concentration of DMI: 0.08M, liquid and gas flow rates: 40 ml min $^{-1}$.

4.8.2 Influence of the substrate concentration

As was performed for the shake-flask reactor, it is desirable to increase the TOF with regard

to possible commercial application for the ion exchange resin. Different concentrations of

DMI were investigated in order to optimize the TOF using substrate to catalyst ratios of 26,

60, 121, 227, 500 and 1000 as shown in Table 4.10. In addition, the catalyst was re-used by

performing a second reaction with the same catalyst to assess if any loss of activity was

observed. The recyclability tests were conducted for the lowest two ratios of 26 and 60. For a substrate to catalyst ratio of 26, a dramatic drop in catalyst activity was observed when going from first to second cycle which was also accompanied by a substantial drop in the *ee*, from 94 to 26%. On the other hand, recycling the catalyst for a substrate to catalyst ratio of 60 had less detrimental impact upon catalyst activity and enantioselectivity. For this ratio, the initial reaction rate dropped to third its initial value, with a halving of DMI conversion and TOF, while *ee* decreased from 95 to 90%.

Possible reasons for catalyst deactivation are polarity of solvent, catalyst poisoning and adsorption of reactants and/or products into the catalyst. Simons *et al*. (2004) studied the influence of polarity of solvent on Rh leaching during the enantioselective hydrogenation of DMI over [Rh ((R,R)-Me-DuPhos)(COD)]BF_4 catalyst in an autoclave reactor. The catalyst was immobilized by straightforward ion exchange, using a three-dimensional mesoporous aluminosilicate (AlTUD-1). In their study, leaching of Rh showed a significant dependence on the polarity of the solvent in which the catalysis was performed. The highest leaching of Rh (15 – 23%) experienced with methanol could be overcome by switching to less polar solvents. With the less polar 2-propanol as solvent, leaching of Rh could be reduced by a factor of 6. It was believed that this could be due to the increasing ability to stabilise species with increasing polarity of solvent. They concluded that methanol has the capability to stabilise both cations and anions, explaining the large leaching of Rh experienced with this solvent.

Barbaro (2006) reported that despite their potential to be reused up to 5-15 times with constant *ee* in each cycle, asymmetric hydrogenation catalysts immobilized into ion-exchange resins may suffer from a significant decrease of the reaction rates in the second and following cycles. In his review article, Barbaro (2006) also stated that a loss of catalytic activity after the first cycle is invariably displayed by the supported catalysts regardless of the resin type or

the ligand nature. It was hypothesised that the decrease in the reaction rate after recycling could be due to a stronger binding interaction between the sulfonate groups from the resin and the rhodium centres after the first hydrogenation step.

Therefore, a Sheldon test was performed in this study to investigate Rh leaching into the solution (Lempers and Sheldon, 1998). The reaction liquors of the first and second cycles were put in two separate flasks. Then, an amount of DMI that gave the corresponding substrate to catalyst ratio was added to the solution and reaction was started by bubbling hydrogen through. After running reactions for about an hour, no changes in the products concentrations were observed, and hence it was concluded that no catalytically active complex could have leached from the support. Another possible reason for deactivation may be partial oxidation of the catalyst precursor complex due to some inevitable exposure to air during sampling for GC analysis.

Table 4.10 and Figure 4.12 also show that reaction rate increased proportionally with increasing substrate to catalyst ratio up to 227, after which it decreased slightly for substrate to catalyst ratio of 500 before plummeting to almost quarter of its highest value at the highest substrate to catalyst ratio of 1000. The TOF also increased with increasing substrate to catalyst ratio to reach its highest value of 330 h^{-1} at a ratio of 500, before demonstrating an abrupt decrease at the highest ratio of 1000 as shown in Figure 4.12. The decrease in initial reaction rate observed at substrate to catalyst ratios higher than 227 could be caused by the substantial coverage of the rhodium surface by DMI, leading to reduction of the number of available sites for hydrogen to adsorb and react. Considering that the reported initial reaction rates were calculated after 20 min from the start of the reaction, the highest TOF achieved with a substrate to catalyst ratio of 500 could be due to the higher number of available DMI molecules to react afterwards once more active sites become available, while excessive coverage of the active catalytic sites by DMI at the highest substrate to catalyst ratio of 1000

155

could severely restrict hydrogen accessibility thus diminishing TOF. At the conditions

implemented in the TBR, the wetting efficiency of the catalyst bed was calculated to be 0.99

based on a correlation developed by Julcour-Lebigue *et al*. (2009).

Run	DMI concentration (mol l^{-1})	Substrate/catalyst molar ratio	Cycle	Initial reaction rate*	% Conversion	TOF (h^{-1})	% *ee*
18	0.035	26	1	0.0011	98	25	94
			2	0.00008	10	3	26
19	0.08	60	1	0.0027	98	59	95
			2	0.0009	47	20	90
20	0.16	121		0.0056	100	121	96
21	0.3	227		0.0096	100	227	99.9
22	0.662	500		0.0076	96	330	95
23	1.324	1000		0.0027	14	110	90

Table 4.10. Results from testing different concentrations of DMI in the TBR. In 15 ml solvent (50%$_{v/v}$ MeOH in water), 20 °C temperature, atmospheric pressure, 1 g of support, 0.012 g complex/g support, liquid and gas flow rates: 40 ml min $^{-1}$. * mol DMI l^{-1} min^{-1}; calculated after 20 min from the start of the reaction.
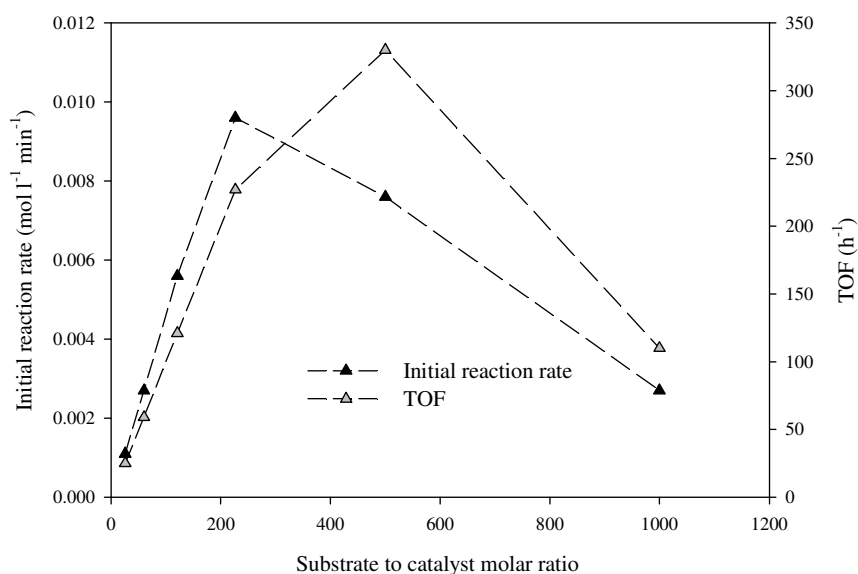
Figure 4.12. Effect of substrate to catalyst molar ratio upon initial reaction rate and TOF in the TBR. In 15 ml solvent (50%$_{v/v}$ MeOH in water), 20 °C temperature, atmospheric pressure, 1 g of support, 0.012 g complex/g support, liquid and gas flow rates: 40 ml min $^{-1}$.

4.8.3 Kinetics

Since the reaction between DMI and hydrogen is a bimolecular reaction involving the catalyst complex immobilised upon the catalyst surface, possible kinetic schemes must allow for the formation of intermediate complexes between these reactants and the catalyst surface. Table 4.10 shows a strong dependence of the initial reaction rate on the substrate concentration, suggesting that the substrate concentration has a significant effect on the rate. However the possible role of hydrogen concentration upon the rate of the insertion step must also be considered. The dependence of the rate on the substrate concentration and on the contact between the catalyst and the substrate are reflected on the kinetic model introduced by Osborn *et al*. (1966) and is shown in Figure 4.13 below.
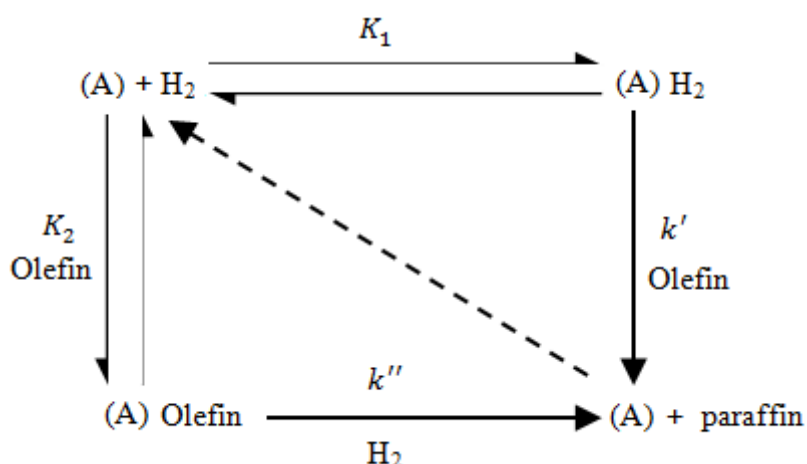
Figure 4.13. Osborn – Wilkinson Catalytic Cycle (Osborn *et al*. 1966).

The rate determining step in this model can be either one or both of two possible paths: (1) attack of uncomplexed olefin on the dihydrido-complex at the vacant site giving a transition state in which both hydrogen and olefin are bound to the metal; (2) attack of molecular hydrogen on the olefin complex leading to the same transition state.

The rate according to the mechanism of Figure 4.13 can be expressed by the following equation (Osborn *et al*. 1966):

$$R = -\frac{d[S]}{dt} = \frac{(k'K_1 + k''K_2)p[S][A]}{1 + K_1p + K_2[S]} \qquad (4.2)$$

Although this kinetic model is valid for a dissolved complex in liquid phase, its resemblance

to Langmuir-Hinshelwood and Eley-Rideal kinetic models proposed for heterogeneous

catalysts (Fogler, 1999, Rode *et al*. 2006), was the incentive for utilizing it in this work. The

assumed elementary steps for the above model are also incorporated in Langmuir-

Hinshelwood kinetics, which involve adsorption, surface reaction and desorption phenomena

for reactions involving either single- or dual-site mechanisms (Fogler, 1999). Accordingly,

equation (4.2) was regressed to the experimental data at four different initial DMI

concentrations using the least squares method. A solver function of MS Excel software was

used to minimize the sum of the squares of the difference between experimental and

predicted points for DMI concentrations simultaneously. A constraint was imposed that the

rate and equilibrium constants must be greater than or equal to zero. The fit of the

experimental results to model curves is shown in Figure 4.14. A comparison between the

experimental and modelled initial reaction rates is also provided in Figure 4.15. Table 4.11

shows the corresponding fitted values of the constants in equation (4.2). As can be seen in

Table 4.11, the value of the equilibrium constant K_1 is greater than that of K_2 by a factor of

1.6, meaning that the formation of the dihydrido-complex is favoured. The finding is in

agreement with reported findings for the catalytic hydrogenation of DMI in a biphasic

cyclohexane-water system and in a [Triton X-100/1-pentanol]/cyclohexane/water

microemulsion using the water-soluble catalyst complex Rh-TPPTS (Milano-Brusco *et al*.

2008). Although their obtained values for K_1, 1460 and 1570 l mol^{-1}, are close to the value

for K_1 obtained in this work (1552 l mol^{-1}) , their obtained values for K_2 are significantly

lower than that predicted in this work. The relatively high value of K_2 in this work, together

with the very low value of k'' indicates that the olefin complex could not activate molecular hydrogen. Osborn *et al.* (1966), using RhCl(PPh$_3$)$_3$ homogeneous catalyst, obtained the same conclusion after investigating the effect of the admission of hydrogen on the colour of a benzene solution containing the olefin(ethylene)-complex, and the effect of the reversed procedure, which is the admission of the olefin into a benzene solution containing the dihydrido-complex. In the former case, the solution maintained its bright yellow colour, which is a hallmark of the olefin complex. In the latter case, admission of ethylene resulted in a small rapid absorption and the solution again assumed the yellow colour of the olefin complex. Therefore, it was concluded that this was an indication that the olefin complex could not activate molecular hydrogen and hence in their kinetic studies k'' was assumed to be zero. However, the value obtained for k'' in this work, although very low, was not zero designating some activation of molecular hydrogen which might be due to the nature of the immobilised catalyst complex giving different interactions with hydrogen molecules. Moreover, this could also be a result of the high value of the equilibrium constant K_2 shifting the reaction toward path (2). The presumed high adsorption of DMI into the catalyst surface, as well as into the vacant sites of the ion exchange resin, could lead to diminished uncomplexed DMI, resulting in low value of k' as shown in Table 4.11.

Figure 4.14. Fit of the kinetic model represented by eq 4.2 to experimental concentration vs time profiles of the hydrogenation of DMI in the TBR. In 15 ml solvent (50%$_{v/v}$ MeOH in water), 20 ^{o}C temperature, atmospheric pressure, 1 g of support, 0.012 g complex/g support, liquid and gas flow rates: 40 ml min $^{-1}$.
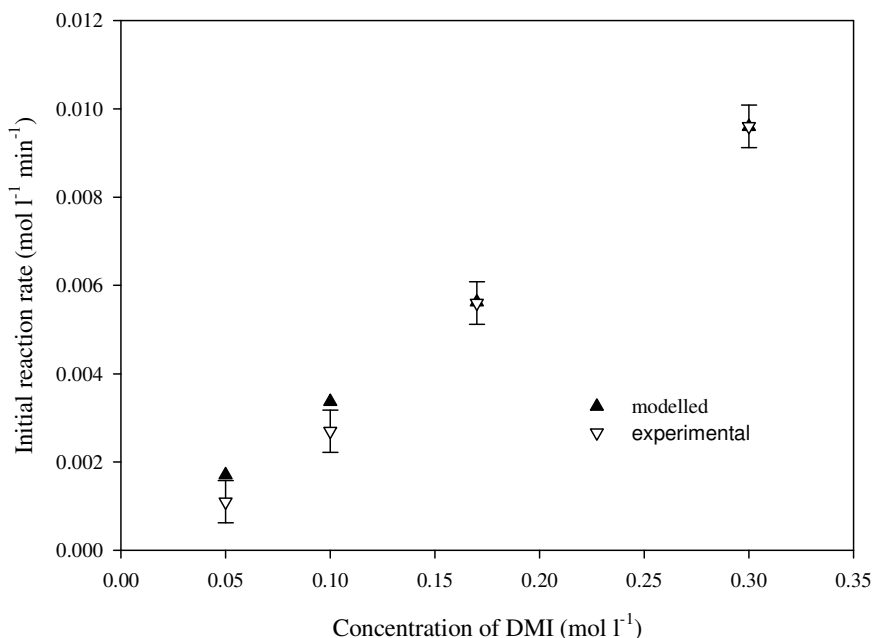
Figure 4.15. Fit of the kinetic model represented by eq 4.2 to experimental initial reaction rates of the hydrogenation of DMI in the TBR. In 15 ml solvent (50%$_{v/v}$ MeOH in water), 20 ^{o}C temperature, atmospheric pressure, 1 g of support, 0.012 g complex/g support, liquid and gas flow rates: 40 ml min $^{-1}$.

k'/l mol^{-1} s^{-1}	k''/ l mol^{-1} s^{-1}	K_1/l mol^{-1}	K_2 / l mol^{-1}
83	2	1552	959

Table 4.11. Rate and equilibrium constants for the hydrogenation of DMI in the TBR. Values of constants were predicted using excel solver.

4.9 Conclusion

The results show that ion-exchange resins can be an ideal support for the development of heterogenized asymmetric catalysts suitable for easy recycling along with clear economical and environmental benefits. The complex [Rh (NBD){(S,S)-DIOP}]BF$_4$ has shown to provide promising results in terms of reaction rate but not enantioselectivity. By using 50% mixture of methanol and water as a solvent, the highest reaction rate with full conversion have been achieved.

The enantioselective hydrogenation of DMI, over [Rh (COD){(R,R)-Me-DuPHOS}]BF$_4$ supported on 50WX2-100 ion-exchange resins, can be successfully carried out in a trickle bed reactor to produce dimethyl (S)-(-)-methylsuccinate. Under optimized conditions in the TBR, the catalyst gave high enantioselectivity of 99.9% and TOF of 330 h^{-1}, with results comparable to those obtained in shake-flask reactor. The experimental data could be fitted well by means of a kinetic model based on the Osborn-Wilkinson reaction mechanism. Applying Osborn-Wilkinson kinetics to the reaction indicated that complexation with the hydrogen before reaction with the olefin was the preferred path.

CHAPTER 5

ENANTIOSELECTIVE HYDROGENATION OF DIMETHYL ITACONATE OVER

{Rh (COD)[(R,R)-Me-DuPHOS]}BF$_4$ SUPPORTED ON ALUMINA

5.1 Introduction

In this chapter, the catalytic hydrogenation of dimethyl itaconate (DMI) was studied in lab-scale shake flask and transferred to continuous flow with recirculation in a trickle bed reactor (TBR). The catalyst complex [Rh((R,R)-Me-DuPhos)(COD)]BF$_4$ was anchored to powder and trilobe alumina supports using phosphotungstic acid (PTA) as an anchoring agent. For the powder alumina, tests were conducted in the shake flask to ensure that the reaction was not influenced by mass transfer limitations by varying the stirrer speed (§5.2.1) and catalyst mass (§5.2.3), thus ensuring the reported data are in the kinetic regime. In the shake flask, the substrate to catalyst molar ratio was optimized (§5.2.2) and the concentration profiles of DMI were fitted according to Osborn-Wilkinson kinetic expression (§5.2.4). §5.2.5 compares the effectiveness of the trilobe alumina with the alumina powder in the shake-flask reactor. The TBR was operated in the trickle flow regime using the trilobe support. In the TBR, the effect of catalyst loading (g complex/ g support) and substrate to catalyst molar ratio were discussed in §5.3.1 and §5.3.2. In §5.3.2, the concentration profiles of DMI were fitted according to Osborn-Wilkinson kinetic expression. §5.3.3 discusses the influence of hydrodynamics in the TBR upon conversion of DMI and enantioselectivity of reaction, followed by conclusions §5.4.

5.2 Reactions in the shake-flask reactor

5.2.1 Base case

Reactions conducted in lab-scale shake-flask reactor were taken as base cases for comparison with the TBR; an initial substrate to catalyst ratio of 9 was selected as a basis for optimisation (Table 5.1). At this condition, a TOF of about 9 h^{-1} and *ee* of 97% were obtained. The rotational speed (rpm) of the agitator affects mixing and thus mass transport between gas-liquid and liquid-solid. This was quantified in terms of the dependence of initial reaction rate on the speed of agitation. As shown in Figure 5.1, the initial reaction rate increased with an increasing speed of agitation up to 200 rpm, after which it was independent of agitation speed. Therefore, all experiments were conducted at 200 rpm to eliminate external particle mass transfer resistance as a limiting factor for the powdered catalyst. The impact of other mass transfer resistances upon the results is discussed in §5.2.3.

Run	DMI concentration (mol l^{-1})	Substrate/catalyst molar ratio	Initial reaction rate[a]	% Conversion	TOF (h^{-1})	% *ee*
14	0.01	9	0.0003	97	9	97
16	0.03	26	0.0011	98	25	96
17	0.08	61	0.0021	99.9	60	96
18	0.16	122	0.0023	100	99	97
19	0.26	196	0.0028	33	45	94
20	0.412	311	0.0014	19	31	93

Table 5.1. Results from testing different concentrations of DMI in the shake-flask reactor with powdered immobilised catalyst. In 15 ml ethanol, 20 °C temperature, atmospheric pressure, 20 µmol of catalyst precursor complex, H$_2$ flow of 100 ml min^{-1} and shaking speed of 200 rpm.
[a] mol DMI / (l of solution · min);calculated after 10 minutes from the start of the reaction.
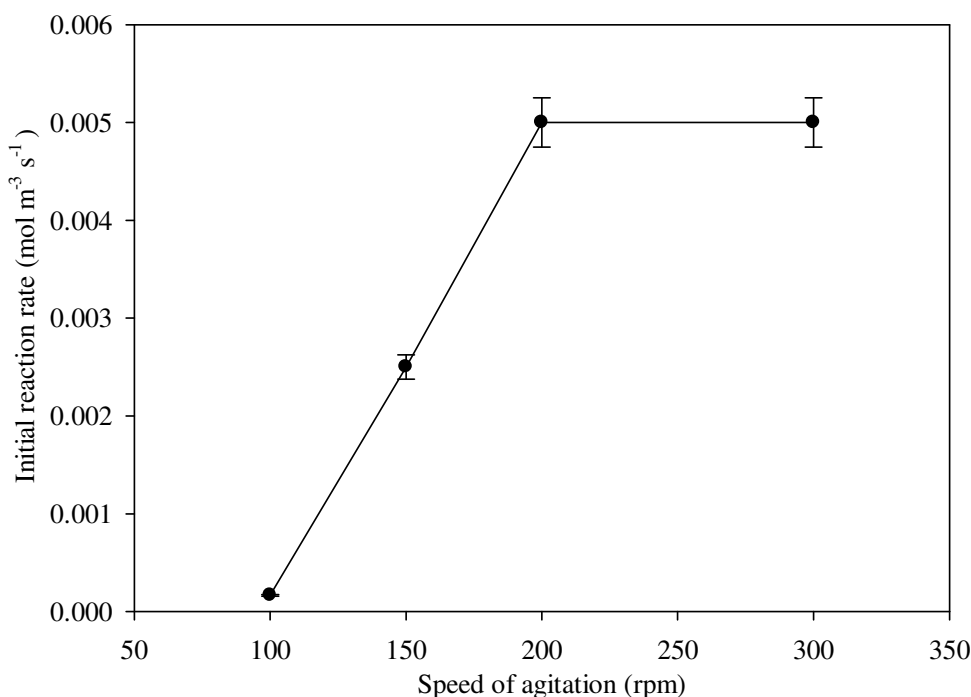
Figure 5.1. Effect of speed of agitation on initial reaction rate in the shake-flask reactor with powdered immobilised catalyst. Conditions: In 15 ml ethanol, 20 ^{o}C temperature, atmospheric pressure, H$_2$ flow of 100 ml min^{-1}, 20 µmol (20 × 10^{-6} mol) of catalyst precursor complex, substrate to catalyst ratio : 9.

5.2.2 Influence of the substrate concentration

The TOF of 9 h^{-1} was relatively low compared with the values of 4000-7000 h^{-1} reported by Augustine *et al*. (2004), and the values of 2000-19000 h^{-1} reported by Brandts and Berben (2003). However, these high TOFs were achieved by conducting reactions in an autoclave at H$_2$ pressures between 3.3 × 10^5 and 6.6 × 10^5 Pa and/or temperatures of up to 323.15 K, whilst the results presented here were taken at ambient conditions. Higher pressures and temperatures would be expected to increase H$_2$ solubility in the liquid phase as well as increasing the rate of reaction.

In order to scale up such processes for application in industry it would be desirable to achieve high TOFs, such as observed by Augustine *et al*. (2004) and Brandts and Berben (2003). However in practice issues concerning catalyst stability, deactivation pathways, reaction

kinetics and mass transfer effects could each play a part in causing a lower TOF to be observed. This chapter systematically investigates these effects in order to elucidate the limitations of carrying out enantioselective hydrogenations in the shake-flask and trickle bed reactor and suggests possible ways in which they may be overcome.

Among several methods of immobilising catalyst complexes upon a support, each may have advantages and disadvantages. The catalysts used by Brandts and Berben (2003) were prepared following a procedure in which the cationic metal – precursor [Rh(COD)$_2$]BF$_4$ was first immobilised into γ-alumina followed by a modification of (R,R)-MeDuPHOS. Brandts and Berben (2003) claim that such immobilisation tends to give better reproducibility results in terms of activity and leaching stability. However the method of Augustine in which the catalytic species is attached to the support through the metal atom of the complex via a heteropoly acid as the anchoring agent offers the advantage that it does not lead to modification of the chiral ligand. Thus the immobilised ligand is expected to have the same functionality as the homogeneous complex, resulting in a high enantioselectivity as was observed in the base case of 97 % *ee* in this work.

Augustine *et al*. (2004) pointed out that many previously reported asymmetric hydrogenations were carried out at substrate to catalyst ratios (turnover numbers (TONs) with all of the reaction going to completion) near 100 and therefore an important goal is to increase the ratio to values which are more commercially significant. They reported with TONs in the range 1000-50000, together with a high rate or TOF (Augustine *et al*. 2004). TOFs are expected to vary with the reaction TONs and thus the substrate concentration. Therefore optimisation of the TOF in the current study was carried out by changing the DMI concentrations. The results, given in Table 5.1 for the powder alumina support, show that the initial reaction rate increased with increasing concentration of DMI. The rate reached its maximum at a substrate to catalyst ratio of 196 after which it dropped to half this value at

substrate to catalyst ratio of 311. For substrate to catalyst ratios between 9 and 122 the *ee* was 96 - 97% and dropped to ~94% at the highest substrate to catalyst ratios of 196 and 311. It is noteworthy that the optimum turnover frequency (TOF) of 99 h^{-1} (2.8 × 10^{-2} s^{-1}) is still quite low when compared to the above reported literature values, but nevertheless the optimisation shows an order of magnitude improvement.

5.2.3 Determination of mass transfer effects

Due to the relatively low TOFs observed, investigations were carried out to determine whether the reaction is limited by external mass transfer at the catalyst particle or diffusional limitations within the catalyst pores.

Figure 5.2 shows a plot of C_i/R_A versus $1/m$, and according to the straight line form of equation (3.2) the value of the gas bubble resistance r_b was determined from the intercept and the catalyst resistance r_{cr} from the slope of the line. The catalyst resistance incorporates combined resistance to internal diffusion, reaction, and external diffusion. From Figure 5.2 it can be deduced that the catalyst resistance was greater than the gas bubble resistance at the conditions implemented in the reactions, since the line passes almost through the origin, showing negligible value of the intercept. Since the external mass transfer resistance was already determined to be negligible in § 5.2.1, the role of internal mass transfer resistance in the catalyst pores was evaluated by calculating the internal effectiveness factor, which was estimated for the trilobe from the expression for a spherical catalyst particle (Fogler, 1999):

$$\eta = \frac{3}{\phi_1^2} \left(\phi_1 \coth \phi_1 - 1 \right) \tag{5.1}$$

Where for a cylindrical catalyst pellet:

$$\phi = (R/2) \sqrt{k_1 \, S_a \, \rho_c / D_e} \qquad (5.2)$$

In calculating the value of the Thiele Modulus, ϕ, the intrinsic rate constant was taken from the value determined for powder supported catalyst, which is not subject to internal diffusion limitation. The value of the effectiveness factor for the pellets, η was found to be in the range 0.98 – 1, and therefore the catalyst is not subject to internal diffusion limitations. Consequently, under the experimental conditions employed, all diffusional resistances (inter particle and intra particle) are not rate limiting and therefore it was possible to detect true kinetics from the experimental observations.
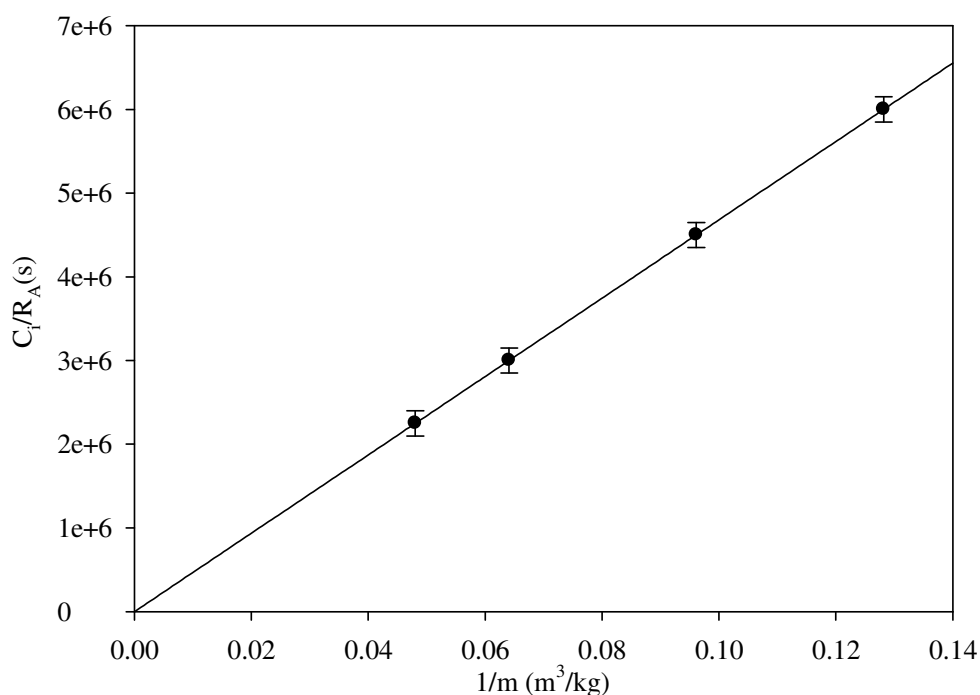
Figure 5.2. Effect of catalyst mass: Plot to delineate controlling resistance in the shake-flask reactor with powdered immobilised catalyst. Conditions: In 15 ml ethanol, 20 $^{\circ}$C temperature, atmospheric pressure, H$_2$ flow of 100 ml min^{-1}, shaking speed of 200 rpm and 0.08 mol l^{-1} of DMI.

5.2.4 Kinetics

As was performed for the catalyst complex [Rh((R,R)-Me-DuPhos)(COD)]BF$_4$ supported on 50WX2-100 ion-exchange resins (Chapter 4, § 4.8.3), it was desirable to fit Osborn – Wilkinson Catalytic Cycle (Figure 4.13) to DMI concentration profiles obtained in § 5.2.2. Accordingly, equation (4.2) was regressed to the experimental data at four different initial DMI concentrations using the least squares method. The fit of the experimental results to model curves is shown in Figure 5.3. Table 5.2 shows the corresponding fitted values of the constants in equation (4.2).

As can be seen in Table 5.2, the value of the equilibrium constant K_2 is much greater than that of K_1, meaning that the formation of the olefin complex is favoured. Osborn *et al*. (1966), using RhCl(PPh$_3$)$_3$ homogeneous catalyst, obtained the same conclusion after investigating the effect of the admission of hydrogen on the colour of a benzene solution containing the olefin(ethylene)-complex, and the effect of the reversed procedure, which is the admission of the olefin into a benzene solution containing the dihydrido-complex. In the former case, the solution maintained its bright yellow colour, which is a hallmark of the olefin complex. In the latter case, admission of ethylene resulted in a small rapid absorption and the solution again assumed the yellow colour of the olefin complex. Therefore, it was concluded that this was an indication that the olefin complex could not activate molecular hydrogen and hence in their kinetic studies k'' was assumed to be zero. The finding is in agreement with that found for the catalytic hydrogenation of DMI in a biphasic cyclohexane-water system and in a [Triton X-100/1-pentanol]/cyclohexane/water microemulsion using the water-soluble catalyst complex Rh-TPPTS (Milano-Brusco *et al*. 2008). However, the value obtained for k'' in this work, although very low, was not zero designating some activation of molecular hydrogen which might be due to the nature of the immobilised catalyst complex giving different interactions with hydrogen molecules. Moreover, this could also be a result of the high value

of the equilibrium constant K_2 shifting the reaction toward path (2). The presumed high adsorption of DMI into the catalyst surface, as well as into the vacant sites of powder alumina support, could lead to diminished uncomplexed DMI, resulting in zero value of k' as shown in Table 5.2.
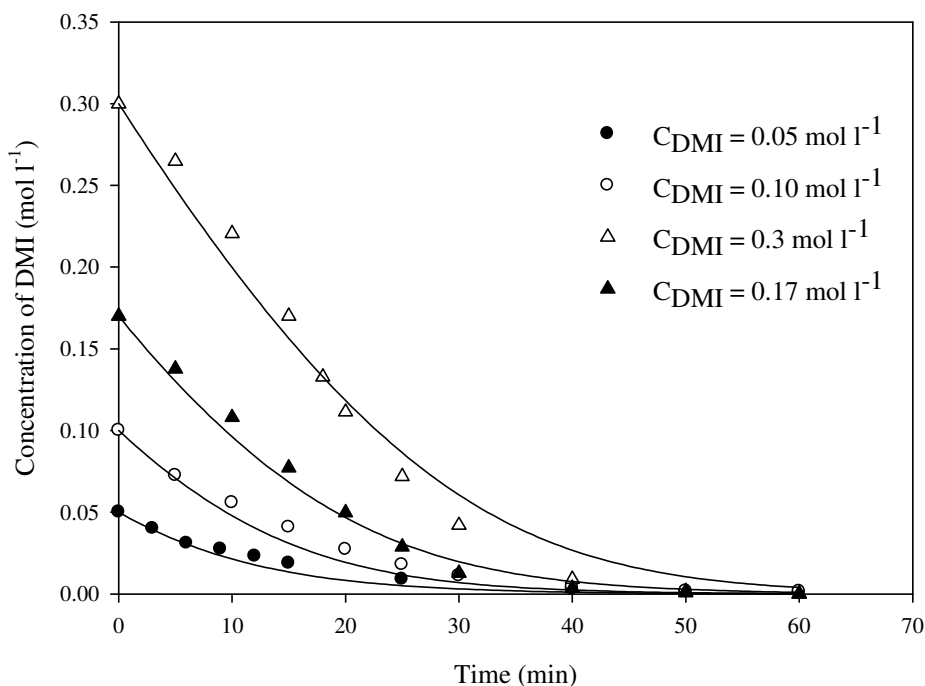

Figure 5.3. Fit of the kinetic model represented by equation (4.2) to experimental concentration vs time profiles of the hydrogenation of DMI in the shake-flask reactor. Conditions: In 15 ml ethanol, 20 $^{\circ}$C temperature, atmospheric pressure, H$_2$ flow of 100 ml min^{-1}, shaking speed of 200 rpm and 20 µmol (20×10^{-6} mol) of catalyst precursor complex.

	k'/l mol^{-1} s^{-1}	k''/ l mol^{-1} s^{-1}	K_1/l mol^{-1}	K_2 / l mol^{-1}
Shake-flask reactor	0	1.26×10^{-3}	201	196×10^3
TBR	0	2.46×10^{-3}	943	196×10^3

Table 5.2. Rate and equilibrium constants for the hydrogenation of DMI in the shake-flask and trickle-bed reactors. Values of constants were predicted using excel solver.

5.2.5 Influence of the type of support

For the purpose of comparing the effectiveness of the trilobe alumina with the alumina powder, a reaction was carried out in the shake-flask reactor using [Rh((R,R)-Me-DuPhos)(COD)]BF$_4$ immobilised onto trilobe alumina and the results are shown in Figure 5.4 and Table 5.3. As expected, the reaction rate when the complex was immobilised onto powder alumina was higher than when it was immobilised onto trilobe alumina. This could possibly be attributed to mass transfer limitations in the pellets as well as the larger surface area provided by powder alumina particles, offering BET surface areas of 258 m^2 g^{-1} for the powder compared with 149 m^2 g^{-1} for trilobe, as shown in Table 3.2.

The experiments conducted in the shake-flask reactor made it possible to assess the efficiency of the implemented immobilisation procedure under well controlled conditions. Furthermore, the optimized TON and TOF serve as a basis for comparisons with the TBR.
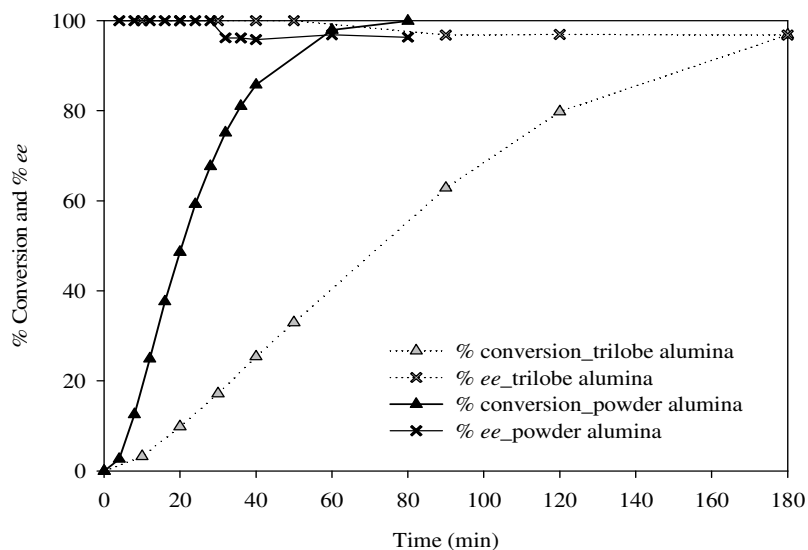
Figure 5.4. Conversion of DMI and *ee* profiles for the reaction catalyzed by [Rh(Me-DuPhos)(COD)]BF$_4$ immobilised into powder and trilobe alumina in the shake-fask reactor. Conditions: In 15 ml ethanol, 20 °C temperature, atmospheric pressure, H$_2$ flow of 100 ml min^{-1}, shaking speed of 200 rpm, 20 µmol (20 × 10^{-6} mol) of catalyst precursor complex and substrate/ catalyst ratio: 60.

Run	support	Surface area (m^2 g^{-1})	Initial reaction rate[a]	% Conversion	% ee	Time (min)
21	Powder alumina	258	0.00192	99.9	96	72
25	Trilobe alumina	149	0.0009	97	97	180

Table 5.3. Comparison of powder and trilobe alumina supports in the shake-flask reactor. In 15 ml ethanol, 20 ^{o}C temperature, atmospheric pressure, substrate/ catalyst ratio:60, 20 µmol (20 × 10^{-6} mol) of catalyst precursor complex, H$_2$ flow of 100 ml min^{-1} and shaking speed of 200 rpm.
[a] mol DMI / (l of solution · min).

5.3 Reactions in the trickle bed reactor (TBR)

In this section results for the TBR are presented and compared with those obtained in the shake flask for powder and pellets. Thereafter kinetic modelling of reactions in the TBR and optimisation of hydrodynamic conditions are presented.

Depending on the gas and liquid flow rates and the physical properties of the liquid, various flow regimes may exist in the TBR. Consequently, knowledge of this is important in understanding the hydrodynamics and mass transfer characteristics.

At low liquid rate, the flow pattern is defined as 'trickling', where the liquid trickles over the packing in a laminar flow. As a result, liquid and gas flow rates were selected based on Baker flow map for the reaction to fall in the trickle flow regime (Figure 5.5). Figure 5.6 shows a comparison between the trickle-bed reaction at these conditions and the results from the shake-flask. After 16 min reaction time, the initial reaction rates in the trickle-bed and shake-flask reactors were 0.0017 mol l^{-1} min^{-1} and 0.0019 mol l^{-1} min^{-1}, respectively. Although the initial reaction rate was faster in the shake-flask reactor, both reactors achieved high conversions of > 99% and ee of ~96% after 70 minutes. The difference in reaction rates could be due to the suspension of the catalyst particles in the shake-flask resulting in higher intraparticle diffusion and hence a more efficient utilization of the catalyst. Frequent problems in packed bed reactors such as non-uniform flow distribution with flow channelling

could have caused concentration gradients affecting the performance of the TBR (Nedovic and Willaert, 2004).
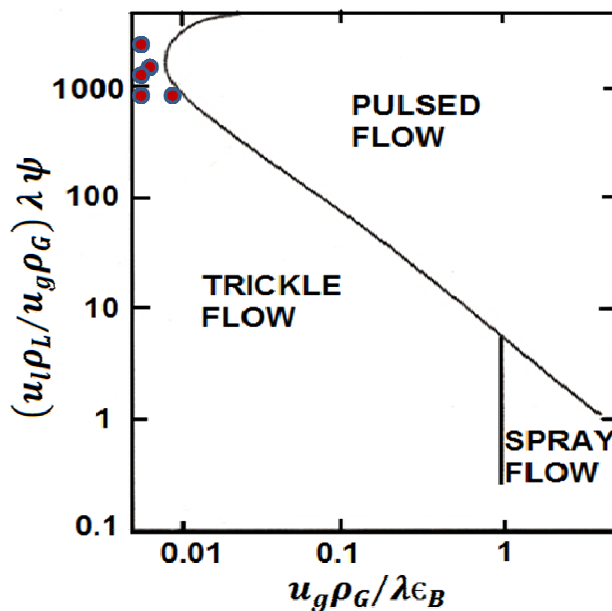
Figure 5.5. The correspondence of the TBR operating conditions in Baker's flow map.
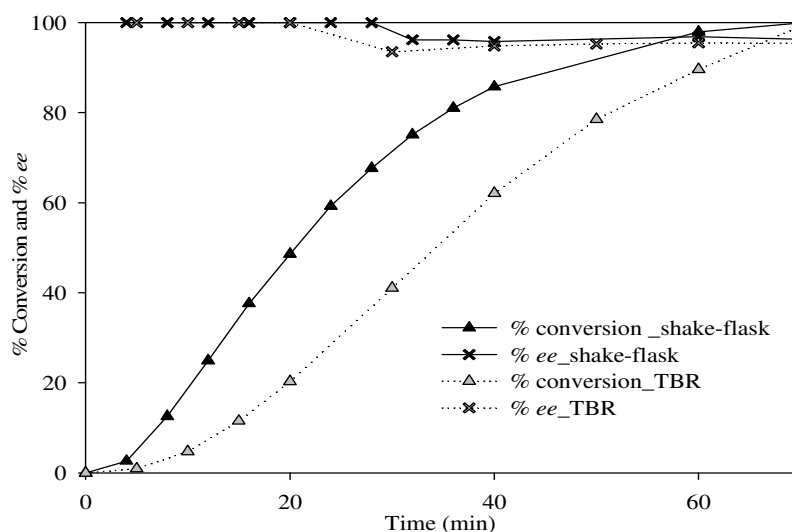
Figure 5.6. Comparison of DMI conversion and *ee* profiles in the shake-flask and trickle-bed reactors. Conditions: In 15 ml ethanol, 20 °C temperature, atmospheric pressure, H$_2$ flow of 100 ml min^{-1}, shaking speed of 200 rpm, 20 µmol (20 × 10^{-6} mol) of catalyst precursor complex and substrate/ catalyst ratio: 60.

5.3.1 Effect of catalyst loading

In order to achieve the optimum complex to support ratio in the catalyst bed, two different catalyst loadings upon the support were tested in the TBR and the results are summarized in Table 5.4. A conversion of 70% with 80% *ee* was achieved when a catalyst loading of 12.2×10^{-3} g complex/g support was used. However, when the loading was decreased to 4.4×10^{-3} g complex/g support, 99% conversion with 95% *ee* was obtained with more than four-fold increase in reaction rate.

As reported in Chapter 4, the effect of catalyst loading can be explained by the *site isolation theory* presented by Pugin (1996). Isolated sites are those attached to the support in sufficiently low density that they do not interact with each other, and thus are able to maintain their activity and selectivity. In contrast, if the complexes are packed onto the support too densely, they have a strong tendency to react irreversibly with each other, forming dimers that are no longer active. Pugin (1996) developed a mathematical rate model on these bases which matched very well with their experimental data.

Run	Catalyst loading (g complex/g support)	Initial Reaction rate[a]	% Conversion	% *ee*	Time (min)
24	12.2×10^{-3}	0.0004	70	80	330
25	4.4×10^{-3}	0.002	99	95	70

Table 5.4. Optimizing catalyst bed by testing different catalyst loadings. In 15 ml ethanol, 20 $^{\circ}$C temperature, atmospheric pressure, 1.3×10^{-3} mole DMI, H$_2$ flow of 100 ml min^{-1} and liquid flow of 20 ml min^{-1}. Complexes were immobilised onto 2.7 g of trilobe alumina support.
[a] mol DMI / (l of solution $\cdot$ min).

5.3.2 Influence of the substrate concentration

As was performed for the powder support, it is desirable to increase the TON and TOF with regard to possible commercial application for the trilobes. Different concentrations of DMI were investigated in order to optimize these parameters using substrate to catalyst ratios of

85, 128, 179 and 223 as shown in Table 5.5. In addition, the catalyst was re-used by performing up to three reactions with the same catalyst to assess if any loss of activity was observed. The recyclability tests were conducted for the lowest and highest substrate to catalyst ratios implemented in this study. For a substrate to catalyst ratio of 85, a slight decrease in initial reaction rate and conversion when going from first to second cycle was observed while *ee* was maintained at about 96%. However, when going from second to third cycle, the initial reaction rate plummeted to almost quarter of its initial value accompanied by a substantial drop in conversion, from 97% to 17%, while a very high *ee* of 99.9% was obtained. This very high *ee* is expected for the very low conversion achieved since the decrease in ee with increasing conversion is well known [e.g. Coleman-Kammula and Duim-Koolstra, 1983, Jacobsen *et al*. 2005].

Possible reasons for catalyst deactivation are polarity of solvent, catalyst poisoning and adsorption of reactants and/or products into the catalyst. Brandts *et al*. (2003) focused on the possibility of leaching of the complex from the support when using alcoholic solvents. Leaching of the Rh complexes was found to decrease from MeOH > EtOH > isopropyl alcohol whilst in cyclohexane no leaching was observed (Brandts *et al*. 2003). In this study, a Sheldon test was performed to check for leaching (Lempers and Sheldon, 1998). The reaction liquors of the first and second cycles were separated from the support by filtration. Then, an amount of DMI that gave the corresponding substrate to catalyst ratio was added to the solution and reaction was started by bubbling hydrogen through. After running reactions for about an hour, no changes in the products concentrations were observed, and hence it was concluded that no catalytically active complex could have leached from the support. Another possible reason for deactivation may be partial oxidation of the catalyst precursor complex due to some inevitable exposure to air during sampling for GC analysis.

Table 5.5 also shows that as expected, reaction rate increased with increasing concentration of DMI, as more molecules would be available to occupy the catalytic sites for reaction. The best results were obtained with the highest ratio of 223 giving conversion and *ee* of 99% and 99.9%, respectively. However, there was again a notable loss of activity upon recycling of the catalyst, with a halving of the rate and drop in conversion to 52% while *ee* decreased to 94%. Again, application of the Sheldon test showed no presence of leached active complex.

The Osborn-Wilkinson kinetic equation (4.2) was again fitted to the experimental data obtained from the TBR as shown in Figure 5.7. Rate and equilibrium constants are displayed in Table 5.2. While the value of K_2 is the same for both reactors (Table 5.2), the values of K_1 and k'' obtained for the TBR are larger. This possibly indicates increased complexation of hydrogen with the catalyst, which could be due to a better mixing of gas and liquid at the top of the TBR resulting in more hydrogen molecules available to complex with the catalyst and to attack the olefin-complex.

Run	DMI concentration (mol l^{-1})	Substrate/catalyst molar ratio	Cycle	Initial reaction rate[a]	% Conversion	TOF (h^{-1})	% *ee*
26	0.105	85	1	0.0017	99	85	95
			2	0.0014	97		96
			3	0.0005	17		99.9
27	0.170	128		0.0017	97	82	86
28	0.237	179		0.0019	97	79	87
29	0.300	223	1	0.0026	99	114	99.9
			2	0.0011	52		94

Table 5.5. Results from testing different concentrations of DMI in the TBR. In 15 ml ethanol, 20 °C temperature, atmospheric pressure, 20 µmol (20 × 10^{-6} mol) of catalyst precursor complex supported on 2.7 g of trilobe alumina, H$_2$ flow of 100 ml min^{-1} and liquid flow of 20 ml min^{-1}.
[a] mol DMI / (l of solution · min); calculated after 30 minutes from the start of the reaction.
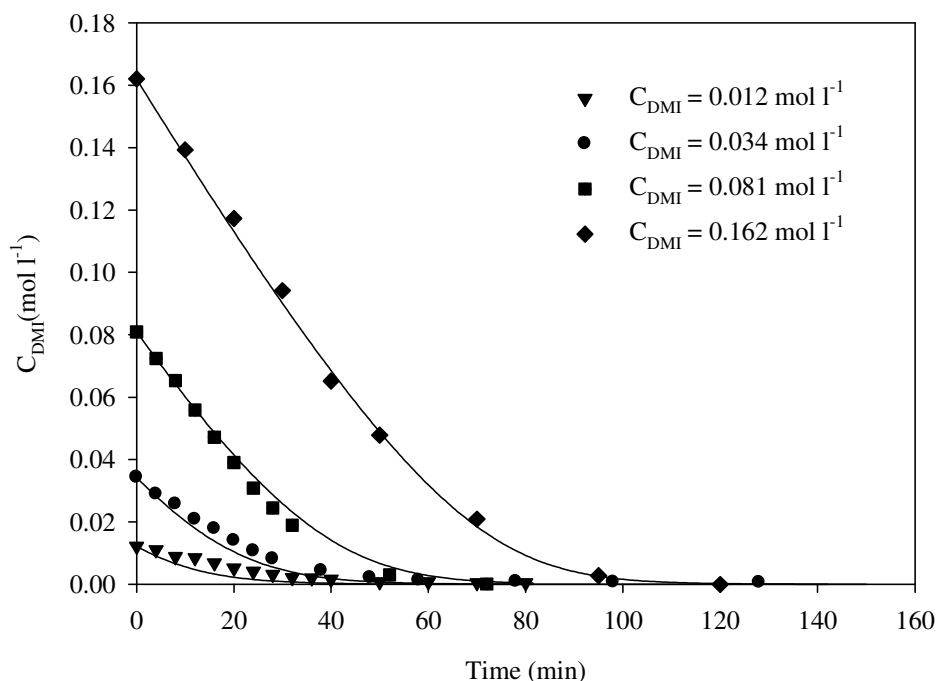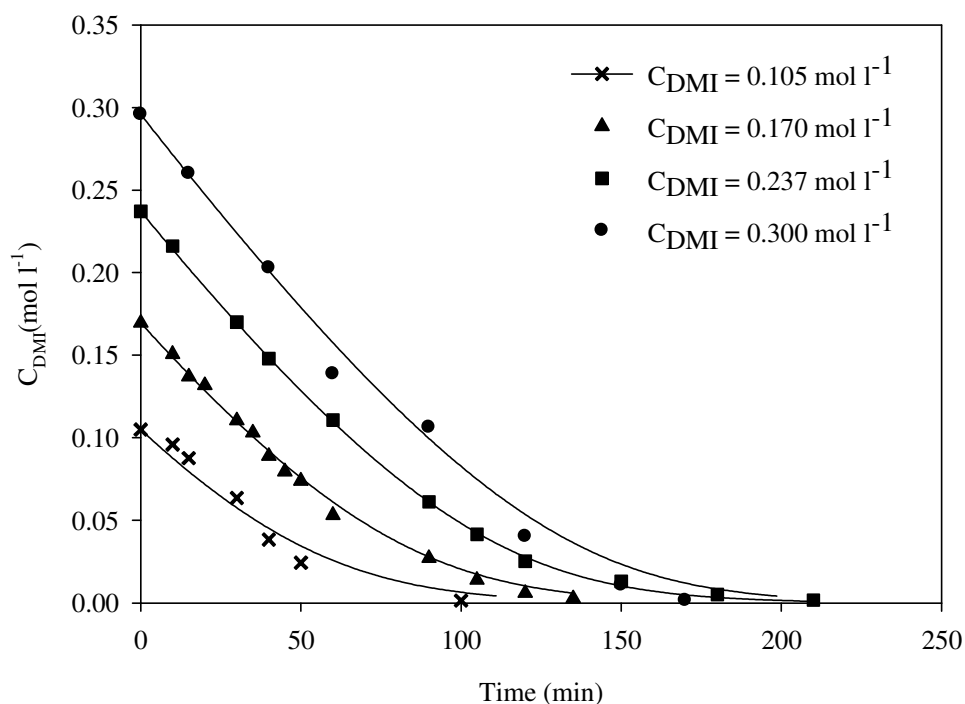
Figure 5.7. Fit of the kinetic model represented by equation (4.2) to experimental concentration vs time profiles of the hydrogenation of DMI in the TBR.

5.3.3 Influence of the hydrodynamics

In the TBR, maintaining effective contact of the gas and liquid with the catalyst active sites becomes a significant design consideration in comparison with the well mixed shake flask reactor. Therefore investigation of the hydrodynamics within the TBR is vital for evaluating the performance of the reactor. A suitable selection of gas and liquid flow rates is crucial when basic phenomena such as wetting efficiency of the catalyst bed and mass transfer are evaluated. Therefore, the effect of gas and liquid flow rates on the rate and selectivity of the reaction is discussed in the following sections.

5.3.3.1 Effect of gas flow rate

The results obtained from testing different gas flow rates are shown in Table 5.6 and the conversion profiles are shown in Figure 5.8. Increasing hydrogen flow from 50 to 100 ml min^{-1} increased both reaction rate and enantioselectivity. However, increasing hydrogen flow

from 100 to 200 ml min^{-1}, although increasing the initial reaction rate, decreased overall reaction rate and led to a decrease in enantioselectivity from 99.9 to 94%. Increasing the gas velocity may have led to a decrease in the thickness of liquid film upon the catalyst due to the drag force of gas flowing through the void space. In turn this could have led to a lower liquid hold up and hence decreased residence time of liquid, which would explain the lower reaction rate. However, it is interesting to observe that as gas flow rate was increased from 100 to 200 ml min^{-1} the flow regime approached pulsed flow (Figure 5.5). Ramachandran and Chaudhari (1983) reported that the transition from trickle to pulse flow is generally characterized by a sharp increase in the root mean square pressure fluctuation for a small increase in gas or liquid flow rate. Owing to the higher interaction between the gas and liquid phases in the pulsing regime some workers have sought to induce pulsing by cycling the liquid feed on and off (Boelhouwer *et al*. 2002, Wilhite *et al*. 2003). Wilhite *et al*. (2003) found that this approach was not effective for a system under mild gas limitation as better performance is achieved in steady flow. In contrast, Boelhouwer *et al*. (2002) found that periodic pulsing operation led to an improvement of 400 % in reaction rate for the hydrogenation of α-methyl styrene. However in the study reported here, it appears that operation in steady flow at lower gas flow rate leads to higher liquid hold up and residence time, in turn giving higher reaction rate and enantioselectivity. Künzle *et al*. (2002) reported that enantioselectivity is influenced by the competitive adsorption of all reaction components and possibly some impurities. Therefore, a general positive or negative correlation between hydrogen flow and enantioselectivity cannot be expected, thus explaining the lower enantioselectivity observed at high gas flow rates in this work.

Run	Liquid flow rate (ml min^{-1})	Gas flow rate (ml min^{-1})	Initial reaction rate[a]	% Conversion	% ee
30	20	50	0.0024	98	87
29	20	100	0.0026	99	99.9
31	20	200	0.0029	97	94
32	10	100	0.0013	96	93
33	15	100	0.0019	96	98
29*	20	100	0.0026	99	99.9

Table 5.6. Effect of gas and liquid flow rates in the TBR. In 15 ml ethanol, 20 ^{o}C temperature, atmospheric pressure, 20 µmol (20 × 10^{-6} mol) of catalyst precursor complex supported on 2.7 g of trilobe alumina, substrate/catalyst molar ratio: 223.
[a] mol DMI / (l of solution · min); [run 29,30 and 31] : calculated after 10 minutes from the start of the reaction; [run 32,33 and 29*]: calculated after 60 minutes from the start of the reaction.
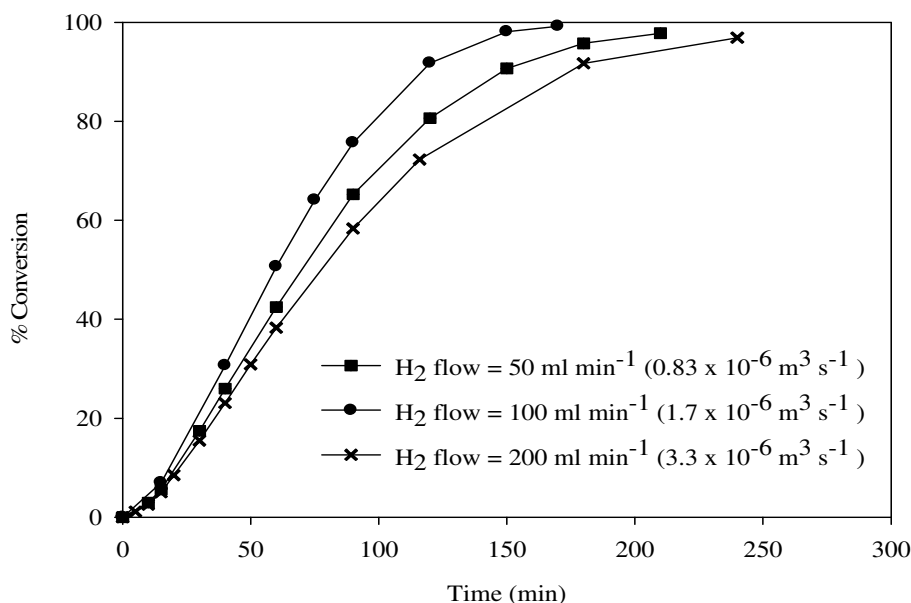
Figure 5.8. Conversion profiles of different gas flow rates in TBR at constant liquid flow rate of 20 ml min^{-1} (3.3 × 10^{-7} m^3 s^{-1}). In 15 ml (15 × 10^{-6} m^3) ethanol, 20 ^{o}C (293.15 K), atmospheric pressure (101317 Pa), 20 µmol (20 × 10^{-6} mol) of catalyst precursor complex supported on 2.7 g of trilobe alumina, substrate/catalyst molar ratio: 223.

5.3.3.2 Effect of liquid flow rate

The results obtained from investigating different liquid flow rates are summarized in Table 5.6 and the conversion profiles are shown in Figure 5.9. The initial reaction rate and

enantioselectivity increased with increasing liquid flow rate with the optimum

enantioselectivity obtained at liquid flow rate of 20 ml min^{-1}.

The wetting efficiencies were calculated based on a correlation developed by Julcour-Lebigue *et al*. (2009):

$$f = 1 - \exp[-1.986 Fr_L^{0.139} Mo_L^{0.0195} {}_B^{-1.55}] \tag{5.3}$$

The correlation uses a bounded function and only three dimensionless groups (liquid Froude and Morton numbers and bed porosity) and has been shown to predict wetting efficiency with very good precision (Julcour-Lebigue *et al*. 2009).

Mass transfer coefficients were calculated using a correlation by Winterbottom *et al*. (1999) for the transport of hydrogen from bulk liquid-to-solid interface:

$$Sh' = 0.266 Re_l^{1.15} Sc^{1/3} \tag{5.4}$$

A value for the diffusivity of hydrogen into ethanol required for calculation of the Sherwood (Sh) and Schmidt numbers (Sc) was obtained using (Coulson and Richardson, 1999):

$$D = (1.173 exp^{-16} \emptyset_B^{0.5} M_B^{0.5} T) / \mu V_A^{0.6} \tag{5.5}$$

The increase in initial reaction rate with liquid velocity could be explained by the improved wetting efficiency and mass transfer coefficient accompanying the increase in liquid superficial velocity as demonstrated in Table 5.7. High liquid velocities in TBRs result in the catalyst particles being completely covered by the liquid reactant, and the gaseous reactant must penetrate the liquid film for the reaction to take place. However, at low liquid velocities,

the surface of the catalyst might not be fully covered by liquid giving a chance for the gaseous reactant to enter into the liquid filled pores through the dry regime without any liquid film resistance. In this case, as the liquid flow rate is increased, the wetting efficiency increases. For gas limited reactions, an increase in wetting efficiency increases the resistance to the transfer of the gaseous reactant from the gas phase to the catalytic sites (Mogalicherla *et al*. 2009). This results in a decrease in the overall rate of reaction even though the liquid-solid mass-transfer coefficient increases (Herskowitz *et al*. 1979). However, since the wetting efficiencies obtained from the investigated liquid flow rates are high, as shown in Table 5.7, and because reactions were not gas limited, the only resistance remaining is the transport of gas from bulk liquid-to-solid interface, Therefore, an increase in liquid flow rate increases mass transfer coefficient which in turn increases reaction rate.

Although high enantioselectivities were maintained throughout the optimisation studies, the TONs and TOFs are relatively low compared to what has been achieved by this catalyst (Brandts and Berben, 2003, Augustine *et al*. 2004) at higher temperatures and pressures. Therefore, for the operation in continuous flow with a single pass to be feasible, further optimisations are required. To achieve high TONs and TOFs, further parameters such as temperature, pressure and solvent effects, which have been found to have a remarkable effect upon the performance of the catalyst, need to be carefully examined.
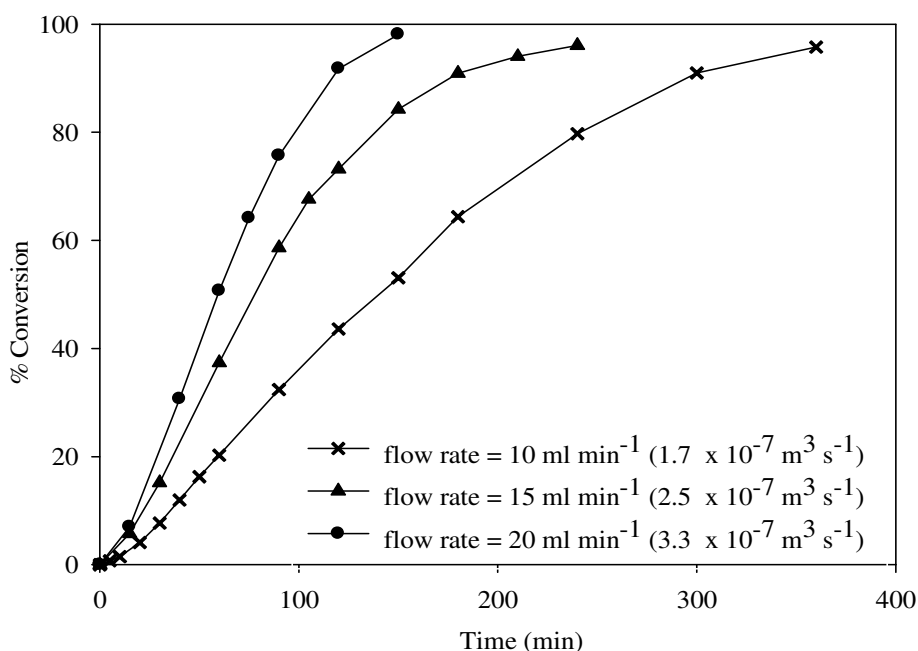
Figure 5.9. Conversion profiles of different liquid flow rates in TBR at constant gas flow rate of 100 ml min^{-1} (1.7 × 10^{-6} m^3 s^{-1}). In 15 ml ethanol (15 × 10^{-6} m^3), 20 °C (293.15 K) temperature, atmospheric pressure (101317 Pa), 20 µmol (20 × 10^{-6} mol) of catalyst precursor complex supported on 2.7 g of trilobe alumina, substrate/catalyst molar ratio: 223.

Run	Liquid flow rate (ml min^{-1})	Liquid superficial velocity (m s^{-1})	Froude number (Fr_L)	Reynolds number (Re)	Wetting efficiency	Mass transfer coefficient (× 10^{-4} m s^{-1})
32	10	0.00589	0.00124	8.448	0.915	0.744
33	15	0.00883	0.00279	12.673	0.936	1.158
29	20	0.01178	0.00497	16.897	0.949	1.590

Table 5.7. Wetting efficiencies and mass transfer coefficients of different liquid flow rates in the TBR. Diffusivity of H$_2$ into ethanol was calculated using correlation (5.5) to be 7.48 × 10^{-9} m^2 s^{-1}; Sc number was calculated to be 203.246; Mo_L was calculated to be 1.62 × 10^{-9}; porosity of bed (ε_B) = 0.6.

5.4 Conclusions

The enantioselective hydrogenation of DMI, over [Rh((R,R)-Me-DuPhos)(COD)]BF$_4$ supported on trilobe alumina, can be successfully carried out in a trickle bed reactor to produce dimethyl (S)-(-)-methylsuccinate. The catalyst gave high enantiomeric excesses in the TBR with results comparable to those obtained in the shake flask batch reactor. After elimination of all diffusional resistances, the experimental data could be fitted well by means of a kinetic model based on the Osborn-Wilkinson reaction mechanism. In the shake-flask [substrate to catalyst molar ratio of 60, atmospheric pressure, room temperature, H$_2$ flow rate of 100 ml min^{-1} and agitation speed of 200 rpm], a turnover frequency (TOF) of 50 h^{-1} was achieved with powder alumina support in comparison to a TOF of 20 h^{-1} obtained with the trilobes. Under these conditions, the enantioselectivities obtained from immobilising the catalyst complex onto the powder and trilobe supports were 96% and 97%, respectively. Fitting Osborn-Wilkinson kinetics to the concentration profiles of DMI indicated that complexation with the olefin before reaction with hydrogen was the preferred path. The trickle bed reactor (TBR) was operated in the trickle flow regime using the trilobe support. Initial reaction rate and enantioselectivity in the TBR could be promoted by optimizing liquid flow rate which was found to be directly proportional to wetting efficiency of the catalyst bed as well as mass transfer of H$_2$ from bulk liquid to catalyst surface. Under optimized conditions in the TBR (Table 5.5), 99% conversion and enantioselectivity of up to 99.9% were achieved.

CHAPTER 6

SELECTIVE HYDROGENATION OF 1-HEPTYNE

6.1 Introduction

In recent years tremendous research has been dedicated to understanding how to control the rate and selectivity of catalytic reactions. The main aim has been to minimize reaction times as well as reducing the amount of waste by-products. Various parameters have been reported in the literature for controlling the catalytic performance such as reactor design and operating conditions. Among these parameters, selection of solvent or mixture of solvents as a medium in which to conduct the reaction has particularly demonstrated a crucial impact upon the reaction behaviour (Hu *et al*. 2007, Bennett *et al*. 2009). Moreover, Toukoniitty *et al*. (2003) stated that a bad selection of the solvent leads to a complete loss of selectivity and/or activity, thus destroying the possible utilization of a potentially efficient process in practice. Consequently, the choice of a solvent and a comprehensive understanding of its effects are vital for optimisation of any catalytic process, and thus needs a careful investigation.

Selective hydrogenation of 1-heptyne has been carried out successfully for almost a decade, achieving selectivities to 1-heptene of up to 95% at 95% total conversion of 1-heptyne (Quiroga *et al*. 2005). However, it is noteworthy that the majority of these reactions (L'Argentière *et al*. 2002; L'Argentière *et al*. 2003; Lederhos *et al*. 2005; Lederhos *et al*. 2006; Liprandi *et al*. 2006; Quiroga *et al*. 2007; Somboonthanakij *et al*. 2007; Liprandi *et al*. 2009; Mekasuwandumrong *et al*. 2009; Lederhos *et al*. 2010; Mekasuwandumrong *et al*. 2010) have deployed toluene as a solvent at a common reaction conditions of 303 K and 150 kPa. The increasing pressure for moving towards green chemistry has been a major incentive to develop replacement solvents, which are attractive for reasons of safety, toxicity, emissions, and other aspects in order to comply with government regulations. There is clearly a need, then, to search for alternative solvents for the hydrogenation of 1-heptyne that are

more environmentally friendly than toluene. Unfortunately, this search is quite complicated as the solvating characteristics of the replacements should match those of toluene as closely as possible, and the yield of the reaction should not be compromised.

Despite the significant research conducted to investigate the effects of different bulk solvents, and solvent mixtures across the full range of compositions (Bennett *et al.* 2009), it has recently been reported that addition of small amounts of water or base to a reaction conducted in another solvent could have a significant impact upon the reaction performance (Kobayashi *et al.* 2000; Tike and Mahajani, 2007).

Hydrodynamic studies of TBRs are vital for the design and prediction of their performance. Referring to Chapter 4 and Chapter 5, and considering the noticeable effect of hydrodynamics upon the performance of the catalytic system, it was interesting to explore the influence of such phenomenon upon the selective hydrogenation of 1-heptyne. Hydrodynamics were found to have a remarkable effect upon the selective hydrogenation of alkynes. Rebrov *et al.* (2009) investigated the influence of hydrodynamics upon the selective hydrogenation of 2-methyl-3-butyn-2-ol (MBY) to 2-methyl-3-buten-2-ol (MBE) over Pd catalysts. At constant gas flow rate, liquid flow rate was found to have a noticeable effect upon the catalytic behaviour. The MBY conversion decreased with increasing liquid flow rate, while the selectivity to MBE remained constant at a value > 90%. The influence of liquid flow rate was ascribed to variations in liquid residence time and liquid hold up in the reactor.

Previously reported studies for 1-heptyne hydrogenation were mainly carried out in stirred autoclave reactors. Whilst this type of reactor is traditionally used, catalyst separation at the end of the reaction becomes an issue. Toukoniitty *et al.* (2002) reported that fine chemicals are usually produced on a batch-slurry basis and because of the expected increase in the production volumes; the replacement of batch operations with continuous ones is a natural step forward.

The aims of this work were to study the hydrogenation of 1-heptyne in the trickle bed reactor over a 2 wt. % Pd/Al_2O_3 catalyst, with the objective to transfer from batch processing to continuous operation with optimisation of conditions to maximize 1-heptene selectivity. The results presented in this chapter are for batch-recirculation in the trickle bed reactor, although some test results were also carried out for fully continuous operation (§6.5). Studies of the reactor hydrodynamics and kinetic fitting of the results are also presented (§6.3 and §6.4), in order to provide information that could be used to scale up the process. In order to optimize the reaction, several different solvents were selected for investigation (§6.2), including comparisons between 2-propanol, hexane and mixtures of these two solvents. The influence of adding small quantities of water and sodium hydroxide was then investigated and compared with previous studies. This work is intended to serve as a firm basis for further optimisations towards greener conditions of this industrially important reaction. The novel aspects are the use of a flow reactor together with new insights in to the effects of solvent mixtures upon the hydrogenation of 1-heptyne.

6.2 Influence of solvent selection

6.2.1 Reactions in pure and mixed solvents

The catalytic performance of 2 % Pd/Al_2O_3, which is a proven catalyst for selective hydrogenation of alkynes (§ 2.9), was evaluated in the trickle bed reactor operating in batch-recycle mode, using a 100 ml mixture containing 5 % v/v 1-heptyne in the corresponding solvent at the temperature 20 ^{o}C and atmospheric pressure of H_2. The reactions were operated with gas and liquid flow rates of 100 and 10 ml min^{-1}, respectively based on Baker flow map in order for the reaction to fall in the trickle flow regime (Ramachandran and Chaudhari, 1983).

The catalytic performance in the liquid phase semi-hydrogenation was evaluated using a range of solvents, with the polar, protic solvent, isopropanol (IPA) being first investigated. As discussed further in Section 6.3, catalyst wetting was at least 91 % in all experiments. This corresponds to relatively high wetting and utilization of the available catalyst surface compared with, for example, the study of Gladden *et al*. (2003), in which wetting efficiency of up to 57 % was observed by MRI measurements of air and water in a trickle bed reactor. As can be seen in the reaction profile shown in Figure 6.1, a complete conversion of 1-heptyne was obtained after 4 h of reaction. 1-heptyne was initially converted to 1-heptene, but 3h after the beginning of the reaction, heptane started to appear and its concentration increased rapidly with time of operation, thus, indicating that overhydrogenation of 1-heptene took place. A maximum conversion to 1-heptene of 77 % was achieved after 210 min from the start of the reaction, while the selectivity to 1-heptene was retained above 95 % up until 2 h, which corresponded to a total conversion of 1-heptyne of 49 %. As the reaction proceeded further, a decrease in the 1-heptene selectivity to 93 % occurred after 180 min, correspoding to 81 % conversion of 1-heptyne. Thereafter, a dramatic decrease in selectivity occurred, indicating over-hydrogenation of 1-heptene owing to competition between the alkene and alkyne for adsorption sites upon the metal surface.
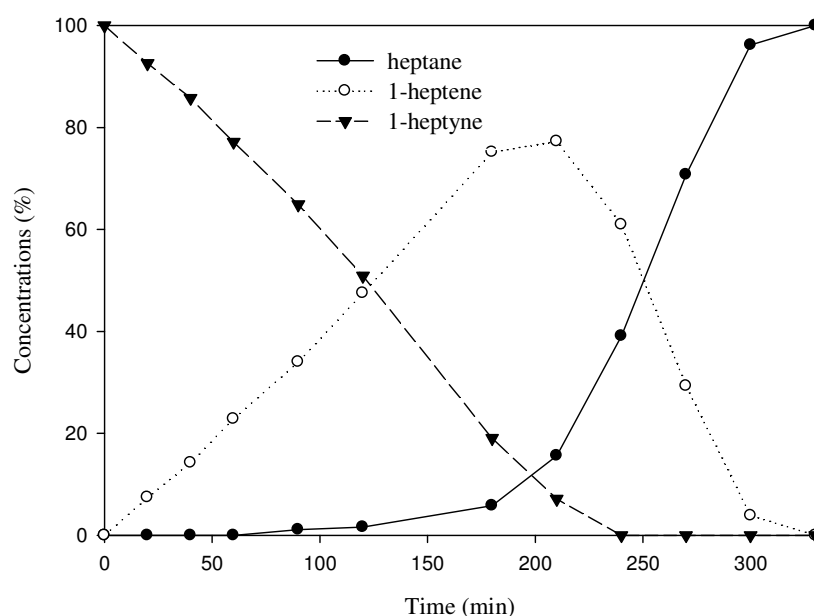
Figure 6.1. Reaction profile for 1-heptyne hydrogenation in IPA. Conditions: 100 ml mixture (5 % v/v 1-heptyne in isopropanol), H_2 flow rate of 100 ml min^{-1}, liquid flow rate of 10 ml min^{-1}, 20 ^{o}C temperature and atmospheric pressure.

Figure 6.2 is a plot of the weight percentage (on a solvent-free basis) of 1-heptyne (a), 1-heptene (b), and heptane (c) versus time-on-stream, corresponding to the runs conducted with the various solvents. Typical profiles for a consecutive reaction alkyne-alkene-alkane were attained in all cases. No substances other than 1-heptyne, 1-heptene and heptane were detected in the reactant solutions in any of the conducted experiments.

Purwanto *et al*. (1996) reported that hydrogen solubility decreases in solvents of increasing polarity, therefore less polar hexane was chosen as one of the solvent to investigate, for which the rate of reaction was indeed remarkably higher than in isopropanol (Figure 6.2a). Complete conversion of 1-heptyne was achieved in hexane after 75 min in comparison with 240 min in isopropanol, making the overall reaction time faster in hexane by a factor of 3.2. Table 6.1 shows the initial rates of reaction in all solvents, also indicating a much higher rate of reaction in hexane than isopropanol. However, the maximum concentration and

corresponding selectivity of 1-heptene were considerably higher with isopropanol (Figure 6.3). Very high selectivity of 100 % up to a total conversion of about 23% was observed with isopropanol, and thereafter significantly decreased. For the reaction in hexane, the selectivity was around 93 % up to a conversion of 21 %, decreasing steadily thereafter. The higher solubility of hydrogen in hexane (Katayama and Nitta, 1976) contributes to the much higher reaction rate in hexane compared with isopropanol, while high availability of hydrogen would also lead to over-hydrogenation, reducing 1-heptene selectivity. Katayama and Nitta (1976) reported the solubility of hydrogen and nitrogen in n-propanol and n-hexane, with Henry's constants at 25 °C reported as 4270 atm and 1430 atm for these respective solvents. Therefore under these conditions hydrogen is 2.98 times more soluble in hexane than isopropanol. Previous studies in our group have shown a strong correlation between reaction rate, bubble size and hydrogen solubility with solvent composition in isopropanol/water mixtures in the hydrogenation of 2-butyne-1,4-diol upon a palladium catalyst in a stirred autoclave (Hu *et al*. 2007). The solubility of hydrogen in isopropanol was found to be approximately 3.85 mol m^{-3} and the reaction rate was found to be proportional to the concentration of dissolved hydrogen divided by the mean bubble size ($r_{H2} \alpha C_{H2}/d_{32}$). Studies of the hydrogenation of 2-pentyne in a stirred autoclave with a bacteria supported palladium catalyst were reported by Bennett *et al*. (2009), who also observed strong effects of solvent selection upon the reaction rate and selectivity.

The different adsorption strengths of 1-heptyne and/or 1-heptene upon the catalyst could also explain the better selectivity obtained in isopropanol in this work. These selectivity differences could occur if 1-heptene is weakly adsorbed upon the catalyst in isopropanol and hence its further hydrogenation to heptane is limited. A series of adsorption experiments were conducted by Bennett *et al*. (2009) to determine the change in concentration of a 2-pentyne solution after being allowed to equilibrate with a high loading of Pd/Al$_2$O$_3$ catalyst for 1 h at

40 °C. It was found that in isopropanol, the concentration of 2-pentyne decreased by 11% and remained almost unchanged after 1 h in heptane (1% change in concentration). An experiment using 2-pentene in isopropanol containing Pd/Al$_2$O$_3$ catalyst showed only a small decrease in the alkene concentration, approximately 5 times less than that observed with the alkyne (Bennett *et al*. 2009). Therefore, the increased selectivity to 1-heptene obtained with isopropanol in this work could be due to much higher adsorption of 1-heptyne onto the catalyst and thus hydrogenation of 1-heptene was suppressed till most of 1-heptyne was hydrogenated as shown in Figure 6.1.

When a mixed solvent system of 50/50 (v/v) hexane/isopropanol was used activity was lower than that observed in hexane (Figure 6.2 (a)), which could be due to lower hydrogen solubility. However, selectivity values to 1-heptene (Figure 6.3) were almost the same for both solvents. The effect of solvent upon rate/selectivity of catalytic hydrogenation is a complex phenomenon and can be attributed to several effects. Therefore, correlation of reaction rate/selection with one variable would not necessarily be expected.
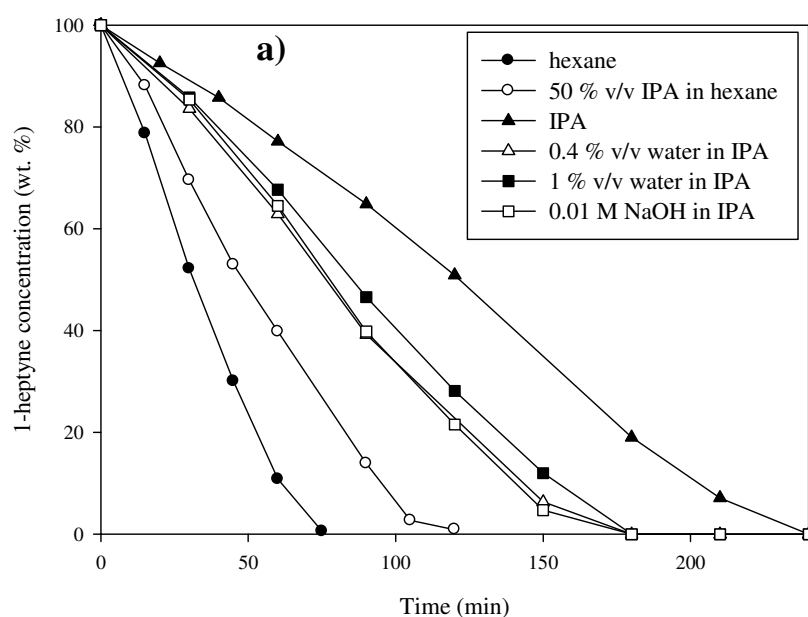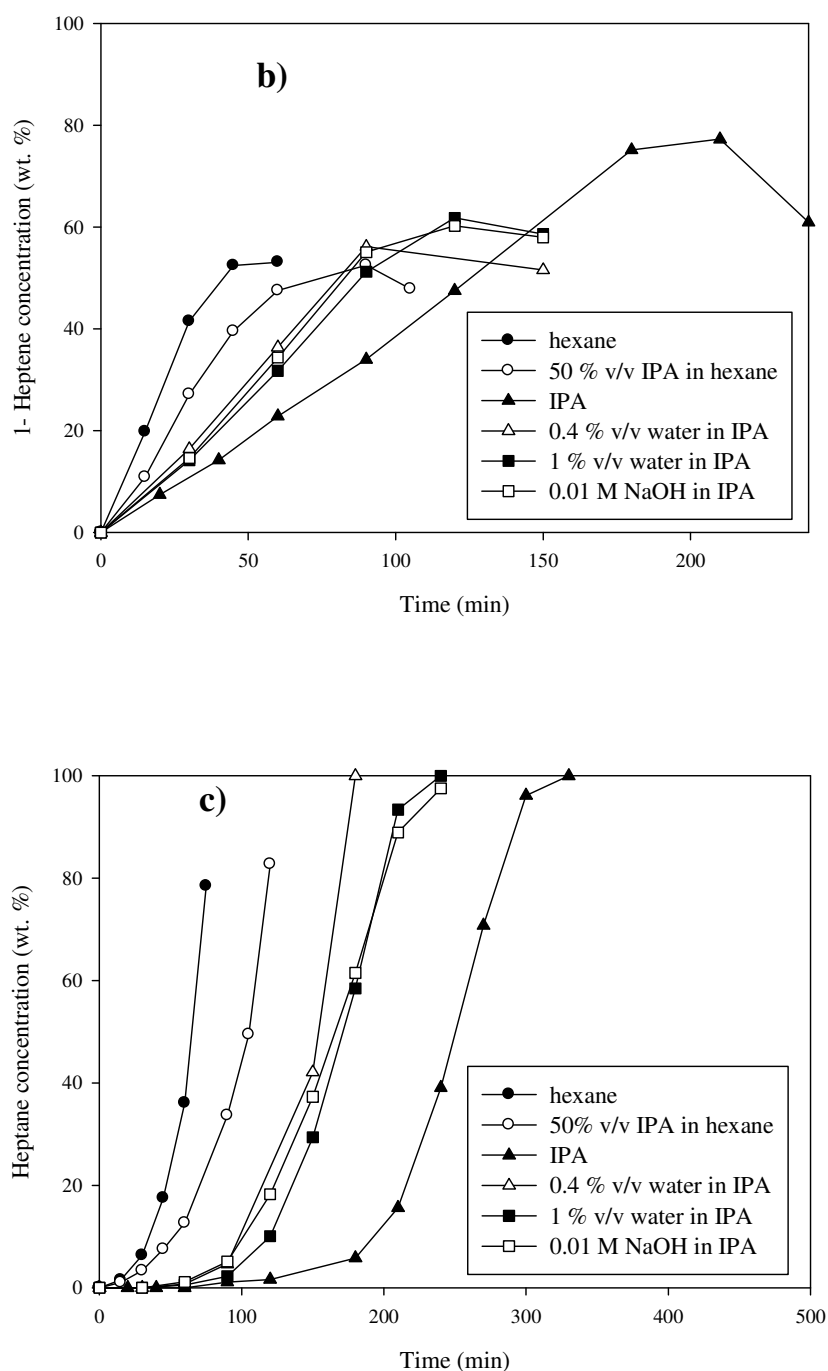
Figure 6.2. Plots of 1-heptyne (a), 1-heptene (b), and heptane (c) versus time profiles, corresponding to the runs conducted with the various solvents. Conditions: 100 ml mixture (5 % v/v 1-heptyne in the corresponding solvent), H_2 flow rate of 100 ml min^{-1}, liquid flow rate of 10 ml min^{-1}, 20 $^{\circ}$C temperature and atmospheric pressure.
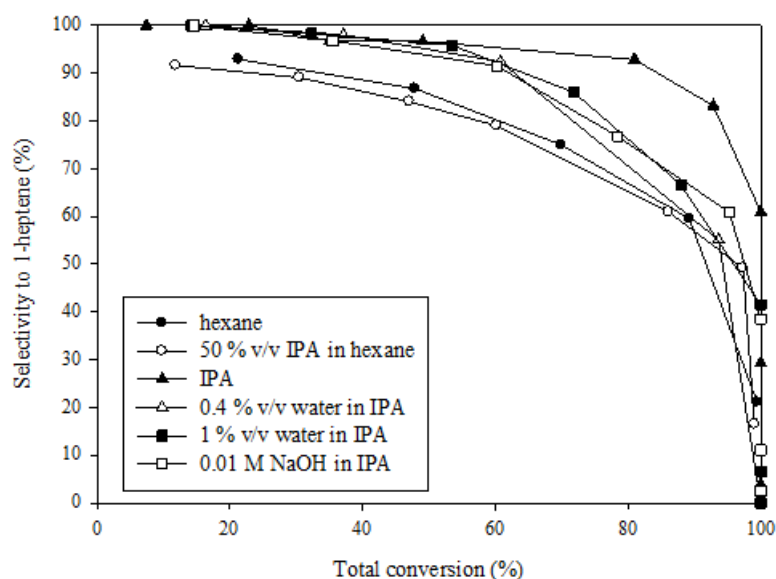
Figure 6.3. Selectivity to 1-heptene (%) vs. total 1-heptyne conversion (%), corresponding to the runs conducted with the various solvents. Conditions are given in Figure 6.2.

Run	Solvent	Initial reaction rate of 1-heptyne (mol l^{-1} min^{-1})*	TOF (h^{-1})	Maximum conversion to 1-heptene (%)	Maximum selectivity to 1-heptene (%)
1	IPA	0.0013	17	77	>96 (plateau-shaped up to 81% 1-heptyne conv.)
2	50 % IPA in hexane	0.0038	43	52	~92 (monotonously decreasing)
3	Hexane	0.0060	64	53	~93(monotonously decreasing)
4	0.4 % water in IPA	0.0022	27	56	~98 (monotonously decreasing)
5	1 % water in IPA	0.0018	23	62	>95 (plateau-shaped up to 53% 1-heptyne conv.)
6	0.01 M NaOH in IPA	0.0018	26	60	>95 (plateau-shaped up to 36% 1-heptyne conv.)

Table 6.1. Comparison of catalytic activity, maximum conversion and selectivity to 1-heptene values corresponding to the runs conducted with the various solvents. Conditions are given in Figure 6.2.
* calculated after 30 min from the start of the reaction.

6.2.2 Effect of water and base addition

To understand the mechanistic role of water, the effects of the addition of small volumes of water (0.4 % v/v and 1 % v/v) to a 100 ml mixture containing 5 % v/v 1-heptyne in isopropanol were investigated. Complete conversion of 1-heptyne was achieved when 0.4 % v/v and 1 % v/v of water were added to isopropanol as can be seen in Figure 6.2a. 1-heptyne was fully hydrogenated within 180 min upon the addition of 0.4 % v/v and 1 % v/v of water, thus indicating the rate accelerating effect of water addition. From Table 6.1, the initial rates of reaction were increased when water was added, compared with pure isopropanol. It is possible that the addition of water affects the adsorption equilibrium at the catalyst surface. Ning *et al*. (2007) studied the influence of adding some water into the solvent of ethanol upon the selective hydrogenation of *p*-chloronitrobenzene (*p*-CNB) to *p*-chloraniline (*p*-CAN) over ruthenium catalyst. The hydrogenation rate was found to increase remarkably with elevating the content of water in solvent up to 30 % v/v. The promoting effect of water was believed to be attributed to competitive adsorption of water and *p*-CAN on catalyst surface and to the hydrogen bonds between *p*-CAN and water in the solvent. Based on a study by Ronchin and Toniolo (2001), in selective hydrogenation of benzene to cyclohexene, hydrogenation of benzene to cyclohexane was thermodynamically favoured to its partial hydrogenation to cyclohexene. Nevertheless, cyclohexene could be obtained when water was used in the system suggesting that the addition of water might wet the catalyst surface, resulting in the formation of water films that influence the adsorption equilibria of cyclohexene. The selection of solvent or solvent mixture could also influence the rate of proton diffusion, which will be influenced by the hydrogen bonding structure of the solvent. This structure could be disrupted by the addition of water or base and thus the rate of hydrogen ion diffusion would be altered. Most likely the modification of adsorption equilibria at the catalyst surface led to the observed changes in rate and selectivity in this work. Weber *et al*.

(2009) used NMR relaxation to study the hydrogenation of 2-butanone and found that water has a strong surface interaction with the catalyst, which can lead to preferential adsorption of water on the surface of the palladium catalyst. The rate enhancing effect of water was highest for the smaller concentration of 0.4 % v/v, and decreased slightly for the larger addition of water at 1 % v/v. Possibly the smaller quantity of water leads to competitive adsorption with the alkyne and possibly enhanced proton diffusion above, leading to enhanced rate observed. However larger quantities of water may form a film across the catalyst surface, causing a larger decrease in adsorption of reactants, or could cause the catalyst particles to agglomerate in to clusters, leading to diffusion limitations of the reactants (Rajadhyaksha and Karwa, 1986). It has also been reported that the addition of small volumes of isopropanol into water decreases bubble size and, as a result, leads to improved reaction rates than in water alone (Hu *et al*. 2007b). Less likely, water could facilitate the donation of a proton, i.e. being involved in the reaction, to assist in the hydrogenation.

Although the addition of small volumes of water improved the reaction rate, the trends of selectivity to 1-heptene vs 1-heptyne conversion were generally lower than those obtained in pure isopropanol (Figure 6.3). A possible explanation could be that water competes with alcohol on surface adsorption leading to a decreased content of alcohol on catalyst surface. This could result in strong adsorption of 1-heptene on surface and hence its over-hydrogenation is favoured.

The addition of a small amount of inorganic base, 0.01 M NaOH to isopropanol, resulted in an improved reaction rate compared to that with isopropanol, but quite similar performance to isopropanol containing a small amount of water (Figure 6.2a). The influence of the base could be through interaction with the substrate or the catalyst surface. The quantity of base is low relative to 1-heptyne (0.01 M versus 0.38 M), while the number of moles of base is in excess of the number of moles of palladium, at 0.01 M compared to 0.005 M. This suggests

that interaction of the base with the catalyst surface would have a larger effect than interaction with the substrate directly. This theory is supported by observations from the literature, for example Wang *et al.* (1998) demonstrated substantial improvements in the rate of NO decomposition with Pd/Al_2O_3 catalyst that was pre-coated with NaOH. It was proposed that the promotional effect of NaOH coating could be ascribed to a formation of additional sites that can strongly adsorb the substrate molecules. As the alkyne triple bond interacts more strongly with the metal than the double bond of the alkene, it is possible that addition of NaOH could enhance the adsorption of 1-heptyne and 1-heptene. This would explain the observed improvement in reaction rate with NaOH added, while decreasing the selectivity to 1-heptene due to its over-hydrogenation to heptane (Figure 6.3).

The selectivity plots displayed in Figure 6.3 demonstrate some solvents with plateau behaviour in a broad range of 1-heptyne total conversion followed by a decreasing tendency, while others decrease monotonously.

Trends and selection of the best catalytic systems are drawn based on two criteria: (a) maximum conversion values to 1-heptene versus 1-heptyne total conversion and (b) maximum selectivity values to 1-heptene, and the range of 1-heptyne total conversion in which they are self-maintained. These are summarized in Table 6.1. Although the highest initial reaction rate of 1-heptyne and eventually the highest TOF were achieved using hexane as solvent for reaction, IPA gave the best results in terms of maximum conversion and selectivity to 1-heptene, and therefore, IPA was selected for further optimisation studies.

6.3 Influence of hydrodynamics

In view of the major role of hydrodynamics, besides its influence upon the wetting efficiency of the catalyst bed, liquid hold up as well as mass transfer in the reactor, the effect of liquid flow rates on the rate and selectivity of the reaction is discussed in the following sections.

For each run the gas flow rate was kept constant at 100 ml min^{-1} and the liquid flow rate was gradually increased in steps of 5 ml min^{-1}. The flow rates were chosen to reside within the trickle flow regime as demonstrated in Figure 6.4 below.
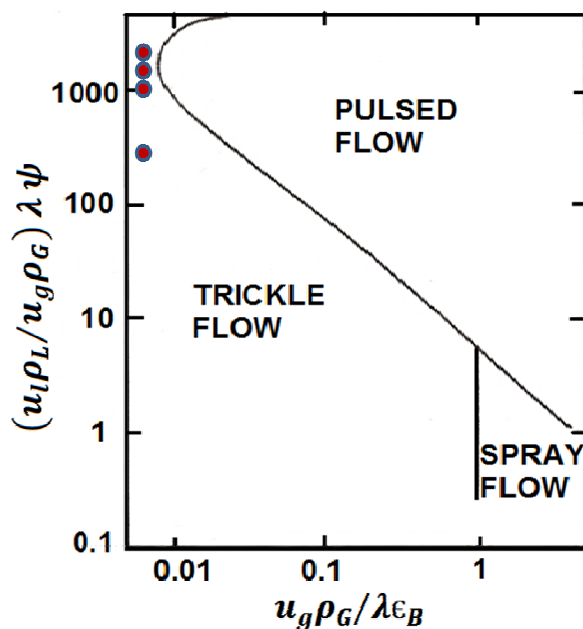
Figure 6.4. The correspondence of the TBR operating conditions in Baker's flow map.

Table 6.2 demonstrates the influence of liquid flow rate on the catalytic activity during the hydrogenation of 1-heptyne. Increasing liquid flow rate increased the rate of 1-heptyne hydrogenation from 0.0015 mol l^{-1} min^{-1} at a flow of 5 ml min^{-1} to 0.0028 mol l^{-1} min^{-1} at a flow of 15 ml min^{-1}, the largest increase occurring between 10 and 15 mL min^{-1}, thereafter levelling off for the highest two flow rates. The conversion profiles of 1-heptyne are plotted in Figure 6.5. A similar trend was observed for the rate of 1-heptene production as shown in Figure 6.6.

Run	Liquid flow Rate (ml min^{-1})	reaction rate of 1-heptyne (mol l^{-1} min^{-1})	TOF (h^{-1})	Maximum conversion to 1-heptene (%)	Maximum selectivity to 1-heptene (%)
7	5	0.0015	17	68	>95 (plateau-shaped up to 55 % 1-heptyne conv.)
1	10	0.0018	17	77	>96 (plateau-shaped up to 81% 1-heptyne conv.)
8	15	0.0028	25	89	>95 (plateau-shaped up to 93% 1-heptyne conv.)
9	20	0.0026	25	89	100 (plateau-shaped up to 84% 1-heptyne conv.)

Table 6.2. Comparison of catalytic activity, maximum conversion and selectivity to 1-heptene values corresponding to the runs conducted with different liquid flow rates. Conditions: 100 ml mixture (5 % v/v 1-heptyne in isopropanol), H_2 flow rate of 100 ml min^{-1}, 20 ^{o}C temperature and atmospheric pressure.

As can be seen in Figure 6.6, the rate of 1-heptene production increased upon increasing liquid flow rate and remained unchanged for the highest two liquid flow rates implemented in this study. The conversion to 1-heptene versus 1-heptyne total conversion profiles are displayed in Figure 6.7. At total conversion of 1-heptyne lower than 60% the conversion to 1-heptene was similar for all investigated liquid flow rates. Differences were observed at higher conversion levels. At 5 ml min^{-1} liquid flow rate, conversion to 1-heptene reached a maximum of 68% at 1-heptyne total conversion of 91%, and then decreased as the heptane conversion increased. Conducting the reaction with a liquid flow rate of 10 ml min^{-1} achieved a maximum conversion to 1-heptene of 77% at 93% 1-heptyne total conversion, after which a sharp decrease was experienced. The better performance, however, corresponded to the highest liquid flow rates of 15 and 20 ml min^{-1}, at which the conversion to 1-heptene reached

a maximum of about 89%. Beyond this point the conversion to 1-heptene decreased to 83% at the final full conversion of 1-heptyne.
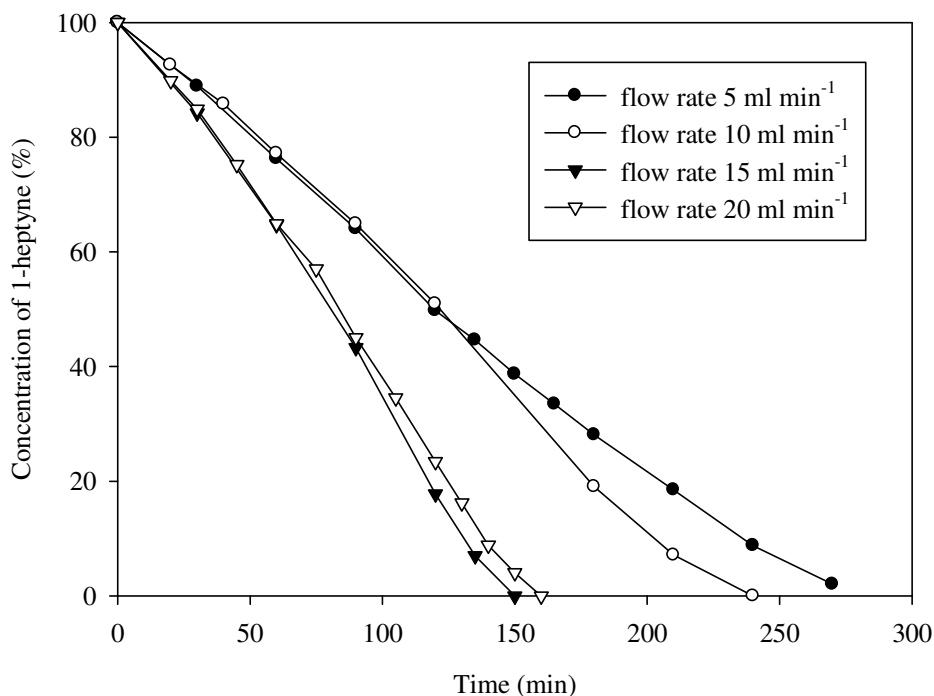
Figure 6.5. Plot of 1-heptyne versus time profiles, corresponding to the runs conducted with different liquid flow rates. Conditions: 100 ml mixture (5 % v/v 1-heptyne in isopropanol), H_2 flow rate of 100 ml min^{-1}, 20 ^{o}C temperature and atmospheric pressure.

The profiles of 1-heptene selectivity versus total conversion of 1-heptyne are displayed in Figure 6.8, and a summary of the trends is provided in Table 6.2. The selectivity to 1-heptene values displayed in Figure 6.8 also demonstrate the better catalytic behaviour obtained at the highest two liquid flow rates with the best behaviour observed at the highest flow rate of 20 ml min^{-1}. At a total conversion lower than 20% the selectivity was almost the same for all liquid flow rates. However, at higher values of 1-heptyne total conversion the differences become evident. The selectivity to 1-heptene at 20 ml min^{-1} started with very high up value of 100% which remained constant up to a total conversion of about 77%, and then decreased gradually to reach 93% at a total conversion of 96% followed by a sharp decrease to 83% at full conversion of 1-heptyne. At a liquid flow rate of 15 ml min^{-1}, the selectivity to 1-heptene

197

was 100 % at total conversion of 16% and then decreased to 98% at 35% 1-heptyne conversion keeping constant value up to total conversion of 82%, after which it decreased to 95% at 93% total conversion followed by an abrupt decrease to 84% at full conversion of 1-heptyne. The selectivity to 1-heptene values at 10 and 5 ml min^{-1} demonstrated a similar behaviour, starting at selectivity values higher than 98% at total conversion of 23%, which then decreased gradually to 96% at around 50 % conversion of 1-heptyne followed by a dramatic decrease to less than 60% at the full conversion of 1-heptyne.
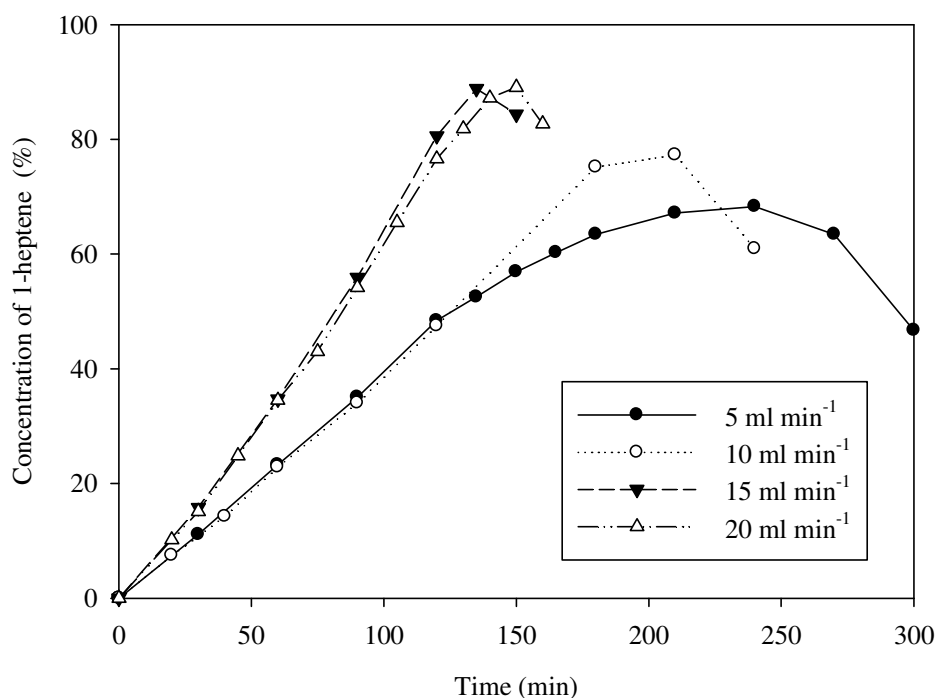
Figure 6.6. Plot of 1-heptene versus time profiles, corresponding to the runs conducted with different liquid flow rates. Conditions: 100 ml mixture (5 % v/v 1-heptyne in isopropanol), H_2 flow rate of 100 ml min^{-1}, 20 ^{o}C temperature and atmospheric pressure.
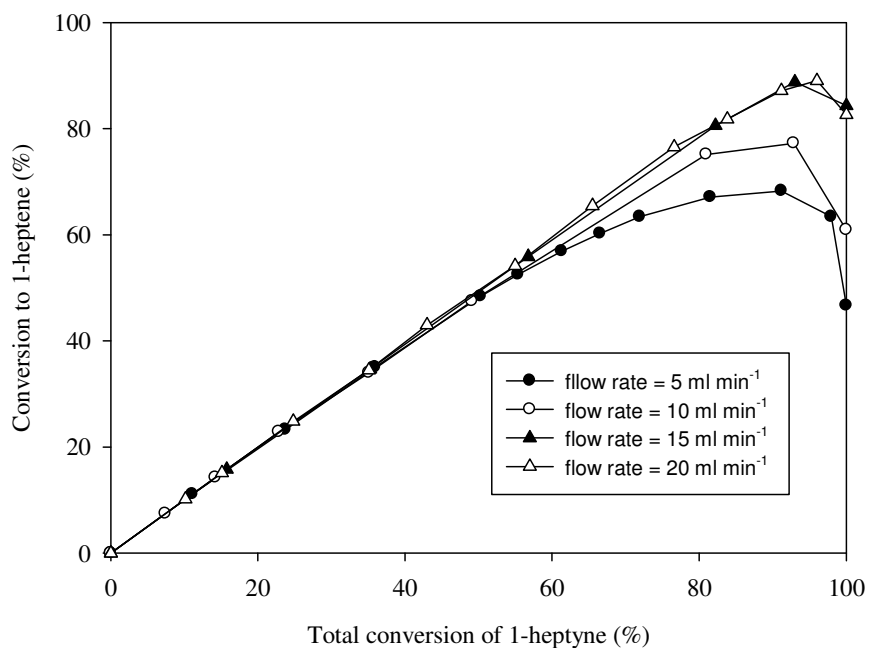
Figure 6.7. Conversion to 1-heptene (%) versus total 1-heptyne conversion (%), corresponding to the runs conducted with different liquid flow rates at a constant gas flow rate of 100 ml min^{-1}.
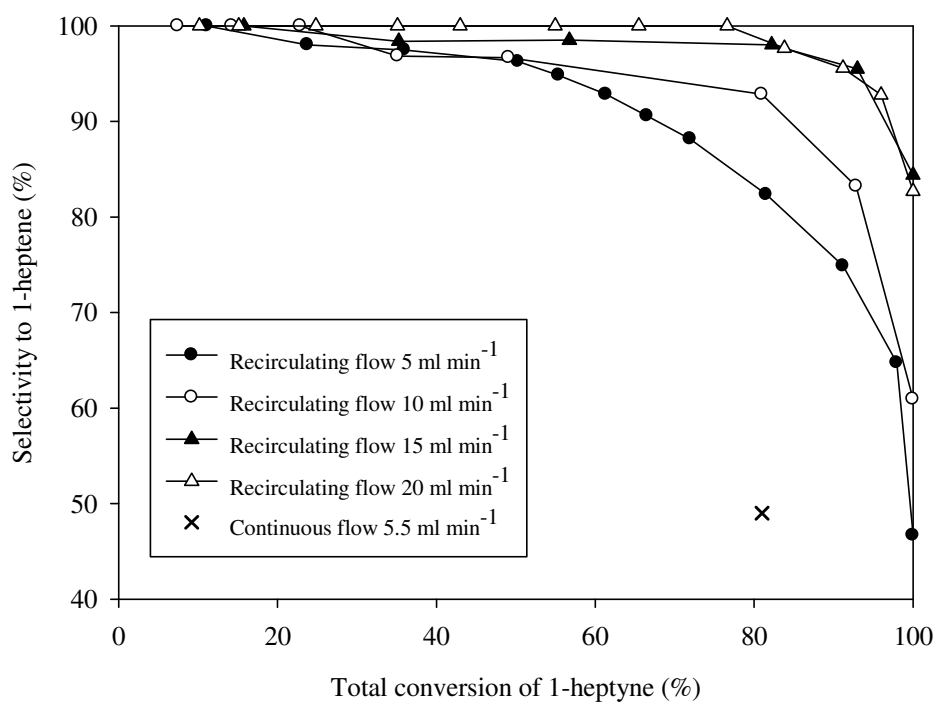
Figure 6.8. Selectivity to 1-heptene (%) versus total 1-heptyne conversion (%), corresponding to the runs conducted with different liquid flow rates, at a constant gas flow rate of 100 ml min^{-1}.

The wetting efficiencies and mass transfer coefficients corresponding to the investigated liquid flow rates were calculated using the correlations introduced in Chapter 5 (Eqs 5.3 and 5.4), and are displayed in Table 6.3. As can be seen in Table 6.3, high wetting efficiencies of greater than 91% were achieved for all liquid flow rates, corresponding to efficient utilization of catalyst bed in the reactor. The wetting efficiency increased from 0.915 at 2.9×10^{-3} m s^{-1} liquid superficial velocity reaching as high up as 0.974 at liquid superficial velocity of 11.8×10^{-3} m s^{-1}. Over the same range of flowrates the mass transfer coefficient increased from 0.96×10^{-5} to 4.5×10^{-5} m s^{-1}. It appears that at the lowest flowrate there may be some slight effects of partial catalyst wetting and mass transfer limitation, which become less significant at the highest flowrate, where the reaction may be expected to fall within the kinetic regime.

Liquid flow rate (ml min^{-1})	Liquid superficial velocity ($\times 10^{-3}$ m s^{-1})	Froude number (Fr_L) $\times 10^{-3}$	Reynolds number (Re_L)	Wetting efficiency	Mass transfer coefficient ($\times 10^{-5}$ m s^{-1})^a
5	2.9	0.4	0.95	0.915	0.96
10	5.9	1.8	1.9	0.950	2.1
15	8.9	4	2.9	0.965	3.2
20	11.8	7	3.8	0.974	4.5

Table 6.3. Wetting efficiencies and mass transfer coefficients corresponding to different liquid flow rates. [a] Diffusivity of H_2 into isopropanol was calculated using correlation (5.5) to be 3.7×10^{-9} m^2 s^{-1}; Sc number was calculated to be 827; Mo_L was calculated to be 3.6×10^{-8}; porosity of bed (ε_B) = 0.6.

It was also noted that the total liquid hold up ($\varepsilon_{L,t}$), defined as the total volume fraction of the liquid phase in the catalyst bed volume would vary with liquid flowrate. Total liquid holdup ($\varepsilon_{L,t}$) is composed of static and dynamic fractions. The dynamic liquid holdup ($\varepsilon_{L,d}$) is the freely flowing liquid volume relative to the reactor volume, while the static liquid holdup

($\varepsilon_{L,st}$) is the fraction of the liquid that is trapped in catalyst pores and stagnant liquid between catalyst particles. Total and dynamic liquid holdups were calculated using correlations by Lange *et al*. (2005):

$$\varepsilon_{L,t} \; = \; 0.16(d_R/d_P)^{0.33}Re_L^{0.14} \tag{6.1}$$

$$\varepsilon_{L,d} \; = \; 0.002(d_R/d_P)^{1.28}Re_L^{0.38} \tag{6.2}$$

The correlations, based on the drainage method, were derived for very low liquid Reynolds numbers while the effect of gas flow rate was claimed to be negligible. The total and dynamic holdups are mainly a function of the liquid Reynolds number, which includes liquid properties and superficial velocity, as well as the reactor diameter to particle diameter ratio. In their study, Lange *et al*. (2005) found that increasing the liquid Reynolds number resulted in an increase in the liquid hold up, which is consistent with the calculated holdups of this study. Increasing liquid superficial velocity and thus liquid Reynolds number (Table 6.3), increased total liquid holdup as can be seen in Figure 6.9. Figure 6.10 presents a plot of ($\varepsilon_{L,t}$) versus ($\varepsilon_{L,d}$). It was observed, as expected, the total holdup (($\varepsilon_{L,t}$) is considerably higher than the dynamic holdup ($\varepsilon_{L,d}$).
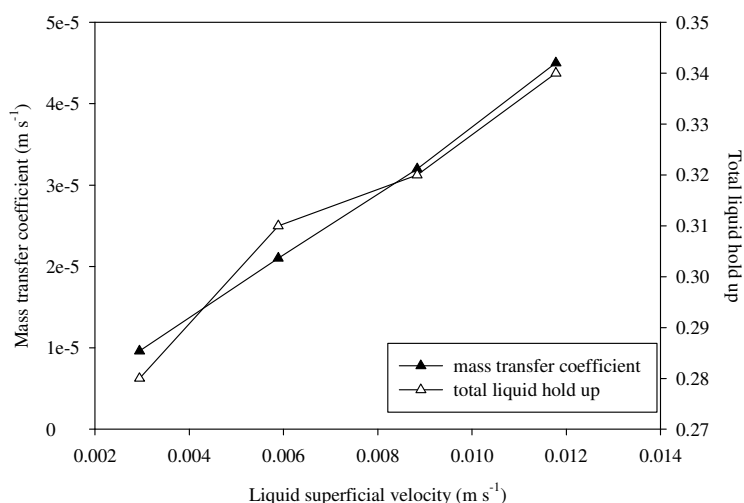
Figure 6.9. Mass transfer coefficient and total liquid holdup corresponding to runs conducted with different liquid velocities.
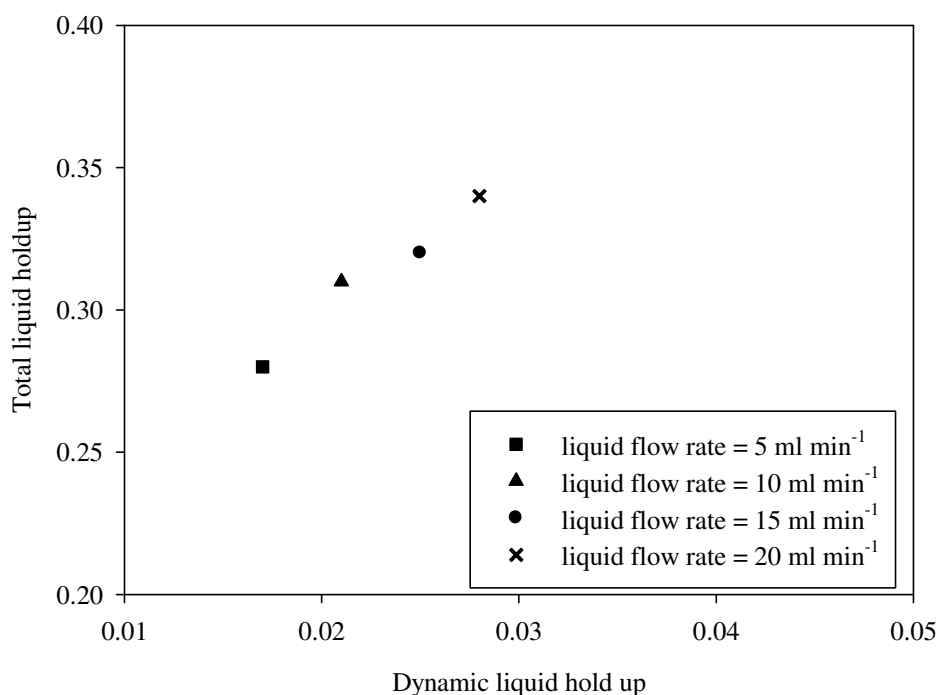
Figure 6.10. Plot of dynamic liquid holdup versus total liquid holdup.

Estimation of the total liquid holdup enabled the average residence time per pass and number of passes to achieve 65 % conversion of 1-heptyne to be calculated at different flowrates, as shown in Table 6.4. The mean residence time was estimated using the total liquid holdup and liquid flow, rather than the combined flow of the gas and liquid, since the liquid trickles over the catalyst whilst the gas may flow much faster through the interstitial voids. The total liquid holdup was used, since although some of the liquid is static between the particles and in the pores, exchange by mass transfer processes occurs with the dynamic liquid flow. In small trickle beds which have not been diluted with fine particles there will actually be a wide distribution of residence times (Kulkarni *et al*. 2005), owing to the dynamic and static liquid fractions and therefore the mean residence time is used. It is noted that the larger number of passes at higher flowrates lead to improved rate of reaction and thus complete conversion in shorter times.

It was earlier mentioned that the highest selectivities occur at the higher flowrates (Figure 6.8). This significant improvement in the selectivity to 1-heptene with increasing flowrate resulted from a reduction of liquid residence time from 8.94 s to 2.71 s upon increasing the flowrate from 5 ml min^{-1} to 20 ml min^{-1}. The lower residence time ensures that the 1-heptene formed in the reactor is quickly washed off the catalyst surface rather than over-hydrogenating to 1-heptane. Weekman (1969) reported a profound effect of the residence time upon the catalytic cracking selectivity in fixed-bed reactors. It was found that the gasoline selectivity was poorer at longer residence times. Kohler and Richarz (1985) also reported a significant decrease in the selectivity at increasing residence times during the hydrogenation of aniline in a trickle bed reactor. A plot of liquid velocities versus average residence times and the maximum obtained selectivities to 1-heptene is also shown in Figure 6.11. For consistent comparison, selectivities to 1-heptene were calculated at 65 % conversion of 1-heptyne. As can be seen from Table 6.4 and Figure 6.11, increasing liquid superficial velocity decreased residence time and increased the selectivity to 1-heptene. The selectivity to 1-heptene increased from 91% at the lowest liquid velocity of 2.9×10^{-3} m s^{-1} up to 100% at the highest liquid superficial velocity of 11.8×10^{-3} m s^{-1}. The highest selectivity of 100% obtained with the highest liquid velocity of 11.8×10^{-3} m s^{-1} remained high up and constant up until 80% conversion of 1-heptyne, after which it started to decrease, which could be ascribed to a stronger competition of 1-heptene on the active catalytic sites and thus overhydrogenation to heptane was inevitable. However other effects could also influence the selectivity, for example at flows where wetting is improved the contact of hydrogen with the catalyst would be reduced.

It is well established in the literature that high alkene selectivities require low hydrogen pressures (Lederhos *et al*. 2005). Therefore, all experiments were conducted at a fixed gas flow rate of 100 ml min^{-1} and no further investigation regarding this variable was performed.

Liquid superficial velocity (x 10^{-3} m s^{-1})	Residence time per pass (s)	No of passes to achieve 65% conversion of 1-heptyne	% Selectivity to 1-heptene at 65% conversion of 1-heptyne
2.9	8.94	1072	91
5.9	4.93	1785	95
8.9	3.48	1687	98
11.8	2.71	2273	100

Table 6.4. Average residence time and selectivity to 1-heptene corresponding to different liquid velocities. Conditions: 100 ml mixture (5 % v/v 1-heptyne in isopropanol), H$_2$ flow rate of 100 ml min^{-1}, 20 ^{o}C temperature and atmospheric pressure.
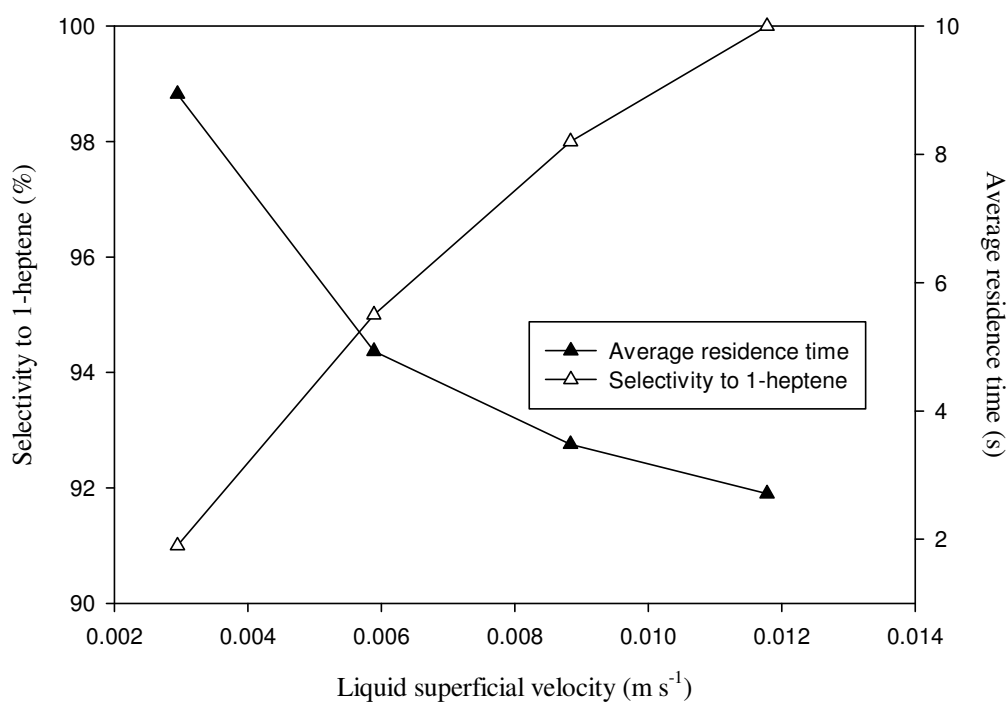
Figure 6.11. Average residence time and maximum selectivity to 1-heptene versus liquid superficial velocity.

6.4 Effect of 1-heptyne initial concentration and kinetic modelling

The influence of 1-heptyne initial concentration was investigated under the previously optimized conditions: 100 ml mixture (5 % v/v 1-heptyne in isopropanol), H_2 flow rate of 100 ml min^{-1}, 20 ^{o}C temperature and atmospheric pressure. For this set of experiments the liquid flow rate of 20 ml min^{-1} was used, owing to the highest selectivity and rate of reaction occurring at highest flowrate. Intraparticle mass transfer limitations were considered by crushing the catalyst up to one quarter of the original size and using the obtained samples to carry out the hydrogenation reaction. Reaction rate and conversion values, equal to those obtained with the uncrushed catalyst (Figure 6.12), proved that this type of limitation is absent at the implemented conditions of this work.
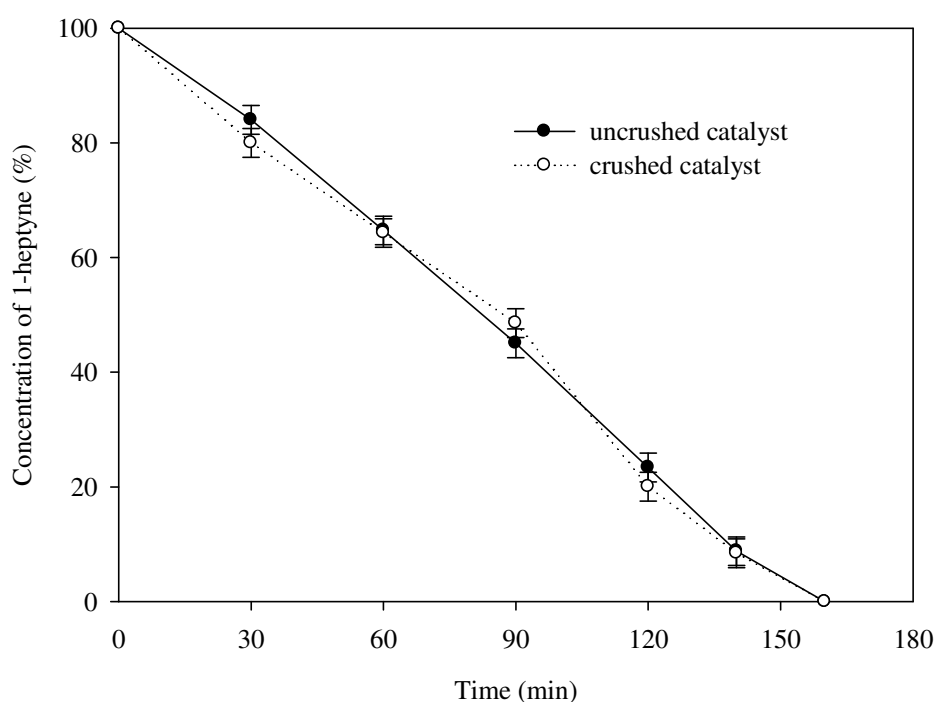
Figure 6.12. Investigation of intraparticle mass transfer. Conditions: 100 ml mixture (5 % v/v 1-heptyne in isopropanol), H_2 flow rate of 100 ml min^{-1}, liquid flow rate of 20 ml min^{-1}, 20 ^{o}C temperature and atmospheric pressure.

The influence of 1-heptyne initial concentration on the rate and selectivity was studied for concentrations from 0.1 to 0.5 mol l^{-1} (M). Figure 6.13 shows that the 1-heptyne concentration-time profiles follow almost the same slope until the latest stage of each reaction, thus suggesting that the reaction is zero order. This would result from excess reagents being present in the solution, such that the substrates do not limit the reaction rate. At the lowest 1-heptyne initial concentration of 0.1 mol l^{-1} and towards the end of the reactions of the higher starting concentrations, the profile becomes curved, indicating first order behaviour with limiting concentration of 1-heptyne. Table 6.5 shows that initial reaction rate increased upon increasing initial concentration of 1-heptyne up to 0.3 mol l^{-1}, and decreased to 0.0022 mol l^{-1} min^{-1} at the highest initial concentrations of 0.4 and 0.5 mol/l. Table 6.5 also shows that TOF increased upon increasing 1-heptyne initial concentration up to 0.3 mol l^{-1} and decreased afterwards at the highest concentrations of 0.4 and 0.5 mol l^{-1}. The highest obtained concentration of 1-heptene (Figure 6.14) and thus the highest conversion to 1-heptene versus 1-heptyne conversion (Table 6.5) were obtained at 1-heptyne initial concentration of 0.4 M. The best selectivity-trend to 1-heptene was also observed for 1-heptyne initial concentration of 0.4 M as can be seen in Figure 6.15.
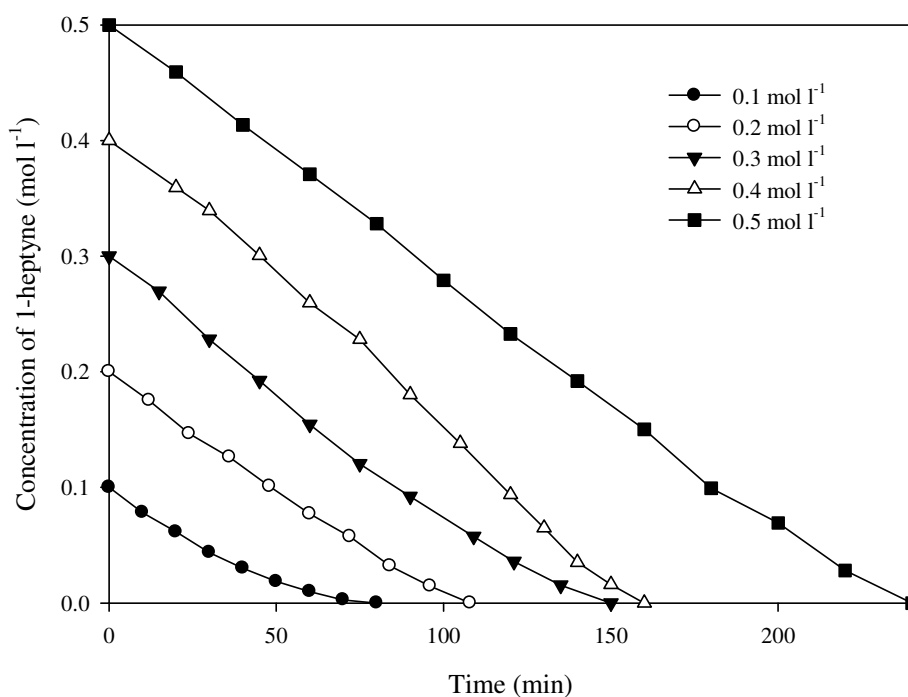
Figure 6.13. Plot of 1-heptyne versus time profiles, corresponding to the runs conducted with different initial concentrations of 1-heptyne. Conditions: 100 ml mixture (5 % v/v 1-heptyne in isopropanol), H_2 flow rate of 100 ml min^{-1}, liquid flow rate of 20 ml min^{-1}, 20 $^{\circ}$C temperature and atmospheric pressure.
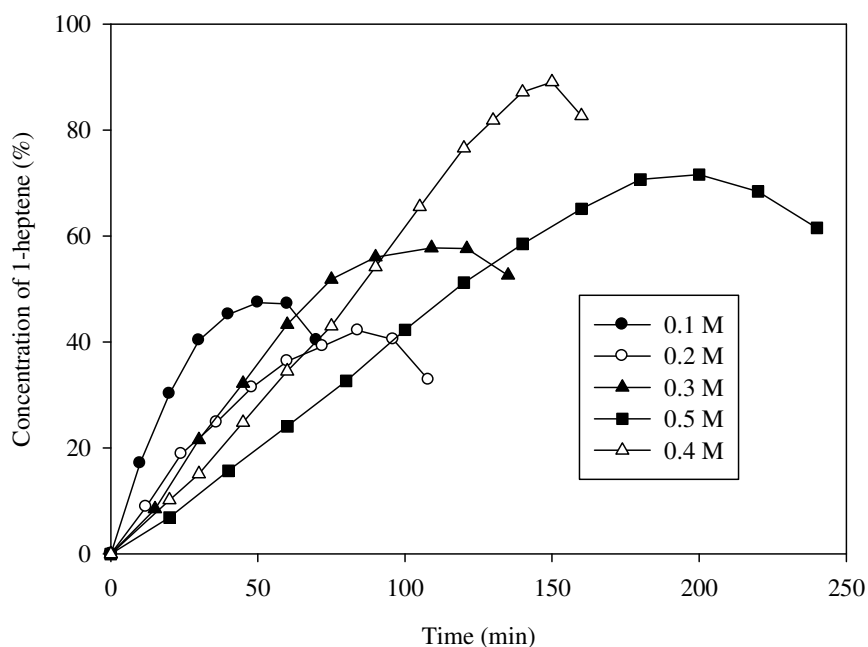
Figure 6.14. Plot of 1-heptene versus time profiles, corresponding to the runs conducted with different initial concentrations of 1-heptyne. Conditions: 100 ml mixture (5 % v/v 1-heptyne in isopropanol), H_2 flow rate of 100 ml min^{-1}, liquid flow rate of 20 ml min^{-1}, 20 $^{\circ}$C temperature and atmospheric pressure.

207

Run	Initial concentration of 1-heptyne $(\text{mol } l^{-1})$	TON	Initial reaction rate of 1-heptyne $(\text{mol } l^{-1} \text{ min}^{-1})*$	Maximum conversion to 1-heptene (%)	TOF (h^{-1})	Maximum selectivity to 1-heptene (%)
10	0.1	18	0.0017	47	16	79
11	0.2	36	0.0021	42	22	71
12	0.3	54	0.0024	58	26	90
9	0.4	72	0.0022	89	25	100
13	0.5	90	0.0022	72	23	96

Table 6.5. Maximum conversion and selectivity to 1-heptene values corresponding to the runs conducted with different initial concentration of 1-heptyne. * calculated after 40 min from the start of the reaction.
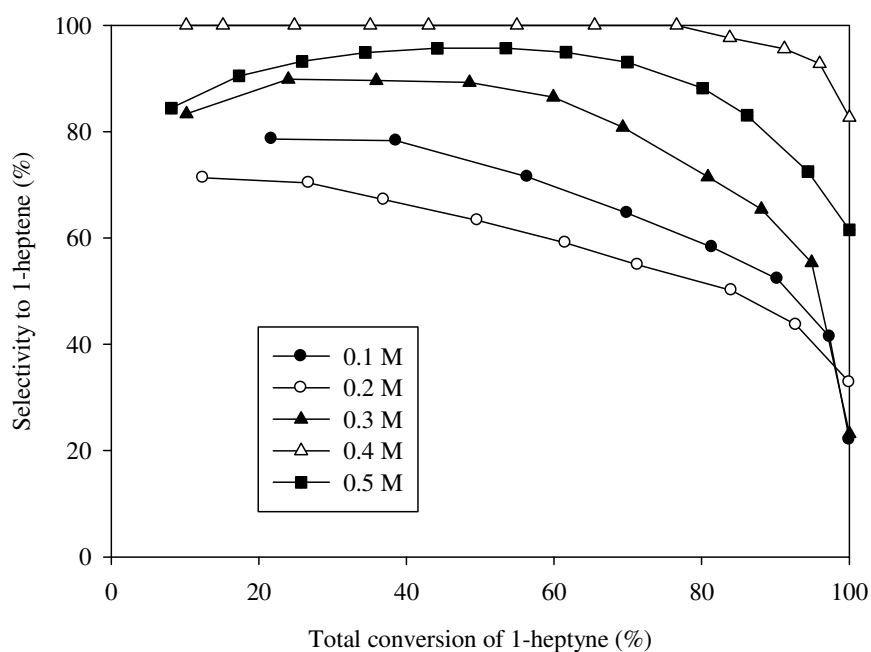
Figure 6.15. Selectivity to 1-heptene (%) vs. total 1-heptyne conversion (%), corresponding to the runs conducted with different initial concentrations of 1-heptyne. Conditions: 100 ml mixture (5 % v/v 1-heptyne in isopropanol), H_2 flow rate of 100 ml min^{-1}, liquid flow rate of 20 ml min^{-1}, 20 $^{\circ}$C temperature and atmospheric pressure.

Alkyne hydrogenation reactions typically follow Langmuir-Hinshelwood-type kinetic expression of the type (Rode *et al*. 2006):

$$R_1 = -\frac{dC_{1-heptyne}}{dt} = \frac{mk_1 C_{H_2} C_{1-heptyne}}{(1 + K_{1-heptyne} C_{1-heptyne} + K_{1-heptene} C_{1-heptene})^2} \quad (6.3)$$

Assuming a small adsorption constant of heptane and taking also into consideration a weak hydrogen adsorption on Pt group metals (Singh and Albert Vannice, 2000) and its low bulk concentration of 0.0084 kmol m^{-3}; $K_{heptane} C_{heptane}$ and $K_{H_2} C_{H_2}$ could be neglected in the denominator.

For the alkene hydrogenation, the rate is given by

$$R_2 = \frac{mk_2 C_{H_2} C_{1-heptene}}{(1 + K_{1-heptyne} C_{1-heptyne} + K_{1-heptene} C_{1-heptene})^2} \quad (6.4)$$

Thus, the rate of consumption of alkene is determined by the difference of the aforementioned rates:

$$\frac{dC_{1-heptene}}{dt} = R_1 - R_2 \quad (6.5)$$

The rate of production of alkane is found from the rate of consumption of alkene:

$$\frac{dC_{heptane}}{dt} = R_2 \quad (6.6)$$

As 1-heptyne concentration profile tends towards zero order at the highest initial concentrations of 0.4 and 0.5 kmol m^{-3} (Figure 6.13), Langmuir-Hinshelwood model was fitted to lower initial concentrations of 1-heptyne. For 1-heptyne initial concentrations of 0.1, 0.2 and 0.3 kmol m^{-3}, (eqs 6.3-6.6) were fitted to the experimental data points using a solver function of MS Excel software to minimize the sum of the squares of the difference between experimental and calculated points. A constraint was imposed that the coefficient must be greater than or equal to zero. The dissolved concentration of hydrogen in isopropanol was determined by Hu $et\ al.$ (2007) to be $\sim$ 6 times higher than the dissolved concentration in water, and thus was used to estimate the concentration of hydrogen in isopropanol (0.0084 kmol m^{-3}) (Wood $et\ al.$ 2009). The catalyst loading used was 0.54 kg m^{-3}. The fitted values of the kinetic and adsorption parameters are shown in Table 6.6, and the lines shown in Figures

6.16a, 6.16b and 6.16c display the calculated concentration profiles for the same fitted constants.

k_1 ((m^3)^2/kmol kg s)	$K_{1-heptyne}$ (m^3/kmol)	k_2 ((m^3)^2/kmol kg s)	$K_{1-heptene}$ (m^3/kmol)
12.49	5.58	5.99	0

Table 6.6. Values of rate and adsorption constants determined by fitting eqs 6.3-6.6 to the experimental data shown in Figure 6.13.
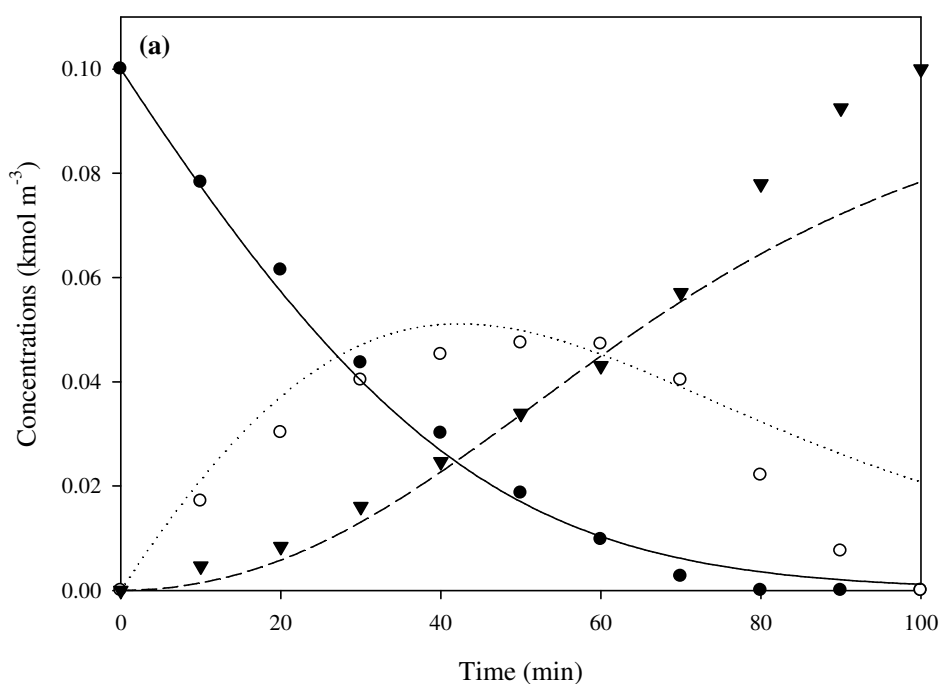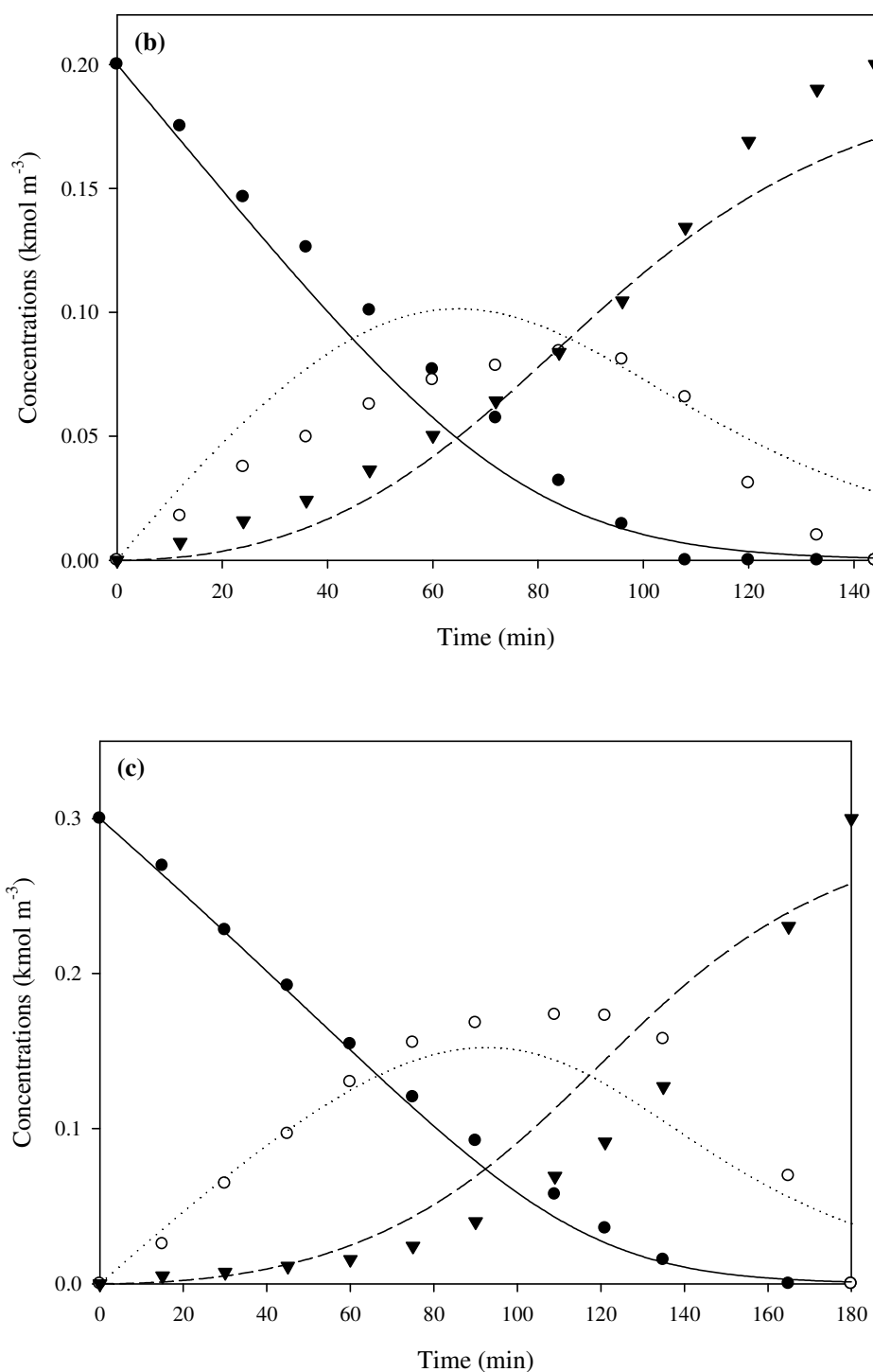
Figure 6.16. Fit of Langmuir-Hinshelwood expression represented by equations 6.3-6.6 to experimental concentration vs time profiles of the hydrogenation of 1-heptyne. (a) Concentration profiles at 0.1 kmol m^{-3} initial concentration of 1-heptyne (b) Concentration profiles at 0.2 kmol m^{-3} initial concentration of 1-heptyne. (c) Concentration profiles at 0.3 kmol m^{-3} initial concentration of 1-heptyne. Experimental data points: ($\bullet$) 1-heptyne, ($\circ$) 1-heptene and ($\blacktriangledown$) heptane. Lines shown are the best fits of the model equations to the experimental data points ((—) 1-heptyne, ($\cdots$) 1-Heptene, and (- - -) heptane).

As shown in Figure 6.16, the calculated values of 1-heptyne concentration show a good agreement at all times, and for 0.2 kmol m^{-3} concentration, the calculated values are slightly lower than the experimental values up until 95 min and are slightly higher after 95 min. In Figure 6.16a, the calculated and experimental values for 1-heptene and heptane display good agreement until 60 min reaction time, after which the calculated values are over-predicted for 1-heptene and under-predicted for heptane. In Figure 6.16b, the experimental values for heptane show good fit to the model, although under-predicted by the model after 120 min, and for 1-heptene, the experimental values were generally over-predicted by the model. In Figure 6.16c, the calculated and experimental values of 1-heptene and heptane display good agreement at all times; however, at ~ 68-138 min the experimental values are under-predicted for 1-heptene and over-predicted for heptane.

The adsorption coefficient $K_{1-heptene}$ is predicted to be zero, as shown in Table 6.6, which suggests that adsorption of alkene does not occur in isopropanol. The finding is in agreement with experimental studies of the adsorption coefficient that have been performed for the pentyne/pentene system over a Pd/Al$_2$O$_3$ catalyst by Bennett et al. (2009). In their work, adsorptions of 2-pentyne and 2-pentene were investigated by observing the change in concentration of a 2-pentyne or 2-pentene solution after being allowed to equilibrate with a high loading of Pd/Al$_2$O$_3$ catalyst for 1 h at 40 ^{o}C. The concentration of 2-pentyne experienced a significant reduction of about 11%, while 2-pentene exhibited a small decrease in concentration (~5 times less than that observed with the alkyne). Their finding together with the predicted adsorption coefficient for 1-heptene in this work indicates that alkene adsorption upon palladium is much lower than alkyne adsorption. This could explain the rapid hydrogenation of alkene after the depletion of the alkyne from the solution. Figure 6.17 shows a plot of initial reaction rate versus initial concentration of 1-heptyne. The rates are calculated after 40 min from the start of the reaction and demonstrated an increasing

behaviour with increasing initial concentration of 1-heptyne, except for the highest initial concentrations of 0.4 and 0.5 mol l^{-1}, where a decrease in reaction rate was observed. In the limiting cases, the mathematical form of the rate equation described in eq 6.3 suggests that, first-order behaviour would occur at low concentrations of 1-heptyne, whereas a negative reaction order in 1-heptyne may result at high concentrations (Wood *et al*. 2009). Referring to Figure 6.13, the concentration profiles of 1-heptyne demonstrated first order behaviour except for the highest concentrations of 0.4 and 0.5 mol l^{-1} that were closer to zero order behaviour for a wide range of the reaction time. The inhibiting effect at the highest concentrations of 0.4 and 0.5 mol l^{-1} could be due to a competitive adsorption between 1-heptyne and hydrogen with the former much more strongly adsorbed onto the catalyst surface, thus preventing the adsorption of hydrogen and therefore slowing the reaction.
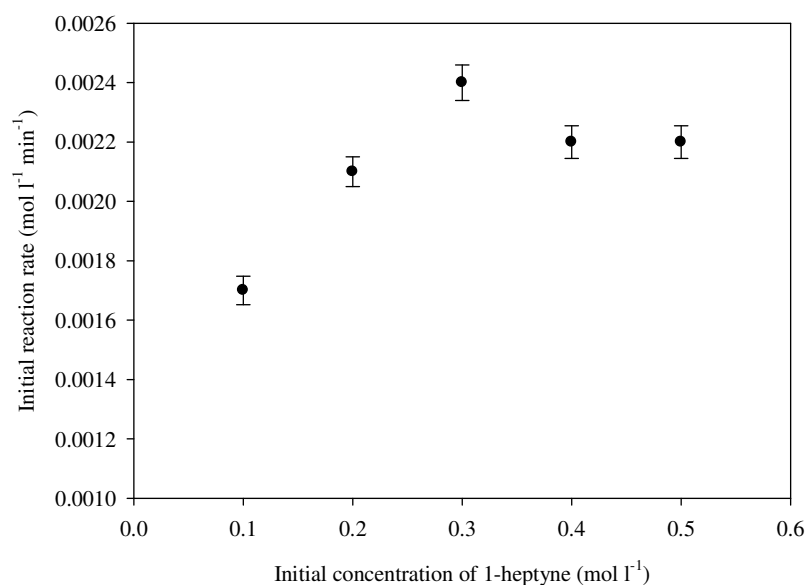
Figure 6.17. Initial reaction rate versus initial concentration of 1-heptyne.

6.5 Converting the recirculating batch into continuous operation

An attempt has been made to investigate the feasibility of continuous operation with a single pass of reaction mixture through the catalyst bed. To achieve this objective, the previously optimized conditions, in particular initial concentration of 1-heptyne and liquid flow rate

needed to be scaled down in order to obtain acceptable conversion levels of 1-heptyne per pass into the catalyst bed. The optimum conditions of 100 ml mixture (5 % v/v 1-heptyne in isopropanol), H_2 flow rate of 100 ml min^{-1}, liquid flow rate of 20 ml min^{-1}, 20 ^{o}C temperature and atmospheric pressure, were taken as a basis for calculating the required parameters. To start with, the conversion obtained at these conditions was calculated per minute of reaction. The required concentration of 1-heptyne and liquid flow rate were then calculated to be 0.0273 mol l^{-1} and 2.8 ml min^{-1}, respectively. When the reaction was carried out at these conditions, a full conversion of 1-heptyne and 25% selectivity to 1-heptene were achieved upon passing the whole mixture into the catalyst bed. The influence of liquid flow rate upon the catalytic performance was then investigated and the results are shown in Table 6.7. As can be seen in Table 6.7, increasing liquid flow rate from 2.8 to 5.5 ml min^{-1} decreased 1-heptyne conversion from 100% to 81%, whereas further increase in liquid flow rate to 10.5 ml min^{-1} diminished the conversion. On the other hand, the selectivity to 1-heptene increased from 25% to 49% upon increasing the liquid flow rate from 2.8 to 5.5 ml min^{-1}. The decrease in 1-heptyne conversion and the increase in the selectivity to 1-heptene accompanied the increase in liquid flow rate from 2.8 to 5.5 ml min^{-1} could be attributed to residence time effects as explained previously. For batch recycle operation data in which at a flow of 5 ml min^{-1}, conversion of 81 %, 1-heptene selectivity was approximately 83 % (Figure 6.8). Comparing this with continuous operation data of Table 6.7, for a similar flowrate of 5.5 ml min^{-1}, conversion of 81 %, 1-heptene selectivity was 49 %. Figure 6.8 also shows this point for continuous operation for purposes of comparison with batch recycle operation. Therefore it appears that the longer residence time required for continuous operation leads to considerably lower selectivity compared with the equivalent batch recycle conditions.

Catalyst deactivation is known to affect the performance of catalytic reactions and could be caused by several factors including substrate impurities. In this work, catalyst deactivation

was investigated by conducting a continuous reaction for 6 h under liquid flow rate of 3.5 ml min^{-1} and the results are displayed in Figure 6.18. As shown in Figure 6.18, catalyst performance remained unaffected during the entire reaction period, totalling a TON of 60. Thus it appeared that the catalyst did not deactivate during the course of an extended experiment, although further studies of catalyst recycling would be required to confirm whether it could be effectively recycled.

Run	Liquid flow rate (ml min^{-1})	Reaction time (min)	Average residence time (s)	% conversion of 1-heptyne	% selectivity to 1-heptene
14	2.8	36	14.72	100	25
15	3.5	29	12.15	90	40
16	4	25	10.83	83	44
17	5.5	18	8.24	81	49
18	10.5	9.5	4.72	0	0

Table 6.7. Effect of liquid flow rate upon the catalytic performance with single pass of reaction mixture through the catalyst bed. Conditions: 100 ml mixture (0.0273 mol l^{-1} of 1-heptyne in isopropanol), H$_2$ flow rate of 100 ml min^{-1}, 20 $^{\circ}$C temperature and atmospheric pressure.
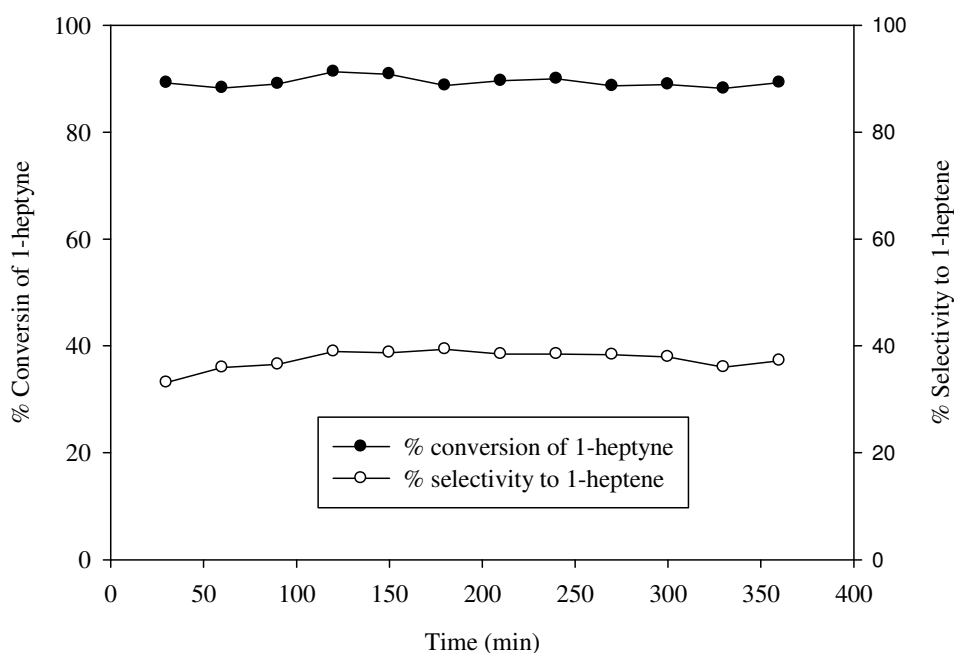
Figure 6.18. Investigation of catalyst deactivation. Reaction conditions: 100 ml mixture (0.0273 mol l^{-1} of 1-heptyne in isopropanol), H$_2$ flow rate of 100 ml min^{-1}, liquid flow rate of 3.5 ml min^{-1}, 20 $^{\circ}$C temperature and atmospheric pressure.

6.6 Conclusion

The hydrogenation of 1-heptyne over 2 wt. % Pd/Al$_2$O$_3$ catalyst was studied in a fixed-bed reactor working under trickle flow regime. The hydrogenation of 1-heptyne was carried out in isopropanol and hexane solvents, with the addition of small quantities of either water or sodium hydroxide base. Influence of solvent selection showed that there was a tradeoff between obtaining a fast reaction rate and a high selectivity to 1-heptene. The addition of water and sodium hydroxide to isopropanol solvent caused a noticeable increase in the reaction rate, with the fastest reaction obtained when only hexane was used as the solvent. The highest selectivity to 1-heptene was achieved in isopropanol, although the rate was faster in the other solvents. Reaction rate and selectivity could be promoted by optimizing liquid flow rate which was found to be directly proportional to wetting efficiency of the catalyst bed, liquid holdup as well as mass transfer of H$_2$ from bulk liquid to catalyst surface. The best selectivity trend was observed at the highest liquid flow rate of 20 ml min^{-1} that corresponded

216

to the lowest residence time of reaction mixture in the catalyst bed. The effect of 1-heptyne initial concentration was investigated and it was shown that increasing the alkyne concentration increased initial reaction rate to a maximum value, after which the reaction rate decreased. The inhibiting effect at the highest concentrations of 0.4 and 0.5 mol l^{-1} was thought to be due to a competitive adsorption between 1-heptyne and hydrogen into the catalyst surface. The concentration profiles of 1-heptyne as a function of time were fitted satisfactorily using a Langmuir-Hinshelwood expression. The expression was fitted to the experimental data points using a solver function of MS Excel software. The adsorption coefficient $K_{1-heptene}$ was predicted to be zero which suggests that adsorption of alkene does not occur in isopropanol. Performing reaction in one pass is feasible but long residence time of liquid phase leads to overhydrogenation of 1-heptene to heptane.

CHAPTER 7

SELECTIVE HYDROGENATION OF SOYABEAN OIL

7.1 Introduction

Hydrogenation of vegetable oils is an important process in the fats and oils industry due to its wide applications, such as modification of the oils physical characteristics for specific uses and increase of its stability towards oxidation (Belkacemi *et al*. 2006). Figure 7.1 demonstrates the simplified reaction scheme for hydrogenation of soybean oil, with the various intermediates generated through *cis-trans* isomerisation. Belkacemi *et al*. (2006) reported that the *trans* fatty acids (TFA) content of the hydrogenated oils obtained by means of the existing industrial technology is high (15-30% of total fatty acids) which largely exceeds the 5%-recommended level, thus constituting its major drawback. Moreover, Fernández *et al*. (2009) stated that in common industrial hydrogenation processes it has not been possible to produce partially hydrogenated oil with low *trans*-isomer content.

Among various noble catalysts used for the hydrogenation of vegetable oils, palladium represents a better compromise between higher activity and lower selectivity towards TFA formation via isomerization (Belkacemi *et al*. 2006). Fernández *et al*. (2009) pointed out that use of Pd catalysts in the hydrogenation of edible oils is attractive due to their higher activity than the commonly used Ni catalysts, and because the operation can be carried out under softer conditions.

Hydrogenation of triglycerides (TAG) incorporates chemical reaction as well as mass and heat transfers, where maximizing the interface between the hydrogen, the catalyst and the edible oil is required. Transport limitations on hydrogen and triglycerides to the active sites of the catalyst, have a strong influence on both selectivity (Beenackers and Swaaij van, 1993) and TFA production (Jonker *et al*. 1998; Schmidt, 2000). Balakos and Hernandez (1997) reported that among the factors influencing mass and heat transfers, the efficient

218

solubilisation of hydrogen in the oil, the transport of hydrogen and triglycerides to the catalyst surface and the available surface of the catalyst are very critical in hydrogenation reaction. Although fixed-bed reactors are known to provide a large interfacial area between the oil and hydrogen (Heldal *et al*. 1989), their potential for use in the hydrogenation of soyabean oil has only been investigated in a limited number of studies. Fixed-bed reactors also keep the catalyst working at its maximum efficiency in supplying hydrogen and thus result in a minimum amount of *trans* fatty acids produced at any given temperature.

This chapter reports studies of the behaviour of a recirculating fixed-bed reactor for partial hydrogenation of soyabean oil, with specific focus on the influence of temperature (§7.2) and hydrodynamics (§7.3). The catalytic performance of 2 wt. % Pd/Al_2O_3 catalyst in the selective hydrogenation was evaluated using 12.5 ml of soyabean oil at atmospheric pressure of H_2. The reactions were operated with gas and liquid flow rates of 250 and 3.5 ml min^{-1}, respectively that corresponded to a trickle flow regime. The influence of soyabean oil volume at optimized conditions is discussed in §7.4.

The performance of the 2 wt. % Pd/Al_2O_3 catalyst in the TBR was assessed in terms of reaction rate, selectivity toward *cis*-C18:1 and formation of the saturated product C18:0. An *et al*. (1998) stated that the overall degree of oil hydrogenation is usually quantified by the iodine value (IV), which is expressed in terms of the number of centigrams of iodine absorbed per gram of oil (I_2 reacts with the double bonds of unsaturated fatty acids). In the present study, the IV of hydrogenated oil was calculated from the composition obtained by GC analysis using Equation 7.1 (Pétursson, 2002):

$$IV = (\%C18:1 \times 0.8598) + (\%C18:2 \times 1.7315) + (\%C18:3 \times 2.6152) \qquad (7.1)$$

A specific aim of this study was the hydrogenation of oils with the maximum formation of *cis* oleic acid and a minimum increase in the amount of stearic acid (C18:0), maintaining a low *cis-trans* isomerization. The optimized results from the TBR are compared with those of slurry based systems in §7.5.
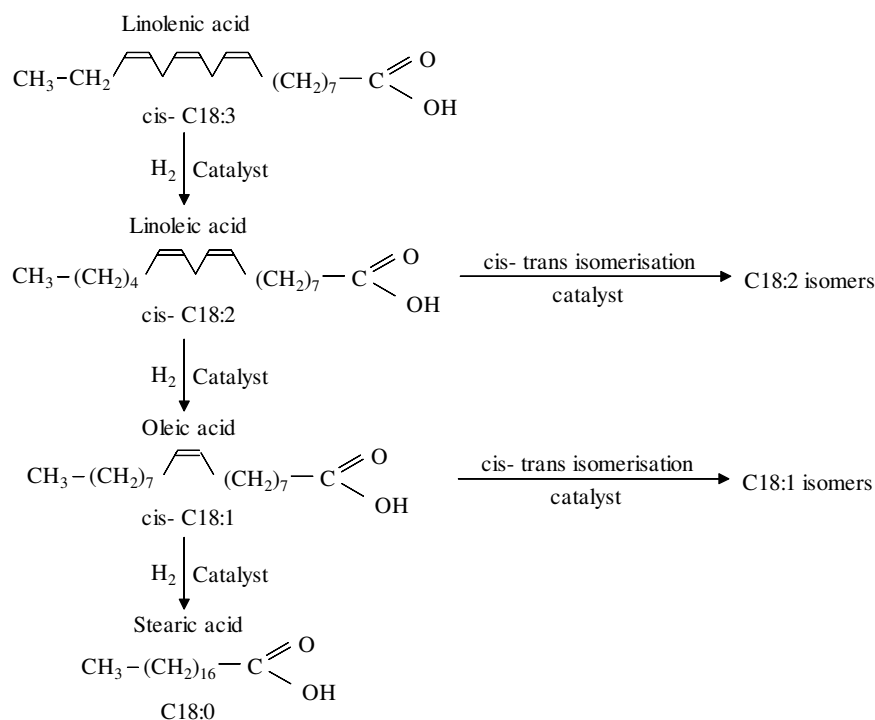
Figure 7.1. Soybean oil hydrogenation and isomerisation network in presence of solid catalyst (Nohair *et al*. 2005).

7.2 Effect of temperature

It is desirable to operate at high temperatures due to higher reaction rates; however, higher temperatures conventionally also lead to increased formation of TFAs. Moreover, Drozdowski and Szukalska (2000) reported that the isomerization coefficient for soyabean oil is 0.5~0.6 and that the use of low temperature reduces trans-isomer formation. In order to study the effect of temperature, experiments were conducted in the temperature range from 50 to 105 ºC.

Figure 7.2 depicts the fatty acid profiles of soyabean oil hydrogenated at an initial reaction temperature of 50 ºC. As shown, linolenic acid (C18:3) was completely hydrogenated within

240 min of reaction, while linoleic acid (C18:2) achieved 90% conversion within same reaction time. The level of *cis* oleic acid (C18:1) initially increased, then levelled-off and subsequently decreased; on the other hand, *trans* oleic acid (C18:1) demonstrated a steady increase to a final value of 22% after a reaction time of 240 min. Furthermore, the content of stearic acid (C18:0) experienced a steady increase for 180 min but thereafter started to build up significantly, reaching a high value of 40% of total fatty acids after 240 min of reaction time.
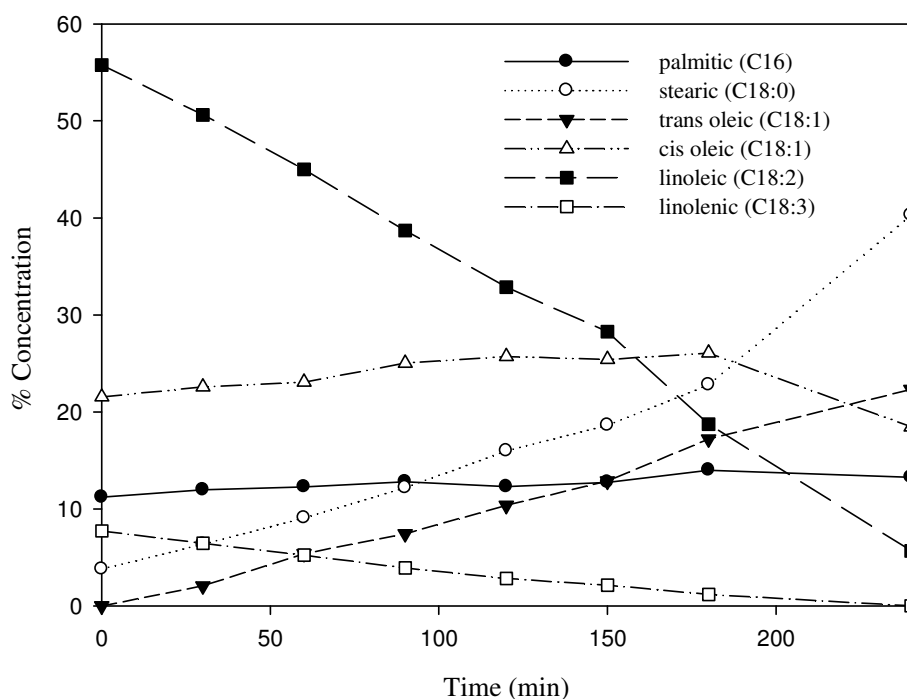
Figure 7.2. Fatty acid profiles of soyabean oil hydrogenated with 2 % Pd/Al_2O_3 catalyst. Conditions: 50 °C, atmospheric pressure, hydrogen flow rate of 250 ml min^{-1} and liquid flow rate of 3.5 ml min^{-1}.

7.2.1 Effect of temperature on hydrogenation rate

Figure 7.3 shows the effect of temperature on hydrogenation rate expressed in terms of iodine value (IV). As can be seen in Figure 7.3, the reduction in IV increased with an increase in temperature and levelled off at the highest two temperatures of 85 and 105 °C.
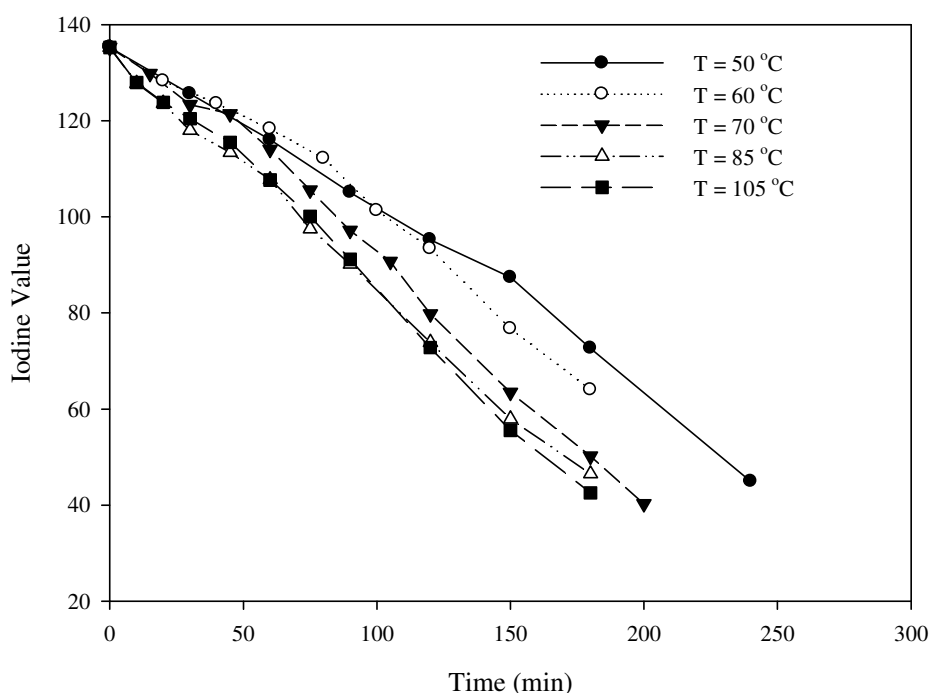
Figure 7.3. Effect of reaction temperature on reduction in IV during hydrogenation of soyabean oil. Conditions: atmospheric pressure, hydrogen flow rate of 250 ml min^{-1} and liquid flow rate of 3.5 ml min^{-1}.

The obtained concentration and conversion profiles of linoleic acid (C18:2) are also shown in Figure 7.4 and 7.5, respectively. Figures 7.3-7.5 show that the overall hydrogenation activity increased as temperature increased. Belkacemi and Hamoudi (2008) pointed out that an increase in temperature involves a viscosity drop, thus favouring the gas-liquid, liquid-solid and intraparticle transfers. Furthermore, the increase in the temperature is expected to increase reaction rate constant, thus affecting the overall hydrogenation rate of the reaction.
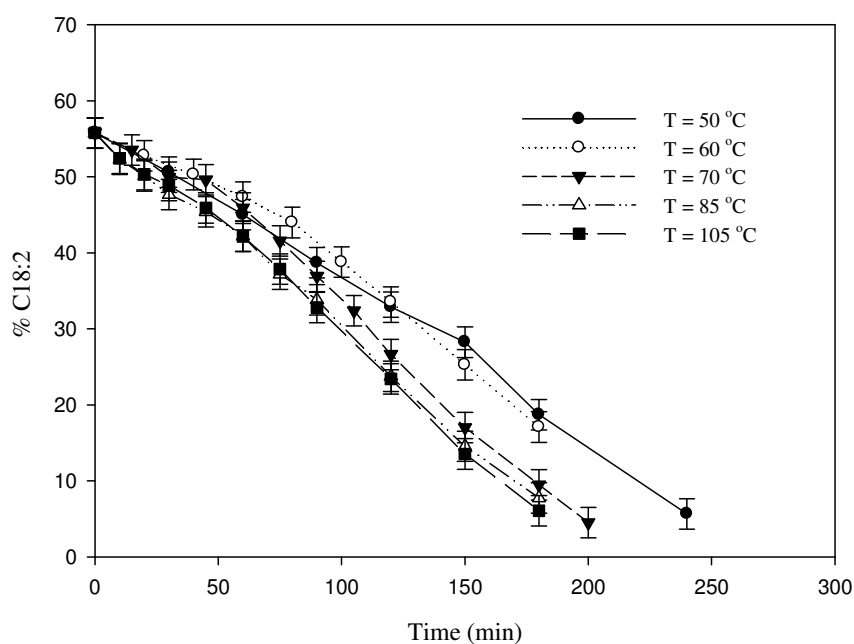
Figure 7.4. Comparison of linoleic acid (C18:2) concentration profiles at different reaction temperatures. Conditions: atmospheric pressure, hydrogen flow rate of 250 ml min^{-1} and liquid flow rate of 3.5 ml min^{-1}.
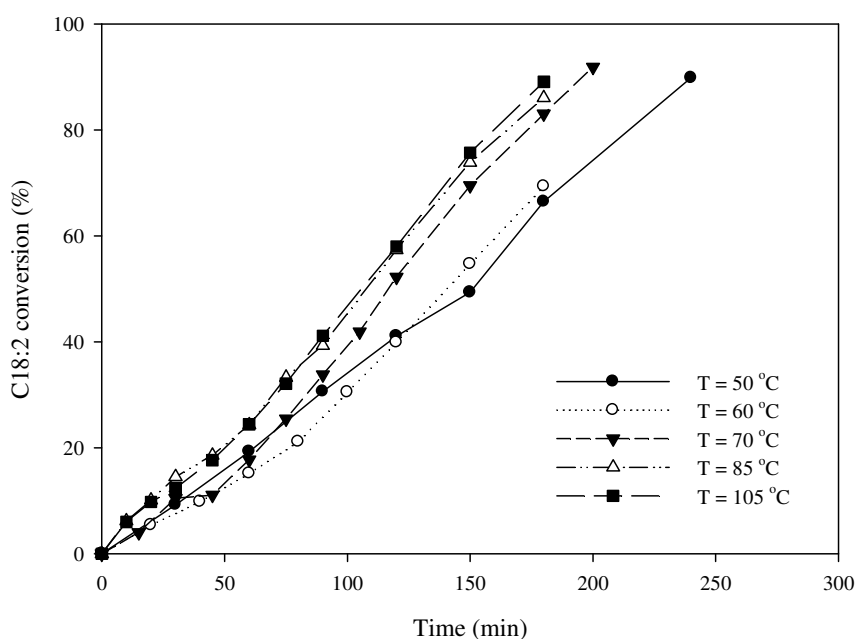
Figure 7.5. Comparison of linoleic acid (C18:2) conversion profiles at different reaction temperatures. Conditions: atmospheric pressure, hydrogen flow rate of 250 ml min^{-1} and liquid flow rate of 3.5 ml min^{-1}.

7.2.2 Effect of temperature on selectivity

In soyabean oil hydrogenation, the notation of selectivity is important. The hydrogenation selectivity describes the preference of hydrogenation of polyenes over monoenes. The hydrogenation selectivity is deemed high if no saturated acid is formed until almost all polyene has been hydrogenated (Coenen, 1976). Therefore, it is useful to introduce selectivities that describe hydrogenation towards the desired products. A well-known and accepted method to determine the selectivity is from the ratio of reaction rate constants (Satterfield, 1970) governing the reaction as shown in Eq. 2.6 below.

$$\text{Liolenic acid} \xrightarrow{k_1} \text{Linoleic acid} \xrightarrow{k_2} \text{Oleic acid} \xrightarrow{k_3} \text{Stearic acid}$$

$$\text{(C18:3)} \qquad\qquad \text{(C18:2)} \qquad\qquad \text{(C18:1)} \qquad\qquad \text{(C18:0)} \qquad (2.6)$$
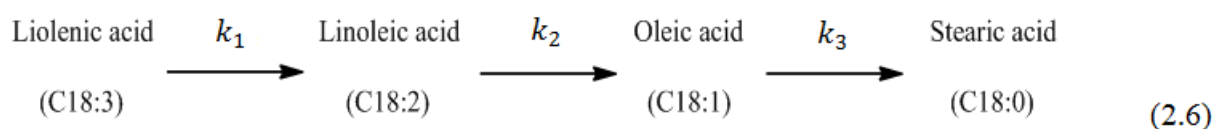
The concept of "traditional" selectivity has therefore been introduced in the literature, which describes the preference for hydrogenation of polyenes over monoenes by the ratio of rate constant. Thus:

$$S_{Ln} = \frac{k_1}{k_2} \tag{2.11}$$

$$S_L = \frac{k_2}{k_3} \tag{2.12}$$

Where S_{Ln} and S_L represent the linolenic and linoleic selectivity, respectively.

For industrial hardening, S_L is the most important parameter and hydrogenation is considered to be selective when S_L is higher than 10 (Albright, 1965). A very low value of S_L (<5) designates a significant formation of stearic acid (C18:0) from the beginning of the reaction, whereas high value of S_L indicates that its formation is held back until the linoleic acid is almost eliminated (Coenen, 1976). Accordingly, the present work aims to obtain hydrogenated product that contains less than 1% linolenic (C18:3) without substantial increase in stearic acid (C18:0). The values of the rate constants in this work were obtained

from a fit to the data (An example of the fit of data for 50 ºC is shown in Appendix B, P 305). The various selectivities computed as above for the investigated reaction temperatures are presented in Table 7.1.

Run	Temperature (ºC)	k_1 (min^{-1})	k_2 (min^{-1})	k_3 (min^{-1})	S_{Ln}	S_L
1	50	0.0365	0.208	0.105	0.1755	1.981
2	60	0.0483	0.216	0.118	0.2236	1.831
3	70	0.0483	0.262	0.190	0.1843	1.379
4	85	0.0511	0.268	0.190	0.1907	1.410
5	105	0.0525	0.279	0.190	0.1882	1.468

Table 7.1. Effect of temperature on linolenic and linoleic selectivities. Conditions: atmospheric pressure, hydrogen flow rate of 250 ml min^{-1} and liquid flow rate of 3.5 ml min^{-1}.

Referring to Table 7.1, the obtained rate constants were found to follow the order $k_2 > k_3 > k_1$, which indicates that three double bonds are hydrogenated more slowly than two and single double bonds in the corresponding molecules. Moreover, the values of the rate constants were generally found to increase with an increase in reaction temperature. Over the range of investigated temperatures, the linolenic selectivity values were very low (<0.25), that increased slightly upon increasing reaction temperature from 50 to 60 ºC and maintained a lower value of about 0.19 at higher reaction temperatures. The linoleic selectivity, on the other hand, decreased with an increasing reaction temperature achieving a maximum value of about 2 at the lowest temperature of 50 ºC. The low value of the linoleic selectivity indicates a significant formation of stearic acid from the beginning of the reaction.

Figure 7.6 is a plot of *cis* oleic content versus conversion of linoleic acid. For reaction temperature of 50, 60 and 70 ºC, the content of *cis* oleic increased slightly up to 40%

conversion of linoleic acid and dropped gradually afterwards to lower than 19% at the final achieved conversion of linoleic acid. For reaction temperature of 85 and 105 ℃, *cis* oleic retained its initial value up to 40% conversion of linoleic acid before dropping to lower than 19 % at the final conversion of linoleic acid.
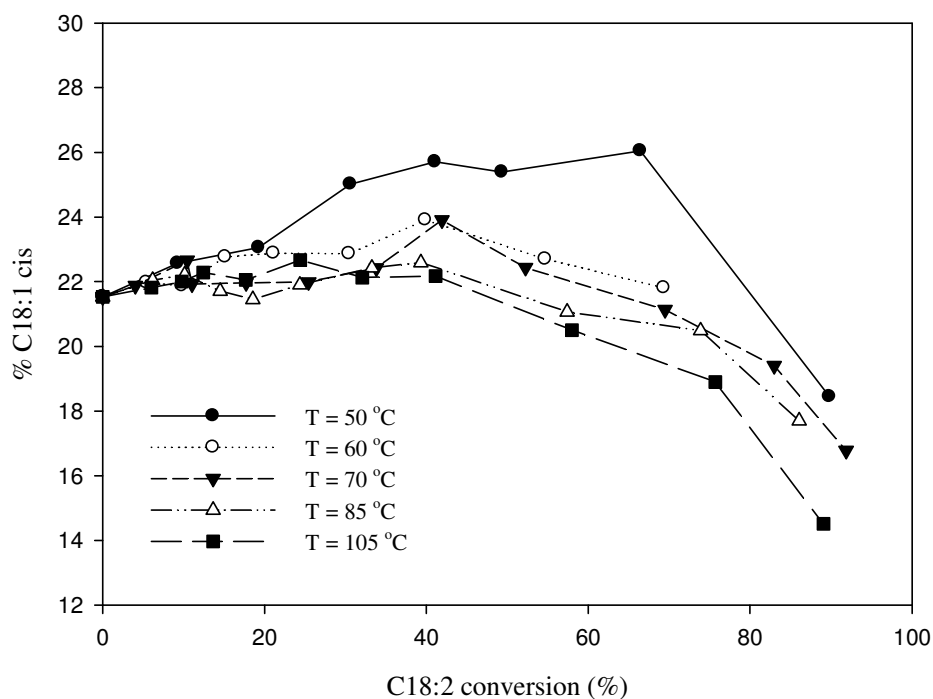
Figure 7.6. Comparison of *cis* oleic concentration profiles obtained at different reaction temperatures.

7.2.3 Effect of temperature on *trans* and saturated fatty acid formation

In a traditional three phase slurry reactor an increase in temperature increases the rate of hydrogen consumption which in turn increases hydrogen starvation of the catalyst and therefore leads to higher TFA formation (Singh, 2009). The TBR, however, keeps the catalyst working at its maximum efficiency thorough a continuous supply of hydrogen, and therefore is expected to result in a minimum amount of *trans* fatty acids produced at any given temperature. Figure 7.7 demonstrates the effect of increasing temperature upon the formation of *trans* C18:1 during hydrogenation in the TBR. As can be seen in Figure 7.7, similar amounts of *trans* C18:1(of about 22%) were obtained over the range of investigated

temperatures at the maximum conversion of C18:2. The minor influence of temperature on TFA formation can be attributed to similar hydrogen concentrations at the catalyst surface.
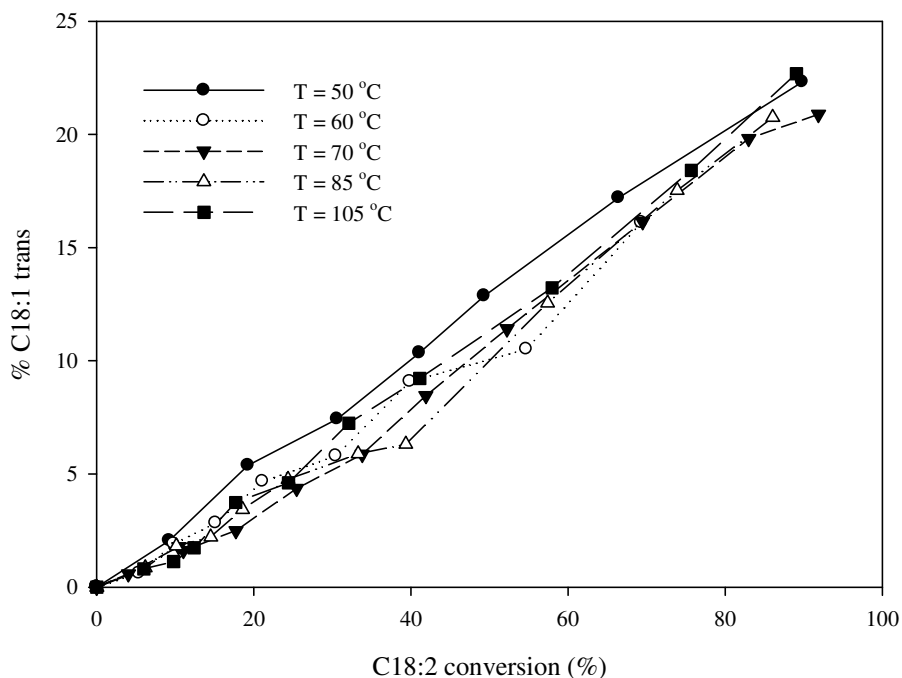
Figure 7.7. *Trans* fatty acid content (C18:1) as a function of C18:2 conversion at different reaction temperatures.

Figure 7.8 represents the influence of temperature upon the evolution of the C18:0 as a function of the C18:2 conversion. As shown in Figure 7.8, the content of C18:0 demonstrated a steady increase during the course of the reaction for all investigated temperatures. It is noteworthy that the lowest rate of C18:0 formation was obtained with the lowest temperature of 50 °C, although a similar content of C18:0 (~42%) was obtained with all temperatures at the highest conversion of C18:2.
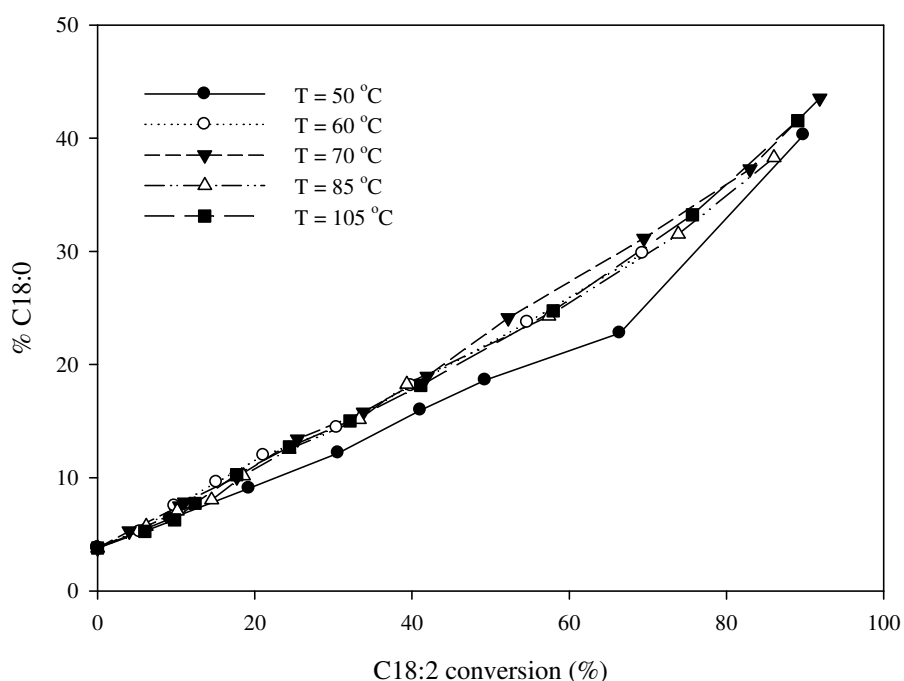
Figure 7.8. Stearic acid content (C18:0) as a function of C18:2 conversion at different reaction temperatures.

7.2.4 Kinetic model

7.2.4.1 Rate expression in terms of IV

It is well known that the saturation of double bonds follows first order simple kinetics with respect to reduction of IV (Tike and Mahajani, 2006). Consequently, dependence between rate and reactant concentration in terms of IV can be expressed as (Tike and Mahajani, 2006):

$$\text{r} = -\frac{d(IV)}{dt} = k_{IV}(IV) \tag{7.2}$$

The value of k_{IV} was evaluated at different temperatures (50, 60, 70, 85 and 105 °C) and was found to be 0.366, 0.398, 0.492, 0.495 and 0.519, respectively, under the conditions employed during hydrogenation. From the temperature dependence of the reaction rate constant, the energy of activation was found to be 6.718 kJ/mol (Figure 7.9). The reaction activation energy obtained is much smaller than that for general chemical reaction (60-250 kJ/mol) (Cheng-wei *et al.* 2009). This suggests that mass transfer limitations were present in the reactions.

228
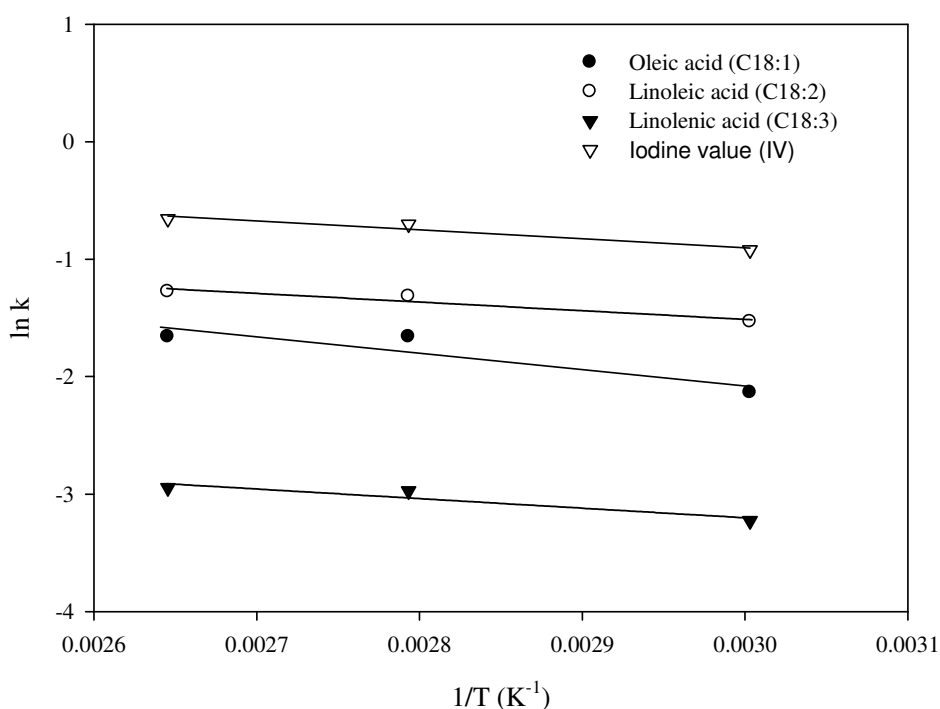
Figure 7.9. Temperature dependence of the reaction rate constants.

7.2.4.2 Rate expression in terms of fatty acid concentration

In order to obtain a thorough understanding of the reaction mechanism in the TBR, it was thought beneficial to find the rate expressions in terms of fatty acid concentrations. As can be seen clearly in Figure 7.1, hydrogenation of soyabean oil is a complex chemical reaction involving hydro isomerization. Moreover, the various reactants compete with each other for the active catalytic sites. During the hydrogenation reaction fatty acids compete with hydrogen through adsorption into the catalyst where they are gradually converted to the saturated state.

Thus the reduction of polyunsaturated fatty acid and the formation of monounsaturated fatty acid can be described as first order consecutive reaction as shown in Eq. 2.6. To illustrate the procedure describing the overall hydrogenation pseudo-kinetics, all reactions were considered to be irreversible and first order with respect to substrate.

With these simplification and assumptions, the apparent reaction rates depicted in Eq. 2.6 can be expressed as (Tike and Mahajani, 2006):

$$-\frac{d(C_{linolenic\ acid})}{dt} = k_1(C_{linolenic\ acid}) \tag{2.7}$$

$$-\frac{d(C_{linoleic\ acid})}{dt} = k_1(C_{linolenic\ acid}) - k_2(C_{linoleic\ acid}) \tag{2.8}$$

$$-\frac{d(C_{oleic\ acid})}{dt} = k_2(C_{linoleic\ acid}) - k_3(C_{oleic\ acid}) \tag{2.9}$$

$$-\frac{d(C_{stearic\ acid})}{dt} = k_3(C_{oleic\ acid}) \tag{2.10}$$

Where $(C_{linolenic\ acid}) = (C_{linolenic\ acid})_0$, $(C_{linoleic\ acid}) = (C_{linoleic\ acid})_0$, $(C_{oleic\ acid}) = (C_{oleic\ acid})_0$, and $(C_{stearic\ acid}) = (C_{stearic\ acid})_0$ at t=0.

For the reactions at each temperature, Eqs 2.7-2.10 were fitted to the experimental data points, to minimize the sum of the squares of the difference between experimental and predicted points for the concentrations of the fatty acids simultaneously, using a solver function of MS Excel software. A constraint was imposed that the apparent reaction rate constants k_1, k_2 and k_3 must be greater than or equal to zero.

The fitted values of the apparent reaction rate constants are shown in Table 7.2, and the lines shown in Figures 7.10 display the calculated concentration profiles for the same fitted constants for the reaction at 50 °C. The fitted concentration profiles from the other reaction temperatures are provided in Appendix B, p 306 & 307. The RSS in Table 7.2 represents the sums of the squares of the difference between the experimental and predicted composition of fatty acid profile of soyabean oil. As shown in Table 7.2 and Figure 7.10, the best agreement between the experimental and the predicted values was found for reaction temperature of 50°C.

Temperature (ºC)	k_1 (min^{-1})	k_2 (min^{-1})	k_3 (min^{-1})	RSS
50	0.0045	0.0040	0.0048	16.5
60	0.0045	0.0040	0.0062	100
70	0.0053	0.0052	0.0086	248
85	0.0051	0.0053	0.0087	83
105	0.0053	0.0054	0.0091	108

Table 7.2. Apparent reaction rate constants and RSS for kinetic model (Eqs. (2.7)-(2.10)).
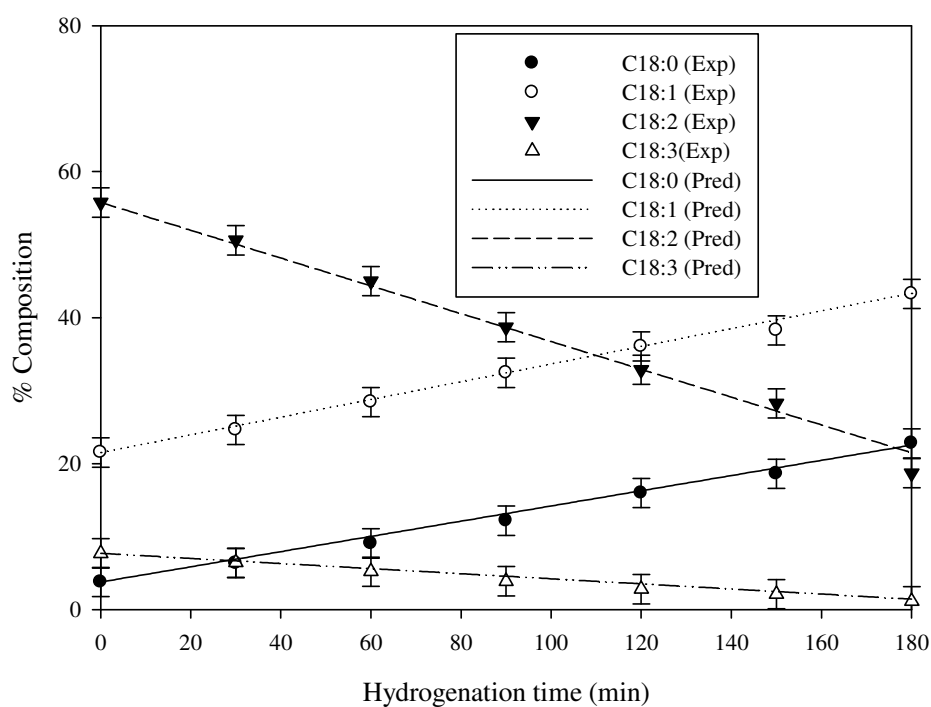
Figure 7.10. % Composition of fatty acids in soyabean oil under reaction temperature of 50 ºC (Points denote experimental values and lines are fitted models to the data).

7.3 Influence of the hydrodynamics

In a traditional slurry reactor the concentration of hydrogen in the bulk oil influences the catalyst's surface coverage of hydrogen and therefore affects the rate of hydrogenation (Dijkstra, 2006). Consequently, an increase in the solubility of hydrogen in oil would be expected to lower the formation of TFAs which are formed through the dissociation and isomerization of the unstable intermediates at low hydrogen concentration. Since the first development of the hydrogenation process in the 1920s, a number of investigations studied the kinetics and mass transfer. Albright (1973), Bern *et al*. (1976), Marangonizis *et al*. (1977) and Chen *et al*. (1983) reported that mass transfer is the rate-limiting step in most of the commercial reactors. Hsu *et al*. (1988) observed a reaction order of 0.6 with respect to hydrogen during hydrogenation of soyabean oil using $Pd-Al_2O_3$. Moreover, other authors have observed reaction orders in the range of 0.2-1.6 for palladium in slurry reactors (Singh, 2009).

In the TBR, maintaining effective contact of the gas and oil with the catalyst active sites becomes a significant design consideration in comparison with the well mixed stirred tank reactor. Therefore investigation of the hydrodynamics within the TBR is vital for evaluating the performance of the reactor. A suitable selection of gas and liquid flow rates is crucial when basic phenomena such as wetting efficiency of the catalyst bed and mass transfer are evaluated. Therefore, the effect of gas and liquid flow rates on the rate and selectivity of the reaction is discussed in the following sections.

The influence of the hydrodynamics was investigated by changing either gas or liquid flow rate while keeping the rest of the reaction conditions the same. The gas and liquid flow rates were selected as for the reaction to fall in the trickle flow regime as demonstrated in Figure 7.11. For rapid testing purposes, the effect of the hydrodynamics was studied under a temperature of 105 ℃ that gave the highest reaction rate (as demonstrated in § 7.2.1). The

optimized gas and liquid flow rates were then used to conduct a reaction at 50 ℃ that gave

the best linolenic selectivity (Table 7.1) as well as the best selectivity to *cis* oleic acid (Figure

7.6).
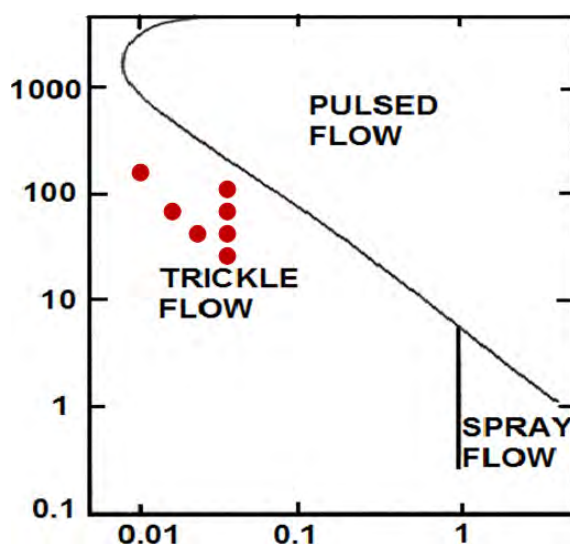
Figure 7.11. The correspondence of the TBR operating conditions in Baker's flow map.

7.3.1 Effect of gas flow rate

7.3.1.1 Effect of gas flow rate on hydrogenation rate

Figure 7.12 shows the effect of gas flow rate on hydrogenation rate expressed in terms of

iodine value (IV). As can be seen in Figure 7.12, the reduction in IV increased with an

increase in gas flow rate with the highest reduction obtained at the highest gas flow rate of

1000 ml min^{-1}. The obtained concentration and conversion profiles of linoleic acid (C18:2)

are also shown in Figure 7.13 and 7.14, respectively. Figures 7.12-7.14 show that the overall

hydrogenation activity increased with an increase in gas flow rate. Several authors found that

increasing gas flow rate in TBR enhances the quality of the liquid distribution over the

catalyst particles (Weekman and Myers, 1964; Saroha *et al*. 1998; Winterbottom *et al*. 2000;

Kundu and Saroha, 2001; Llamas *et al*. 2009). Therefore, the improved hydrogenation rate of

soyabean oil with increasing gas flow rate could be ascribed to improved liquid distribution and thus efficient utilization of the catalyst bed in the reactor.

Figure 7.12. Effect of gas flow rate on reduction in IV during hydrogenation of soyabean oil. Conditions: atmospheric pressure, 105 °C temperature and liquid flow rate of 3.5 ml min^{-1}.

Figure 7.13. Comparison of linoleic acid (C18:2) concentration profiles at different gas flow rates. Conditions: atmospheric pressure, 105 °C temperature and liquid flow rate of 3.5 ml/min.

Figure 7.14. Comparison of linoleic acid (C18:2) conversion profiles at different gas flow rates. Conditions: atmospheric pressure, 105 °C temperature and liquid flow rate of 3.5 ml min^{-1}.

7.3.1.2 Effect of gas flow rate on selectivity

The linolenic and linoleic selectivities were calculated for the various gas flow rates and are presented in Table 7.3. As shown in Table 7.3, the reaction rate constants increased with increasing gas flow rate. However, the gas flow rate does not seem to have an impact upon linolenic and linoleic selectivities which maintained low values of less than 5%. The profiles of *cis* C18:1 content versus total conversion of C18:2 obtained from the various gas flow rates are shown in Figure 7.15. For gas flow rates of 250, 500 and 750, the content of *cis* oleic acid maintained its initial value of 21.5% up to 40% conversion of linoleic acid after which *cis* oleic acid started to decrease. The best performance was obtained with the highest gas flow rate of 1000 ml min^{-1} at which the content of *cis* oleic increased slightly to 23.5% and remained constant up until 60% conversion of linoleic acid before starting to decrease.

Run	Gas flow rate (ml min^{-1})	k_1 (min^{-1})	k_2 (min^{-1})	k_3 (min^{-1})	S_{Ln}	S_L
5	250	0.0525	0.279	0.206	0.188	1.354
6	500	0.083	0.435	0.257	0.191	1.7
7	750	0.0851	0.467	0.269	0.182	1.736
8	1000	0.112	0.588	0.345	0.190	1.70

Table 7.3. Effect of gas flow rate on linolenic and linoleic selectivities. Conditions: atmospheric pressure, 105 ºC temperature and liquid flow rate of 3.5 ml min^{-1}.
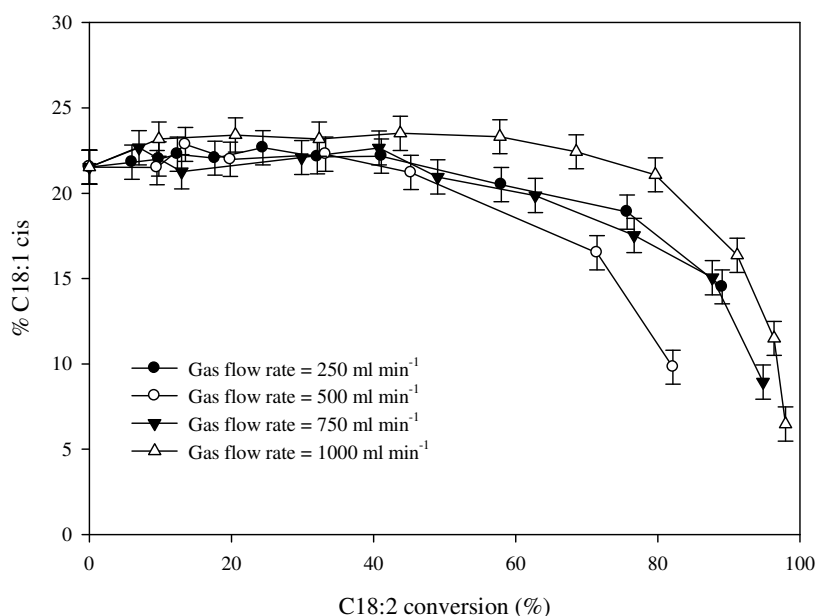
Figure 7.15. Comparison of *cis* oleic concentration profiles obtained at different gas flow rates.

7.3.1.3 Effect of gas flow rate on *trans* and saturated fatty acid formation

The profiles of *trans* oleic acid concentration versus total conversion of linoleic acid are displayed in Figure 7.16. As can be seen, the highest production rate of *trans* oleic acid was obtained with the highest gas flow rate of 1000 ml min^{-1}. Considering the reported low solubility of hydrogen in oil of about 0.00235 mol l^{-1} (Ganguli and Van den Berg, 1978), the

highest activity obtained with the highest gas flow rate could lead to the starvation of oil from hydrogen and thus favouring the formation of *trans* oleic acid.

On the other hand, increasing the gas velocity may have led to a decrease in the thickness of oil film upon the catalyst due to the drag force of gas flowing through the void space. In turn this could have led to a lower liquid hold up and hence decreased residence time of liquid, which would explain the lowest production rate of C18:0 obtained at the highest gas flow rate of 1000 ml min^{-1} as shown in Figure 7.17. Figure 7.18 is a plot of fatty acids concentrations vs time at the optimized gas flow rate of 1000 ml min^{-1}.
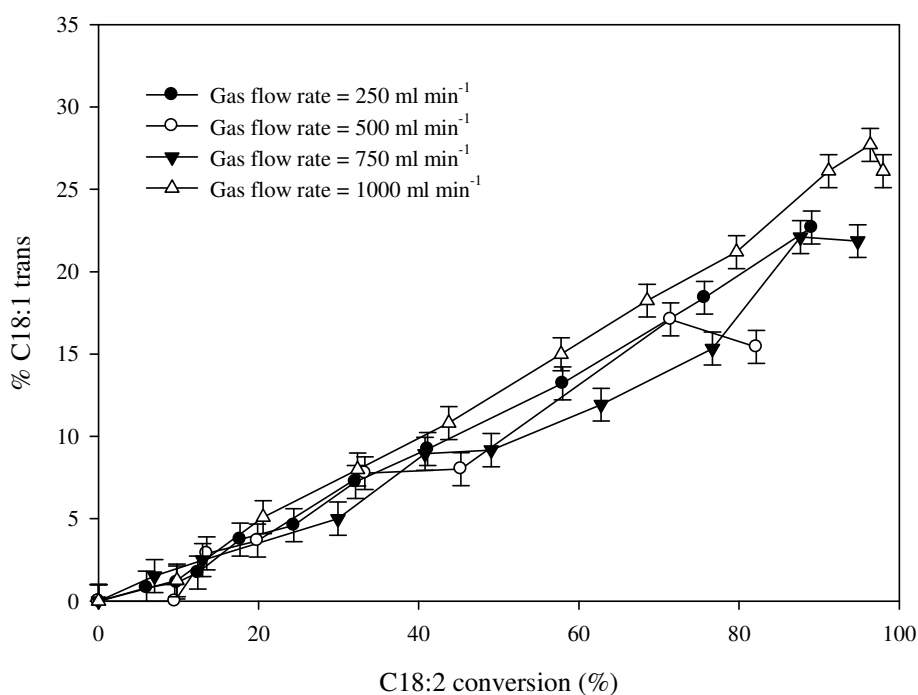
Figure 7.16. Trans fatty acid content (C18:1) as a function of C18:2 conversion at different gas flow rates.
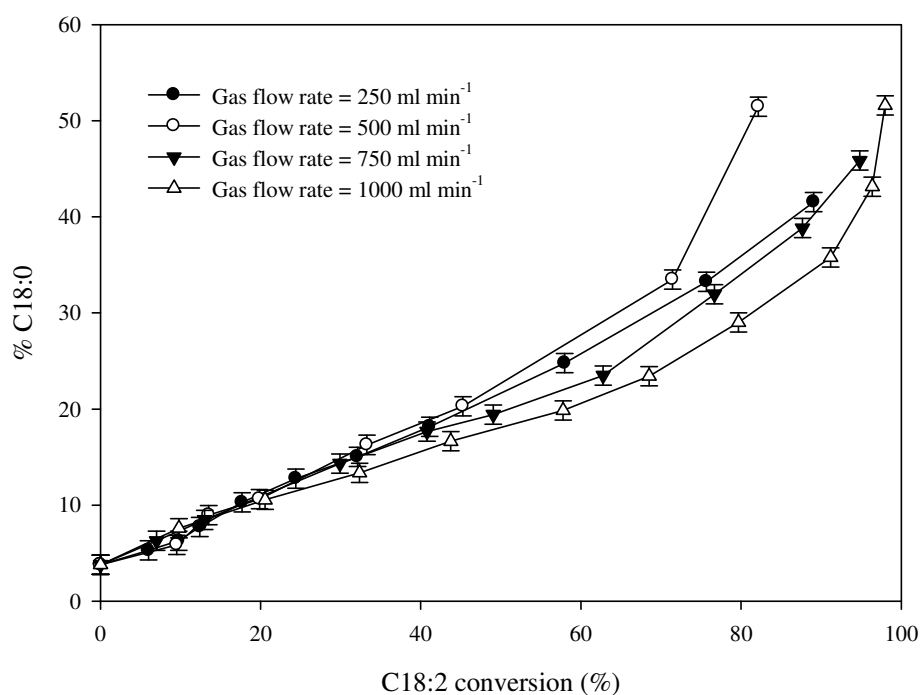
Figure 7.17. Stearic acid (C18:0) content as a function of C18:2 conversion at different gas flow rates.
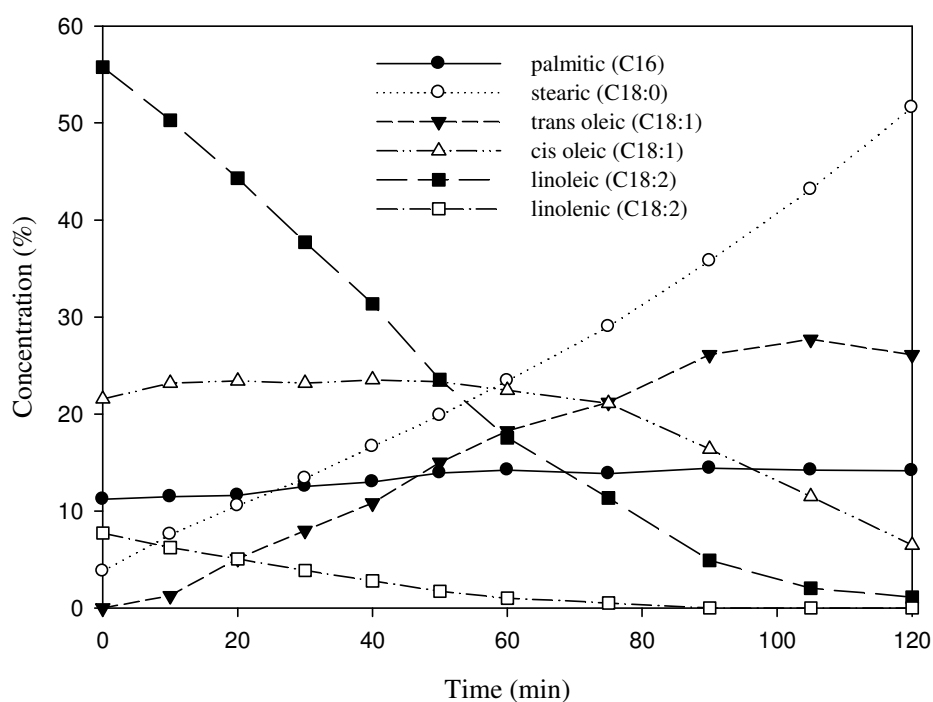
Figure 7.18. Fatty acid profiles of soyabean oil hydrogenated with 2 % Pd/Al$_2$O$_3$ catalyst.
Conditions: 105 ºC, atmospheric pressure, hydrogen flow rate of 1000 ml min^{-1} and liquid flow rate of 3.5 ml min^{-1}.

238

7.3.2 Effect of liquid flow rate

7.3.2.1 Effect of liquid flow rate on hydrogenation rate

For each run the gas flow rate was kept constant at 1000 ml min^{-1}, as this flow rate provided the best compromise between reaction rate and selectivity values, and the liquid flow rate was gradually increased stepwise. Figure 7.19 shows the effect of liquid flow rate on hydrogenation rate expressed in terms of iodine value (IV). The obtained concentration and conversion profiles of linoleic acid (C18:2) are also shown in Figure 7.20 and 7.21, respectively. Figures 7.19-7.21 show that the overall hydrogenation activity decreased at the highest two liquid flow rates of 6.5 and 8 ml min^{-1}.
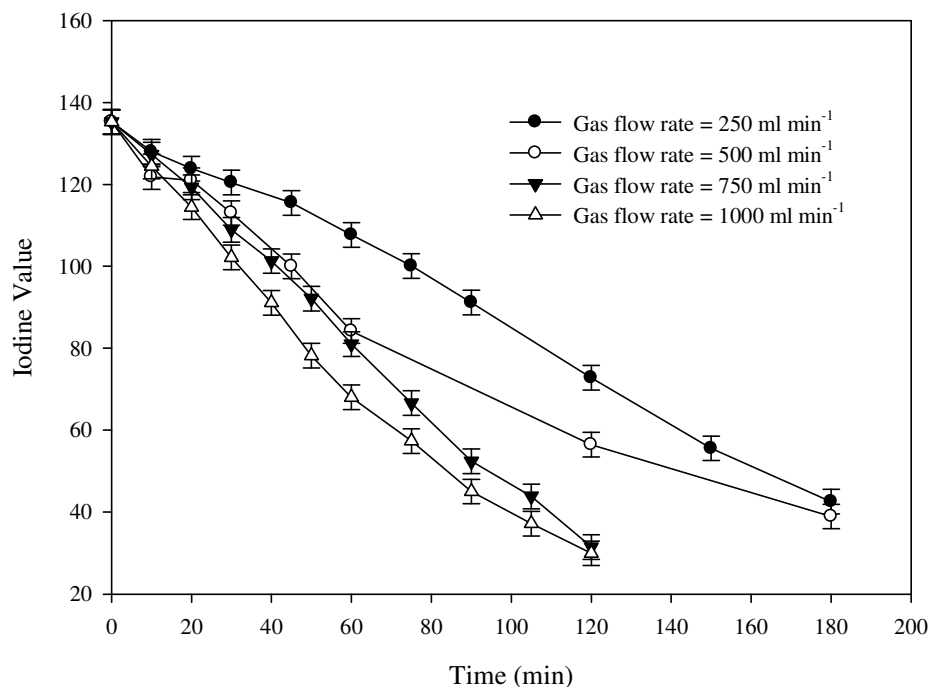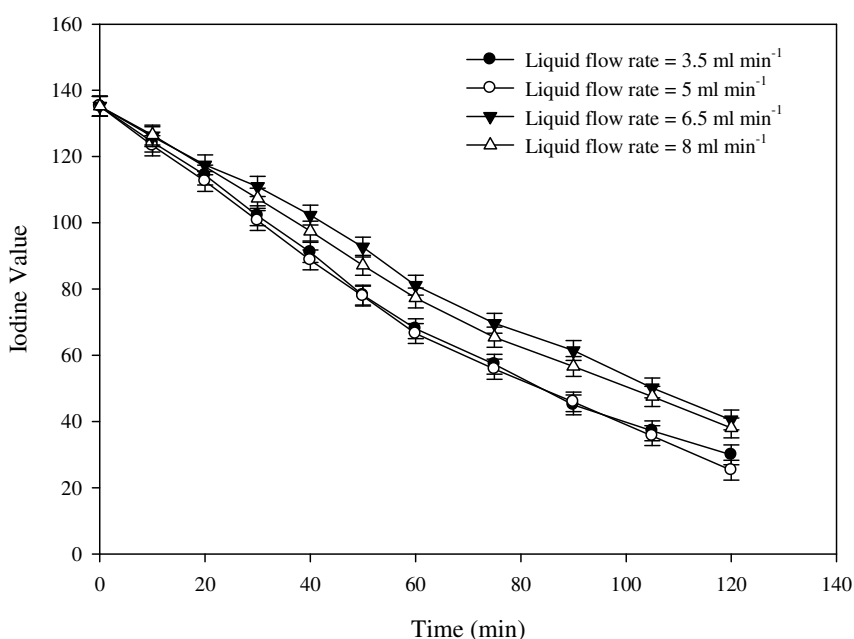

Figure 7.19. Effect of liquid flow rate on reduction in IV during hydrogenation of soyabean oil. Conditions: atmospheric pressure, 105 ℃ temperature and hydrogen flow rate of 1000 ml min^{-1}.
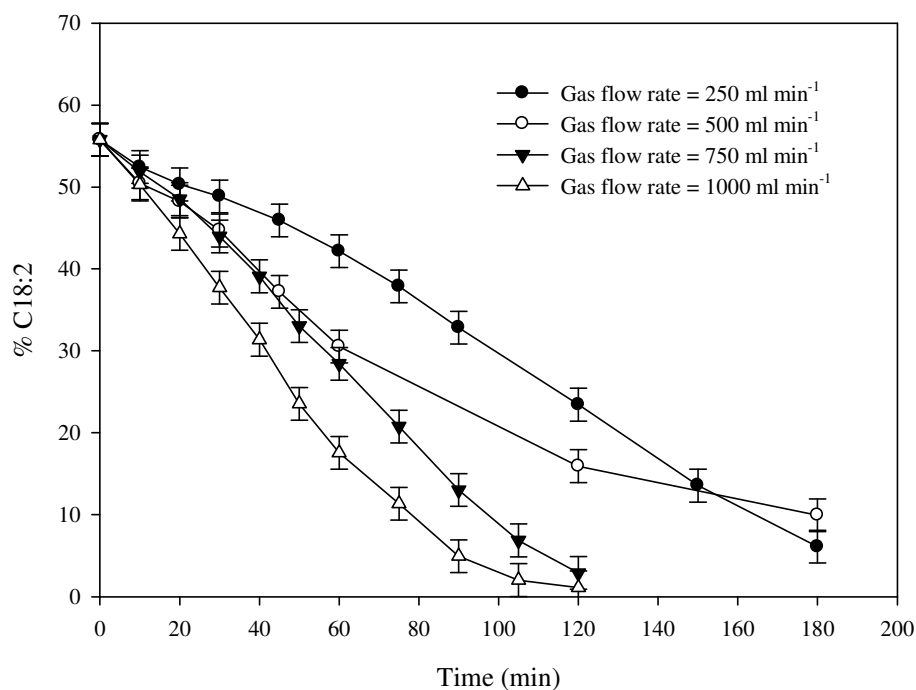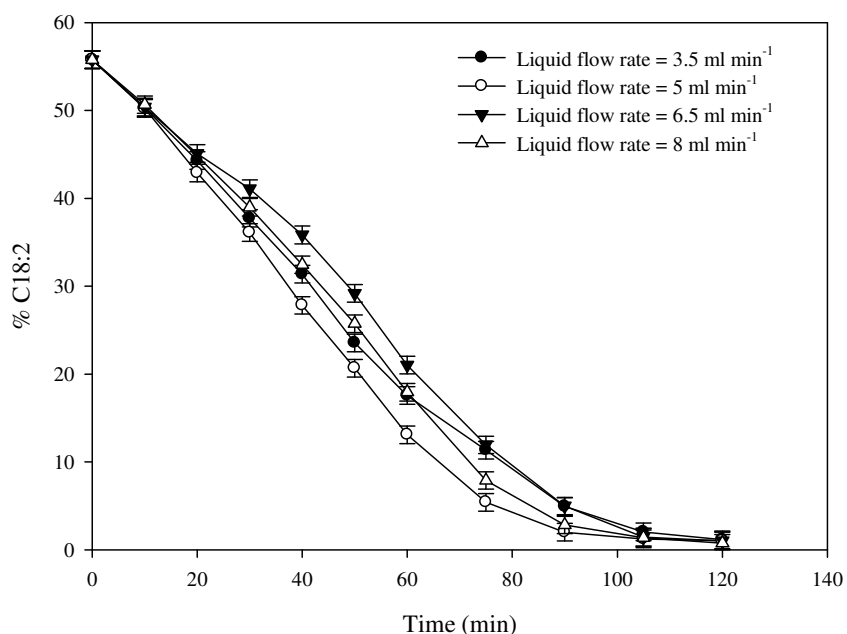
Figure 7.20. Comparison of linoleic acid (C18:2) concentration profiles at different liquid flow rates. Conditions: atmospheric pressure, 105 °C temperature and hydrogen flow rate of 1000 ml min^{-1}.
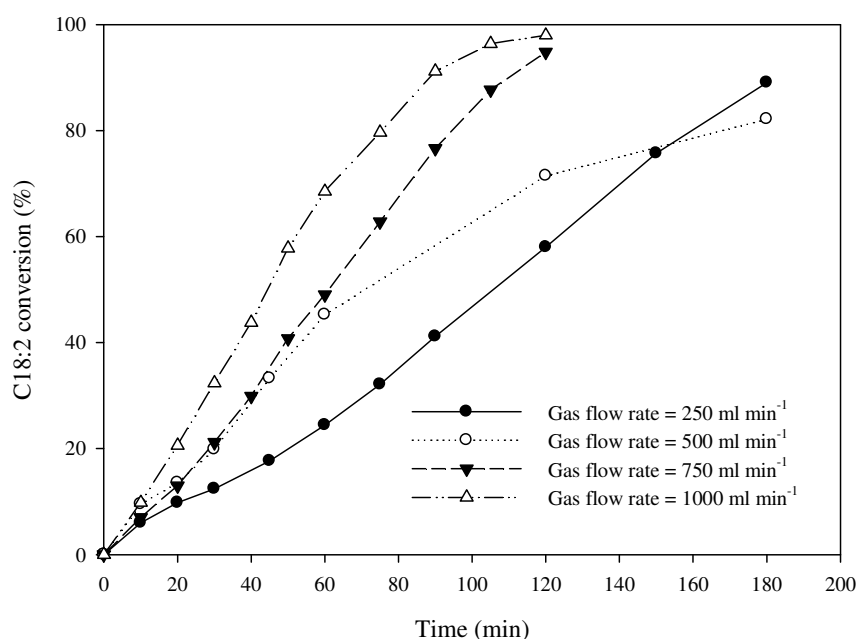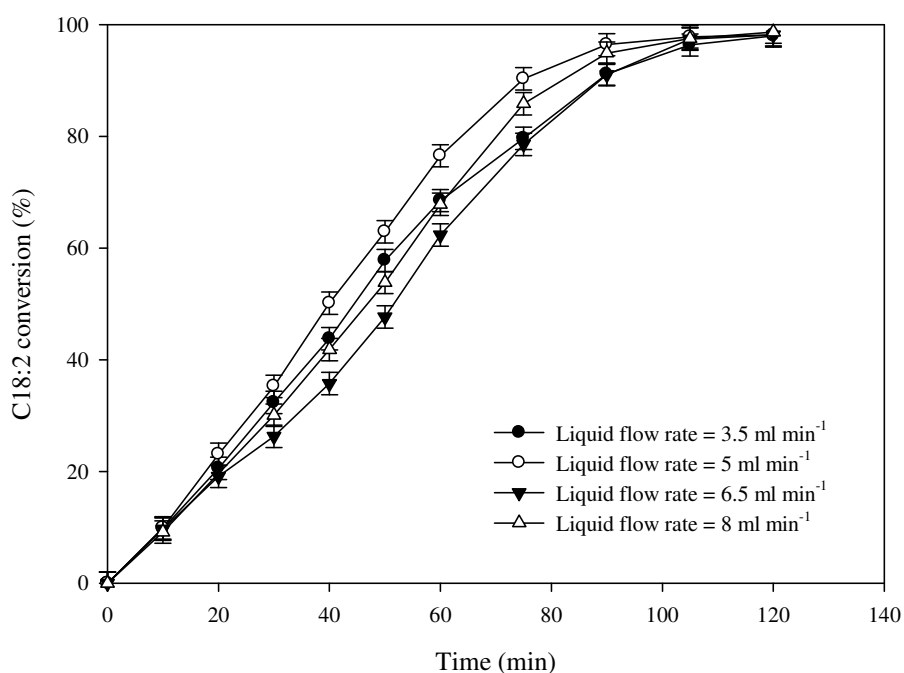

Figure 7.21. Comparison of linoleic acid (C18:2) conversion profiles at different liquid flow rates. Conditions: atmospheric pressure, 105 °C temperature and hydrogen flow rate of 1000 ml min^{-1}.

The wetting efficiencies and mass transfer coefficients corresponding to the investigated

liquid flow rates were calculated using the correlations introduced in Chapter 5, and are

displayed in Table 7.4. The physical properties of soybean oil required for calculating mass transfer coefficients and wetting efficiencies are shown in Table 7.5.

A value for the diffusivity of hydrogen into soyabean oil required for calculation of the Sherwood (Sh) and Schmidt numbers (Sc) was obtained using (Andersson *et al*. 1974):

$$D = (1.173\exp^{-16}\emptyset_B^{0.5}M_B^{0.5}T)/\mu V_A^{0.6} \tag{7.3}$$

As can be seen in Table 7.4, high wetting efficiencies of greater than 90% were achieved for all liquid flow rates, which indicate efficient utilization of catalyst bed in the reactor. The wetting efficiency increased from 0.930 at 2×10^{-3} m s^{-1} liquid superficial velocity to 0.965 at liquid superficial velocity of 4.7×10^{-3} m s^{-1}. The slight improvement of wetting efficiency with increasing liquid flow rate might partly explain the slight decrease in the observed catalytic activity at the highest two liquid flow rates of 6.5 and 8 ml min^{-1}. At the lowest two liquid velocities, the surface of the catalyst might not be fully covered by liquid giving a chance for the gaseous reactant to enter into the liquid filled pores through the dry regime without any liquid film resistance. In this case, increasing liquid flow rates increases rate of reaction. However, at the highest two liquid flow rates of 6.5 and 8 ml min^{-1}, the catalyst particles might be completely wetted by the liquid, which could restrict the accessibility of H_2 into the catalyst pores and hence decreasing the catalytic activity. Despite the improvement in mass transfer coefficient and liquid holp up accompanying the increase in liquid velocity (Figures 7.22, 7.23), the decrease in catalytic activity at the highest liquid flow rates could also be explained by the average residence time of oil in the catalyst bed. Table 7.6 demonstrates the calculated average residence time per pass and total number of passes through the catalyst bed corresponding to the various liquid velocities. As shown in Table 7.6, increasing liquid superficial velocity decreased residence time of oil from 11.18 s at $2 \times$

10^{-3} m s^{-1} to 5.49 s at 4.7×10^{-3} m s^{-1}. Although higher liquid velocities incorporate more passes through the catalyst bed as shown in Table 7.6, it could also result in a stronger competition of fatty acids on the active sites giving less time for linoleic acid molecules to get adsorbed on the catalyst surface and thus affecting its hydrogenation rate.

Liquid flow rate (ml min^{-1})	Liquid superficial velocity ($\times 10^{-3}$ m s^{-1})	Froude number (Fr_L) $\times 10^{-4}$	Reynolds number (Re_L)	Wetting efficiency	Mass transfer coefficient ($\times 10^{-5}$ m s^{-1})^a
3.5	2	2.2	0.3	0.930	1.1
5	2.9	4.4	0.4	0.947	1.7
6.5	3.8	7.4	0.5	0.957	2.2
8	4.7	11.3	0.7	0.965	2.8

Table 7.4. Wetting efficiencies and mass transfer coefficients corresponding to different liquid flow rates. ^{a} Diffusivity of H_2 into soyabean oil was calculated using correlation (7.3) to be 2.47×10^{-8} m^2 s^{-1}; Sc number was calculated to be 289; Mo_L was calculated to be 6×10^{-7}; porosity of bed (ε_B) = 0.6.

Properties	Values	Remarks
molecular weight (kg kmol^{-1})	Mw = 875	Fillion and Morsi, 2000
viscosity (kg m^{-1} s^{-1})	$\log_{10}\mu_L = -3.073 + 46.6 \times 10^6/T^3$	Haighton $et\ al.$ 1972
density (kg m^{-3})	$\rho_L = 1108 - 0.65 \times T$	Bailey, 1979
surface tension (N m^{-1})	$\sigma_L = 0.0517 - 5.71 \times 10^{-5}T$	Bartsch, 1995

Table 7.5. Physical properties of soyabean oil.
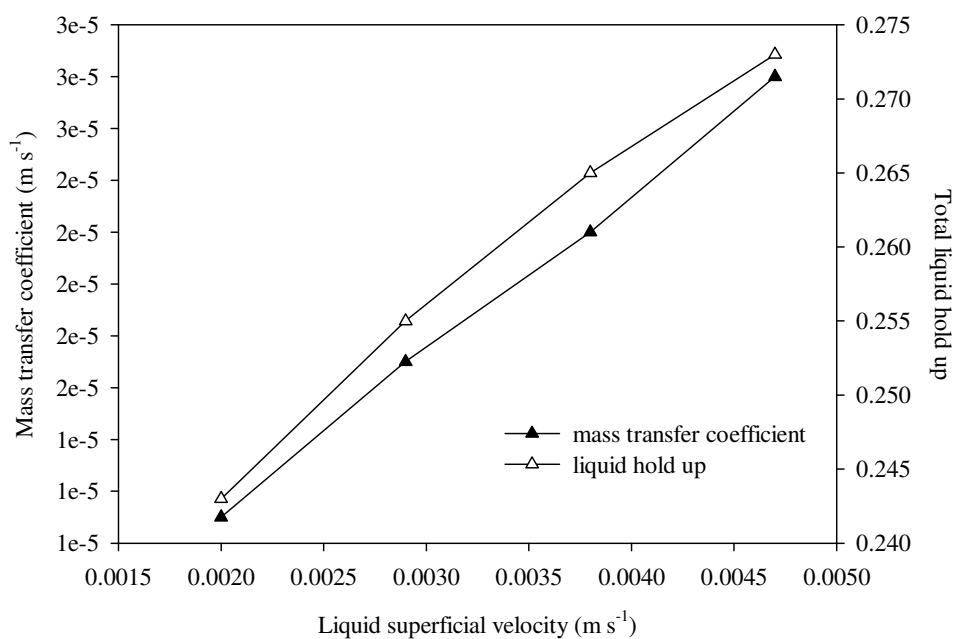
Figure 7.22. Mass transfer coefficient and total liquid hold corresponding to runs conducted with different liquid velocities.
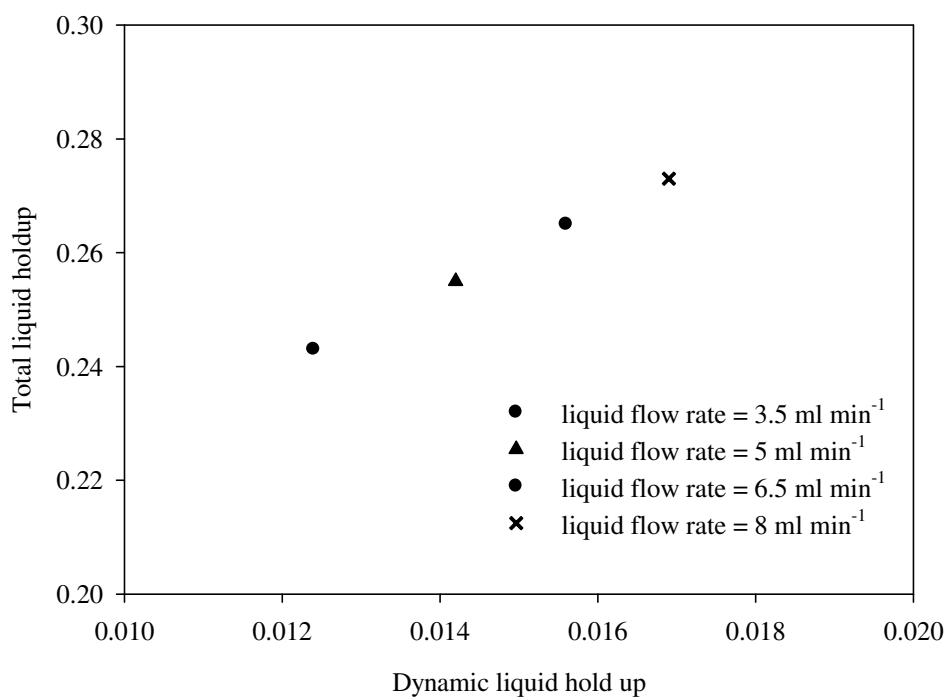
Figure 7.23. Plot of dynamic liquid holdup versus total liquid holdup corresponding to runs conducted with different liquid velocities.

Liquid superficial velocity ($\times 10^{-3}$ m s^{-1})	Average residence time per pass (s)	Total number of passes to achieve 70% conversion of linoleic acid	% Concentration of *cis* oleic acid at 70% conversion of linoleic acid.
2	11.18	333	22
2.9	8.23	394	27
3.8	6.57	621	30.6
4.7	5.49	677	31.2

Table 7.6. Comparison of average residence time and total number of passes for the various investigated liquid flow rates.

7.3.2.2 Effect of liquid flow rate on selectivity

The linolenic and linoleic selectivities were calculated for the various liquid flow rates and are presented in Table 7.7. As can be seen in Table 7.7, linolenic selectivity maintained low values of < 0.2 for all liquid flow rates. The linoleic selectivity, on the other hand, increased systematically from 1.7 at a liquid flow rate of 3.5 ml min^{-1} to 4.5 at the highest liquid flow rate of 8 ml min^{-1}. Figure 7.24 shows the concentration profiles of *cis* oleic acid plotted against total conversion of linoleic acid (C18:2). As shown in Figure 7.24, a noticeable increase was observed in the content of *cis* oleic acid upon increasing liquid flow rate. At about 70% conversion of linoleic acid, the concentration of *cis* oleic acid increased from 23.5% at a liquid flow rate of 3.5 ml min^{-1} to 31.5% at the highest two liquid flow rates of 6.5 and 8 ml min^{-1}. The improved linoleic selectivity as well as the content of *cis* oleic acid accompanied the increased in liquid flow rate could be attributed to the residence time of the fatty acids in the catalyst pores. Draguez de Hault and Demoulin (1984) reported that the longer the residence time at the active sites, the greater is the probability of occurrence for all reactions, i.e. hydrogenation, isomerization or conjugation. A plot of the maximum obtained

content of *cis* oleic acid and calculated average residence time versus liquid superficial

velocity is show in Figure 7.25.

Run	Liquid flow rate (ml min^{-1})	k_1 (min^{-1})	k_2 (min^{-1})	k_3 (min^{-1})	S_{Ln}	S_L
8	3.5	0.112	0.588	0.345	0.19	1.7
9	5	0.128	0.699	0.260	0.18	2.7
10	6.5	0.108	0.579	0.144	0.19	4
11	8	0.117	0.646	0.144	0.18	4.5

Table 7.7. Effect of liquid flow rate on linolenic and linoleic selectivity. Conditions: atmospheric pressure, 105 ºC temperature and hydrogen flow rate of 1000 ml min^{-1}.
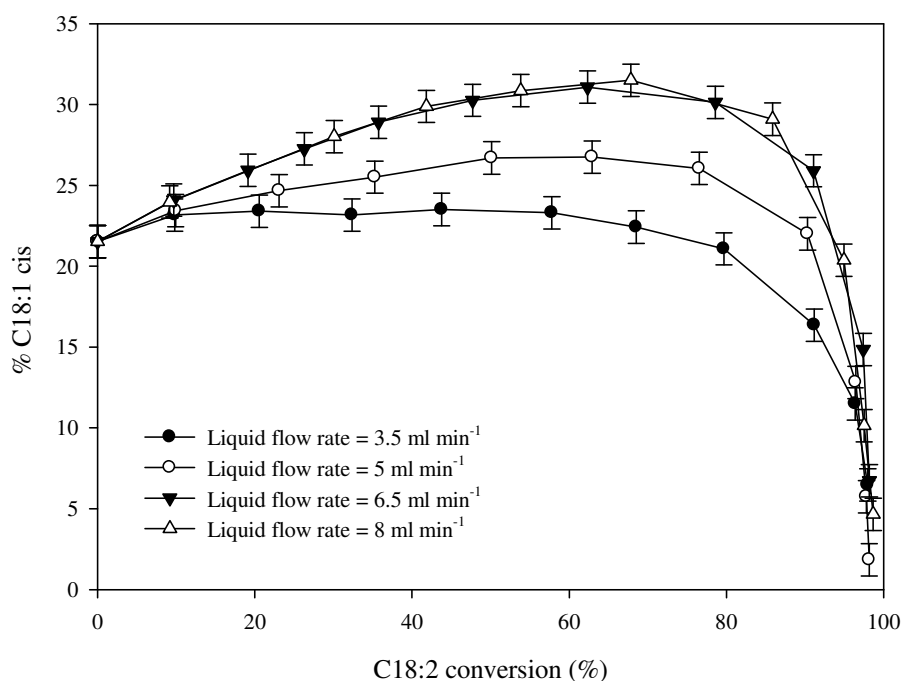
Figure 7.24. Comparison of *cis* oleic concentration profiles obtained at different liquid flow rates. Conditions: atmospheric pressure, 105 ºC temperature and hydrogen flow rate of 1000 ml min^{-1}.
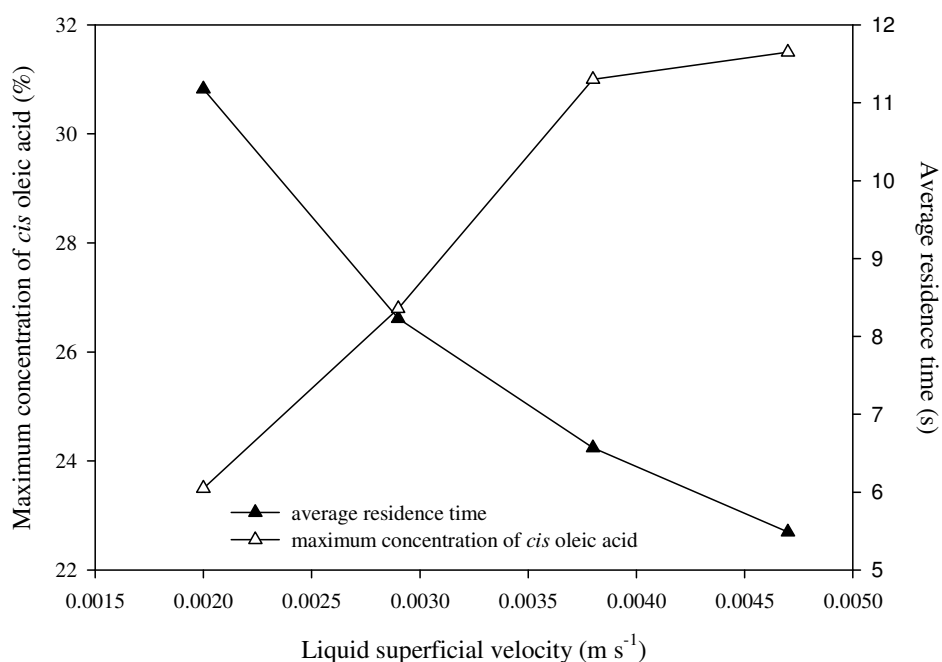
Figure 7.25. Average residence time and maximum concentration of *cis* oleic versus liquid superficial velocity.

7.3.2.3 Effect of liquid flow rate on *trans* and saturated fatty acid formation

The profiles of *trans* oleic acid concentration versus total conversion of linoleic acid are displayed in Figure 7.26. As shown, similar production rates of *trans* oleic acid were observed up to 60% conversion of linoleic acid and that differences were observed at higher conversion levels of linoleic acid. At conversion levels of linoleic acid higher than 60%, the production rate of *trans* oleic acid increased with an increase in liquid flow rate.
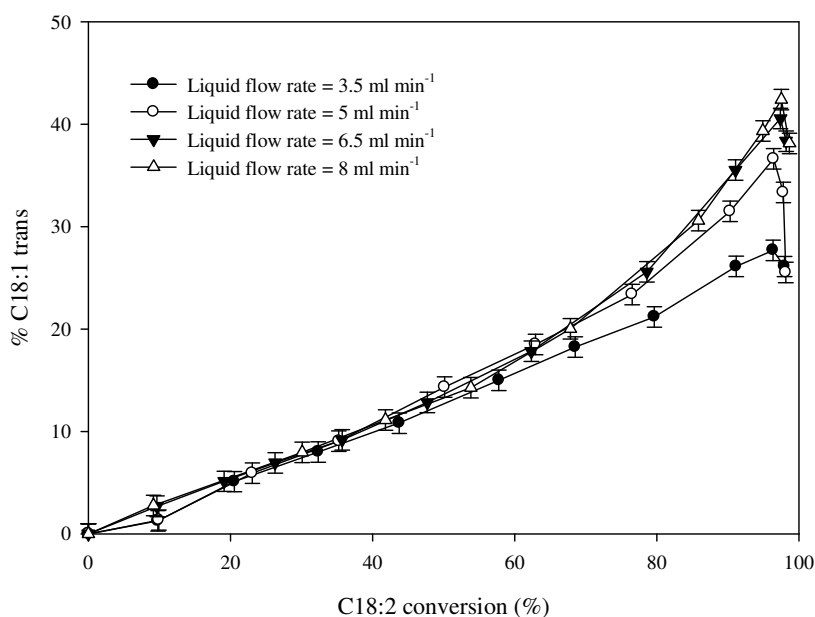
Figure 7.26. *Trans* fatty acid content (C18:1) as a function of C18:2 conversion at different liquid flow rates. Conditions: atmospheric pressure, 105 °C temperature and hydrogen flow rate of 1000 ml min^{-1}.

Figure 7.27 shows the influence of liquid flow rate upon the evolution of the C18:0 as a function of the C18:2 conversion. As can be seen in Figure 7.27, the production rate of C18:0 was significantly reduced upon increasing liquid flow rate. At about 90% conversion of linoleic acid, 32% of stearic acid was produced at the lowest liquid flow rate of 3.5 ml min^{-1} that decreased to about 24% at liquid flow rate of 5 ml min^{-1} reaching its lowest content of 17% at the highest liquid flow rates of 6.5 and 8 ml min^{-1}. The decrease in residence time of oil in the catalyst bed with increasing oil flow rate (Table 7.6), coupled with the reported difference in the affinity of dienic and monoenic acids and the stronger adsorption of the former on Pd-catalyst (Kitayama *et al*. 1996; Kitayama *et al*. 1997) could favour the formation of monoenic acids rather than stearic acid. Figure 7.28 is a plot of fatty acids concentrations vs time at the optimized liquid flow rate of 8 ml min^{-1}.
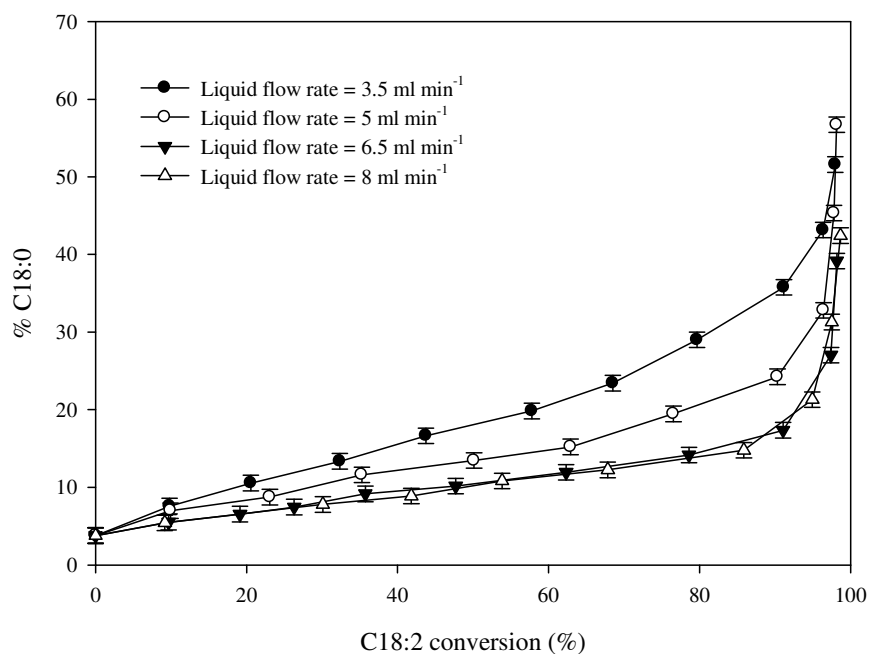
Figure 7.27. Stearic acid (C18:0) content as a function of C18:2 conversion at different liquid flow rates.
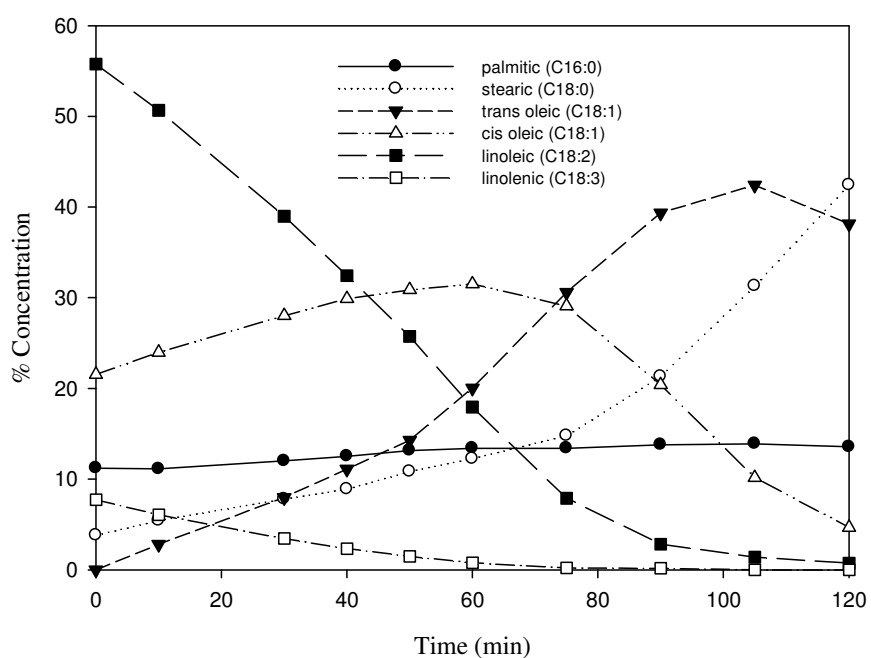
Figure 7.28. Fatty acid profiles of soyabean oil hydrogenated with 2 % Pd/Al$_2$O$_3$ catalyst. Conditions: 105 ºC, atmospheric pressure, hydrogen flow rate of 1000 ml min^{-1} and liquid flow rate of 8 ml min^{-1}.

A reaction was then conducted at the optimized gas and liquid flow rates of 1000 and 8 ml min^{-1}, respectively, and under a temperature of 50 ºC that gave the best linolenic selectivity as

well as the best selectivity to *cis* oleic acid (§ 7.2). The fatty acids compositions from the reaction conducted at these conditions are demonstrated in Figure 7.29. Table 7.8 shows the calculated selectivities for both temperatures at the optimized gas and liquid flow rates. As can be seen, the linoleic selectivity increased from 4.5 at 105 ºC to 7 at 50 ºC. Figures 7.30 shows a comparison of *cis* oleic acid composition versus time profiles for both temperatures. As expected, the content of *cis* oleic acid increased noticeably upon decreasing the reaction temperature. At about 80% conversion of linoleic acid, a concentration of 28% of *cis* oleic was obtained at 105 ºC in comparison to 38% obtained at 50 ºC. Interestingly, the production rate of *trans* oleic acid decreased upon decreasing temperature from 105 to 50 ºC (Figure 7.31), which contrasts the trend obtained in Figure 7.7 for these two temperatures. This could be due to the much higher difference in reaction rates obtained after optimisation of hydrodynamics leading to more catalyst starvation of hydrogen and thus favouring the production of *trans* oleic acid. Conducting the reaction at 50 ºC also led to an impressive reduction in the production rate of stearic acid as can be seen in Figure 7.32.

Run	Temperature (ºC)	k_1 (min^{-1})	k_2 (min^{-1})	k_3 (min^{-1})	S_{Ln}	S_L
11	105	0.117	0.646	0.144	0.18	4.5
12	50	0.043	0.214	0.0315	0.2	7

Table 7.8. Effect of temperature on linolenic and linoleic selectivities. Conditions: atmospheric pressure, gas flow rate of 1000 ml min^{-1} and liquid flow rate of 8 ml min^{-1}.
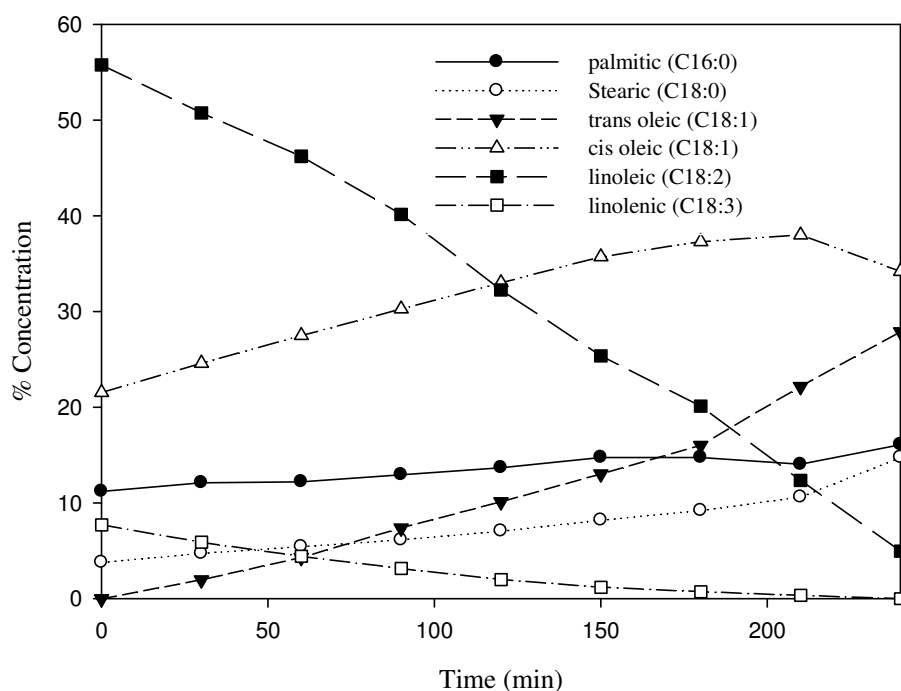
Figure 7.29. Fatty acid profiles of soyabean oil hydrogenated with 2 % Pd/Al$_2$O$_3$ catalyst. Conditions: 50 °C, atmospheric pressure, hydrogen flow rate of 1000 ml min^{-1} and liquid flow rate of 8 ml min^{-1}.
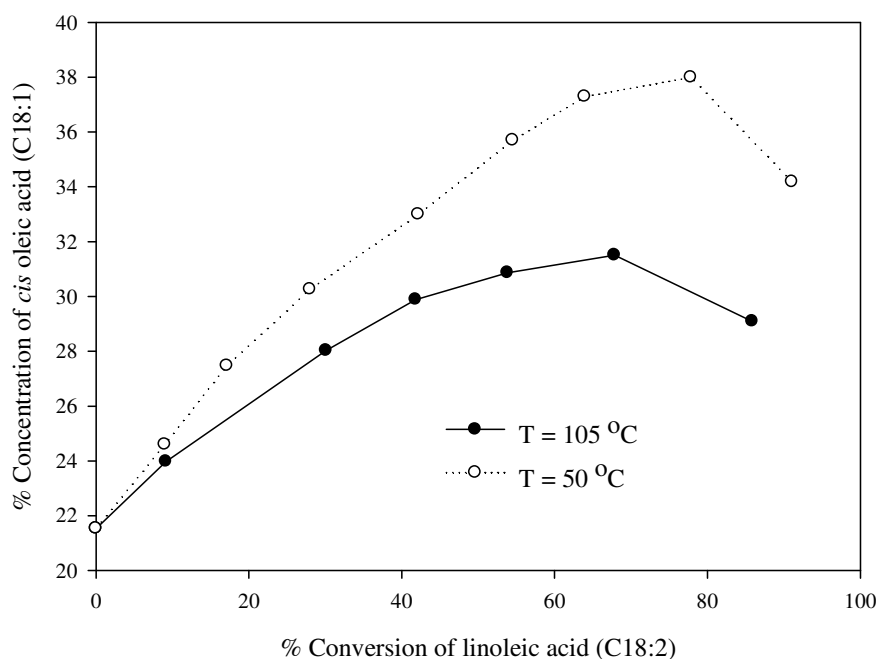
Figure 7.30. A comparison of *cis* oleic concentration profiles as a function of linoleic acid conversion at temperatures of 50 and 105 °C. Conditions: atmospheric pressure, hydrogen flow rate of 1000 ml min^{-1} and liquid flow rate of 8 ml min^{-1}.
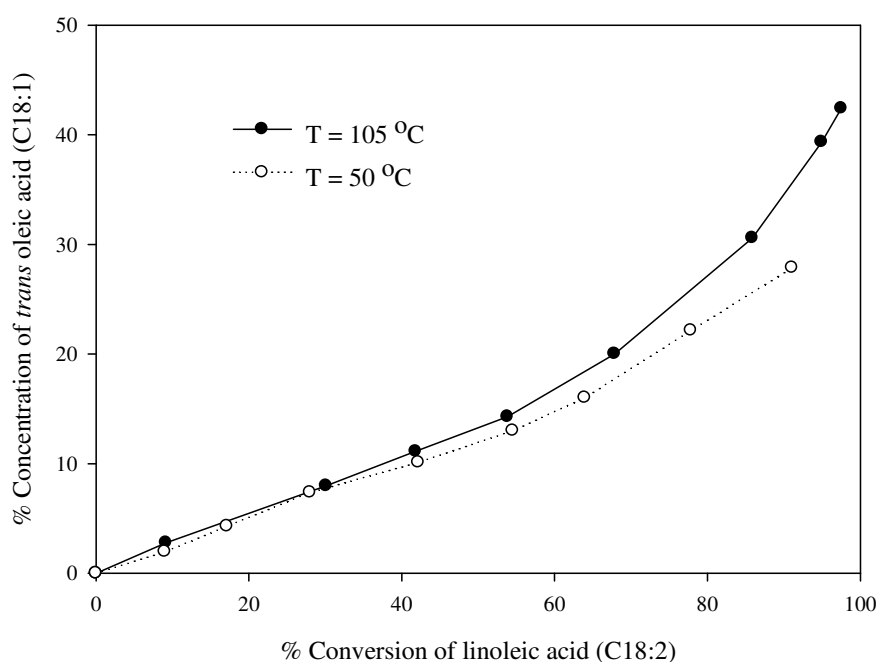
Figure 7.31. A comparison of *trans* oleic concentration profiles as a function of linoleic acid conversion at temperatures of 50 and 105 ºC. Conditions: atmospheric pressure, hydrogen flow rate of 1000 ml min^{-1} and liquid flow rate of 8 ml min^{-1}.
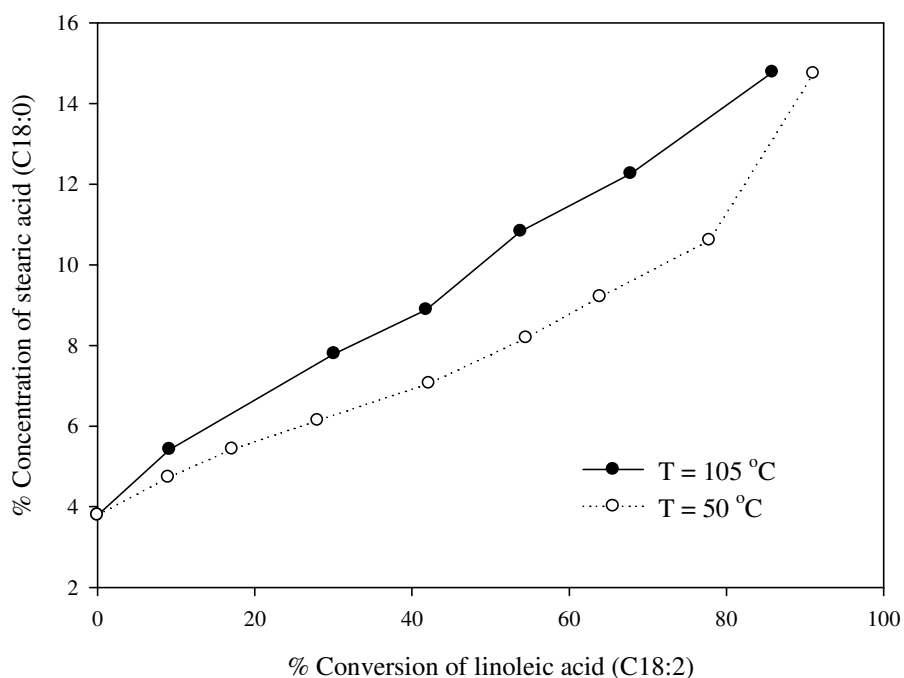
Figure 7.32. Effect of temperature on production rate of stearic acid. Conditions: atmospheric pressure, hydrogen flow rate of 1000 ml min^{-1} and liquid flow rate of 8 ml min^{-1}.

7.4 Optimisation of soyabean oil volume

To optimize volume of soyabean oil and thus substrate to catalyst molar ratio, an experiment was conducted using a doubled amount of 25 ml of soyabean oil under the previously optimized conditions; temperature of 50 ºC, gas flow rate of 1000 ml min^{-1} and liquid flow rate of 8 ml min^{-1}. The fatty acids compositions from the reaction conducted at these conditions are demonstrated in Figure 7.33. It is noteworthy that for this reaction side products were observed after 180 min which reached values up to 8% at a reaction time of 480 min. Figure 7.34 compares the hydrogenation rate of both oil volumes in terms of iodine value. As can be seen Figure 7.34, and as expected, doubling oil volume led to almost halving of reaction rate as there are more molecules competing for the active metal sites. However, doubling oil volume increased linoleic selectivity by almost 4% as shown in Table 7.9. A comparison of stearic acid profiles for both oil volumes as a function of linoleic acid conversion is also shown in Figure 7.35. At about 79% conversion of linoleic acid, 11% of stearic acid was produced with 12.5 ml of oil in comparison to 7% produced with 25 ml of oil. Moreover, at the same conversion level of linoleic acid, the *cis* oleic composition achieved 44% with 25 ml of oil compared to 38% with 12.5 ml of oil as shown in Figure 7.36. Considering the higher adsorption of linoleic acid compared to oleic acid, the higher content of *cis* oleic obtained with 25 ml of oil could be due to the higher number of linoleic acid molecules involved in the reaction which could suppress the reaction of oleic acid leading to reduced production of stearic acid. On the other hand, the higher hydrogenation rate obtained with 12.5 ml of oil could reduce the availability of hydrogen at the catalyst surface thus favouring a higher formation of *trans* oleic acid as compared to 25 ml of oil as shown in Figure 7.37.
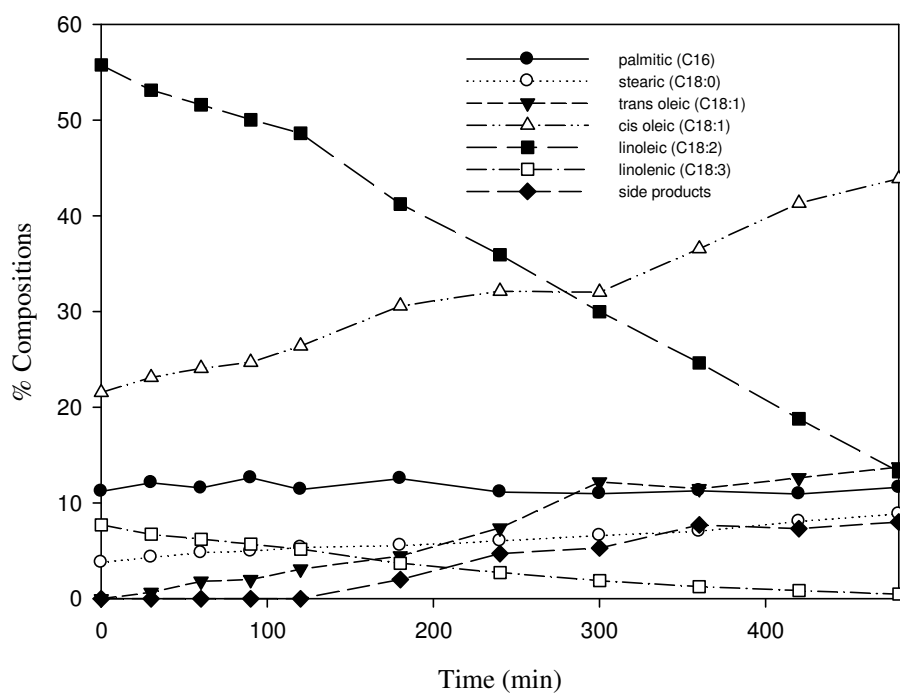
Figure 7.33. Fatty acid profiles of soyabean oil hydrogenated with 2 % Pd/Al$_2$O$_3$ catalyst. Conditions: 25 ml of soyabean oil, 50 ºC, atmospheric pressure, hydrogen flow rate of 1000 ml min^{-1} and liquid flow rate of 8 ml min^{-1}.

Figure 7.34. Effect of oil volume on reduction in IV during hydrogenation of soyabean oil. Conditions: 50 ºC, atmospheric pressure, hydrogen flow rate of 1000 ml min^{-1} and liquid flow rate of 8 ml min^{-1}.

Run	Oil volume (ml)	Substrate/catalyst molar ratio	k_1 (min^{-1})	k_2 (min^{-1})	k_3 (min^{-1})	S_{Ln}	S_L
12	12.5	21	0.043	0.214	0.0315	0.2	7
13	25	42	0.019	0.090	0.008	0.21	11

Table 7.9. Effect of oil volume on linoleic and linolenic selectivities. Conditions: 50 ºC, atmospheric pressure, hydrogen flow rate of 1000 ml min^{-1} and liquid flow rate of 8 ml min^{-1}.
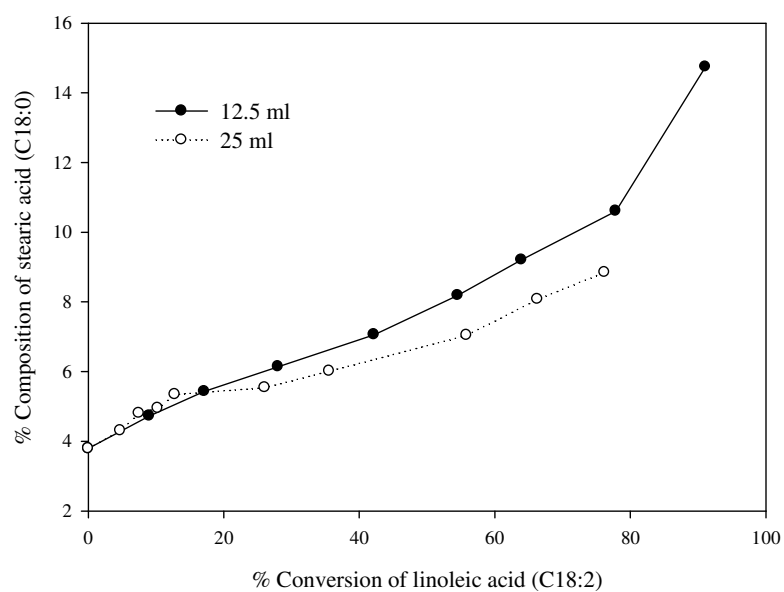

Figure 7.35. Effect of oil volume on production rate of stearic acid as a function of C18:2 conversion. Conditions: 50 ºC, atmospheric pressure, hydrogen flow rate of 1000 ml min^{-1} and liquid flow rate of 8 ml min^{-1}.
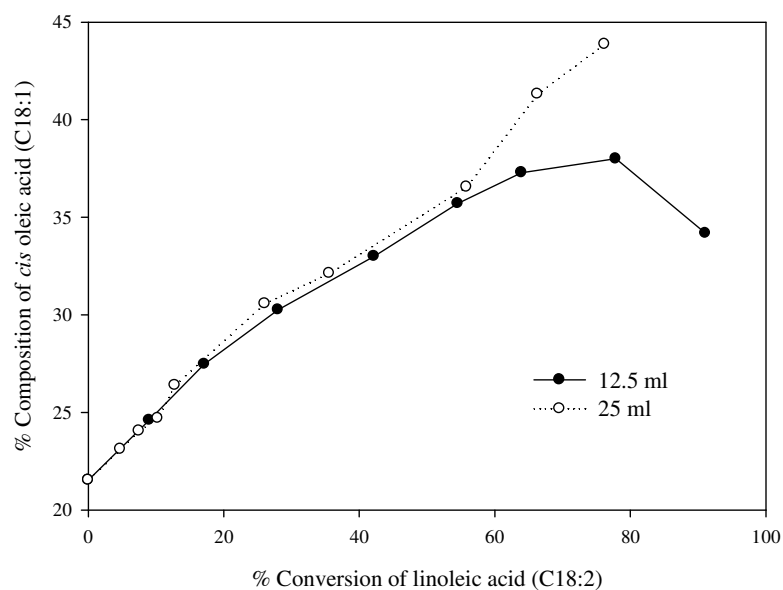
Figure 7.36. Effect of oil volume on production rate of *cis* oleic acid as a function of C18:2 conversion. Conditions: 50 ºC, atmospheric pressure, hydrogen flow rate of 1000 ml min^{-1} and liquid flow rate of 8 ml min^{-1}.
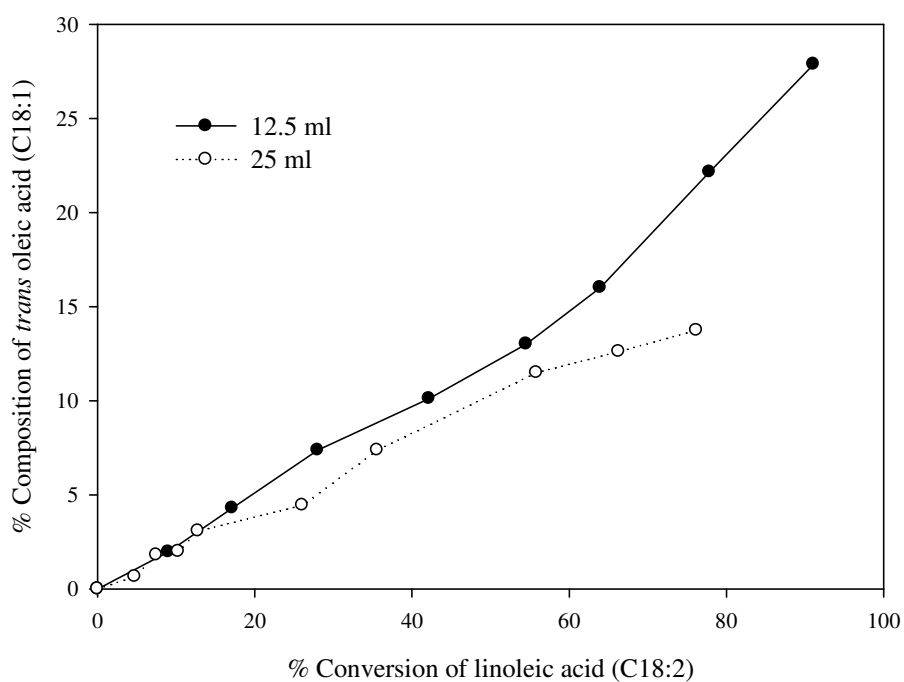
Figure 7.37. Effect of oil volume on production rate of *trans* oleic acid as a function of C18:2 conversion. Conditions: 50 ºC, atmospheric pressure, hydrogen flow rate of 1000 ml min^{-1} and liquid flow rate of 8 ml min^{-1}.

7.5 Comparison between recirculating batch and batch hydrogenation

To compare recirculating batch (TBR) with batch hydrogenation, 3 runs were carried out in the Baskerville autoclave at the optimal conditions of the TBR (50° C and 1 bar hydrogen pressure). The experiments were conducted using three different catalysts, namely 5% (w/w) palladium on alumina powder and two BioPd catalysts (5 wt% Pd/P. *vulgaris* and 5 wt% Pd/S. *marcescens*) supplied by School of Bioscience, University of Birmingham. The reactions were conducted at an optimized stirring speed of 800 rpm using 50 ml of soyabean oil. To promote the solubility of hydrogen, soyabean oil was mixed with 200 ml of hexane prior to reaction. Although reaction conditions in both reactors could not be exactly the same, the comparisons were on the basis of the optimal conditions applied to both reactors which were expected to give a fast rate of hydrogenation and a maximum selectivity to reaction products. For consistent comparison of both reactors, the reduction rate of IV was normalised per gram of catalyst.

Figure 7.38 compares the hydrogenation rate of the four catalysts in terms of iodine value, and the reaction rates normalised per gram of catalyst are shown in Figure 7.39 plotted against Pd loading in catalysts. As shown in Figure 7.38, the rate is much slower for both of the BioPd catalyst, with the desired product *cis* C18:1 being formed at small rate together with a trace amount of *trans* C18:1 and C18:0. In contrast, the Pd/Al$_2$O$_3$ catalysts gave high conversion levels of C18:2 of about 80% with the highest hydrogenation rate obtained with 5% Pd/Al$_2$O$_3$ powder as shown in Figure 7.38. However, the normalised reaction rates (Figure 7.39) show that BioPd catalysts are better than the 2% Pd/Al$_2$O$_3$. This could be due to the suspension of the catalyst particles in the autoclave which together with the high stirring speed would be expected to result in higher intraparticle diffusion and hence a more efficient utilization of the catalyst. The better catalytic activity in the autoclave obtained with Pd/Al$_2$O$_3$ catalyst compared with BioPd catalyst was also observed by Bennett *et al*. (2010),

for the hydrogenation of 2-pentyne. They suggested that the increased activity of alumina support with respect to biomass could be due to the former adsorbing spillover hydrogen once the palladium active sites are covered with reactive hydrogen. This would act as a local reservoir of the gas substrate, in close proximity to palladium with adsorbed C18:2. In contrast, the biomass may be inert to hydrogen adsorption and hence would not offer the reservoir effect leading to lower rate of hydrogenation.
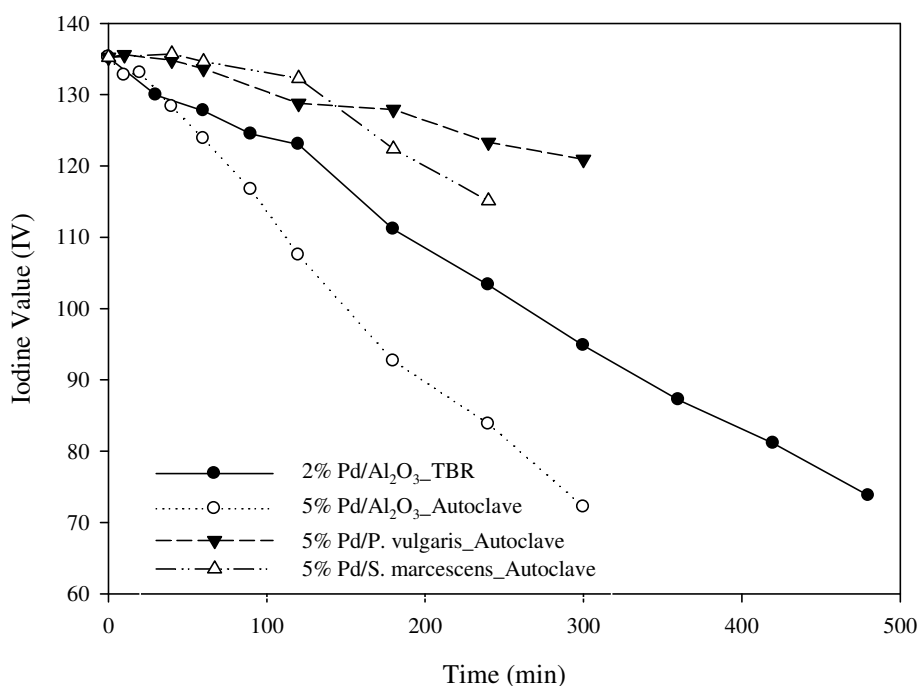
Figure 7.38. Influence of catalyst on the hydrogenation rate of soyabean oil in the TBR and the autoclave. TBR conditions: reaction medium: 25 ml of soyabean oil, 50 °C, atmospheric pressure, hydrogen flow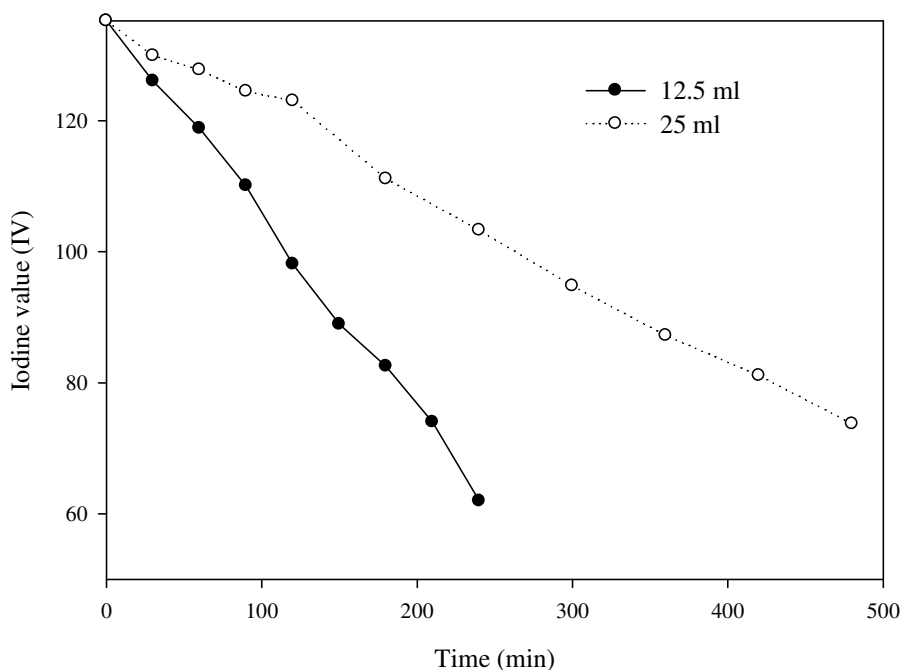 rate of 1000 ml min^{-1} and liquid flow rate of 8 ml min^{-1}. Autoclave conditions: reaction medium: 50 ml of soyabean oil in 200 ml of hexane, 50 °C, 1 bar hydrogen pressure and stirring speed of 800 rpm.

257
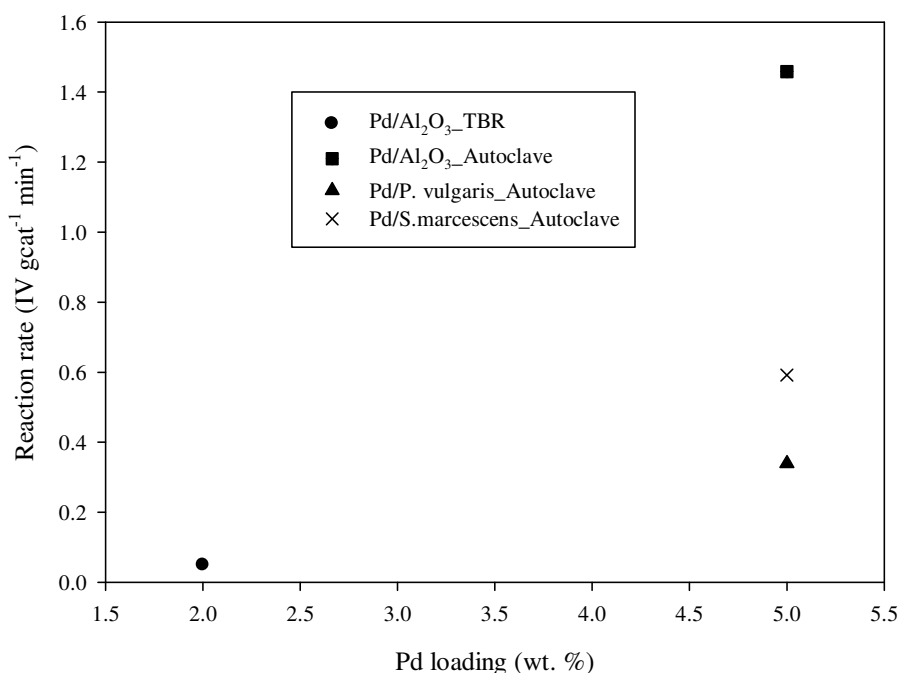
Figure 7.39. Normalised reaction rates as a function of Pd loading in catalysts.

The fatty acids compositions of the reaction conducted in the autoclave using 5% Pd/Al$_2$O$_3$ powder is demonstrated in Figure 7.40. It is noteworthy that for this reaction side products reached up to 7.86% at a reaction time of 3 h. The linolenic and linoleic selectivities achieved with 5% Pd/Al$_2$O$_3$ are similar to those obtained from 2% Pd/Al$_2$O$_3$ in the TBR as shown in Table 7.10. However, a higher content of *cis* oleic acid (C18:1) was achieved in the TBR compared to that obtained from the autoclave as shown in Figure 7.41. At 76% conversion of linoleic acid, the TBR produced 44 % of *cis* oleic acid compared to 31% in the autoclave. Furthermore, a higher production rate of *trans* oleic acid was observed in the autoclave compared to the TBR as demonstrated in Figure 7.42. At 76% conversion of linoleic acid, the TBR produced 13.7 % of *trans* oleic acid compared to 22% in the autoclave, that could be linked to the higher catalytic activity in the autoclave. Although the initial production rate of stearic acid (C18:0) was higher in the TBR, both reactors achieved same content of about 8.8% at 76% conversion of linoleic acid as shown in Figure 7.43.
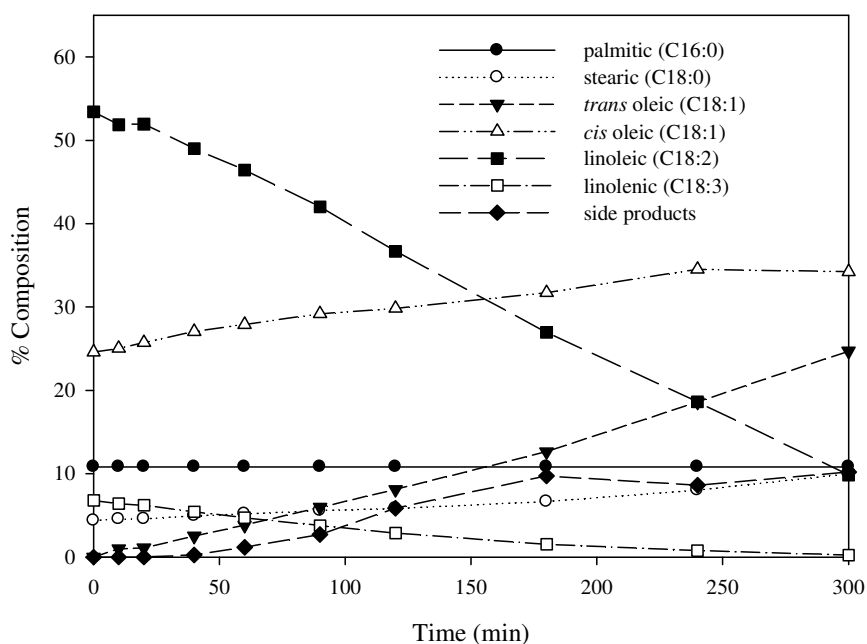
Figure 7.40. Fatty acid profiles of soyabean oil hydrogenated with the 5 % Pd/Al$_2$O$_3$ powder catalyst in the autoclave. Conditions: reaction medium: 50 ml of soyabean oil in 200 ml of hexane, 50 ºC, 1 bar hydrogen pressure and stirring speed of 800 rpm.

Catalyst	k_1 (min^{-1})	k_2 (min^{-1})	k_3 (min^{-1})	S_{Ln}	S_L
2 % Pd/Al$_2$O$_3$ (TBR)	0.019	0.090	0.008	0.21	11
5 % Pd/Al$_2$O$_3$ (autoclave)	0.03	0.149	0.0125	0.20	12

Table 7.10. Influence of catalyst on the linolenic and linoleic selectivities in the TBR and the autoclave. TBR conditions: reaction medium: 25 ml of soyabean oil, 50 ºC, atmospheric pressure, hydrogen flow rate of 1000 ml min^{-1} and liquid flow rate of 8 ml min^{-1}. Autoclave conditions: reaction medium: 50 ml of soyabean oil in 200 ml of hexane, 50 ºC, 1 bar hydrogen pressure and stirring speed of 800 rpm.
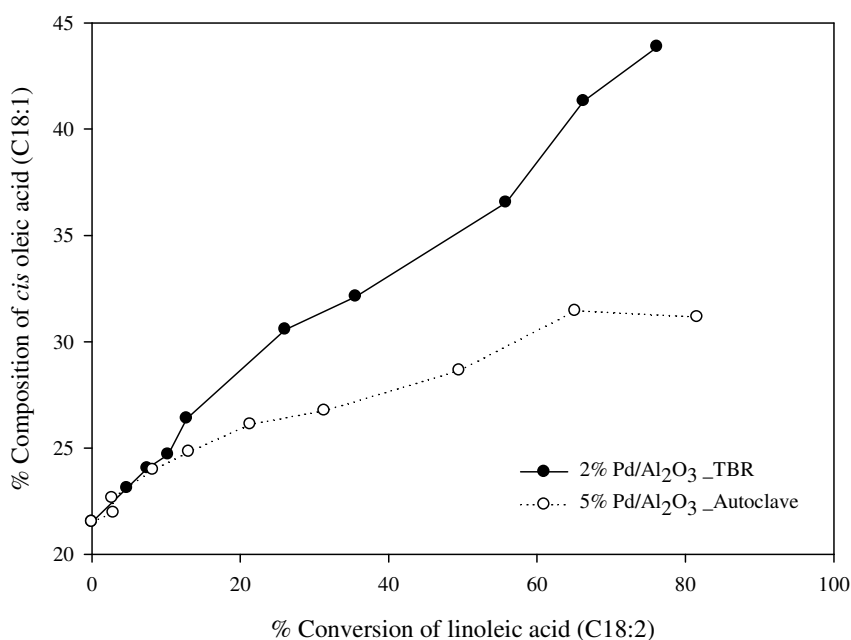
Figure 7.41. Comparison of *cis* oleic acid content obtained from the TBR and the autoclave. TBR conditions: reaction medium: 25 ml of soyabean oil, 50 °C, atmospheric pressure, hydrogen flow rate of 1000 ml min^{-1} and liquid flow rate of 8 ml min^{-1}. Autoclave conditions: reaction medium: 50 ml of soyabean oil in 200 ml of hexane, 50 °C, 1 bar hydrogen pressure and stirring speed of 800 rpm.
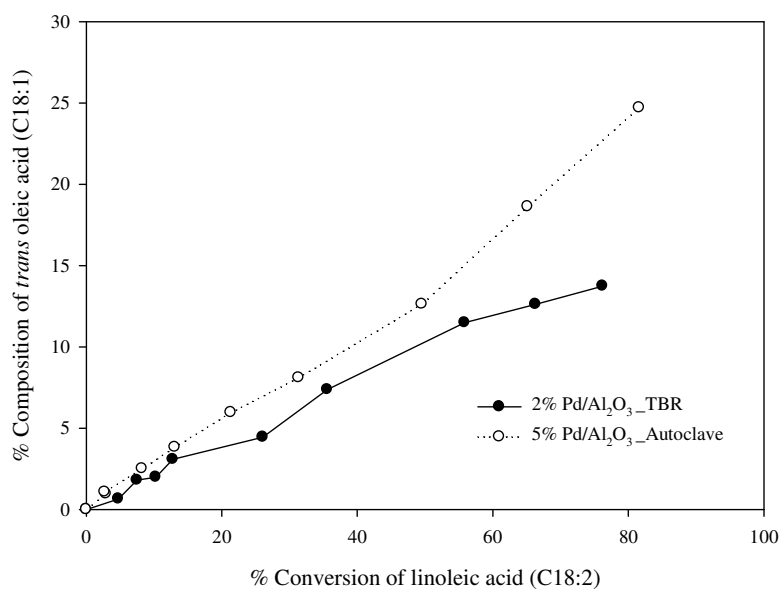
Figure 7.42. Comparison of *trans* oleic acid content obtained from the TBR and the autoclave. TBR conditions: reaction medium: 25 ml of soyabean oil, 50 °C, atmospheric pressure, hydrogen flow rate of 1000 ml min^{-1} and liquid flow rate of 8 ml min^{-1}. Autoclave conditions: reaction medium: 50 ml of soyabean oil in 200 ml of hexane, 50 °C, 1 bar hydrogen pressure and stirring speed of 800 rpm.
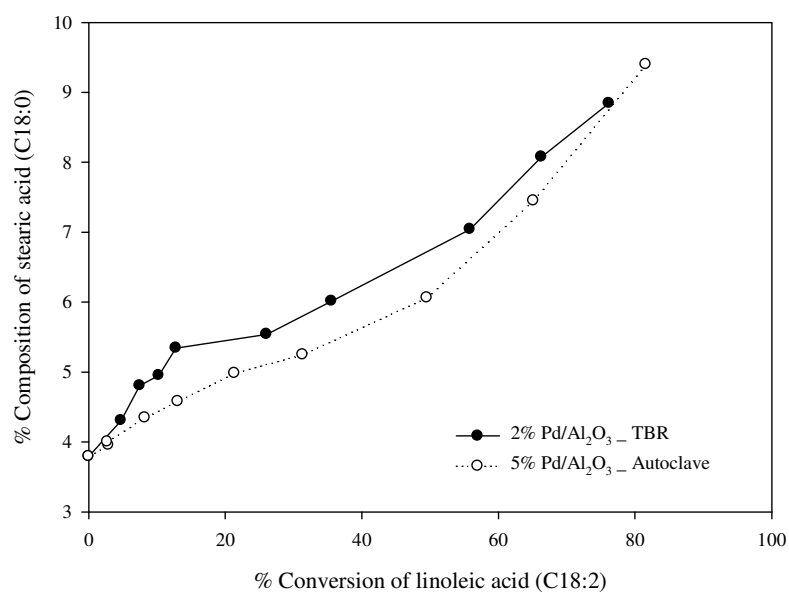
Figure 7.43. Comparison of stearic acid content obtained from the TBR and the autoclave.

7.6 Conclusion

The hydrogenation of soyabean oil over 2 wt. % Pd/Al$_2$O$_3$ catalyst was studied in a fixed-bed reactor working under trickle flow regime. The reduction rate of iodine value increased with an increase in temperature and levelled off at the highest two temperatures of 85 and 105 ^{o}C. The maximum content of *cis* oleic acid (C18:1) and the lowest production rate of stearic acid (C18:0) were obtained at the lowest investigated temperature of 50 ^{o}C. The calculated apparent activation energy (6.718 kJ/mol) is much smaller than that for general chemical reaction (60-250 kJ/mol). This shows that mass transfer limitations were present at the implemented reaction conditions. The experimental data from various temperatures were well described with pseudo-first order kinetic model. The reduction rate of IV increased with an increase in gas flow rate which could be ascribed to improved liquid distribution and thus efficient utilization of the catalyst bed in the reactor. The highest gas flow rate of 1000 ml min^{-1} gave the best selectivity to *cis* oleic acid and the lowest production rate of stearic acid (C18:0) although resulting in the highest production rate of *trans* oleic acid. Although increasing liquid flow rate increased gas-solid mass transfer and total liquid hold up, it

261

decreased the reduction rate of IV which could be explained by the wetting efficiency of the catalyst bed and the residence time of the oil in the reactor. Increasing liquid flow rate led to a noticeable improvement in the linoleic selectivity and the obtained content *cis* oleic acid which also resulted in the lowest production rate of stearic acid. Doubling the amount of soyabean oil used in the reaction resulted in a further improvement in the reaction results although prolonging reaction time. The results of this work also demonstrate that trickle-bed hydrogenation with recirculating oil is capable of reducing the unsaturates in soyabean oil to the same degree as a batch hydrogenation under low reaction temperature. Trickle-bed hydrogenation also demonstrated similar linolenic and linoleic selectivities as a batch hydrogenation, with better selectivity to *cis* oleic acid, a lower formation of *trans* oleic acid and comparable production rate of stearic acid. Although the *trans*-isomer concentration is still high for food application, this work shows that, under proper operating conditions, 2 wt. % Pd/Al$_2$O$_3$ catalyst can be used in a TBR to produce base oils for lubricants.

CHAPTER 8

CONCLUSIONS AND FUTURE WORK RECOMMENDATIONS

8.1 Conclusions

Chapter 4. Enantioselective hydrogenation of dimethyl itaconate over Rh complexes supported on 50WX2-100 ion-exchange resins.

- Investigation of various combinations of ligand and support has shown that the complex [Rh (NBD){(S,S)-DIOP}]BF$_4$ supported on 50WX2-100 is promising in terms of reaction rate (66 % conversion of DMI), but not enantioselectivity (23%).

- The reaction rate could be promoted by addition of water to the deployed methanol solvent. Using 50% mixture of methanol and water as a solvent the reaction rate increased by a factor of 1.3 and full conversion of DMI was obtained.

- The influence of DIOP/Rh molar ratio was investigated and it was shown that a molar ratio of 0:1 gave the highest reaction rate (full conversion of DMI in 9 min), but didn't show enantiomeric enhancement. The optimized ratio of 1:1 gave full conversion of DMI and an *ee* of 23% in 20 min.

- Under optimized conditions in the TBR, the catalyst [Rh (COD){(R,R)-Me-DuPHOS}]BF$_4$ supported on 50WX2-100 ion-exchange resins, gave high enantioselectivity of 99.9% and TOF of 330 h^{-1}, with results comparable to those obtained in the shake-flask reactor.

- The experimental data could be fitted well by means of a kinetic model based on the Osborn-Wilkinson reaction mechanism. Applying Osborn-Wilkinson kinetics to the reaction indicated that complexation with the hydrogen before reaction with the olefin was the preferred path.

Chapter 5. Enantioselective hydrogenation of dimethyl itaconate over [Rh (COD){(R,R)-Me-DuPHOS}]BF$_4$ supported on alumina.

- The catalyst complex [Rh((R,R)-Me-DuPhos)(COD)]BF$_4$ was anchored to powder and trilobe alumina supports using phosphotungstic acid (PTA) as an anchoring agent.

- For the powder alumina, tests were conducted in the shake-flask to ensure that the reaction was not influenced by mass transfer limitations by varying the stirrer speed and catalyst mass, thus ensuring the reported data are in the kinetic regime.

- Under optimized conditions in the shake-flask reactor, a TOF of 50 h^{-1} was achieved with powder alumina support in comparison to a TOF of 20 h^{-1} obtained with the trilobes. Under these conditions, the enantioselectivities obtained from immobilizing the catalyst complex onto powder and trilobe supports were 96% and 97%, respectively.

- Fitting Osborn-Wilkinson kinetics to the concentration profiles indicated that complexation with the olefin before reaction with hydrogen was the preferred path.

- The trickle bed reactor (TBR) was operated in the trickle flow regime using trilobe support. Optimal gas and liquid flow rates of 100 and 20 ml min^{-1} were selected which were found to have a noticeable effect on initial reaction rate and enantioselectivity. Under optimized conditions in the TBR, 99% conversion and enantioselectivity of up to 99.9% were achieved.

Chapter 6. Selective hydrogenation of 1-heptyne.

- Hydrogenation of 1-heptyne has been demonstrated in the TBR which was operated in the trickle flow regime.

- 2-propanol (IPA) has been identified as a suitable solvent giving best selectivity (> 96 % (plateau-shaped up to 81% 1-heptyne conversion)) at expense of slower rate than for e.g. hexane. Complete conversion of 1-heptyne was achieved in hexane after 75 min in comparison with 240 min in IPA, which could be due to lower H_2 solubility in protic solvents.

- Reaction rate and selectivity could be promoted by increasing the liquid flow rate from 5 to 20 ml min^{-1}, which was found to influence the wetting efficiency of the catalyst bed, liquid holdup, as well as mass transfer of hydrogen from bulk liquid to catalyst surface. The highest selectivity (100% (plateau-shaped up to 84% 1-heptyne conversion)) was observed at the highest liquid flow rate of 20 ml min^{-1}, corresponding to the lowest residence time (2.71 s) of reaction mixture in the catalyst bed.

- Increasing 1-heptyne concentration at constant hydrodynamic conditions did not lead to expected increase in rate suggesting that number of active sites on the catalyst becomes limiting.

- Under non-limited conditions, Langmuir-Hinshelwood kinetics show promise for fitting to the experimental data. The adsorption coefficient $K_{1-heptene}$ is predicted to be zero which suggests that adsorption of alkene does not occur in isopropanol.

- It was shown that the reaction can be carried out in continuous flow without recycle of reagents and that catalyst deactivation is not an issue during the timeframe of the experiments reported in this work.

- The results could be used to provide insights and information as to how hydrogenations in the autoclave could be transferred to continuous flow reactors.

Chapter 7. Selective hydrogenation of soyabean oil

- Hydrogenation of soyabean oil has been demonstrated in the TBR which was operated in the trickle flow regime.

- The reduction rate of iodine value (IV) increased with an increase in temperature and levelled off at the highest two temperatures of 85 and 105 °C. At a reaction temperature of 50 °C a final IV of 45 was obtained at 240 min in comparison to IV of 42 at 180 min at a temperature of 105 °C.

- The maximum content of *cis* oleic acid (C18:1) of 26 % and the lowest production rate of stearic acid (C18:0) were obtained at the lowest investigated temperature of 50 °C, which was believed to be due to higher H_2 concentration at the catalyst surface compared to that at higher temperatures.

- The calculated apparent energy (6.7 kJ/mol) is much smaller than that for general chemical reaction (60-250 kJ/mol), which indicates that mass transfer limitations were present at the implemented reaction conditions.

- The experimental data from various temperatures (50, 60, 70, 85 and 105 °C) were well described with pseudo-first order kinetic model, with the best fit obtained for a reaction temperature of 50 °C.

- The reduction rate of IV increased with an increase in gas flow rate which could be due to improved liquid distribution and thus efficient utilization of catalyst bed in the reactor. At a gas flow rate of 250 ml min a final IV of 42 was obtained at 180 min in comparison to IV of 30 at 120 min at a gas flow rate of 1000 ml min^{-1}.

- At 105 °C reaction temperature, the highest gas flow rate of 1000 ml min^{-1} gave the best selectivity trend to *cis* oleic acid (C18:1), at which the content of *cis* oleic maintained a value of 23% up until 60% conversion of linoleic acid. The highest gas

flow rate of 1000 ml min^{-1} gave the lowest production rate of stearic acid (C18:0) although resulting in the highest production rate of *trans* oleic acid.

- Although increasing liquid flow rate increased gas-solid mass transfer and total liquid holdup in the reactor, it decreased the reduction rate of IV, which could be explained by the wetting efficiency of catalyst bed as well as the residence time of the oil in the reactor.

- Increasing liquid flow rate led to a noticeable improvement in the linoleic selectivity and the obtained content of *cis* oleic acid (C18:1) along with the lowest production rate of stearic acid (C18:0).

- Doubling the amount of soyabean oil used in the reaction resulted in a further improvement in the results at the expense of prolonged reaction time.

- Compared to a batch reactor, TBR offered similar linolenic and linoleic selectivities, with better selectivity to *cis* oleic acid (C18:1), a lower formation of *trans* oleic acid and comparable production rate of stearic acid (C18:0).

- Although the *trans*-isomer content from the optimized conditions in the TBR is still high for food application, this work shows that, under proper operating conditions, 2wt. % Pd/Al$_2$O$_3$ catalyst can be used in a TBR to produce base oils for lubricants.

8.2 Recommendations for future work

Due to financial, equipment and time constrains several experiments/analysis could not be performed in the scope of this work and hence are recommended as future work. They are as follows:

- To further elucidate the results obtained from different combinations of catalyst ligand and support (Chapter 4), and the results obtained from supporting [Rh

(COD){(R,R)-Me-DuPHOS}]BF4 catalyst onto 50WX2-100 ion-exchange resins, powder and trilobe alumina supports (Chapter 5), catalyst characterization techniques should be performed such as:

> ➢ ICP-AES (inductively coupled plasma atomic emission spectroscopy).
>
> ➢ EDS analysis (energy dispersive X-ray spectrometery) coupled to ESEM microscopy (environmental scanning electron microscopy) (Barbaro, 2006).

- Possible oxidation of the air-sensitive catalysts used for the enantioselective hydrogenation of dimethyl itaconate (Chapters 4 and 5), could be eliminated by performing catalyst manipulations in a Shlenk apparatus.

- Further parameters such as temperature and pressure could be investigated for the selective hydrogenation of 1-heptyne with one pass through the catalyst bed, in order to study the influence upon selectivity to 1-heptene.

- Further hydrodynamic study in pulsing regime could be carried out to investigate the influence upon reaction rate, selectivity and validity of implemented kinetic models.

- Ability to measure hydrogen consumption in the reactors would be useful to understand mass transfer of hydrogen during the reactions and obtain accurate concentrations for kinetic modelling studies.

- It is desirable to operate the TBR under higher pressure and temperature to mimic those implemented industrially as such conditions are expected to influence hydrodynamics and mass transfer which in turn could influence reaction rate and selectivity of the studied reactions.

REFERENCES

Albright, L. (1973). "Application of partial hydrogenation theory to the design of commercial reactors for hydrogenating triglyceride oils." Journal of the American Oil Chemists' Society 50(7): 255-259.

Albright, L. F. (1965). "Quantitative measure of selectivity of hydrogenation of triglycerides." Journal of the American Oil Chemists' Society. 42(3): 250-253.

Alves, J. A., Bressa, S. P., Martínez, O. M., Barreto, G. F. (2011). "Kinetic study of the liquid-phase selective hydrogenation of 1-butyne in presence of 1-butene over a commercial palladium-based catalyst." Chemical Engineering Research and Design 89(4): 384-397.

Andersson, K., Hell, M., Löwendahl, L., Schöőn, N. (1974). "Diffusivities of hydrogen and glyceryl trioleate in cottonseed oil at elevated temperature." Journal of the American Oil Chemists' Society 51(4): 171-173.

An, W., Hong, J. K., Pintauro, P. N. (1998). "Current efficiency for soybean oil hydrogenation in a solid polymer electrolyte reactor." Journal of Applied Electrochemistry 28(9): 947-954.

Arterburn, J. B., Pannala, M., Gonzalez, A. M., Chamberlin, R. M. (2000). "Palladium-catalyzed transfer hydrogenation in alkaline aqueous medium." Tetrahedron Letters 41(41): 7847-7849.

Atencio, R., Bohanna C., Esteruelas, M. A., Lahoz, F. J., Oro, L. A. (1995). "Synthesis, reactivity and catalytic activity of [RuH(-OCMe$_2$)(CO)$_2$(PPri$_3$)$_2$]BF$_4$." Journal of the Chemical Society, Dalton Transactions(13): 2171-2181.

Augustine, R. L., Goel, P., Mahata, N., Reyes, C., Tanielyan, S.K. (2004). "Anchored homogeneous catalysts: high turnover number applications." Journal of Molecular Catalysis A: Chemical 216(2): 189-197.

Augustine, R. L., Tanielyan, S.K., Mahata, N., Gao, Y., Zsigmond, A., Yang, H. (2003). "Anchored homogeneous catalysts: the role of the heteropoly acid anchoring agent." Applied Catalysis A: General 256(1-2): 69-76.

Babaee, Z., Nikoopour H., and Safafar., (2007). "A Comparison of Commercial Nickel Catalysts Effects on Hydrogenation of Soyabean Oil". World Applied Sciences Journal 2 (6): 621-626.

Baiker, A. (1997). "Progress in asymmetric heterogeneous catalysis: Design of novel chirally modified platinum metal catalysts." Journal of Molecular Catalysis A: Chemical 115(3): 473-493.

Bailar, J. C. (1971). "The Homogeneous Hydrogenation of Soyabean Oil Methyl Ester." Platinum Metals Review 15(1): 2-8.

Bailey, A. E. (1979). "Bailey's Industrial Oil and Fat Products." Volume 2, 4th ed.; John Wiley & Sons: New York.

Baker, O. (1954). "Simultaneous Flow of Oil and Gas." Oil Gas Journal, 53, 185.

Balakos, M. W., Hernandez, E. E. (1997). "Catalyst characteristics and performance in edible oil hydrogenation." Catalysis Today 35: 415-425.

Barbaro, P., Bianchini, C., Giambastiani, G., Oberhauser, W., Bonzi, L. M., Rossi, F., Santo, V. D. (2002). "Recycling asymmetric hydrogenation catalysts by their immobilization onto ion-exchange resins." Supplementary data, The Royal Society of Chemistry.

Barbaro, P. (2006). "Recycling Asymmetric Hydrogenation Catalysts by Their Immobilization onto Ion-Exchange Resins." Chemistry-A European Journal 12: 5666-5675.

Barnard, C. F. J., Rouzaud, J., Stevenson, S. H. (2005). "Straightforward Preparation of Highly Enantioselective Anchored Chiral Homogeneous Catalysts." Organic Process Research & Development 9(2): 164-167.

Bartsch, A. (1995). Beschleunigung des Stoffaustaustausches von Gas-Flussigkeits-Reaktionen durch Schallwellen am Beispiel der Fetthartung. Z. Naturforsch 50(2): 228-234.

Beenackers, A. A. C. M., Swaaij van, W. P. M. (1993) "Mass transfer in gas-liquid slurry reactors." Chemical Engineering Science, 48 (18): 3109-3139.

Belkacemi, K., Boulmerka, A., Arul, J., Hamoudi, S. (2006). "Hydrogenation of Vegetable Oils with Minimum *trans* and Saturated Fatty Acid Formation Over a New Generation of Pd-catalyst." Topics in Catalysis 37(2): 113-120.

Belkacemi, K., Hamoudi, S. (2008). "Low Trans and Saturated Vegetable Oil Hydrogenation over Nanostructured Pd/Silica Catalysts: Process Parameters and Mass-Transfer Features Effects." Industrial & Engineering Chemistry Research 48(3): 1081-1089.

Bennett, J. A., Creamer, N. J., Deplancheb, K., Macaskieb, L. E., Shannonc, I. J., Wood, J. (2010). "Palladium supported on bacterial biomass as a novel heterogeneous catalyst: A comparison of Pd/Al2O3 and bio-Pd in the hydrogenation of 2-pentyne." Chemical Engineering Science 65(1): 282-290.

Bennett, J. A., Fishwick, R. P., Spence, R., Wood, J., Winterbottom, J. M., Jackson, S. D., Stitt, E. H. (2009). "Hydrogenation of 2-pentyne over Pd/Al$_2$O$_3$ catalysts: Effect of operating variables and solvent selection." Applied Catalysis A: General 364(1-2): 57-64.

Berger, A., de Souza, R. F., Delgado, M. R., Dupont, J. (2001). "Ionic liquid-phase asymmetric catalytic hydrogenation: hydrogen concentration effects on enantioselectivity." Tetrahedron: Asymmetry 12(13): 1825-1828.

Bernas, A., Myllyoja, J., Salmia, T., Murzin, D. Y. (2009). "Kinetics of linoleic acid hydrogenation on Pd/C catalyst." Applied Catalysis A: General 353(2): 166-180.

Bern, L., Lidefelt, J., Schöön, N. (1976). "Mass transfer and scale-up in fat hydrogenation." Journal of the American Oil Chemists' Society 53(7): 463-466.

Bernsmann, H., van den Berg, M., Hoen, R., Minnaard, A. J., Mehler, G., Reetz, M. T., De Vries, J. G., Feringa, B. L. (2005). "PipPhos and MorfPhos:☐ Privileged Monodentate Phosphoramidite Ligands for Rhodium-Catalyzed Asymmetric Hydrogenation." The Journal of Organic Chemistry 70(3): 943-951.

Blaser, H., Pugin, B. and Spindler, F. (2005). "Progress in enantioselective catalysis assessed from an industrial point of view." Journal of Molecular Catalysis A: Chemical 231(1-2): 1-20.

Blaser, H., Pugin, B., Studer, M., in: D.E. De Vos, I.F.J. Vankelecom, P.A. Jacobs (Eds.), Chiral Catalyst Immobilization and Recycling, WILEY-VCH, Germany, 2000, pp. 9-11.

Boelhouwer, J. G., Piepers, H. W., Drinkenburg, A. A. H. (2002). "Liquid-induced pulsing flow in trickle-bed reactors." Chemical Engineering Science 57(16): 3387-3399.

Bogdan, A. R., Mason, B. P., Sylvester, K. T., McQuade, D. T. (2007). "Flow Systmes with a Packed-Bed Microreactor." Angewandte Chemie International Edition 46: 1698-1701.

Bolton, E. R., (1927). Ibid. 46:444T.

Bolton, E. R., (1922). Indian Chemical Society Journal. 41:384R.

Bond, G. C., Dowden, D. A., Mackenzie, N. (1958). "The selective hydrogenation of acetylene." Transactions of the Faraday Society 54: 1537-1546.

Bond, G. C., Wells, P. B. (1965). "The hydrogenation of acetylene: I. The reaction of acetylene with hydrogen catalyzed by alumina-supported platinum." Journal of Catalysis 4(2): 211-219.

Bond, G. C., Wells, P. B. (1966). "The hydrogenation of acetylene: II. The reaction of acetylene with hydrogen catalyzed by alumina-supported palladium." Journal of Catalysis 5(1): 65-73.

Börner, A. and Heller, D. (2001). "The economic use of precious chiral diphosphine ligands-- DuPHOS and its rhodium(I) COD and NBD complexes." Tetrahedron Letters 42(2): 223-225.

Borodzinski, A., Cybulski, A. (2000). "The kinetic model of hydrogenation of acetylene-ethylene mixtures over palladium surface covered by carbonaceous deposits." Applied Catalysis A: General 198(1-2): 51-66.

Borodziński, A. (1999). "Hydrogenation of acetylene–ethylene mixtures on a commercial palladium catalyst." Catalysis Letters 63(1): 35-42.

Brandts, J. A. M. And Berben, P. H. (2003). "Application of Immobilized Rhodium Catalyst Precursors in Enantio- and Chemoselective Hydrogenation Reactions." Organic Process Research & Development 7(3): 393-398.

Burk, M. J. (1991). "C_2-symmetric bis(phospholanes) and their use in highly enantioselective hydrogenation reactions." Journal of the American Chemical Society 113(22): 8518-8519.

Burk, M. J. (2000). "Modular Phospholane Ligands in Asymmetric Catalysis." Accounts of Chemical Research 33(6): 363-372.

Chaudhari, R. V., Mills, P. L. (2004). "Multiphase catalysis and reaction engineering for emerging pharmaceutical processes." Chemical Engineering Science 59(22-23): 5337-5344.

Chen, A., McIntire, D., Gibson, P., Covey, J. (1983). "Investigation and modeling of mass transfer in soybean oil hydrogenators." Journal of the American Oil Chemists' Society 60(7): 1326-1330.

Chen, B., Dingerdissen, U., Krauter, J. C. E., Lansink Rotgerik, H.G.J., Mobus K., Ostgard, D. J., Panster, P., Riermeier, T. H., Seebald, S., Tacke, T., Trauthwein, H. (2005). "New developments in hydrogenation catalysis particularly in synthesis of fine and intermediate chemicals." Applied Catalysis A: General 280(1): 17-46.

Cheng-wei, L., Fu-an, W., Tao, Q., Rui-lin, W., Xiao-hong, T., Yong-qiang, Z. (2009). "Apparent kinetics for electrosynthesis process of chromic acid." Chemical Research in Chinese Universities 25(4): 532—536.

Christy, A. A., Xu, Z., Harrington, P. D. B. (2009). "Thermal degradation and isomerisation kinetics of triolein studied by infrared spectrometry and GC-MS combined with chemometrics." Chemistry and Physics of Lipids 158(1): 22-31.

Coenen, J. (1976). "Hydrogenation of Edible oils." Journal of the American Oil Chemists' Society 53(6): 382-389.

Coleman-Kammula, S., Duim-Koolstra, E. T. (1983). "Enantioselective epoxidation of an allylic alcohol catalyzed by (acetylacetonato)-(-N-methylprolinol)dioxomolybdenum. The decrease of enantioselectivity with chemical conversion." Journal of Organometallic Chemistry 246(1): 53-56.

Coulson, J. M., Richardson, J. F. Coulson & Richardson's Chemical Engineering, sixth ed., Butterworth-heinemann, Oxford, 1999.

Crosman, A. And Hoelderich, W. F. (2005). "Enantioselective hydrogenation over immobilized rhodium diphosphine complexes on aluminated SBA-15." Journal of Catalysis 232(1): 43-50.

Dang, T. P. and Kagan, H. B. (1971). "The asymmetric synthesis of hydratropic acid and amino-acids by homogeneous catalytic hydrogenation." Journal of the Chemical Society D: Chemical Communications(10): 481-481.

De Vos D. E., Vankelecom I. F. J., Jacobs P. A. (2000) "Chiral Catalyst Immobilization and Recycling." WILEY-VCH, Germany.

De Vries J. G., Elsevier, C. J. (2007). "Handbook of homogeneous hydrogenation." Wiley-VCH.

Dijkstra, A. J. (2006). "Revisiting the formation of trans isomers during partial hydrogenation of triacylglycerol oils." European Journal of Lipid Science and Technology, 108, (3), 249-264.

D'Oria, E., Karamertzanis, P. G., Price, S. L. (2010). "Spontaneous Resolution of Enantiomers by Crystallization: Insights from Computed Crystal Energy Landscapes." Crystal Growth & Design 10(4): 1749-1756.

Doyle, A. M., S. Shaikhutdinov, K., Jackson, S. D., Freund, H-J. (2003). "Hydrogenation on Metal Surfaces: Why are Nanoparticles More Active than Single Crystals?" Angewandte Chemie International Edition 42(42): 5240-5243.

Draguez de Hault, E., Demoulin, A. (1984). "Partial hydrogenation of polyunsaturated fatty materials." Journal of the American Oil Chemists' Society 61(2): 195-200.

Drozdowski, B. and Szukalska, E. (2000). "Effect of rapeseed oil hydrogenation conditions on trans isomers formation." European Journal of Lipid Science and Technology 102(10): 642-645.

Dudukovic, M.P., Larachi, F., Mills, P.L. (2002). "Multiphase catalytic reactors: a perspective on current knowledge and future trends" Catalysis Reviews Science and Engineering, 44, 123.

Dudukovic, M.P., Larachi, F., Mills, P.L. (1999). "Multiphase reactors – Revisited." Chemical Engineering Science, 54, 1975.

Fabrello, A., Dinoi, C., Perrin, L., Kalck, P., Maron, L., Urrutigoity, M., Dechy-Cabaret, O. (2010). "Probing the stereo-electronic properties of cationic rhodium complexes bearing chiral diphosphine ligands by [103]Rh NMR." Magnetic Resonance in Chemistry 48(11): 848-856.

Fernández, M. B., Sánchez M, J. F., Tonetto, G. M., Damiani, D. E. (2009). "Hydrogenation of sunflower oil over different palladium supported catalysts: Activity and selectivity." Chemical Engineering Journal 155(3): 941-949.

Fessenden, R. J., Fessenden, J. S., Logue, M. W. (1998). "Organic Chemistry 6th Edition." Brooks/Cole Publishing Company: 143-145.

Fillion, B., Morsi, B. I. (2000). "Gas–Liquid Mass-Transfer and Hydrodynamic Parameters in a Soybean Oil Hydrogenation Process under Industrial Conditions." Industrial & Engineering Chemistry Research 39(7): 2157-2168.

Fishwick, R. P., Natividad, R., Kulkarni, R., McGuire, P. A., Wood, J., Winterbottom, J. M., Stitt, E. H. (2007). "Selective hydrogenation reactions: A comparative study of monolith CDC, stirred tank and trickle bed reactors." Catalysis Today 128(1-2): 108-114.

Fogler, H. S. "Elements of Chemical Reaction Engineering" third ed., Prentice-Hall, Inc., New Jersey, 1999.

Formo, M. W. (1968). "General physical and chemical properties of fatty acids. In Fatty acids and their industrial applications." Pattison, E. S., Ed. Marcel Dekker, Inc., New York.

Fu, Y., Guo, X.-X., Zhu, S.-F., Hu, A.-G., Xie, J.-H., Zhou, Q.-L. (2004). "Rhodium-Catalyzed Asymmetric Hydrogenation of Functionalized Olefins Using Monodentate Spiro Phosphoramidite Ligands." The Journal of Organic Chemistry 69(14): 4648-4655.

Gallezot, P., Nicolaus, N., Fle`che, G., Fuertes, P., Perrard, A. (1998). "Glucose Hydrogenation on Ruthenium Catalysts in a Trickle-Bed Reactor." Journal of Catalysis 180(1): 51-55.

Gampp, H. (1987). "Investigation of pH-dependent complex equilibria at low ligand to metal ratio by nonlinear least-squares fit to linear-sweep or cyclic voltammetric data." Analytical Chemistry 59(20): 2456-2460.

Ganguli, K. L., Van den Berg, H. J. (1978). "Edible oil hydrogenation rates in the presence of a homogeneous Ziegler--Natta catalyst in a film reactor." Chemical Engineering Science 33(1): 27-34.

Gao, F., Ng, K. P., Lia, C., Krummela, K. I., Alliana, A. D., Garland, M. (2006). "A versatile and compact experimental apparatus for the on-line spectroscopic study of liquid-phase heterogeneous catalytic systems." Journal of Catalysis 237(1): 49-57.

Gebel, G., Aldebert, P., Pineri, M. (1993). "Swelling study of perfluorosulphonated ionomer membranes." Polymer 34(2): 333-339.

Gierman, H. (1988). "Design of laboratory hydrotreating reactors: Scaling Down of Trickle-flow Reactors." Applied Catalysis, 43, 2, 277.

Gladden, L. F., Lim, M. H. M., Mantle, M. D., Sederman, A. J., Stitt, E. H. (2003). "MRI visualisation of two-phase flow in structured supports and trickle-bed reactors." Catalysis Today 79-80(0): 203-210.

González, B., Calvar, N., Gómez, E., Domínguez, Á. (2007). "Density, dynamic viscosity, and derived properties of binary mixtures of methanol or ethanol with water, ethyl acetate, and methyl acetate at T = (293.15, 298.15, and 303.15) K." The Journal of Chemical Thermodynamics 39(12): 1578-1588.

Grau, R. J., Cassano, A. E., Baltanas, M. A. (1988). "Catalysts and Network Modeling in Vegetable Oil Hydrogenation Processes." Catalysis Reviews-Science and Engineering, 30, (1), 1-48.

Gridnev, I. D., Higashi, N., Asakura, K., Imamoto, T. (2000). "Mechanism of Asymmetric Hydrogenation Catalyzed by a Rhodium Complex of (S,S)-1,2-Bis(tert-butylmethylphosphino)ethane. Dihydride Mechanism of Asymmetric Hydrogenation." Journal of the American Chemical Society 122(30): 7183-7194.

Gunjal, P. R., Kashid, M. N., Ranade, V. V., Chaudhari, R. V. (2005). "Hydrodynamics of Trickle-Bed Reactors: Experiments and CFD Modeling." Industrial & Engineering Chemistry Research 44(16): 6278-6294.

Gupta, M., Yang, J., Roy, C. (2002). "Modelling the Effective Thermal Conductivity in Polydispersed Bed Systems: A Unified Approach using the Linear Packing Theory and Unit Cell Model." The Canadian Journal of Chemical Engineering 80(5): 830-839.

Haighton, A., Van Putte, K., Vermaas, L. F. (1972). "Determination of the solid contents of fats by wide-line nuclear magnetic resonance: The signal of liquid oils." Journal of the American Oil Chemists' Society 49(3): 153-156.

Halpern, J. (1981). "Mechanistic aspects of homogeneous catalytic hydrogenation and related processes." Inorganica Chimica Acta 50: 11-19.

Hamilton, C. A., Jackson, S.D., Kelly, G. J., Spence, R., de Bruin, D.. (2002). "Competitive reactions in alkyne hydrogenation." Applied Catalysis A: General 237(1-2): 201-209.

Hanfan, L., Guoping, M., (1993). "Modification of palladium metallic catalyst with polymer-anchored thioether ligands." Chinese Journal of Polymer Science 11(4): 375-379.

Hastert, R. C., Hydrogenation - A Tool, not an Epithet, Harshaw/Filtrol Partnership, Cleveland, O.

Heiszwolf, J. J., Engelvaart, L. B., van den Eijnden, M. G., Kreutzer, M. T., Kapteijn, F., Moulijn, J. A. (2001). "Hydrodynamic aspects of the monolith loop reactor." Chemical Engineering Science 56(3): 805-812.

Heldal, J., Moulton, K., Fronkel, E. (1989). "Fixed- Bed continuous hydrogenation of soybean oil with palladium- Polymer supported catalysts." Journal of the American Oil Chemists' Society 66(7): 979-982.

Hems, W. P., McMorn, P., Riddel, S., Watson, S., Hancocka, F. E., Hutchings, G. J. (2005). "Asymmetric hydrogenation using chiral Rh complexes immobilised with a new ion-exchange strategy." Organic & Biomolecular Chemistry 3(8): 1547-1550.

Hermán, B., Szőllősi, G., Fülöp, F., Bartók, M. (2007). "Enantioselective hydrogenation of α,β-unsaturated carboxylic acids in fixed-bed reactor." Applied Catalysis A: General 331: 39-43.

Herskowitz, M., Carbonell, R. G., Smith, J. M. (1979). "Effectiveness factors and mass transfer in trickle-bed reactors." American Institute of Chemical Engineers Journal 25(2): 272-283.

Horiuti, I. and Polanyi, M. (1934). "Exchange reactions of hydrogen on metallic catalysts." Transactions of the Faraday Society, 30, 1164 - 1172.

Hsu, N., Dlosady, L., Rubin, L. J. (1988). "Catalytic behavior of palladium in the hydrogenation of edible oils." Journal of the American Oil Chemists' Society 65(3): 349-356.

http://www.manufacturingchemist.com/technical/article_page/Turn_batch_to_continuous_processing/54954, accessed on 05/07/2010.

http://www.sigmaaldrich.com/etc/medialib/docs/Aldrich/Bulletin/al_techbull_al211.Par.0001.File.tmp/al_techbull_al211.pdf, accessed on 01/07/2009.

Hu, B., Fishwick, R. P., Pacek, A. W., Winterbottom, J. M., Wood, J., Stitt, E. H., Nienow, A. W. (2007). "Simultaneous measurement of in situ bubble size and reaction rates with a heterogeneous catalytic hydrogenation reaction." Chemical Engineering Science 62(18-20): 5392-5396.

Hu, B., Nienow, A. W., Stitt, E. H., Pacek, A. W. (2007). "Bubble Sizes in Agitated Water−Hydrophilic Organic Solvents for Heterogeneous Catalytic Reactions." Industrial & Engineering Chemistry Research 46(13): 4451-4458.

Huck, W. R., Bürgi, T., Mallat, T., Baiker, A. (2003). "Palladium-catalyzed enantioselective hydrogenation of 2-pyrones: evidence for competing reaction mechanisms." Journal of Catalysis 219(1): 41-51.

Inoguchi, K., Morimoto, T., Achiwa, K. (1989). "Asymmetric reactions catalyzed by chiral metal complexes : XXXII. Efficient asymmetric hydrogenation of itaconic acid derivatives catalyzed by rhodium complexes of improved (2S,4S)-N-(t-butoxycarbonyl)-4-(diphenylphosphino)-2-[(diphenylphosphino)methyl]pyrrolidine (BPPM) analogues." Journal of Organometallic Chemistry 370(1-3): C9-C12.

Jackson, S. D., Hamilton, C. A., Kelly, G. J., de Bruin, D. (2001). "The Hydrogenation of C-5 Alkynes over Palladium Catalysts." Reaction Kinetics and Catalysis Letters 73(1): 77-82.

Jackson, S. D., Monaghan, A. (2007). "Hydrogenation of unsaturated hydrocarbons--40 years on: Hydrogenation of 1,3-pentadiene over Pd/alumina." Catalysis Today 128(1-2): 47-51.

Jackson, S. D., Shaw, L. A. (1996). "The liquid-phase hydrogenation of phenyl acetylene and styrene on a palladium/carbon catalyst." Applied Catalysis A: General 134(1): 91-99.

Jacobsen, E. E., Andresen, L. S., Anthonsen, T. (2005). "Immobilization does not influence the enantioselectivity of CAL-B catalyzed kinetic resolution of secondary alcohols." Tetrahedron: Asymmetry 16(4): 847-850.

Jonker, G. H., Veldsink, J. W., Beenackers, A. A. C. M. (1998). "Intraparticle Diffusion Limitations in the Hydrogenation of Monounsaturated Edible Oils and Their Fatty Acid Methyl Esters." Industrial & Engineering Chemistry Research 37(12): 4646-4656.

Julcour-Lebigue C., Augier, F., Maffre, H., Wilhelm A., Delmas, H. (2009). "Measurements and Modeling of Wetting Efficiency in Trickle-Bed Reactors: Liquid Viscosity and Bed Packing Effects." Industrial & Engineering Chemistry Research 48(14): 6811-6819.

Katayama, T., Nitta, T. (1976). "Solubilities of hydrogen and nitrogen in alcohols and n-hexane." Journal of Chemical & Engineering Data 21(2): 194-196.

Kerr, J. M., Suckling, C. J. (1988). "Selective hydrogenation by a novel palladium(II) complex." Tetrahedron Letters 29(43): 5545-5548.

Khodadadi-Moghaddam, M., Habibi-Yangjeh, A., Gholami, M. R. (2009). "Solvent effects on the reaction rate and selectivity of synchronous heterogeneous hydrogenation of cyclohexene and acetone in ionic liquid/alcohols mixtures." Journal of Molecular Catalysis A: Chemical 306(1-2): 11-16.

King, J., Holliday, R., List, G., Snyder, J. (2001). "Hydrogenation of vegetable oils using mixtures of supercritical carbon dioxide and hydrogen." Journal of the American Oil Chemists' Society 78(2): 107-113.

Kitayama, Y., Muraoka, M., Takahashi, M., Kodama, T., Itoh, H., Takahashi, E., Okamura, M. (1996). "Catalytic hydrogenation of linoleic acid on nickel, copper, and palladium." Journal of the American Oil Chemists' Society 73(10): 1311-1316.

Kitayama, Y., Muraoka, M., Takahashi, M., Kodama, T., Takahashi, E., Okamura, M (1997). "Catalytic hydrogenation of linoleic acid over platinum-group metals supported on alumina." Journal of the American Oil Chemists' Society 74(5): 525-529.

Klasovsky, F., Claus P., Wolf, D. (2009). "Influence of Preparation Parameters on the Performance of Colloid-derived Oxidic Palladium Catalysts for Selective Hydrogenation of C–C Triple Bonds." Topics in Catalysis 52(4): 412-423.

Knowles, W. S. and Sabacky, M. J. (1968). "Catalytic asymmetric hydrogenation employing a soluble, optically active, rhodium complex." Chemical Communications (London)(22): 1445-1446.

Kobayashi, S., Lam, W. W. L., Manabe, K. (2000). "Remarkable rate enhancement of palladium-catalyzed allylic alkylation in water using a colloidal dispersion system." Tetrahedron Letters 41(32): 6115-6119.

Kohler, M., Richarz, W. (1985). "Experimental Study of a Complex Catalytic Reaction Network in a Trickle-Bed Reactor." Chemical Engineering Communications, 41: 59-72.

Köllner, C., Pugin, B., Togni, A. (1998). "Dendrimers Containing Chiral Ferrocenyl Diphosphine Ligands for Asymmetric Catalysis." Journal of the American Chemical Society 120(39): 10274-10275.

Koritala, S., Moulton Sr, K. J., Friedrich J. P., and Frankel, E. N., (1984). *Ibid*. 61:909.

Kulkarni, R., Natividad, R., Wood, J., Stitt, E. H., Winterbottom, J. M. (2005). "A comparative study of residence time distribution and selectivity in a monolith CDC reactor and a trickle bed reactor." Catalysis Today 105(3-4): 455-463.

Kulkarni, R. (2006). "Studies of trickle bed reactors. "PhD Thesis, University of Birmingham.

Kulkarni, R.; Wood, J.; Winterbottom, J. M. (2005). "Effect of Fines and Porous Catalyst on Hydrodynamics of Trickle Bed Reactors". Industrial & Engineering Chemistry Research. 44 (25), 9497-9501.

Kundu, A., Saroha, A. K., Nigman, D. D. P. (2001). "Liquid distribution studies in trickle-bed reactors." Chemical Engineering Science 56(21-22): 5963-5967.

Kunna, K. (2008), "Catalyst Immobilization via Electrostatic Interactions: Polystyrene-based supports." PhD Thesis, Eindhoven University of Technology.

Künzle, N., Mallat, T., Baiker, A. (2003). "Enantio selective hydrogenation of isopropyl-4,4,4-trifluoroacetoacetate in a continuous flow reactor." Applied Catalysis A: General 238(2): 251-257.

Künzle, N., Soler, J.-W., Mallat, T., Baiker, A. (2002). "Enantioselective Hydrogenation on Palladium - Limitations of Continuous Fixed-Bed Reactor Operation." Journal of Catalysis 210: 466-470.

L'Argentière, P. C., Cagnola, E. A., Quiroga, M. E., Liprandi D. A. (2002). "A palladium tetra-coordinated complex as catalyst in the selective hydrogenation of 1-heptyne." Applied Catalysis A: General 226(1-2): 253-263.

Lange, R., Schubert, M., Bauer, T. (2005). "Liquid Holdup in Trickle-Bed Reactors at Very Low Liquid Reynolds Numbers." Industrial & Engineering Chemistry Research 44(16): 6504-6508.

L'Argentiere, P. C., Quiroga, M. E., Liprandi, D. A., Cagnola, E. A., Roman-Martinez, M. C., Diaz-Aunon, J. A., de Lecea, C. S. M. (2003). "Activated-Carbon-Heterogenized [$PdCl_2(NH_2(CH_2)_{12}CH_3)_2$] for the Selective Hydrogenation of 1-Heptyne." Catalysis Letters 87: 97-101.

Lederhos, C., L'Argentiere, P. C., Coloma-Pascual, F., Figoli, N. S. (2006). "A study about the effect of the temperature of hydrogen treatment on the properties of Ru/Al$_2$O$_3$ and Ru/C and their catalytic behavior during 1-heptyne semi-hydrogenation." Catalysis Letters 110(1): 23-28.

Lederhos, C. R., Badano, J. M., Quiroga, M. E., L'Argentière, P. C., Pascual, F. C. (2010). "Influence of ni addition to a low-loaded palladium catalyst on the selective hydrogenation of 1-heptyne." Química Nova 33: 816-820.

Lederhos, C. R., L'Argentière, P. C., Fígoli, N. S. (2005). "1-Heptyne Selective Hydrogenation over Pd Supported Catalysts." Industrial & Engineering Chemistry Research 44(6): 1752-1756.

Lee, K.-W., Mei, B. X., Bo, Q., Kim, Y.-W and Han, Y. (2007). "Catalytic Selective Hydrogenation of Soyabean Oil for Industrial Intermediates." Industrial & Engineering Chemistry Research, Vol. 13, No. 4, 530-536.

Lempers, H. E. B. and Sheldon, R. A. (1998). "The Stability of Chromium in CrAPO-5, CrAPO-11, and CrS-1 during Liquid Phase Oxidations." Journal of Catalysis 175(1): 62-69.

Lennon, D., Marshall, R., Webb, G., Jackson, S. D. (2000). The effect of hydrogen concentration on propyne hydrogenation over a carbon supported palladium catalyst studied under continuous flow conditions. Studies in Surface Science and Catalysis. F. V. M. S. M. Avelino Corma and G. F. José Luis, Elsevier. Volume 130: 245-250.

Liprandi, D. A., Cagnola, E. A., Quiroga, M. E., L'Argentiere, P. C. (2006). "Rhodium(I) Complex with Hexylamine and Chloride Ligands, Catalytically Active in the Selective Hydrogenation of 1-Heptyne." Industrial & Engineering Chemistry Research 45(17): 5836-5840.

Liprandi, D., Cagnola, E. A., Quiroga, M. E., L'Argentie`re, P. C. (2009). "Influence of the Reaction Temperature on the 3-Hexyne Semi-Hydrogenation Catalyzed by a Palladium(II) Complex." Catalysis Letters 128(3): 423-433.

Li, W., Zhang, X. (2000). "Synthesis of 3, 4-O-Isopropylidene- (3S,4S)-dihydroxy-(2R,5R)-bis(diphenylphosphino)hexane and Its Application in Rh-Catalyzed Highly Enantioselective Hydrogenation of Enamides." The Journal of Organic Chemistry 65(18): 5871-5874.

Llamas, J.-D., Lesage, F., Wild, G. (2008). "Influence of Gas Flow Rate on Liquid Distribution in Trickle-Beds Using Perforated Plates as Liquid Distributors." Industrial & Engineering Chemistry Research 48(1): 7-11.

Lopes, R. J. G. and Quinta-Ferreira R. M. (2009). "Hydrodynamic Simulation of Pulsing-Flow Regime in High-Pressure Trickle-Bed Reactors." Industrial & Engineering Chemistry Research 49(3): 1105-1112.

Lush, E.J., (1923). Ibid. 42:219T.

Lush, E. J., (1930). Oil and Fat Industries 7(5):175.

Marangozis, J., Keramidas, O. B., Paparisvas, G. (1977). "Rate and Mechanism of Hydrogenation of Cottenseed Oil in Slurry Reactors." Industrial & Engineering Chemistry Process Design and Development 16(3): 361-369.

Maranhão, L. C. A., Abreu, C. A. M. (2005). "Continuous Process of Fine Polyols Production in a Trickle-Bed Reactor." Industrial & Engineering Chemistry Research 44(25): 9642-9645.

Mekasuwandumrong, O., Phothakwanpracha, S., Jongsomjit, B. , Shotipruk, A., Panpranot, J . (2010). "Liquid-Phase Selective Hydrogenation of 1-Heptyne over Pd/TiO$_2$ Catalyst Synthesized by One-Step Flame Spray Pyrolysis." Catalysis Letters 136(1): 164-170.

Mekasuwandumrong, O., Somboonthanakij, S., Praserthdam, P., Panpranot, J. (2009). "Preparation of Nano-Pd/SiO$_2$ by One-Step Flame Spray Pyrolysis and Its Hydrogenation Activities: Comparison to the Conventional Impregnation Method." Industrial & Engineering Chemistry Research 48(6): 2819-2825.

Milano-Brusco, J. S., Schwarze, M., Djennad, M., Nowothnick, H., Schomacker, R. (2008). "Catalytic Hydrogenation of Dimethyl Itaconate in a Water–Cyclohexane–Triton X-100 Microemulsion in Comparison to a Biphasic System." Industrial & Engineering Chemistry Research 47(20): 7586-7592.

Mills, P. L., and Chaudhari, R. V. (1997). "Multiphase Catalytic Reactor Engineering and Design for Pharmaceuticals and Fine Chemicals." Catalysis Today, 37, 367.

Miyashita, A., Yasuda, A., Takaya, H., Toriumi, K., Ito, T., Souchi, T., Noyori, R. (1980). "Synthesis of 2,2'-bis(diphenylphosphino)-1,1'-binaphthyl (BINAP), an atropisomeric chiral bis(triaryl)phosphine, and its use in the rhodium(I)-catalyzed asymmetric hydrogenation of .alpha.-(acylamino)acrylic acids." Journal of the American Chemical Society 102(27): 7932-7934.

Mogalicherla, A. K., Sharma, G., Kunzru, D. (2009). "Estimation of Wetting Efficiency in Trickle-Bed Reactors for Nonlinear Kinetics." Industrial & Engineering Chemistry Research 48(3): 1443-1450.

Molnár, Á., Sárkány, A., Varga, M. (2001). "Hydrogenation of carbon-carbon multiple bonds: chemo-, regio- and stereo-selectivity." Journal of Molecular Catalysis A: Chemical 173(1-2): 185-221.

Mondal, K. and Lalvani, S. (2008). "Low temperature soybean oil hydrogenation by an electrochemical process." Journal of Food Engineering 84(4): 526-533.

Mossoba, M., Seiler, A. , Kramer, J. K. G. , Milosevic, V. , Milosevic, M. , Azizian, H., Steinhart, H. (2009). "Nutrition Labeling: Rapid Determination of Total trans Fats by Using Internal Reflection Infrared Spectroscopy and a Second Derivative Procedure." Journal of the American Oil Chemists' Society 86(11): 1037-1045.

Moulton, K. J. and Kwolek , W. F. (1982). "Continuous hydrogenation of soybean oil in a trickle-bed reactor with copper catalyst." Journal of the American Oil Chemists' Society 59(8): 333-337.

Mukherjee, K. D., Kiewitt, I., and Kiewitt, M., (1975). Ibid. 52:282.

Munteanu, M. C. and Larachi, F. (2009). "Flow regimes in trickle beds using magnetic emulation of micro/macrogravity." Chemical Engineering Science 64(2): 391-402.

Natividad, R., Kulkarni, R., Nuithitikul, K., Raymahasay, S., Wood, J., Winterbottom, J. M. (2004). "Analysis of the performance of single capillary and multiple capillary (monolith) reactors for the multiphase Pd-catalyzed hydrogenation of 2-Butyne-1,4-Diol." Chemical Engineering Science 59(22-23): 5431-5438.

Nedovic, V., Willaert , R. (Eds.), Fundamentals of Cell Immobilisation Biotechnology, Kluwer Academic Publishers, Netherlands, 2004, p.418.

Nigam, K. D. P. and Larachi, F. (2005). "Process intensification in trickle-bed reactors." Chemical Engineering Science 60(22): 5880-5894.

Nijhuis, T. A., Koten, G. v., Moulijn, J. A. (2003). "Optimized palladium catalyst systems for the selective liquid-phase hydrogenation of functionalyzed alkynes." Applied Catalysis A: General 238(2): 259-271.

Ning, J., Xu, J., Liu, J., Miao, H., Ma, H., Chen, C., Li, X., Zhou, L., Yu, W. (2007). "A remarkable promoting effect of water addition on selective hydrogenation of p-chloronitrobenzene in ethanol." Catalysis Communications 8(11): 1763-1766.

Nohair, B., C. Especel, C., Lafayea, G., Marécota, P., Hoangb, L., Barbier, J. (2005). "Palladium supported catalysts for the selective hydrogenation of sunflower oil." Journal of Molecular Catalysis A: Chemical 229(1-2): 117-126.

Ojima, I. (2010). "Catalytic asymmetric synthesis." By John Wiley & Sons, Inc., USA.

Osborn, J. A., Jardine, F. H., Young, J. F., Wilkinson, G. (1966). "The preparation and properties of tris(triphenylphosphine)halogenorhodium(I) and some reactions thereof including catalytic homogeneous hydrogenation of olefins and acetylenes and their derivatives." Journal of the Chemical Society A: Inorganic, Physical, Theoretical: 1711-1732.

Pangarkar, K., Schildhauer, T. J., van Ommen, J. R., Nijenhuis, J., Kapteijn, F., Moulijn, J. A. (2008). "Structured Packings for Multiphase Catalytic Reactors." Industrial & Engineering Chemistry Research 47(10): 3720-3751.

Paul, E. L. (1988). "Design of reaction systems for specialty organic chemicals." Chemical Engineering Science 43(8): 1773-1782.

Pestre, N., Meille, V., de Bellefon, C. (2006). "Effect of gas-liquid mass transfer on enantioselectivity in asymmetric hydrogenations." Journal of Molecular Catalysis A: Chemical 252(1-2): 85-89.

Pétursson, S. (2002). "Clarification and expansion of formulas in AOCS recommended practice Cd 1c-85 for the calculation of Iodine value from FA composition." Journal of the American Oil Chemists' Society 79(7): 737-738.

Pfaltz, A., Drury III, W.J. (2004). "Design of chiral ligands for asymmetric catalysis: From C2-symmetric P,P- and N,N-ligands to sterically and electronically nonsymmetrical P,N-ligands ." Proceedings of the National Academy of Sciences of the United States of America 101: 5723-5726.

Pintauro, P. N., Gil, M. P., Warner, K., List, G., Neff, W. (2005). "Electrochemical Hydrogenation of Soybean Oil with Hydrogen Gas." Industrial & Engineering Chemistry Research 44(16): 6188-6195.

Piqueras, C. M., Tonetto, G., Bottini, S., Damiani, D. E. (2008). "Sunflower oil hydrogenation on Pt catalysts: Comparison between conventional process and homogeneous phase operation using supercritical propane." Catalysis Today 133-135: 836-841.

Pugin, B. (1996). "Immobilized catalysts for enantioselective hydrogenation: The effect of site-isolation." Journal of Molecular Catalysis A: Chemical 107(1-3): 273-279.

Purwanto, Deshpande, R. M., Chaudhari, R. V., Delmas, H. (1996). "Solubility of Hydrogen, Carbon Monoxide, and 1-Octene in Various Solvents and Solvent Mixtures." Journal of Chemical & Engineering Data 41(6): 1414-1417.

Quignard, F. Choplin, A., in: J.A. McCleverty, T.J. Meyer (Eds.), Comprehensive Coordination Chemistry II, Elsevier Ltd, 2003, pp. 445-446.

Quiroga, M. E., Liprandi, D., Cagnola, E. A., L' Argentie`re, P. C. (2007). "1-Heptyne semihydrogenation catalized by palladium or rhodium complexes: Influence of: metal atom, ligands and the homo/heterogeneous condition." Applied Catalysis A: General 326(2): 121-129.

Quiroga, M., Liprandi, D., L'Argentière, P., Cagnola, E. (2005). "Obtaining 1-heptene from 1-heptyne semihydrogenation with an anchored rhodium complex on different supports as catalyst." Journal of Chemical Technology & Biotechnology 80(2): 158-163.

Rajadhyaksha, R. A. and Karwa, S. L. (1986). "Solvent effects in catalytic hydrogenation." Chemical Engineering Science 41(7): 1765-1770.

Rajashekharam, M. V., Jaganathan, R., Chaudhari, R. V., (1998) "A trickle bed reactor model for hydrogenation of 2,4-dinitrotoluene: experimental verification", Chemical Engineering Science, 4, 53, 787.

Ramachandran, P. A., and Chaudhari, R. V. (1983). "Three-Phase Catalytic Reactors.", Gordon and Breach, Science Publishers Inc., New York, USA.

Rebrov, E. V., Klinger, E. A., Berenguer-Murcia, A., Sulman, E. M., Schouten, J. C. (2009). "Selective Hydrogenation of 2-Methyl-3-butyne-2-ol in a Wall-Coated Capillary Microreactor with a Pd25Zn75/TiO2 Catalyst." Organic Process Research & Development 13(5): 991-998.

Reetz, M. T., Meiswinkel, A., Mehler, G., Angermund, K., Graf, M., Thiel, W., Mynott, R., Blackmond, D. G. J. (2005). "Why Are BINOL-Based Monophosphites Such Efficient Ligands in Rh-Catalyzed Asymmetric Olefin Hydrogenation?" Journal of the American Chemical Society 127(29): 10305-10313.

Roberts, G.W., and Lamb, H. H. (1995). Journal of Catalysis, 154, 364.

Rode, C. V., Tayade, P. R. Nadgeri, J. M., Jaganathan, R., Chaudhari, R. V. (2006). "Continuous Hydrogenation of 2-Butyne-1,4-diol to 2-Butene- and Butane-1,4-diols." Organic Process Research & Development 10(2): 278-284.

Ronchin, L. and Toniolo, L. (2001). "Selective hydrogenation of benzene to cyclohexene using a Ru catalyst suspended in an aqueous solution in a mechanically agitated tetraphase reactor: a study of the influence of the catalyst preparation on the hydrogenation kinetics of benzene and of cyclohexene." Applied Catalysis A: General 208(1-2): 77-89.

Rylander, P. (1970). "Hydrogenation of natural oils with platinum metal group catalysts." Journal of the American Oil Chemists' Society 47(12): 482-486.

Saroha, A. K., Nigam, K. D. P., Saxena, A. K., Kapor, V. K. (1998). "Liquid distribution in trickle-bed reactors." American Institute of Chemical Engineers Journal 44(9): 2044-2052.

Satterfield. C. N., American Institute of Chemical Engineers Journal 21:209 (1975).

Satterfield, C. N. (1970). "Mass Transfer in Heterogeneous Catalysis." MIT Press, Cambridge, pp. 214-215.

Schmidt, S. (2000). "Formation of trans unsaturation during partial hydrogenation." European Journal of Lipid Science and Technology 102: 646– 648.

Seebach, D., Marti, R. E., Hintermann, T. (1996). "Polymer- and Dendrimer-Bound Ti-TADDOLates in Catalytic (and Stoichiometric) Enantioselective Reactions: Are pentacoordinate cationic Ti complexes the catalytically active species?" Helvetica Chimica Acta 79(6): 1710-1740.

Sekhon, B. S. (2010). " Separation of pharmaceutical enantiomers using supercritical fluid technology." International Journal of PharmTech Research 2(2):1595-1602.

Selke, R., Häupke, K., Krause, H. W. (1989). "Asymmetric hydrogenation by heterogenized cationic rhodium phosphinite complexes." Journal of Molecular Catalysis 56(1-3): 315-328.

Sento, T., Shimazu, S., Ichikuni, N., Uematsu, T. (1999). "Asymmetric hydrogenation of itaconates by hectorite-intercalated Rh-DIOP complex." Journal of Molecular Catalysis A: Chemical 137(1-3): 263-267.

Sharma, S., Mantle, M. D., Gladden, L. F., Winterbottom, J. M. (2001). "Determination of bed voidage using water substitution and 3D magnetic resonance imaging, bed density and pressure drop in packed-bed reactors." Chemical Engineering Science 56(2): 587-595.

Sheldon, R. A. (1993) "Chirotechnology: Industrial Synthesis of Optically Active Compounds." Marcel Dekker, New York, p. 347.

Simons, C., Hanefeld, U., Arends, I.W.C.E., Sheldon, R. A., Maschmeyer, T. (2004). "Noncovalent Anchoring of Asymmetric Hydrogenation Catalysts on a New Mesoporous Aluminosilicate: Application and Solvent Effects." Chemistry – A European Journal 10(22): 5829-5835.

Singh, D. (2009) "Metal Decorated Polymeric Membranes for Low Trans Partial Hydrogenation of Soyabean Oil." PhD Thesis. Kansas State University, Manhattan, Kansas.

Singh, U. K., Albert Vannice, M. (2000). "Liquid-Phase Hydrogenation of Citral over Pt/SiO2 Catalysts: I. Temperature Effects on Activity and Selectivity." Journal of Catalysis 191(1): 165-180.

Sladkova, T. A., Galichaya, N. N., Vasserberg, V. E´. (1985). "Palladium catalysts for selective hydrogenation of acetylenes, produced via complexation in an adsorbed layer." Kinetics and Catalysis 27(2): 516–519.

Snyder. J. M., Mounts, T. L., Schofield, C. R. and Dutton, H. J., (1982), Journal of the American Oil Chemists' Society 59:19.

Somboonthanakij, S., Mekasuwandumrong, O., Panpranot, J., Nimmanwudtipong, T. , Strobel, R., Pratsinis, S. E., Praserthdam, P. (2007). "Characteristics and Catalytic Properties of Pd/SiO$_2$ Synthesized by One-step Flame Spray Pyrolysis in Liquid-phase Hydrogenation of 1-Heptyne." Catalysis Letters 119(3): 346-352.

Stahly, G. P., Starrett, R. M. (1997) "Chirality in Industry II." in: Collins, A. N., Sheldrake, G. N., Crosby, J. (Eds.), Wiley, New York, p. 19.

Steiner, I., Aufdenblatten, R., Togni, A., Blaser, H., Pugin, B. (2004). "Novel silica gel supported chiral biaryl-diphosphine ligands for enantioselective hydrogenation." Tetrahedron: Asymmetry 15(14): 2307-2311.

Stitt, E. H., Fishwick, R. P., Natividad, R., Winterbottom, J. M. Multiphase hydrogenation reactors—past, present and future. In: S.D. Jackson, J.S.J. Hargreaves and D. Lennon, Editors, Catalysis in Application, The Royal Society of Chemistry, London (2003).

Studt, F., Abild-Pedersen, F., Bligaard, T., Sorensen, R. Z., Christensen, C. H., Norskov, J. K. (2008). "On the Role of Surface Modifications of Palladium Catalysts in the Selective Hydrogenation of Acetylene." Angewandte Chemie 120(48): 9439-9442.

Sun, Y., Landau, R. N., Wang, J., LeBlond, C., Blackmond, D. G. (1996). "A Re-Examination of Pressure Effects on Enantioselectivity in Asymmetric Catalytic Hydrogenation." Journal of the American Chemical Society 118(6): 1348-1353.

Sun, Y., Wang, J., LeBlond, C., Landau, R. N., Blackmond, D. G. (1996). "Asymmetric Hydrogenation of Ethyl Pyruvate: Diffusion Effects on Enantioselectivity." Journal of Catalysis 161(2): 759-765.

Taguchi, A. and F. Schüth (2005). "Ordered mesoporous materials in catalysis." Microporous and Mesoporous Materials 77(1): 1-45.

Tang, W.-J, Huang, Y.-Y., He, Y.-M., Fan, Q.-H. (2006). "Dendritic MonoPhos:synthesis and application in Rh-catalyzed asymmetric hydrogenation. " Tetrahedron: Asymmetry 17 (4): 536-543.

Tang, W., Zhang, X. (2003). "New Chiral Phosphorus Ligands for Enantioselective Hydrogenation." Chemical Reviews, 103: 3029-3069.

Teschner, D., Vass, E., Havecker, M., Zafeiratos, S., Schnorch, P., Sauer, H., Knop-Gericke, A., Schloegl, R., Chamam, M., Wootsch, A., Canning, A. S., Gamman, J. J., Jackson, S. D., McGregor, J., Gladden, L. F. (2006). "Alkyne hydrogenation over Pd catalysts: A new paradigm." Journal of Catalysis 242(1): 26-37.

Thomas, J. M.; Maschmeyer, T.; Johnson, B. F. G.; Shephard, D. S. (1999). "Constrained chiral catalysts." Journal of Molecular Catalysis 141: 139-144.

Tike, M. A., Mahajani, V. V., (2007). " Kinetics of hydrogenation of palm stearin fatty acid over Ru/Al$_2$O$_3$ catalyst in presence of small quantity of water." Indian Journal of Chemical Technology 14: 53.

Tike, M. A. and Mahajani, V. V. (2006). "Studies in catalytic transfer hydrogenation of soybean oil using ammonium formate as donor over 5% Pd/C catalyst." Chemical Engineering Journal 123(1-2): 31-41.

Tolman, C. A. (1977). "Steric effects of phosphorus ligands in organometallic chemistry and homogeneous catalysis." Chemical Reviews 77(3): 313-348.

Toukoniitty, E., Mäki-Arvela, P., Kuusisto, J.,Nieminen, V., Päivärinta, J., Hotokka, M., Salmi, T., Murzin, D. Yu. (2003). "Solvent effects in enantioselective hydrogenation of 1-phenyl-1,2-propanedione." Journal of Molecular Catalysis A: Chemical 192(1-2): 135-151.

Toukoniitty, E., Mäki-Arvela, P., Neyestanaki, A. K., Salmi, T., Murzin, D.Yu. (2002). "Continuous hydrogenation of 1-phenyl-1,2-propanedione under transient and steady-state conditions: regioselectivity, enantioselectivity and catalyst deactivation." Applied Catalysis A: General 235(1-2): 125-138.

Toukoniitty, E., Mäki-Arvela, P., Neyestanaki, A. K., Salmi, T., Sjöholm, R., Leino, R., Laine, E., Kooymane, P. J., Ollonqvist, T., Väyrynen, J. (2001). "Batchwise and continuous enantioselective hydrogenation of 1-phenyl-1,2-propanedione catalyzed by new Pt/SiO2 fibers." Applied Catalysis A: General 216(1-2): 73-83.

Turek, F., Chakrabarti, R. K., Lange, R., Geike, R., Flock, W. (1983). "On the experimental study and scale-up of three-phase catalytic reactors: Hydrogenation of glucose on nickel catalyst." Chemical Engineering Science 38(2): 275-283.

Ulan, J. G., Maier, W. F., Smith, D. A. (1987). "Rational design of a heterogeneous palladium catalyst for the selective hydrogenation of alkynes." The Journal of Organic Chemistry 52(14): 3132-3142.

Urbina C., Campos C., Pecchi G., Claver C., Reyes P. (2010). "Chiral Pt/ZrO2 Catalysts. Enantioselective Hydrogenation of 1-phenyl-1,2-propanedione." Molecules 15: 3428-3440.

Van den Berg, M.; Minnaard, A. J.; Haak, R. M.; Leeman, M.; Schudde, E. P.; Meetsma, A.; Feringa, B. L.; de Vries, A. H. M.; Maljaars, C. E. P.; Willans, C. E.; Hyett, D.; Boogers, J. A. F.; Henderickx, H. J. W.; de Vries, J. G. (2003). "Monodentate Phosphoramidites: A Breakthrough in Rhodium-Catalysed Asymmetric Hydrogenation of Olefins." Advanced Synthesis & Catalysis 345(1-2): 308-323.

Vazquez, G., Alvarez, E., Navaza, J. M. (1995). "Surface Tension of Alcohol Water + Water from 20 to 50 .degree.C." Journal of Chemical & Engineering Data 40(3): 611-614.

Veldsink, J. W. B., Schoon, M. J., Beenackers, N. H., Antonie A. C. M. (1997). "Heterogeneous hydrogenation of vegetable oils: a literature review." Catalysis Reviews - Science and Engineering, 39, (3), 253-318.

Wagner, H. H., Hausmann, H., Holderich, W. F. (2001). "Immobilization of Rhodium Diphosphine Complexes on Mesoporous Al-MCM-41 Materials: Catalysts for Enantioselective Hydrogenation." Journal of Catalysis 203(1): 150-156.

Wang, C.-B., Chang, J.-G., Wu, R.-C, Yeh, C.-T. (1998). "Promotion effect of coating alumina supported palladium with sodium hydroxide on the catalytic conversion of nitric oxide." Applied Catalysis B: Environmental 17(1-2): 51-62.

Wang, S. and Kienzle, F. (1998). "Development of a Continuous Homogeneous Metal Complex Catalyzed, Asymmetric Hydrogenation under High Pressure (270 bar)." Organic Process Research & Development 2(4): 226-229.

Weber, D., Mitchell, J., McGregor, J., Gladden, L. F. (2009). "Comparing Strengths of Surface Interactions for Reactants and Solvents in Porous Catalysts Using Two-Dimensional NMR Relaxation Correlations." The Journal of Physical Chemistry C 113(16): 6610-6615.

Weekman, V. W. (1969). "Kinetics and Dynamics of Catalytic Cracking Selectivity in Fixed-Bed Reactors." Industrial & Engineering Chemistry Process Design and Development 8(3): 385-391.

Weekman, V. W., Myers J. E. (1964). "Fluid-flow characteristics of concurrent gas-liquid flow in packed beds." American Institute of Chemical Engineers Journal 10(6): 951-957.

Whitesell, J. K. (1989). "C2 symmetry and asymmetric induction." Chemical Reviews 89(7): 1581-1590.

Wilhite, B. A., Huang, X., McCready, M. J., Varma, A. (2003). "Effects of Induced Pulsing Flow on Trickle-Bed Reactor Performance." Industrial & Engineering Chemistry Research 42(10): 2139-2145.

Willett, W. C., Stampfer, M. J., Manson, J. E., Colditz, G. A., Speizer, F. E., Rosner, B. A., Sampson, L. A., Hennekens, C. H. (1993). "Intake of Trans-Fatty-Acids and Risk of Coronary Heart-Disease among Women." Lancet, 341, (8845), 581-585.

Winterbottom, J. M., Khan, Z., Raymahasay, S., Knight, G., Roukounakis, N. (2000). "A comparison of triglyceride oil hydrogenation in a downflow bubble column using slurry and fixed bed catalysts." Journal of Chemical Technology & Biotechnology 75(11): 1015-1025.

Winterbottom, J. M., King, M. B. (Eds.). (1999). "Reactor Design for Chemical Engineers.", Stanley Thornes, Cheltenham, pp.362-373.

Winterbottom, J. M., Marwan, , H., Natividad, R. (2003). "Selectivity, Hydrodynamics and Solvent Effects in a Monolith Cocurrent Downflow Contactor (CDC) Reactor." The Canadian Journal of Chemical Engineering 81(3-4): 838-845.

Wood, J., Bodenes, L., Bennet, J. Deplanche, K. Macaskie, L. E. (2009). "Hydrogenation of 2-Butyne-1,4-diol Using Novel Bio-Palladium Catalysts." Industrial & Engineering Chemistry Research 49(3): 980-988.

Yang, X., Wang, X., Liang, C., Su, W., Wang, C., Feng, Z., Li, C., Qiu, J. (2008). "Aerobic oxidation of alcohols over Au/TiO2: An insight on the promotion effect of water on the catalytic activity of Au/TiO2." Catalysis Communications 9(13): 2278-2281.

Yan, Y.-Y., RajanBabu, T. V. (2000). "Ligand Substituent Effects on Asymmetric Induction. Effect of Structural Variations of the DIOP Ligand on the Rh-Catalyzed Asymmetric Hydrogenation of Enamides." Organic Letters 2(26): 4137-4140.

Young, J. F., Osborn, J. A., Jardine, F. H., Wilkinson, G. (1965). "Hydride intermediates in homogeneous hydrogenation reactions of olefins and acetylenes using rhodium catalysts." Chemical Communications (London)(7): 131-132.

Yusem, G., Pintauro, P., Cheng, C., An, W. (1996). "Electrocatalytic hydrogenation of soybean oil in a radial flow-through Raney nickel powder reactor." Journal of Applied Electrochemistry 26(10):989-997.

APPENDICES

Appendix A. Data for calculation of flow regime and hydrogen diffusivities

A.1 Determination of flow regime

A.2 Diffusivity of hydrogen in solvent

Appendix B. Results of the influence of solvent and temperature from Chapters 6 and 7

Appendix C. Calibration curves for the GC

Appendix D. Published work

Appendix A. Data for calculation of flow regime and hydrogen diffusivities

This section provides the properties of the fluids used to calculate the flow regime in the TBR. It also supplies some data used to calculate the diffusivities of hydrogen in the solvents used in the studies.

A.1 Determination of flow regime

The flow regime in the trickle bed reactor (TBR) was determined based on Baker flow map shown below (Ramachandran and Chaudhari, 1983):
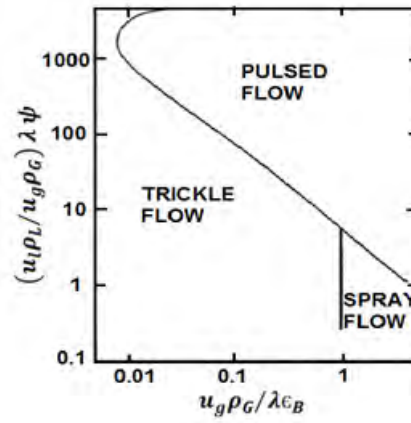
The flow map is in terms of what are known as the Baker (1954) co-ordinates. On the map, $u_l \rho_L \lambda \psi / u_g \rho_G$ vs $u_G \rho_G / \lambda \epsilon_B$ is plotted. The parameters λ and ψ are defined as

$$\lambda = (\frac{\rho_G}{\rho_{air}} \frac{\rho_L}{\rho_{water}})^{0.5} \tag{A.1}$$

$$\psi = \frac{s_{TW}}{s_T} \left[\frac{\mu_L}{\mu_W} \left(\frac{\rho_{water}}{\rho_L} \right)^2 \right]^{1/3} \tag{A.2}$$

Where the parameters are defined in the nomenclature.

The values used to calculate Baker co-ordinates for the studied reactions are presented in Tables A.1 and A.2

ρ_{H2}	ρ_{air}	ρ_{water}	μ_W	S_{TW}
(g/cm³)	(g/cm³)	(g/cm³)	(g/cm/s)	(dyne/cm)
8.99×10^{-5}	0.0012	0.998	0.010	72.8

Table A.1. Properties of H_2, air and water used to calculate Baker co-ordinates.

Liquid	ρ	μ	S_T
	(g/cm³)	(g/cm/s)	(dyne/cm)
50% v/v MeOH in water	0.886*	0.0148*	33.37**
EtOH	0.789	0.0196	22.3
IPA	0.786	0.0243	21.7
Soyabean oil	0.862	0.0616	30

Table A.2. Properties of solvents used to calculate Baker co-ordinates. * obtained from González *et al*. (2007). ** obtained from Vazquez *et al*. (1995).

A.2 Diffusivity of hydrogen in solvent

The diffusivity of hydrogen into ethanol and isopropanol was determined using the following correlation proposed by Coulson and Richardson (1999):

$$D = (1.173exp^{-16}\emptyset_B^{0.5}M_B^{0.5}T)/\mu V_A^{0.6} \qquad \text{(A. 3) or (5.5)*}$$

While the diffusivity of hydrogen into soyabean oil was determined using the following correlation proposed by Andersson *et al*. (1974):

$$D = (1.173exp^{-16}\emptyset_B^{0.5}M_B^{0.5}T)/\mu V_A^{0.6} \qquad \text{(A. 4) or (7.3)*}$$

Where the parameters are defined in the nomenclature.

The values used to calculate the diffusivity of hydrogen into the relevant solvent are presented in Table A.3

Solvent	$\emptyset_B$	M_B
ethanol	1.5	46.07
isopropanol	1.4	60.09
soyabean oil	3.8	875

Table A.3. Values used to calculate the diffusivity of hydrogen into the various solvents used in the studies.

* Equation was labelled based on the order of its appearance in the appendix or in the thesis.

Appendix B. Results of the influence of solvent and temperature from Chapters 6 and 7

This section demonstrates the reaction profiles for the selective hydrogenation of 1-heptyne in the investigated solvents. The fitted concentration profiles for the selective hydrogenation of soyabean oil under various temperatures are also involved.
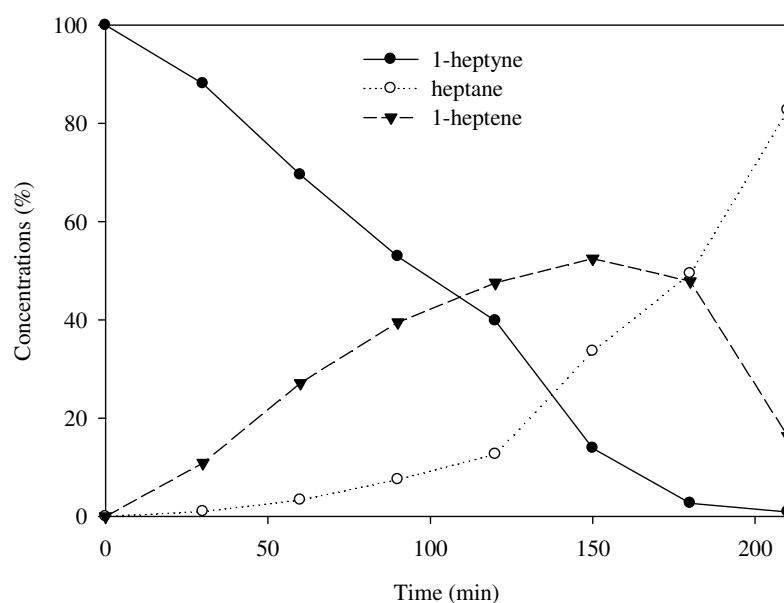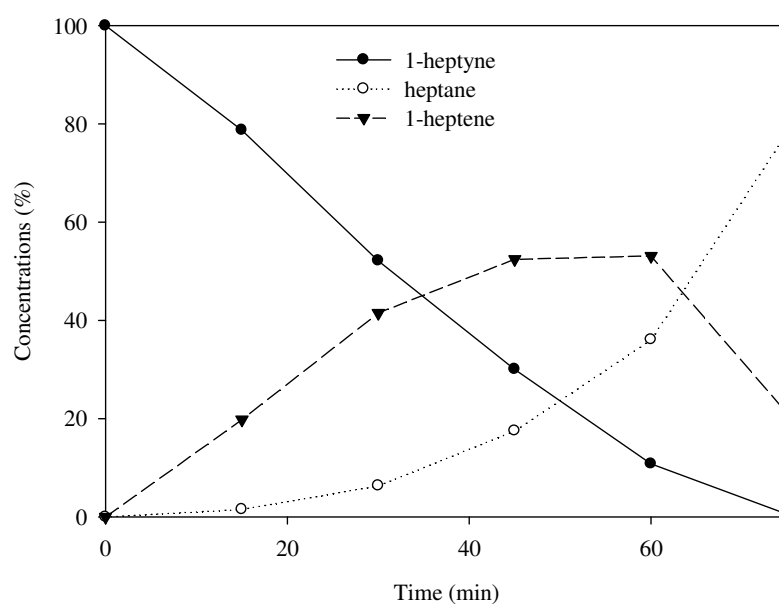

Figure B.1. Reaction profile for 1-heptyne hydrogenation in 0.4 ml water in a 100 ml mixture containing 5 % v/v 1-heptyne in solvent. Conditions: H_2 flow rate of 100 ml min^{-1}, liquid flow rate of 10 ml min^{-1}, 20 °C temperature and atmospheric pressure.
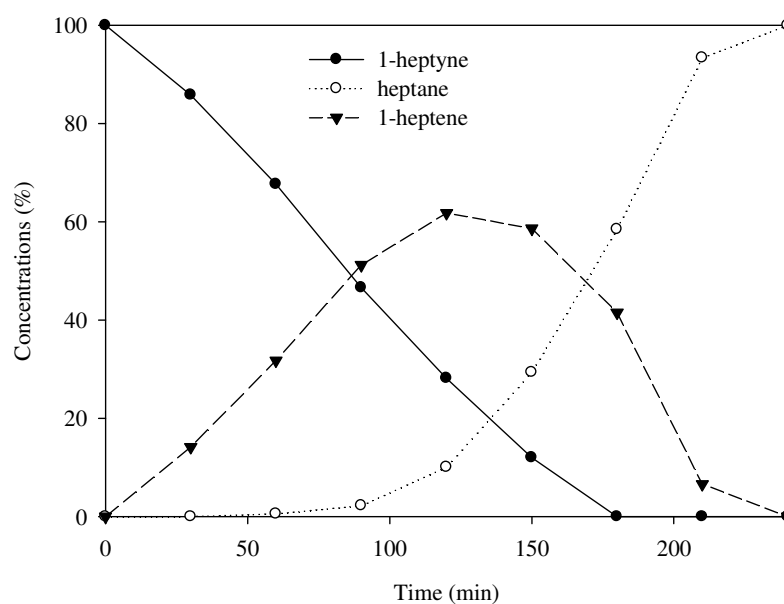
Figure B.2. Reaction profile for 1-heptyne hydrogenation in 1 ml water in a 100 ml mixture containing 5 % v/v 1-heptyne in solvent. Conditions: H_2 flow rate of 100 ml min^{-1}, liquid flow rate of 10 ml min^{-1}, 20 °C temperature and atmospheric pressure.
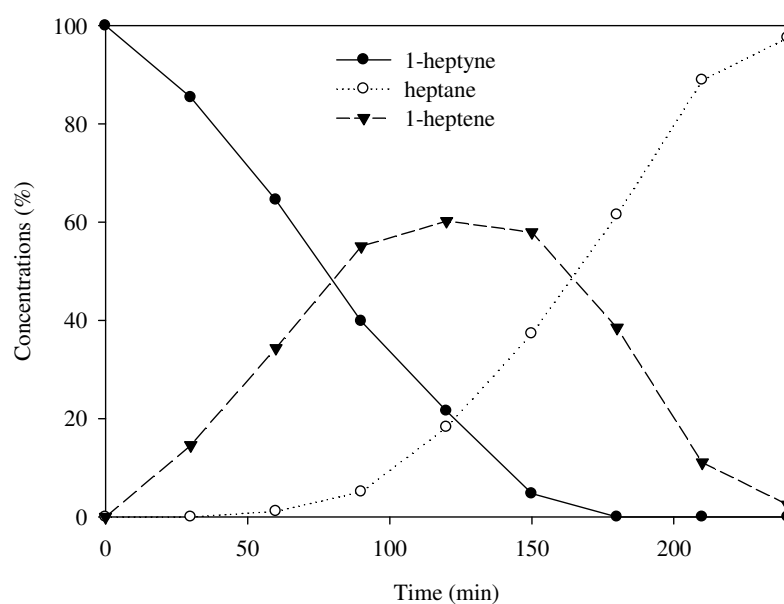
Figure B.3. Reaction profile for 1-heptyne hydrogenation in 1 ml aqueous NaOH in a 100 ml mixture containing 5 % v/v 1-heptyne in solvent. Conditions: H_2 flow rate of 100 ml min^{-1}, liquid flow rate of 10 ml min^{-1}, 20 ^{o}C temperature and atmospheric pressure.
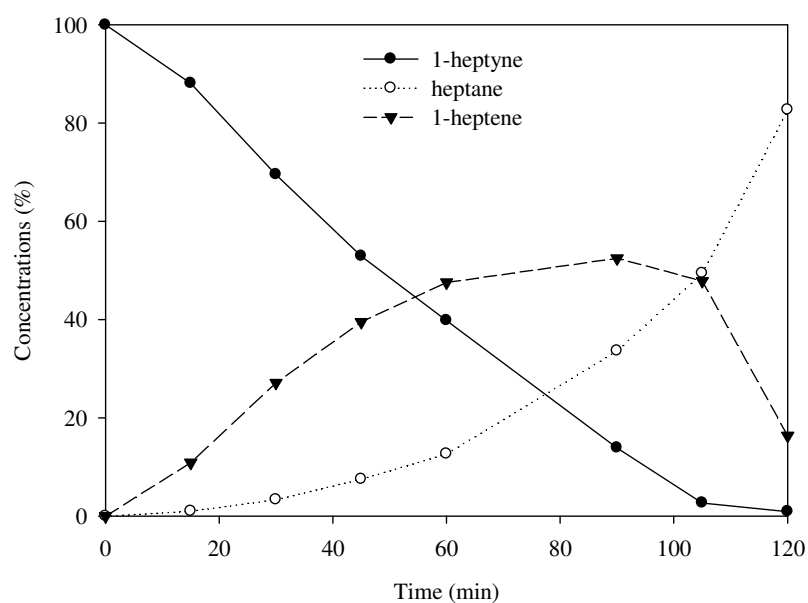
Figure B.4. Reaction profile for 1-heptyne hydrogenation in (50% v/v hexane in isopropanol) in a 100 ml mixture containing 5 % v/v 1-heptyne in solvent. Conditions: H_2 flow rate of 100 ml min^{-1}, liquid flow rate of 10 ml min^{-1}, 20 ^{o}C temperature and atmospheric pressure.

Figure B.5. Reaction profile for 1-heptyne hydrogenation in hexane in a 100 ml mixture containing 5 % v/v 1-heptyne in solvent. Conditions: H_2 flow rate of 100 ml min^{-1}, liquid flow rate of 10 ml min^{-1}, 20 $^{\circ}$C temperature and atmospheric pressure.
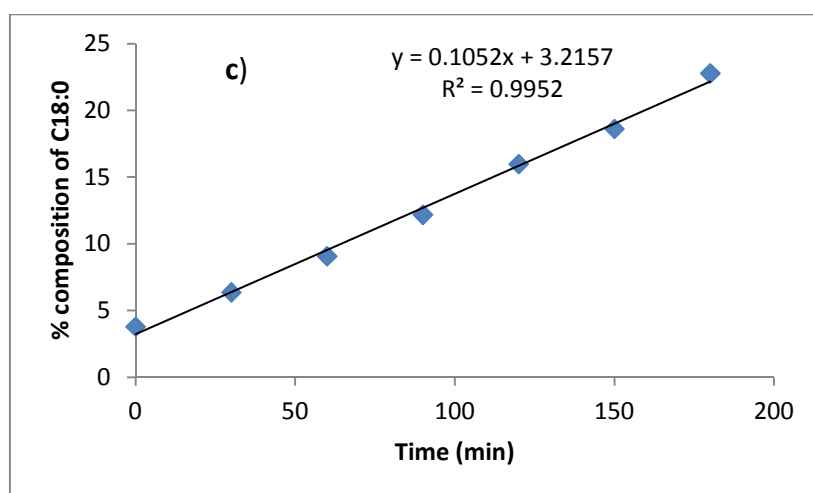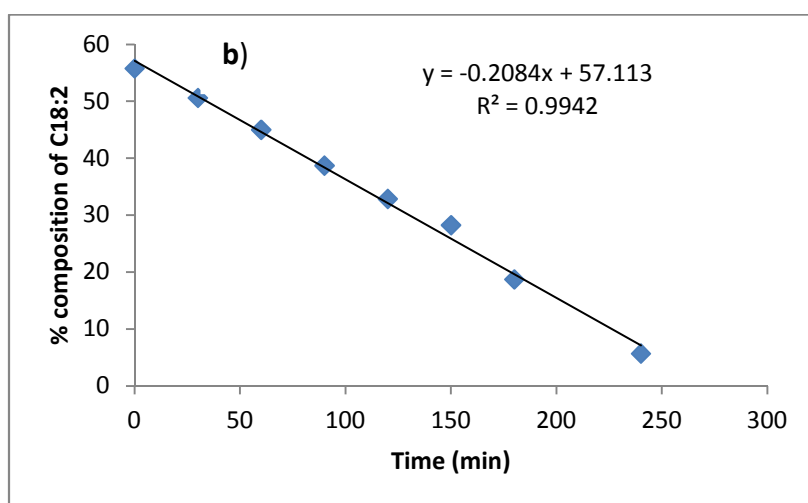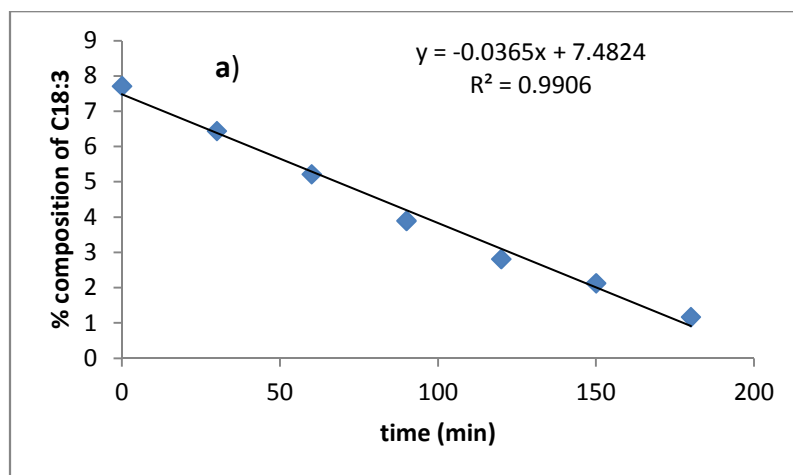
Figure B.6. Plot of % concentration vs time of a) linolenic acid (C18:3), b) linoleic acid (C18:2) and c) stearic acid (C18:0) to determine reaction rate constants for the hydrogenation of soyabean oil at 50 °C.
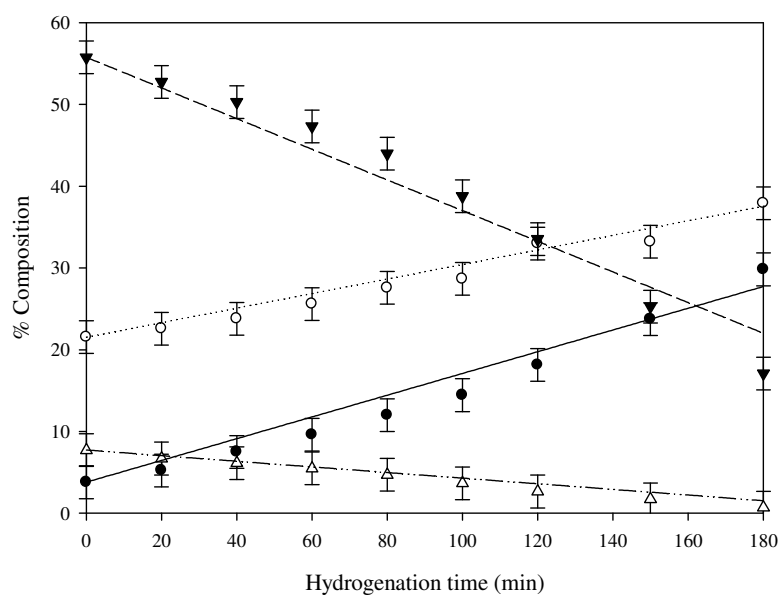
Figure B.7. Comparison of predicted values of % composition of fatty acids in soyabean oil with experimental values under reaction temperature of 60 ℃.
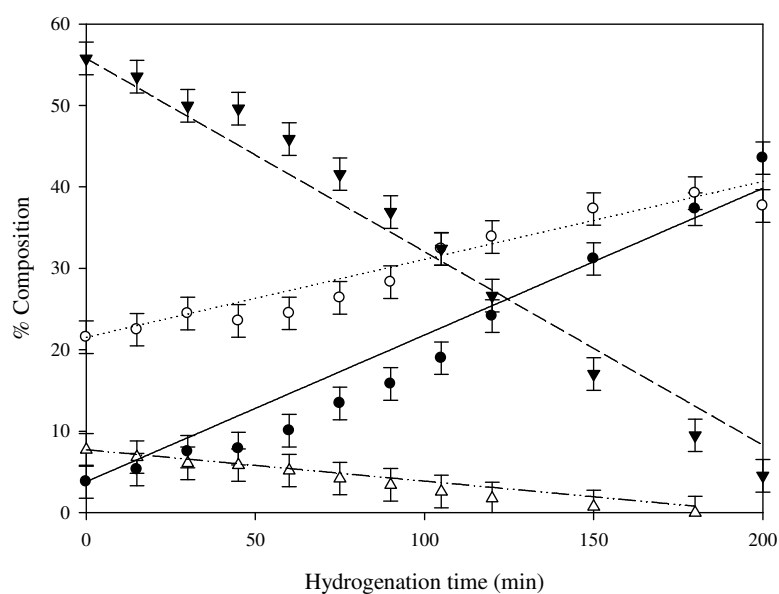
Figure B.8. Comparison of predicted values of % composition of fatty acids in soyabean oil with experimental values under reaction temperature of 70 ℃.
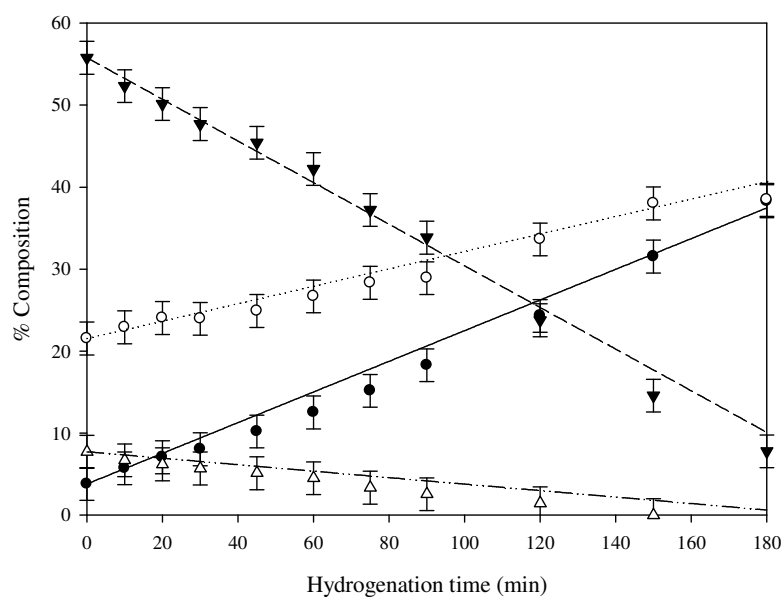
Figure B.9. Comparison of predicted values of % composition of fatty acids in soyabean oil with experimental values under reaction temperature of 85 ℃.
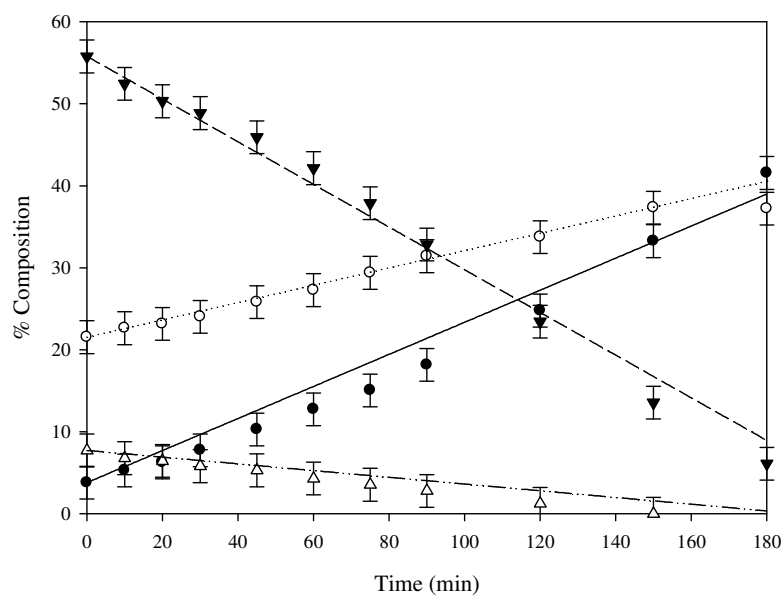
Figure B.10. Comparison of predicted values of % composition of fatty acids in soyabean oil with experimental values under reaction temperature of 105 ℃.

Appendix C. Calibration curves for the GC

This section lists some of the calibration curves used to calculate the activities and selectivities of the studied reactions.
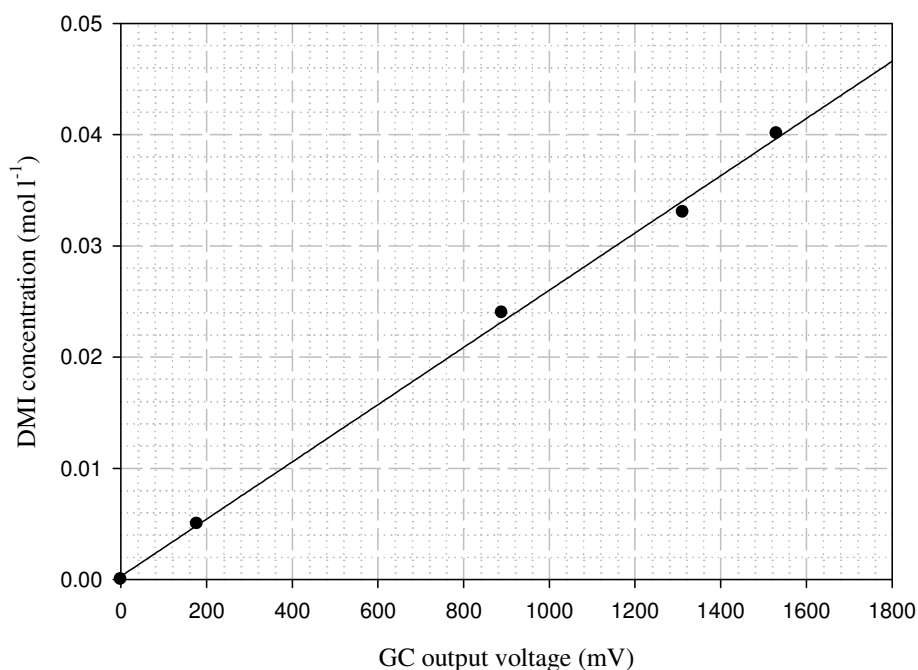
Figure C.1. GC calibration curve for DMI (solvent = 50.0% MeOH + 50.0% water).
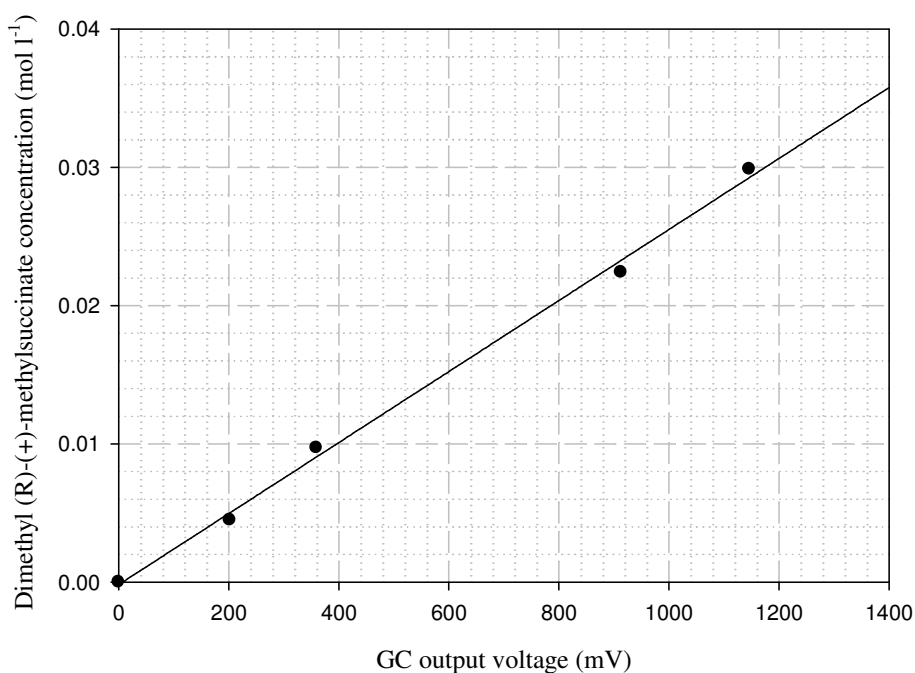
Figure C.2. GC calibration curve for Dimethyl (*R*)-(+)-methylsuccinate (solvent = 50.0% MeOH + 50.0% water).
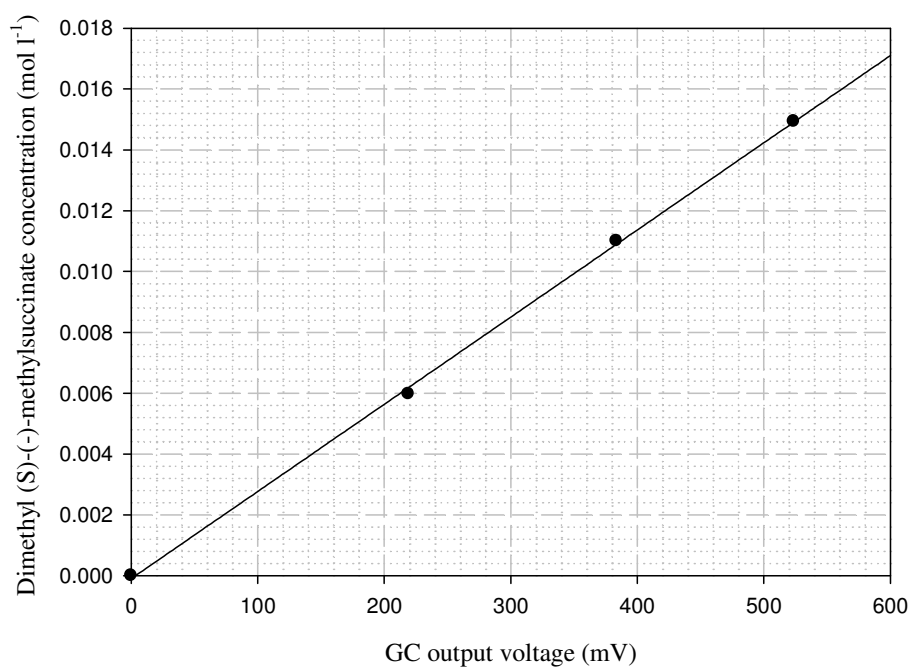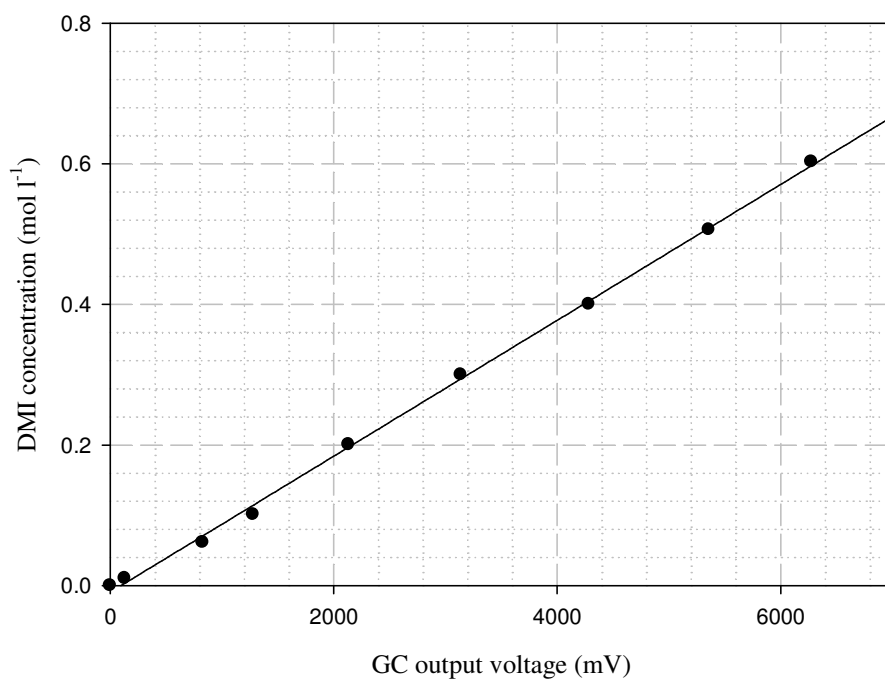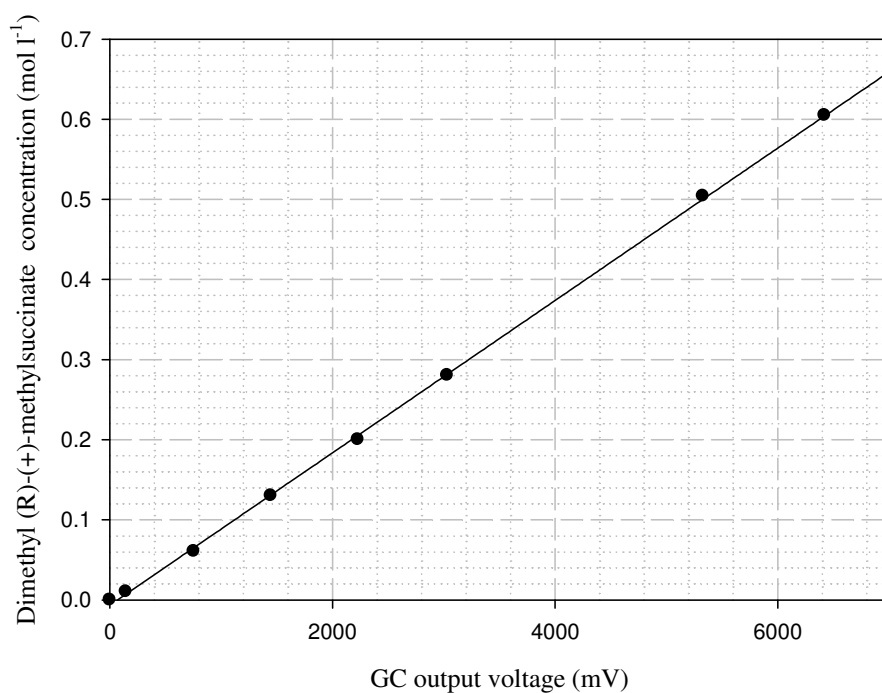
Figure C.3. GC calibration curve for Dimethyl (*S*)-(+)-methylsuccinate (solvent = 50.0% MeOH + 50.0% water).

Figure C.4. GC calibration curve for DMI (solvent = EtOH).

Figure C.5. GC calibration curve for Dimethyl (*R*)-(+)-methylsuccinate (solvent = EtOH).
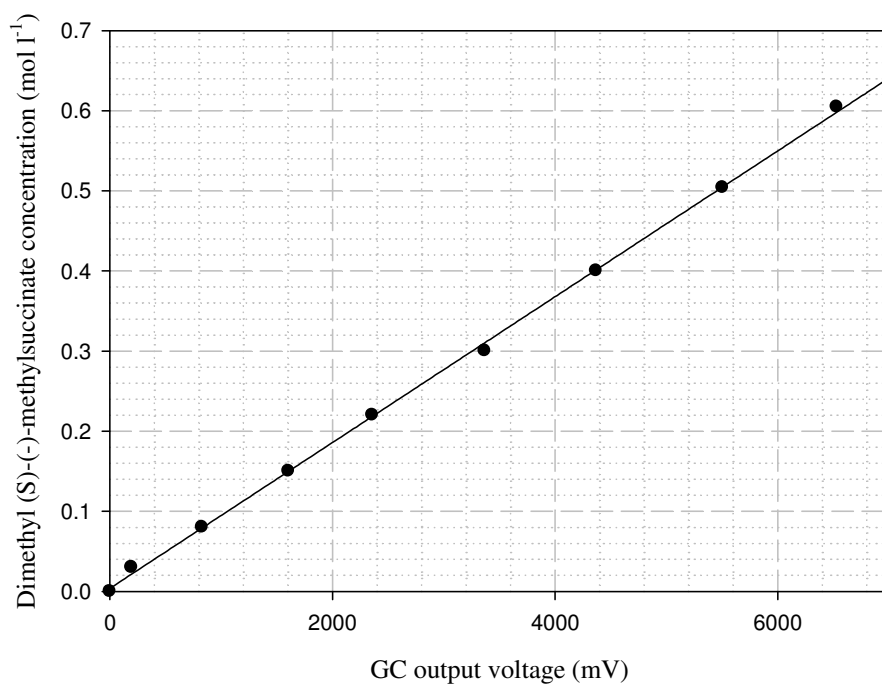

Figure C.6. GC calibration curve for Dimethyl (*S*)-(+)-methylsuccinate (solvent = EtOH).
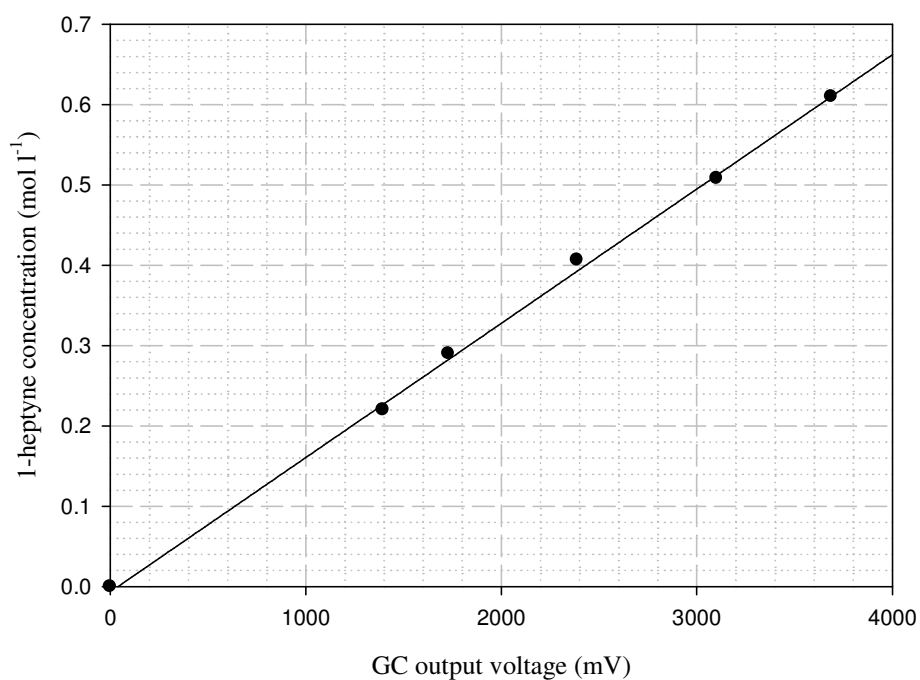
Figure C.7. GC calibration curve for 1-heptyne (solvent = isopropanol).
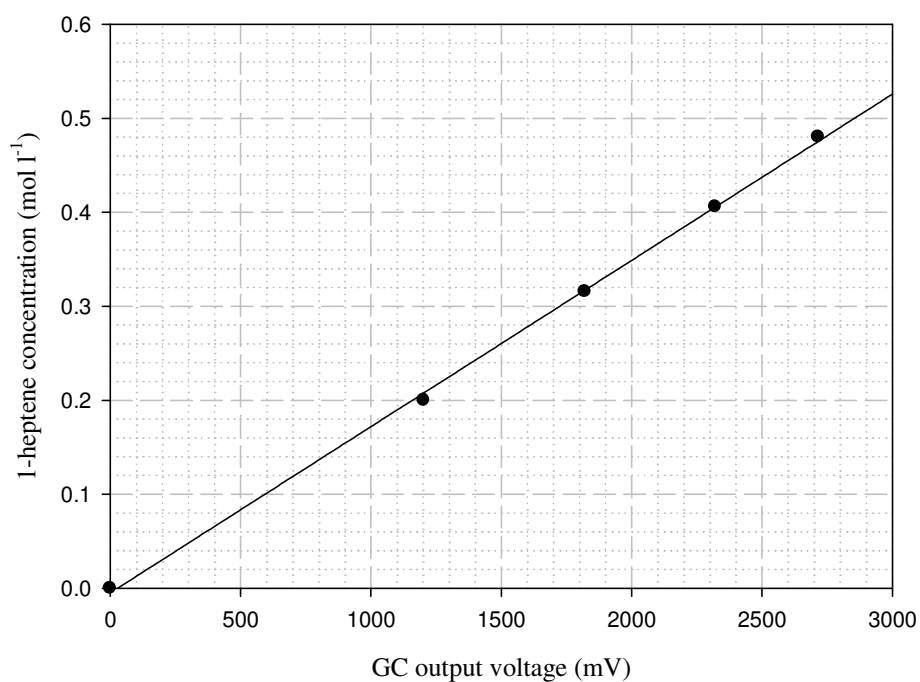

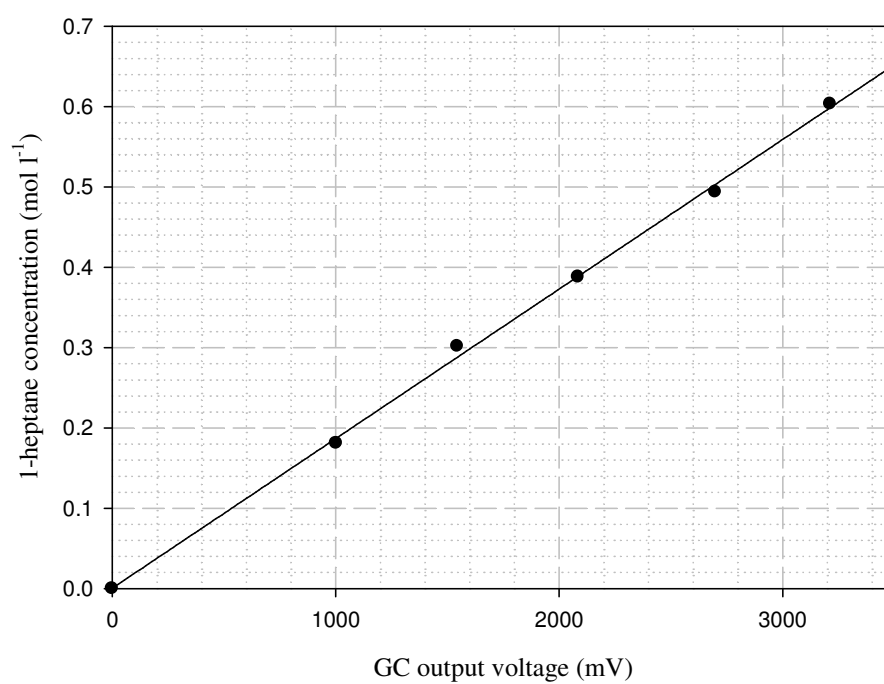**Figure C.8. GC calibration curve for 1-heptene (solvent = isopropanol).**

Figure C.9. GC calibration curve for 1-heptane (solvent = isopropanol).

Appendix D. Published work

Journal publications from the work in this research are listed below.